N77-82335

(NASA-CR-152576)   GODDARD MISSION ANALYSIS
SYSTEM MATHEMATICAL SPECIFICATIONS DOCUMENT
(Martin Marietta Aerospace, Denver, Colo.)
318 p

Unclas

00/12   44424

GODDARD MISSION ANALYSIS SYSTEM
MATHEMATICAL SPECIFICATIONS DOCUMENT

Contract NAS5-20499

January, 1975

Compiled by:

E. D. Vogt
D. V. Byrnes

MARTIN MARIETTA AEROSPACE
P. O. Box 179
Denver, Colorado 80201

for

GODDARD SPACE FLIGHT CENTER
Greenbelt, Maryland

PREFACE

This document describes the mathematical requirements for a general earth-orbital mission analysis system tentatively called the Goddard Mission Analysis System (GMAS). A related document is the GMAS Functional Requirements Document, released 10 October 1974, which summarized the top-level requirements on the system. Previous to that, various documents reviewing mission analysis software and techniques were issued under this effort.

TABLE OF CONTENTS

TABLE OF CONTENTS (continued)

TABLE OF CONTENTS (continued)

TABLE OF CONTENTS (continued)

TABLE OF CONTENTS (continued)

LIST OF FIGURES Page

LIST OF TABLES

1. INTRODUCTION AND SUMMARY

The Goddard Mission Analysis System (GMAS) is to be a coordinated system of computer software that can be used for the mission analysis of general earth-orbital missions. The word "system" implies a set of compatible and complementary elements (data base, utility routine library, program modules, executive programs, interactive graphics equipment and usage, etc.) whose independent functions and mutual interfaces are carefully designed to produce an operation which generates the required data as reliably, efficiently, and easily as possible.

GMAS is to be capable of handling all three phases of mission analyses: pre-flight, in-flight, and post-flight. The basic executive programs will be similar for all phases but different modules and models will be available for each phase. The in-flight capability will of course require real time responsiveness necessitating special mathematical techniques as well as the effective use of interactive graphics and displays.

GMAS will be capable of operating in several mission analysis modes. It will analyze launch opportunity assessment, orbit selection, maneuver targeting and analysis, trajectory propagation, force model sensitivity, mission profile generation, parametric scans, linear error analysis and Monte Carlo error analysis. It will be capable of performing these studies at the levels of depth required by the mission phases discussed above.

GMAS is to be applicable to all earth-orbital missions eventually. Initial development however is to be directed toward four classes of earth-orbital missions: synchronous missions (e.g., CTS, SMS), sun-synchronous missions (e.g., ERTS), drag missions (e.g., AE), and shuttle applications missions. Techniques and software applicable to the first three mission classes currently exist at GSFC. However, these elements are somewhat fragmented and overlapping; the goal of GMAS is to identify the elements common to all three classes and try to coordinate them in an effective general system. The last class is intended to direct attention to identifying the new mission analysis problems associated with the proposed shuttle era.

There are many attractive features of a general system like GMAS if it can be effectively implemented. A modular skeletal structure permits

the basic programs to be easily extended to new problems, techniques and models as they are identified. The commonality of the basic structures with respect to the mission phases results in ease in transferring from the pre-flight to the in-flight to the post-flight phases of mission analysis. Since the basic structures are used for several mission classes (i.e., synchronous, drag, etc.), program users can effectively move from one mission type to another with a minimum of difficulty. Since many of the routines are used by several modules or programs, improvments made to these basic routines immediately improves all the programs that use them, leading to a reduction in costs to maintain the software. Furthermore, this constant use of the same routines and modules results in quick identification of programming errors and thus leads to a continual increase in the reliability of the systems. These advantages can however only be obtained if the system is carefully designed initially so that the time and core requirements are held to a minimum and the program structures are clearly defined.

The first document issued in this initial design effort was the Functional Requirements Document (FRD) which provides a high-level description of the functional requirements to be levied on GMAS. The FRD is currently undergoing revision after review by GSFC personnel. The continually improved document should also improve the efficiency of the actual program construction when begun by having all the mathematical formulation down on paper before beginning any of the coding, thereby demonstrating such things as the required data flow or multiple uses of single modules.

This document, the Mathematical Specifications Document (MSD), is the second in the series. Its function is to identify, organize and display the mathematical models and techniques of GMAS in a single, self-contained report. This will allow knowledgable personnel to review, critique and improve the models and techniques of GMAS before beginning the expensive and sometimes seemingly irreversible process of program coding and assembly.

It is also hoped that this document be of broader use than simply in GMAS development. It is recommended it be maintained as a summary of current mathematical techniques used in mission and operations analysis and support. Then it could foster communication within the mission analysis group by enabling the specialists in each area to see the techniques used by their counterparts in other disciplines and other projects. It could

also serve as an introductory guide to the mission analysis area for un-familiar personnel such as new employees, non-mission analysis special-ists or new contractors.

To accomplish these objectives the editors have tried to make this document as flexible and complete as possible. We have tried to estab-lish a format which allows growth as easily as possible. To improve this we intend to change the numbering of pages, figures, tables and equations to a section basis (e.g., Table 9.1-1, Equation 5.4-3) instead of on the chapter basis (e.g., Table 9-1, Equation 5-24) currently used. This would facilitate the required changes and extensions that we feel are necessary to make this a useful document and not just a dust collector.

For completeness certain topics that have already been addressed in detail in GSFC or other contractor studies have been summarized or re-produced in this report, hopefully always with proper credit given to the original source. In the interest of devoting as much time and effort to the technical analysis and evaluation, the contractor was instructed to minimize the editoral, art and reproduction costs. Thus, where appropri-ate, the original text, equations and artwork from these other sources has been directly reproduced in this report.

The next release of this document from the contractor is due in January 1975. This release will still be in draft form. Eventually GSFC intends to publish this document formally through their own facilities. Any comments or suggestions should be forwarded to the GSFC Technical Monitors: Dr. C. E. Velez or Mr. C. R. Newman, Code 582, Goddard Space Flight Center, or the MMC Program Manager: Dr. E. D. Vogt, Telephone: (303) 794-5211, Ext: 5471.

2. GMAS MISSION SET

Table 1 below defines the four classes of missions to be addressed during this effort. The ordering of the classes is immaterial as the four classes will be treated equally.

Index	Class	Specific Examples
1	Synchronous	SMS-A/B, ATS-F, CTS, IUE, SEOS
2	Sun-Synchronous	ERTS-1/B, SMM, HCMM
3	Drag	AE-D/E, SMM
4	Shuttle Applications	--

TABLE 2-1. Applicable Mission Classes

2.1 Synchronous Missions

The first class covers synchronous missions where a critical problem is the large apogee motor burn. It includes the Synchronous Meteorological Satellite (SMS) Missions A and B. SMS-A was launched 17 May 1974 and SMS-B is scheduled for launch in October, 1974 (Delta launches). Problems with SMS-A (with a six-sigma low apogee in the transfer orbit) pointed up the needs for better apogee maneuver targeting and quick, convenient, parametric search techniques for contingency situations in-flight. The Applications Technology Satellite (ATS-F) was launched (May, 1974) and placed into orbit by a Titan vehicle. The Communications Technology Satellite (CTS) is a joint venture between the U.S. and Canada to be launched in late 1975. GSFC is responsible for getting the satellite on station and Canada takes over at that point. The International Ultraviolet Explorer (IUE) mission

to be launched in mid-1976 is unusual because it is both eccentric and highly inclined to the equator. The Stationary Earth Observatory Satellite is a geostationary equatorial orbiter with minimal north-south drift to provide continuous U.S. coverage.

2.2 Sun-Synchronous Missions

The second class of missions includes the ERTS-type missions which are repeating, sun-synchronous missions with orbital periods of slightly less than two hours. The first Earth Resources Technology Satellite (ERTS-1) is flying now and ERTS-B is scheduled for launch in early 1975. Both are to have 18 day repeating ground tracks and the targeting of ERTS-B will probably involve some phasing constraints to get a net 9 day pattern between the two spacecraft. The Heat Capacitance Mapping Mission, now in preliminary planning, is a sun-synchronous mission that is to obtain near global coverage in about eight days. The Solar Maximum Mission (SMM) launched in 1978 has a sun synchronous orbit that is low enough (about 500 km altitude) to also qualify it as a drag mission.

2.3 Atmospheric Drag Missions

In addition to SMM, the drag missions of the third category include the Atmospheric Explorer (AE) Missions D and E, launched in March and September, 1975, respectively. These missions involve the gradual lowering of perigee into the atmosphere by a sequence where perigee is lowered for one orbit, raised to the previous altitude while data is processed and then if results are safe and predictable, relowered to the new altitude. Some targeting is required in these missions to move periapsis to a location where correlated tests with rockets may be made.

2.4 Shuttle Applications

The fourth class of missions is a somewhat special category as it is intended to start identifying the mathematical models and techniques required for shuttle-era missions. Since GSFC will predominantly be in the role of the shuttle-customer (and not the shuttle-operator) its requirements will largely be to transfer the GSFC satellite from or to orbit where it may be serviced by the shuttle. Possibilities for more complicated orbit phasing maneuvers thus arise. Also the requirement for restartable engines for many of these maneuvers may necessitate the use of longer burns using lower thrust and perhaps vehicle pitching during the maneuver itself.

3. SYSTEM STRUCTURE AND INTERFACES

The basic software components of GMAS may be organized into a hierarchy as follows:

Element	Description
Routine	The smallest unit of software.
Module	A group of functionally related routines.
Program	A collection of modules (and possibly routines) linked to perform a major task.
Subsystem	A set of complementary and coordinated programs.
System	An integrated set of subsystems.

Under these definitions GMAS is a subsystem within the FDS overall system. The detailed design of the system and subsystem structures and interfaces is normally performed after detailing the mathematical specifications of the system. However, these specifications can most efficiently be developed in the context of some structural definition; albeit preliminary. This section will briefly summarize the tentative FDS/GMAS structure.

3.1 FDS Interfaces

The effective design of GMAS requires an understanding of its relation to the other subsystems of the Flight Dynamics System (FDS). The FDS will consist of three subsystems: the Goddard Trajectory Determination System (GTDS), the Attitude Determination and Control System, and the Goddard Mission Analysis System (GMAS).

The GTDS has the prime responsibility for the orbit determination function. It processes telemetered tracking data to estimate the spacecraft orbit and associated uncertainty. In the performance of this task it also includes ephemeris generation (mainly high precision), data simulation, and orbit comparison capabilities. The principal interfaces between the GTDS and the GMAS are that GTDS supplies GMAS with the estimated orbit, covariance, and state transition matrix, while GMAS supplies the GTDS with the nominal maneuver and predicted orbit.

The Attitude Determination and Control System (ADCS) is responsible for the real-time determination and control of the vehicle attitude. There is an active interface between the ADCS and GMAS with GMAS supplying the ADCS with the desired maneuver attitude, ADCS responding with a commanded and achieved attitude, and GMAS determining the acceptability of that attitude.

The basic interface device between the three subsystems will be a common data base in which data required by the three elements will be stored.

3.2 GMAS Modules

A well-designed set of modules is the catalyst that turns a software library into an effective, coordinated system. The GMAS modules provide the basis for a general, flexible, and easily-extended system and allows the simple construction of mission-peculiar software as it is identified. These modules may be divided into two categories as follows:

GMAS Computational Modules

Trajectory Propagation

Optimization and Targeting Algorithms

Orbit Parameter Computation

Instantaneous Parameter Computation

GMAS Executive Modules

Parametric Scan Control

Monte Carlo Analysis Control

Targeting/Optimization Control

The computational modules include those software packages that perform general mathematical computations that are required by several programs. The basic computational module is the trajectory generator which is used by all the programs. An equally important module for mission analysis is the targeting and optimization module for maneuver targeting and orbit selection. Other modules will include the orbit parameter module which computes mission analysis parameters (e.g.

shadow periods) from orbital elements, and the instantaneous parameter module which computes mission analysis parameters (e.g., elevation from a tracking station) from the instantaneous state of the vehicle.

The second class of modules are the executive modules which control the data flow and bookkeeping for specific types of studies. This class includes three similar modules controlling parametric scans, Monte Carlo analyses, and targeting and optimization.

3.3 GMAS Programs

With a proper design of the computational and executive modules defined above, it is a relatively easy job to assemble those modules with supporting (and sometimes mission-peculiar) routines to produce effective GMAS programs. The major GMAS programs are briefly described below.

GMAS Programs

Trajectory Propagation

Launch Opportunity Assessment

Mission Scan

Maneuver Targeting and Analysis

Mission Profile Generation

Linear Error Analysis

Monte Carlo Analysis

Trajectory Propagation Program: This program will contain the trajectory propagation module and the control logic (initialization, input and output control, etc.) necessary to operate it. Trajectory propagation will be available for a variety of force models, mathematical formulations, and numerical quadrature schemes.

Launch Opportunity Assessment: This program will have the capability to scan the launch period/launch window opportunities while evaluating a variety of constraints such as shadowing, attitude during coast and maneuvers, orbital

lifetime, etc.

Mission Scan Analysis: This program will be capable of evaluating a series of orbits defined by a variety of control parameters including impulsive maneuver parameters, launch profile parameters such as launch azimuth and coast time, and orbital elements for broad orbit selection.

Maneuver Targeting and Analysis: This program will be similar to the previous program except that it operates in a targeting or optimization mode instead of a scan mode. It will select the optimal maneuver or mission satisfying equality or inequality constraints while optimizing or requested performance criteria.

Mission Profile Generation: This program will be responsible for the detailed mission profile generation. It will be capable of operating in either the single-case or scan mode, generally with the high- or medium-precision propagation modules and with the instantaneous parameter computation module. Its output will define predicted station passes, shadows, site overflies, etc.

Linear Error Analysis: This program will be capable of performing preflight error analyses for both tracking and maneuvers. The tracking analysis will mirror models actually used in the GTDS in its analysis of the ability to track the vehicles. The maneuver error analysis will identify the impact of injection covariances and orbital maneuver execution errors on fuel budgets and mission design margins.

Monte Carlo Analysis: This program will be composed of the Monte Carlo control module, the selected trajectory propagator, and the desired parameter computation modules. It will be responsible for flying a given mission sequence repeatedly, sampling from input error models to simulate the realities of errors on maneuvers.

4. EXECUTIVE MODULES

The purpose of this contractual effort was to summarize the mathematical specifications of the GMAS. However, in the development of those specifications some consideration was given to several modules performing key executive functions. The detailed definition of the logic and structural design of these modules will be performed in the subsequent design phase of GMAS. However, a toplevel view of several of these modules is worthwhile to demonstrate how several of the computational modules such as the trajectory propagators, the maneuver targeting algorithms, and the mission analysis parameters may be tied together by executive structures. The executive modules discussed below include the following:

        1. Parametric Scan Module

        2. Monte Carlo Module

        3. Targeting Module

        4. Mission Synthesis Module

4.1 Parametric Scan Capability

A frequently-used technique in all phases of mission analysis is the parametric scan. In parametric scans, certain parameters (called control parameters) are varied in a systematic manner (generally over a grid of values) and resulting parameters (called performance parameters) are evaluated for the series of control parameters. The control parameters are generally associated with maneuvers and the performance parameters are generally mission analysis parameters associated with the resulting orbits.

The parametric scan capability required for the GMAS is summarized in Table 4.1-1 on the following page. Generally four types of parametric scans are needed: launch window analysis, launch orbit selection, standard orbit selection, and maneuver targeting. These studies are distinguished by the particular control and performance parameters desired. In launch window analyses, the launch date and launch time-of-day (or longitude of the ascending node) are systematically varied to determine launch periods having adequate daily

Study Type	Fixed Parameters	Varied Parameters	Performance Parameters
1. Launch Window	Launch azimuth Launch site latitude Launch site longitude	Launch data Launch time-of-day or node longitude	Coast time Shadow time Aspect angles at maneuvers Orbit stability Orbit lifetime
2. Launch Orbit Selection	Launch data Site latitude Site longitude	Launch azimuth Launch time-of-day Coast time Injection ΔV vector	Above parameters plus Orbit groundtrack profiles Solar geometry profiles Tracking profiles, etc.
3. Orbit Selection	Initial time	Orbital elements or equivalent orbit parameters	Above parameters
4. Maneuver Targeting/Orbit Selection			
A. Fixed ΔV Magnitude	Initial orbit ΔV Magnitude	Maneuver right ascension Maneuver declination Time of firing	Errors in desired elements ΔV to trim to desired elements. Observability of subsequent trim maneuvers.
B. Fixed Attitude	Initial orbit Maneuver attitude	Time of firing ΔV Magnitude (opt.)	Time to drift to station Orbit groundtrack profiles Solar geometry profiles, etc.
C. Unconstrained Maneuver	Initial orbit	Time of firing Maneuver attitude Maneuver ΔV magnitude	

Table 4.1-1. Mission Analysis Parametric Scan Requirements

launch windows with acceptable orbits. In launch orbit selection, the launch date is held fixed while the standard launch parameters are varied within reasonable limits to determine the range of feasible (with respect to reasonable launch constraints) orbits. In the direct orbit selection, no attempt is made to tie the orbit selection process to launch; the control parameters are simply the orbital elements (or equivalent parameters such as perigee or apogee altitude) varied to optimize the systems design or science return of the mission. The fourth category of maneuver targeting is also related to orbit selection as the maneuver controls are generally selected to optimize the resulting orbit. Three types of maneuvers control constraints are indicated in Table 4.1-1 corresponding to unconstrained controls, and controls limited by fixed V magnitude and fixed attitude. The performance parameters in all three cases are identical however.

The logic flow for any of the scans is essentially identical. The macrologic is indicated in Figure 4.1-1. Whether a general structure can or should be constructed or whether distinct programs should be developed will be a subject for the system design phase.

| Define (input) controls $\underline{k}$ initial values increments $\underline{u}_o$ increments $\Delta \underline{u}$ parameters $\underline{k}_p$ | Increment control parameters $\underline{u} = \underline{u} + \Delta\underline{u}$ systematically | Propagate trajectory to event time(s) if necessary | Evaluate computed parameters $\underline{p}(\underline{u})$ and/or profiles | Print and/or store case data |
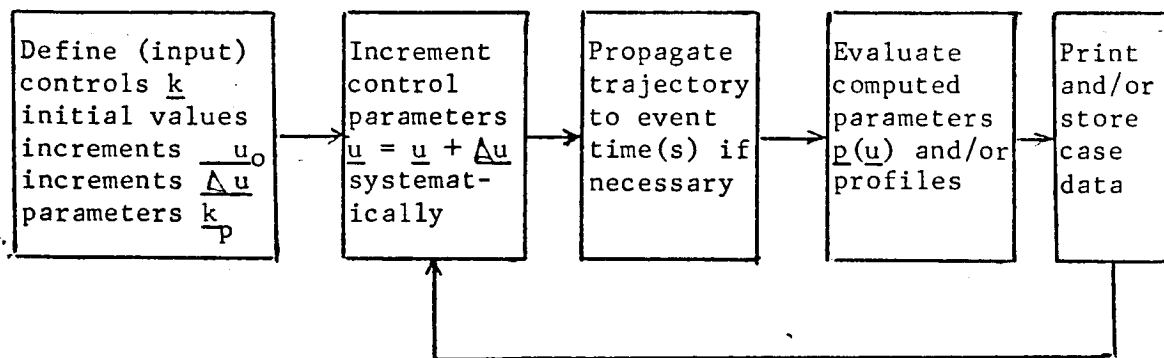
Figure 4.1-1. Parametric Scan Macrologic

4.2 Monte Carlo Capability

A second type of executive control required by the GMAS is a Monte Carlo capability. Monte Carlo analysis is an integral part of maneuver analysis to determine the sensitivity of orbits and their related parameters (e.g., shadowing, station coverage, orbit correction requirements, etc.) to errors made during the maneuver itself.

The types of Monte Carlo analyses needed may be categorized according to the error models used to describe the maneuver (See Table 4.2-1). Certain maneuvers employ a covariance matrix for the error model. Such is the usual case with the injection maneuver from the parking orbit onto the transfer or target orbit. The impulsive error model would generally be used in analyzing a maneuver which takes place during a short increment of orbital true anomaly such as an apogee maneuver or the transfer orbit for a synchronous mission. The finite burn maneuver error model might be required to model a fixed-pitching-rate maneuver used in injecting from a parking orbit onto a synchronous mission transfer orbit. if no injection covariance matrix were available for that maneuver.

Error Model	Error Parameters
Covariance	Covariance matrix (6x6) defining deviations in post maneuver position and velocity
Impulsive Maneuver	Error in impulsive ΔV defined by: proportionality error - $k\ \Delta V$ resolution error - $s\ \Delta V$ pointing errors - α and β
Finite Burn	Error in state following maneuver computed by integrating sample burn defined by: thrust - T mass - m time of initiation - t duration of burn - Δt pointing angles during burn - α, β

Table 4.2-1. Monte Carlo Error Models

Regardless of error models employed, the Monte Carlo analysis proceeds similarly. The error model is sampled repeatedly to generate post-maneuver states. These states are then propagated forward evaluating desired performance variables (See Table 4.1-1). After generating a statistically-reasona le number of samples, the statistics of the resulting performance variables (including pro- bability of success) are re-constructed. The macrologic is essen- tially identical to that of the parametric scan (Figure 4.1-1) except for the second computational block in which the systematic incrementation of the control variables is replaced by the statis- tical sampling of the desired error models. The mathematical details of this sampling are discussed in Section 14.3.

4.3 Targeting Capability

A third executive capability involves the targeting and optimization of orbits and maneuvers. This capability is similar to the previous two capabilities (parametric scan and Monte Carlo scan) in that a series of different orbits are propagated, periodically evaluating a user-defined set of mission analysis parameters. The difference is that the sequence of orbits is determined to iteratively improve a performance function instead of following a user-specified variable grid (parametric scan) or randomly generated error model samples (Monte Carlo analysis).

The targeting module structure thus is identical to the structure pictured in Figure 4.1-1 with one major exception: the second block is replaced by the targeting iteration algorithm. The mathematics of this algorithm are described in detail in Chapter 11. The other primary computational modules include the trajectory propagators (described in Chapter 6) and the mission analysis parameter computations (discussed in Chapter 7).

As with the previous two executive capabilities, there are several distinct studies for which a targeting capability would be desirable. These essentially parallel the studies summarized in Table 4.1-1.

Referring to that table only the launch window study is probably not amenable to targeting and optimization analysis.

The performance function and related constraints of such studies are sufficiently complex and nonlinear to make an iterative targeting algorithm less than effective. Also, the mission designer's subjective evaluation is frequently required in the trades associated with launch window studies. The other studies listed in Table 4.1-1 are all well-suited to optimization analysis. In the categorization of parameters, the "fixed parameters" would be held constant at the input values during the optimization. The "varied parameters" would be the control parameters solved for during the process. The "performance parameters" would be combined and weighted to determine the performance function which would then be minimized (or maximized) during the optimization process.

The preferable mode of implementation would be to develop the targeting/optimization algorithm in a self-contained, modular package that could be used easily in any of these applications. The executive structure that manages the targeting algorithm, the propagator, and the parameter computational modules would be quite similar for each of these studies but may have certain peculiarities for each study.

4.4   Trajectory Synthesis Module

The object of the mission analysis system is to eliminate the need for a new round of programming with each new problem. The cost of such uncoordinated software development in terms of analysis, coding, verification, and documentation is entirely unacceptable. The alternative is to develop a coordinated yet flexible system of executive and computational modules which the user can access to solve his mission analysis problem via a user oriented data deck. Such an approach not only reduces software development costs but also guarantees uniformly high quality analysis and a standard format for supplying data and reporting results.

Fundamental then to this "data-driven" mission analysis system is a means to specify an arbitrary trajectory with a minimum of user supplied data. Such a capability is essential to the targeting/optimization error analysis, parametric scan, and profile generation executive programs. This system-wide demand dictates the need for a computational module to synthesize a full range of earth-orbital trajectories from input data alone.

To be of substantial benefit to the user, such a trajectory synthesizer must be able to function from precisely that data which characterize the trajectory in the user's mind. In other words, the user must not be required to have detailed knowledge of the trajectory to specify it to the system. Typically, the mission analyst thinks of earth orbital missions in segments or phases separated by well defined events. For instance, a synchronous equatorial mission consists of the phases and triggering events shown in Table 4-1. Notice that all of the triggering events are characterized by a specific variable assuming a prescribed value. This triggering variable is not necessarily time. Hence the synthesizer cannot require the user to specify the start time of each phase. The minimal input data structure for the trajectory synthesizer is built upon this event/phase conceptual basis for specifying trajectories.

In order to build the trajectory as it goes, the synthesizer must propagate the equations of motion numerically in time. Next all of the simulation data must be input by phase. Data can be carried over from one phase to the next but each phase must be supplied with all of the essential information pertaining to environment, vehicle characteristics,

initial state conditions, control variables, and propagation techniques so
that each trajectory phase can be constructed from its specified triggering
event to the corresponding event for the succeeding phase.

NO.	TRIGGERING EVENT		PHASE DESCRIPTION
	DESCRIPTION	VARIABLE	
1.	ascent burnout	time	parking orbit coast
2.	first transfer burn ignition	latitude (0°)	transfer ellipse injection
3.	first transfer burn termination	weight of propellant	transfer ellipse coast
4.	second transfer burn ignition	latitude (0°)	apogee motor circularization maneuver
5.	second transfer burn termination	weight of propellant	post circularization tracking coast
6.	phasing burn ignition	time	phasing maneuver
7.	phasing burn termination	time	phasing coast
8.	synchronization burn ignition	longitude	synchronization manpower
9.	synchronization burn termination	time	coast in final synchronized orbit

Table 4.4-1.   Trajectory Characterization by Phases and Triggering
Events for a Synchronous Equatorial Mission

The actual phase specification adheres closely to the user's event/
phase concept of trajectory structure. The simulations are given the same
programmable quality of actual trajectories, that is, subsequent phases can
be adapted to accommodate the outcome of prior phases in order to acheive
desired mission objectives. The order of occurrence of each phase is deter-
mined by its triggering event which is turn defined as the assumption of a

specified value by the triggering variable. In order to treat precedence relations among the phases, each triggering event must be assigned a sequence number by the user. The events are constrained to occur in order of sequence number subject to certain simple rules on event type.

To allow the flexibility in specifying the prospective ordering of phases, three event types can be defined.

1. Primary events are the main sequential events of the simulated trajectory. They must be assigned integral sequence numbers and must occur in increasing order of these numbers.

2. Secondary events are contingency events that may or may not occur during their associated primary phase. They are assigned non-integral sequence numbers, the integral portion of which coincides with the associated primary event and the fractional portion determines the relative order of the secondary events. A secondary event occurs during its associated primary phases whenever its triggering variable assumes its specified value. However, the occurrence of a secondary event nullifies all other secondary events of smaller sequence number. The occurrence of a primary event nullifies all the secondary events associated with its preceding primary event.

3. Roving primary events are events which have no specific predecessor primary event. They are assigned an integral event number and can occur anytime after all of the primary events with lower sequence numbers have occurred. They provide the capability of interrupting the trajectory at any time regardless of the phase number.

In order to detect the end of the current phase, the trajectory synthesizer must monitor a candidate set of triggerent events

1. the next primary event,

2. all the secondary events associated with the current primary event which have not been nullified by the occurence of a subsequent secondary event,

3. all the roving primary events whose immediately preceding primary events have occurred.

The trajectory synthesizer uses an iterative scheme to determine the precise occurrence time of the next triggering event. The triggering

4.4-3

variables of all the events in the candidate set are monitored at each propagation step in time. If one of these passes from above to below or from below to above its specified value between the current and previous propagation steps, it is singled out for precise determination of the cross over point. The macrologic involved is shown in Figure 4-1 for finding the first zero component of an event triggering vector $\underline{g}(t)$. Note that the quadratic interpolation logic makes use of two back values of the triggering variable in addition to the current one. The equations for the interpolating polynomials are given in Section 11.3.2 on the acceleration projected gradient algorithm.

Enter

Build set
$$\mathcal{A}=\left\{i:\ g_i(t_{n-1})g_i(t_n)\leqslant 0\right\}$$

$i^* \leftarrow 0$

Is $\mathcal{A} = \emptyset$?

Yes → Return

No

$k \leftarrow 0$

Has $g(t_{n-2})$ been stored ?

No →
$$\bar{t} \leftarrow t_n$$
$$\underline{t} \leftarrow t_{n-1}$$
For each i
$$\underline{g}_i \leftarrow g_i(\underline{t})$$
$$\bar{g}_i \leftarrow g_i(\bar{t})$$

For each $i \in \mathcal{A}$ find root t_i^*, of line passing through $(\bar{t},\bar{g}_i)$ and $(\underline{t},\underline{g}_i)$

Find i^* such that
$$t_{i^*}^* = \min_{i\in\mathcal{A}}\left\{t_i^*\right\}$$

E

Yes

$$\bar{t} \leftarrow t_n$$
$$\hat{t} \leftarrow t_{n-1}$$
$$\underline{t} \leftarrow t_{n-2}$$

For each $i\in\mathcal{A}$
$$\underline{g}_i \leftarrow g_i(\underline{t})$$
$$\bar{g}_i \leftarrow g_i(\bar{t})$$
$$\hat{g}_i \leftarrow g_i(\hat{t})$$

A

For each $i \in \mathcal{A}$ find appropriate root, t_i^*, of the parabola passing through $(\bar{t},\bar{g}_i)$, $(\hat{t},\hat{g}_i)$ and $(\underline{t},\underline{g}_i)$

Find i^* such that
$$t_{i^*}^* = \min_{i\in\mathcal{A}}\left\{t_i^*\right\}$$

E
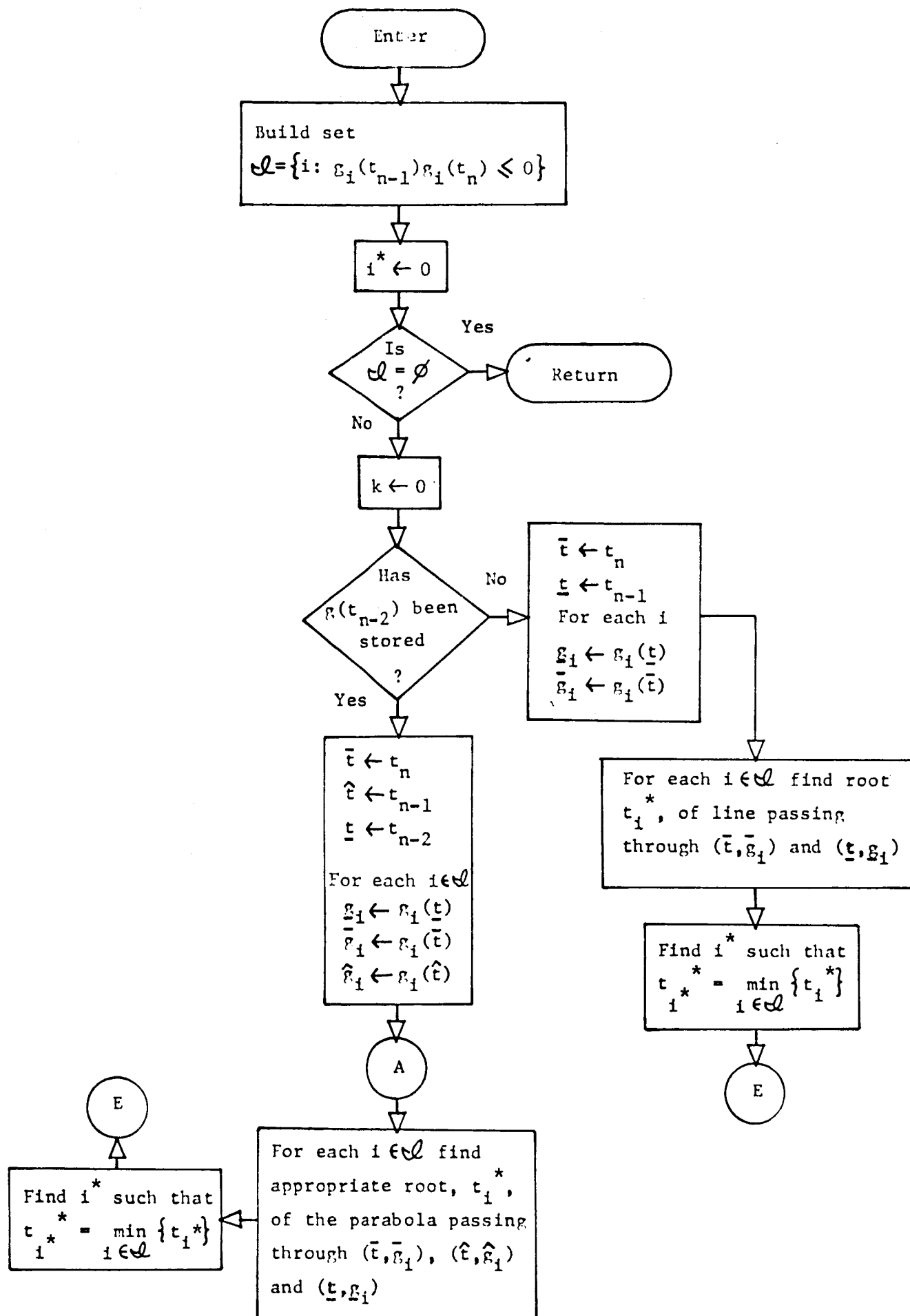
Figure 4.4-1. Macrologic for Precise Determination of Triggering Variable Cross-Over Points

4.4-5

E

Is $\bar{t} - \underline{t} < \varepsilon$?

Yes → Specify that $g_{i^*}(t_{i^*}^*) \approx 0$ → Return

No

$k \leftarrow k + 1$

Is $k > k_{max}$

Yes → Print message that triggering variable could not be approximated sufficiently accurately → Stop

No

For each $i \in \ell$
$g_i^* \leftarrow g_i(t_{i^*}^*)$

Has $\hat{g}$ been stored ?

No → C

Yes

Is $g_{i^*} \bar{g}_{i^*} > 0$?

No

Yes → $\bar{t} \leftarrow \hat{t}$
For each $i \in \ell$
$\bar{g}_i \leftarrow \hat{g}_i$

$\underline{t} \leftarrow \hat{t}$
For each $i \in \ell$
$\underline{g}_i \leftarrow \hat{g}_i$

C

$\hat{t} \leftarrow t_{i^*}^*$
For each $i \in \ell$
$\hat{g}_i \leftarrow g_i^*$

Build set
$\ell = \{ i: \quad \bar{g}_i \underline{g}_i \leqslant 0 \}$ → A
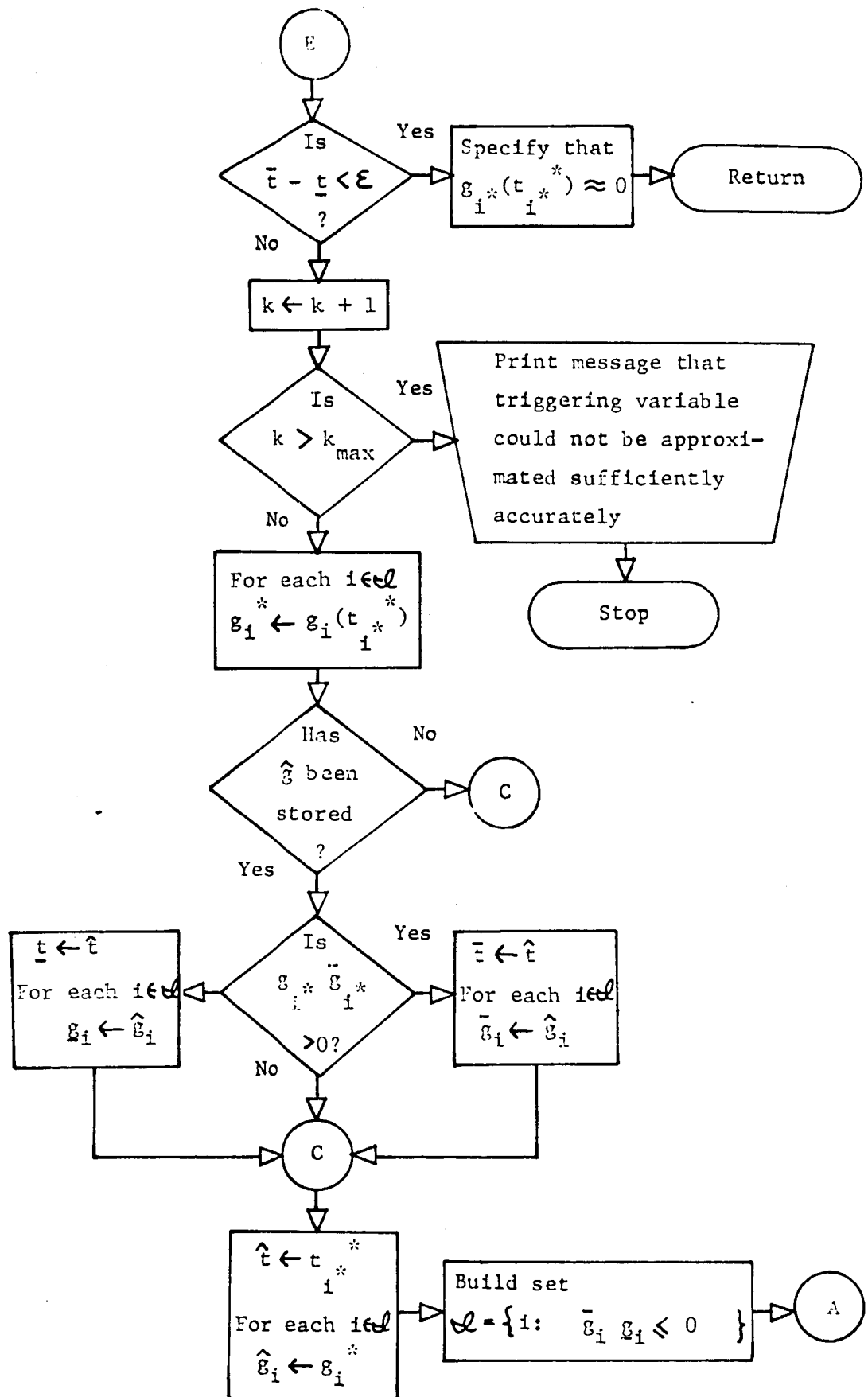
Figure 4.4-1 (completed). Macrologic for Precise Determination of Triggering Variable Cross-Over Points

5.   COORDINATE AND TIME TRANSFORMATIONS

5.1   Introduction

This chapter addresses the coordinate and time transformations to be available in GMAS. It essentially reproduces the development of the same subject in References 5-1 or 5-2 but with some reduction in details. Generally the basic equations are identical but some of the derivations have been deleted. Additions to the material in Reference 5-1 are the inclusion of two additional coordinate frames: the mean ecliptic and equinox coordinate frame and the vehicle-fixed coordinate frame.

Section 5.2 describes the GMAS coordinate systems,, Section 5.3 defines the basic coordinate frames and their transformations, Section 5.4 defines the utility coordinate systems and their transformations and Section 5.5 addresses time systems and transformations.

5.2 COORDINATE SYSTEM DESCRIPTIONS

5.2.1 Body-Centered Inertial (Geocentric, Selenocentric, or Planetocentric)

Origin:	Center of the body
Reference Plane:	Earth equatorial plane of epoch
Principal Direction:	Vernal equinox of epoch
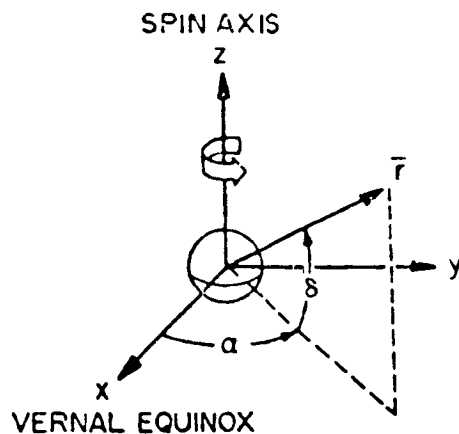
Figure 5.2-1. Body-Centered Inertial
Coordinate System

Rectangular Cartesian Coordinates (see Figure (5.2-1)):

x-axis ~ the principal direction

y-axis ~ the normal to the x-axis and z-axis to form a right-handed system

z-axis ~ the normal to the earth equator of epoch in the direction of the
angular momentum vector

Within the following formulation, $\bar{R}$, X, Y, and Z designate the position vector and Cartesian coordinates referred to the mean equinox and equator of 1950.0. Similarly, $\bar{r}_E$, x_E, y_E, and z_E designate the position vector and Cartesian coordinates referred to the mean equinox and equator of epoch and $\bar{r}$, x, y, and z designate the position vector and Cartesian coordinates referred to the true equinox and equator of epoch.

Spherical Polar Coordinates:

r ~ radial distance from the origin to the point being measured

α ~ right ascension, $\tan^{-1}$ (y/x)

δ ~ declination, $\sin^{-1}$ (z/r)

5.2.2 Body-Centered Rotating (Geographic or Selenographic)

Origin: Center of the body

Reference Plane: Body's equatorial plane (plane perpendicular to the axis of rotation at a given epoch)

Principal Direction: Intersection of the prime meridian with the equator
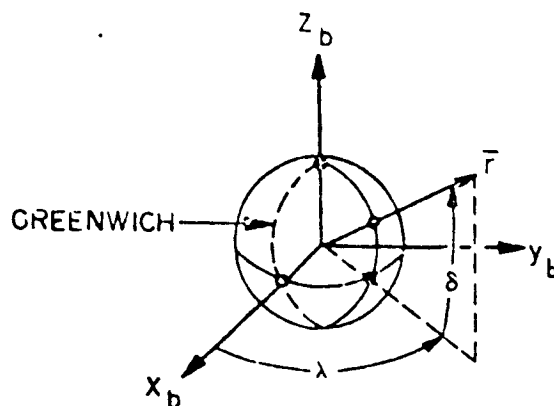
Figure 5.2-2. Body-Centered Rotating Coordinate System

Rectangular Cartesian Coordinates (see Figure 5.2-2):

x_b-axis ~ the principal direction

y_b-axis ~ the normal to the x_b and z_b axes to form a right-handed system

z_b-axis ~ the direction of the axis of rotation toward the north celestial pole

Geocentric Spherical Coordinates:

r_b ~ radial distance from the origin to the point being measured

λ ~ longitude measured east from the prime meridian, $\tan^{-1} (y_b/x_b)$

δ ~ latitude measured from the equator, $\sin^{-1} (z_b/r_b)$

Geodetic Spherical Coordinates (see Figure 5.2-4):

h ~ the perpendicular distance from the surface of the ellipsoid model to the point being measured

λ ~ the same as longitude measured in the geocentric spherical coordinates

ϕ ~ the geodetic latitude angle between the vector normal to the ellipsoid model passing through the point of interest and the equatorial plane

ϕ' ~ the geocentric latitude of a point on the ellipsoid

Geodetic coordinates are used to reference a point from the surface of a body that is an ellipsoid of revolution rather than a sphere.

5.2.3 Local Plane System

Origin:	Center of the reference body
Reference Plane:	The axes are defined independently of a reference plane. The x_{lp} - y_{lp} plane becomes the "reference plane"
Principal Direction:	The principal axis is along the radius vector from the origin to the satellite
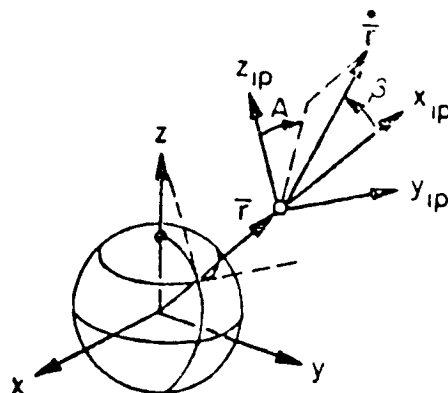
Figure 5.2-3.   Local Plane System

Rectangular Cartesian Coordinates (see Figure 5.2-3).

x_{lp}-axis -- the principal direction

y_{lp}-axis ~ the axis displaced from the inertial y-axis by the satellite's right ascension and lying in the original x-y plane

z_{lp}-axis ~ the direction that forms a right-handed system with x_{lp} and y_{lp}. It is displaced from the inertial z-axis by the satellite's declination

---

Spherical Velocity Coordinates:

V ~ the velocity vector's magnitude ($\dot{r}$)

γ ~ the flight path angle measured from the principal direction to the velocity vector

A ~ the azimuth angle measured clockwise from the z_{lp} axis to the projection of the velocity vector on the y_{lp} - z_{lp} plane

5.2.4 Topocentric Local Tangent (East/North/Up)

Origin: Observer (topocentric)

Reference Plane: Plane tangent to the ellipsoidal earth model at the observer

Principal Direction: Local east direction on the plane tangent to the earth model
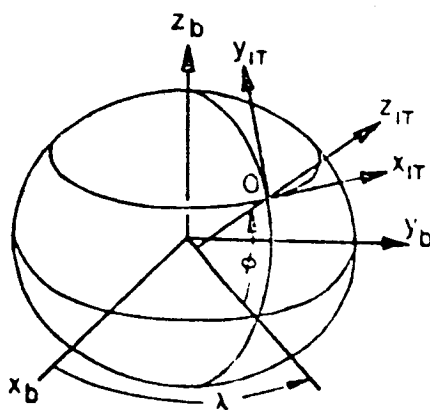
Figure 5.2-4. Topcentric Coordinates

Rectangular Cartesian Coordinates (see Figure 5.2-4):

x_{lt}- axis ~ the principal direction

y_{lt}- axis ~ the axis lying in the reference plane that points north

z_{lt}- axis ~ the upward direction along the geodetic vertical

5.2.5 Orbit Plane

Origin:	Center of the reference body
Reference Plane:	The plane of the orbit
Principal Direction:	The radius vector from the origin to the satellite
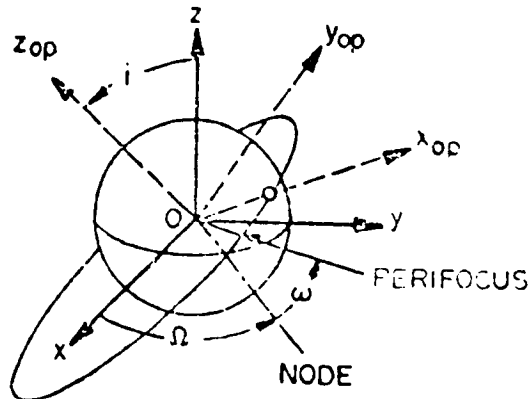
Figure 5.2-5. Orbit Plane Coordinates

Rectangular Cartesian Coordinates (see Figure 5.2-5):

x_{op}-axis ~ the direction along the satellite's position vector, $\bar{r}$ (R)
y_{op}-axis ~ the direction normal to $x_{op} - z_{op}$ plane (T)
z_{op}-axis ~ the direction along the vector $r \times \dot{r}$ (N)

The Cartesian components of the orbit plane system when the satellite is at perifocus are denoted x_p, y_p and z_p (see Figure 5.2-6) or (P,Q,N).
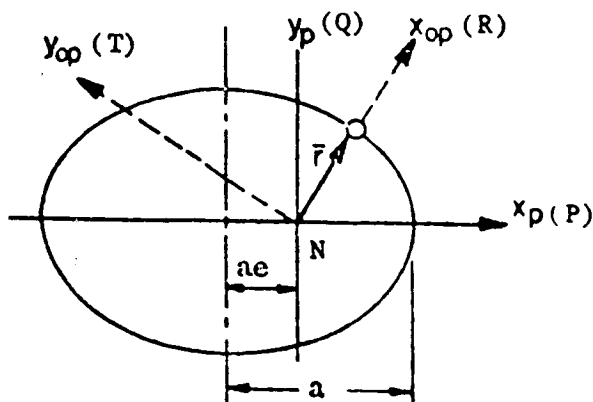
Figure 5.2-6. Orbital Parameters

5.2.6. Keplerian Elements

Origin:	Center of the reference body
Reference Plane:	Equatorial plane perpendicular to the central body's axis of rotation
Principal Direction:	Vernal equinox or prime meridian at a given epoch.

Keplerian Elements (see **Figures** 5.2-5 and 5.2-6):

$a \sim$ the semimajor axis

$e \sim$ the eccentricity specifying the elongation of the orbital conic section

$i \sim$ the inclination specifying the orientation of the satellite's orbital plane to the equator of the central body

$\Omega \sim$ the right ascension of the ascending node, i.e., the angle measured eastward along the equator between the principal direction and the point where the satellite crosses the equator traveling in a northerly direction

$\omega \sim$ the argument of perigee, i.e., angle between the ascending node and the perifocal point measured positive with increasing mean anomaly

$M \sim$ the mean anomaly, i.e., product of the satellite's mean angular motion and the time elapsed since perifocal passage

5.2.7 Vehicle Reference System[*]

Origin: Pre-determined fixed point in vehicle called the reference point origin (RPO)

Reference plane: Plane normal to longitudinal axis containing RPO

Principal direction: Reference direction within body
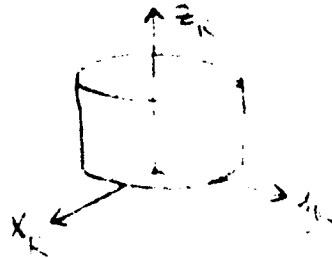
Figure 5.2-7. Vehicle Reference System

Rectangular Cartesian Coordinates (See Figure 5.2-7):

X_R ～ reference direction within body

Y_R ～ direction completing right hand system $(Z_R \times X_R)$

Z_R ～ longitudinal axis fixed in body

[*]This system is used to define tank locations, mounting angles, center-of mass locations, thruster locations, unit thrust vectors, body-fixed sensors, etc. (See Reference 5-3 or 5-4).

5.2.8 Vehicle Attitude System[*]

Origin: Center of gravity of vehicle

Reference Plane: Plane normal to spin axis or longitudinal axis of vehicle

Principal Direction: Projection of reference direction onto reference p plane
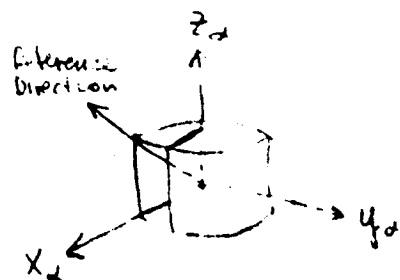
Figure 5.2-8. Vehicle Attitude System

Rectangular Cartesian Coordinates (See Figure 5.2-8):

$$X_\alpha \sim |Y_\alpha \times Z_\alpha|$$

$$Y_\alpha \sim |Z_\alpha \times U_R| \quad \text{where } U_R \text{ is known vector in reference direction}$$

$$Z_\alpha \sim \text{vehicle longitudinal axis}$$

[*]This system has been selected as a compromise between the GTDS format (Reference 5-1) where the Z-axis (third axis) is always the "special" axis and the attitude system of OAMP (Reference 5-3) where the X-axis (first axis) is the vehicle spin axis. The "reference direction" used in OAMP is the Earth-vehicle direction (because the direction so defined is the nadir point -- center of Earth disk -- used for vehicle pitch control). Other "reference directions" considered might include vehicle-to-sun or local north.

5.3 Basic Reference Frames

5.3.1 Introduction

The basic reference frames of GMAS include the following:

1. Inertial equator and equinox of 1950
2. Mean equator and equinox of date
3. Mean ecliptic and equinox of 1950 and of date
4. True equator and equinox of date
5. True equator and prime meridian

This section defines these frames and the transformations required to move from one to another. The fundamental reference frame is the inertial equator and equinox of 1950 to which the other frames are referenced. The other frames are frequently used to describe satellite states.

A coordinate frame is defined by specifying the origin of the coordinates, the reference plane, and the principle direction in the reference plane. A detailed discussion of the background of coordinate transformations is provided in Reference 5-1 or 5-2 from which much of this chapter is excerpted. This chapter will simply summarize the mathematical details of the above transformations.

Some discussion is required to define the relations between the above frames. The equinox, Υ, is defined as the intersection of the planes of the earth's equator and the ecliptic. The equator is defined as being normal to the earth's pole. The primary motion of the equinox is called precession and is due mainly to the precession of the earth's pole. The precessional motion of the mean equinox is due to the combined motions of the two planes, the equator and the ecliptic, that define it.

The motion of the celestial pole or of the equator is due to the gravitational attraction of the sun and moon on the earth's equatorial bulge. It consists of two components: lunisolar precession and nutation. Lunisolar precession is the smooth long-period motion of the equator's pole around the ecliptic pole and has an amplitude of approximately 23.5 degrees and a period of approximately 26,000 years. Nutation is a relatively short-period motion that carries the actual, or the true, pole around the mean pole in a somewhat irregular curve with an aplitude of approximately 9 seconds of arc and a period of approximately 18.6 years.

The word "mean" indicates that nutation is being neglected. The motion of the ecliptic (i.e. the mean plane of the earth's orbit) is due to the planets' gravitational attraction on the earth and consists of a slow rotation of the ecliptic. This motion is known as planetary precession and gives a precession of the equinox of approximately 12 seconds of arc a century and a decrease of the obliquity of the ecliptic, the angle between the ecliptic and the earth's equator, of approximately 47 seconds of arc a century.

5.3.2 Mean Equator and Equinox of Date

The 1950.0 coordinates are transformed into the mean equator and equinox of date by correcting only for precession. Denoting the 1950.0 coordinates by $\bar{R}$ and the mean of date by $\bar{r}_E$ we have

$$\bar{r}_E = A\bar{R} \tag{5.3-1}$$

where the elements of A are

$$a_{11} = -\sin \zeta_0 \sin \xi_p + \cos \zeta_0 \cos \xi_p \cos \theta_p$$

$$a_{12} = -\cos \zeta_0 \sin \xi_p - \sin \zeta_0 \cos \xi_p \cos \theta_p$$

$$a_{13} = -\cos \xi_p \sin \theta_p$$

$$a_{21} = \sin \zeta_0 \cos \xi_p + \cos \zeta_0 \sin \xi_p \cos \theta_p$$

$$a_{22} = \cos \zeta_0 \cos \xi_p - \sin \zeta_0 \sin \xi_p \cos \theta_p \tag{5.3-2}$$

$$a_{23} = -\sin \xi_p \sin \theta_p$$

$$a_{31} = \cos \zeta_0 \sin \theta_p$$

$$a_{32} = -\sin \zeta_0 \sin \theta_p$$

$$a_{33} = \cos \theta_p$$

The angles ζ_0, θ_p, and ξ_p are given by

$$\zeta_0 = 2304.948'' T + 0.302'' T^2 + 0.0179'' T^3$$

$$\xi_p = 2004.255'' T - 0.426'' T^2 - 0.416'' T^3 \tag{5.3-3}$$

$$\theta_p = 2304.948'' T + 1.093'' T^2 - 0.0192'' T^3$$

where

$T =$ the Ephemeris time in Julian centuries (36525 Julian days) elapsed from epoch to 1950.0 (JD 243 3282.5)

$$T = \frac{\text{JD of } t_0 - 2433282.423357}{36525} \tag{5.3-4}$$

The time derivative of A is assumed to be negligble. The velocity coordinates are transformed as follows:

$$\dot{\bar{r}}_E = A\dot{\bar{R}} \tag{5.3-5}$$

5.3-3

5.3.3 Mean Ecliptic and Equinox of Date

Denote the state vector in the mean equator and equinox of date frame by $(r_E, \dot{r}_E)$ and in the mean ecliptic and equinox of date frame by $(r_{EC}, \dot{r}_{EC})$. The sets of vectors are then related by the equations

$$r_{EC} = M\ r_E \qquad\qquad (5.3\text{-}6)$$

$$\dot{r}_{EC} = M\ \dot{r}_E \qquad\qquad (5.3\text{-}7)$$

where the transformation matrix M is given by

$$M = \begin{bmatrix} 1 & 0 & 0 \\ 0 & \cos\bar{\epsilon} & \sin\bar{\epsilon} \\ 0 & -\sin\bar{\epsilon} & \cos\bar{\epsilon} \end{bmatrix} \qquad\qquad (5.3\text{-}8)$$

where the mean obliquity $\bar{\epsilon}$ is given by

$$\bar{\epsilon} = 23.^{\circ}452294 - .^{\circ}130125 \times 10^{-1}\ T_E - .^{\circ}164 \times 10^{-5}$$
$$T_E^2 + .^{\circ}503 \times 10^{-6}\ T_E^3 \qquad\qquad (5.3\text{-}9)$$

and where

$T_E \sim$ the time in Julian centuries (36525 Julian Days) elapsed from epoch to 1900 Jan 0^d 12^h (ET = JD 2415020.0).

5.3.4 True Equator and Equinox of Date

The transformation from the mean equator and equinox of date (5.3.2) to the true of date system involves correcting for the nutation effect. Nutation is measured as cyclic changes in the obliquity, the angle between the equatorial plane and the ecliptic, and the longitude of the equinox. These changes in obliquity, $\delta\epsilon$, and longitude, $\delta\psi$, are assumed known. They are input to GTDS by fitting polynomials through the JPL ephemeris data (Ref. 5.3-3).

Denoting the true of date coordinates by $\underline{r}$, $\underline{\dot{r}}$ and the mean of date by $(\underline{r}_E, \underline{\dot{r}}_E)$ we have

$$\underline{r} = N\underline{r}_E \qquad\qquad (5.3\text{-}10)$$

$$\underline{\dot{r}} = N\underline{\dot{r}}_E$$

where the elemento of N are

$$n_{11} = \cos\delta\psi$$

$$n_{12} = -\sin\delta\psi\cos\tilde\epsilon$$

$$n_{13} = -\sin\delta\psi\sin\tilde\epsilon$$

$$n_{21} = \sin\delta\psi\cos\tilde\epsilon$$

$$(5.3\text{-}11)$$

$$n_{22} = \cos\delta\psi\cos\tilde\epsilon\cos\bar\epsilon + \sin\tilde\epsilon\sin\bar\epsilon$$

$$n_{23} = \cos\delta\psi\cos\tilde\epsilon\sin\bar\epsilon - \sin\tilde\epsilon\cos\bar\epsilon$$

$$n_{31} = \sin\delta\psi\sin\tilde\epsilon$$

$$n_{32} = \cos\delta\psi\sin\tilde\epsilon\cos\bar\epsilon - \cos\tilde\epsilon\sin\bar\epsilon$$

$$n_{33} = \cos\delta\psi\sin\tilde\epsilon\sin\bar\epsilon + \cos\tilde\epsilon\cos\bar\epsilon$$

and where

$\bar\epsilon$ is the mean obliquity given by (5.3-9)

$\tilde\epsilon = \bar\epsilon + \delta\epsilon$ is the true obliquity

$\delta\psi$ is the difference between the longitude of the true and mean equinox of date

with $\delta\epsilon$ and $\delta\psi$ computed as described above.

5.3.5 True Equator and Prime Meridian

The transformation that relates the true of date coordinates to the body-fixed coordinates accounts for two separate effects. The first relates the true vernal equinox to the prime meridian of the rotating planet by means of the angle α_g, variously called the Greenwich sidereal time, the Greenwich hour angle of the true equinox or epoch, or the date right ascention of Greenwich (see Figure 3-9). The second effect, called polar motion, accounts for the fact that the pole of the body-fixed axis, z_b, does not coincide with the body's spin axis, the pole of the true of epoch geocentric axis. The first of these effects transforms the true of date coordinates to pseudo body-fixed coordinates. This pseudo coordinate system would be precisely the body-fixed axes if $z = z_b$, that is, if polar motion is omitted.

5.3.5.1 Psuedo Body-Fixed Transformation

The true of date coordinates transform into the pseudo body-fixed coordinates as follows

$$\bar{r}_{b'} = B_1 \bar{r} \tag{5.3-12}$$

$$B_1(\alpha_g) = \begin{bmatrix} \cos\alpha_g & \sin\alpha_g & 0 \\ -\sin\alpha_g & \cos\alpha_g & 0 \\ 0 & 0 & 1 \end{bmatrix} \tag{5.3-13}$$

where the true Greenwich sidereal time is obtained from the mean Greenwich sidereal time

$$\alpha_{GM} = UT1 + 6^h 38^m 45\overset{s}{.}836 + 8640184\overset{s}{.}542\, T_u + 0\overset{s}{.}0929\, T_u^2 \tag{5.3-14}$$

$UT1 \sim$ seconds of UT1 time (see Section 3.4.5) elapsed from January 1, 1950, 0^h UT1

$T_u \sim$ the number of Julian centries elapsed from 12 hours UT1 January 0, 1900 (JD = 2415020.0) to the UT1 time of Epoch.

by applying the correction $\quad \alpha_g = \alpha_{GM} + \Delta H \tag{5.3-15}$

where

$$\Delta H = \delta\psi \cos(\bar{\epsilon} + \delta\epsilon) \tag{5.3-16}$$

Differentiation yields the velocity transformation

$$\dot{\bar{r}}_{b'} = B_1 \dot{\bar{r}} + \dot{B}_1 \bar{r} \tag{5.3-17}$$

where ($\dot{\alpha}_g =$ constant)

$$\dot{B}_1 = \begin{bmatrix} -\sin\alpha_g & \cos\alpha_g & 0 \\ -\cos\alpha_g & -\sin\alpha_g & 0 \\ 0 & 0 & 0 \end{bmatrix} \dot{\alpha}_g \tag{5.3-18}$$

5.3.5.2 Body-Fixed Transformation

The principal axis of the earth (angular momentum vector) is not coincident with the spin axis (angular velocity vector), and it moves with respect to the latter causing the polar motion effect. The path of the pole on the earth's surface is "semi-regular" but unpredictable due to random shifts in the earth's crust, etc. The motion of the pole is given with respect to the pole at some established epoch. The pole at the established epoch is referred to as the adopted pole (P_A), and the present position of the pole is referred to as the true pole (P_T). There are several adopted poles in the literature. Due to small size of the polar motion correction (it takes place in a square less than 50 meters wide), the polar region of the earth may be considered a plane and the transformation from one adopted pole to another reduces to a simple plane translation. Neglecting the earth's slight curvature at the pole, establish a left-handed rectangular coordinate system centered at P_A with x_b axis directed along the Greenwich merician and the y_b axis along the meridian of 90^0 west. (See Figure 3-10). The coordinates of the instantaneous pole P_T are measured in terms of x_p and y_p components using units of seconds of arc. The measurements of x_p and y_p are performed by the International Polar Motion Service and published by the U.S. Naval Observatory.

$$\bar{r}_b = B_2 \, \bar{r}_b' \qquad (5.3\text{-}19)$$

Since x_p and y_p are small, all cosine terms are equated to unity, all sine terms equated to their angle, and all products neglected. Thus B_2 becomes

$$B_2 = \begin{bmatrix} 1 & 0 & x_p \\ 0 & 1 & -y_p \\ -x_p & y_p & 1 \end{bmatrix} \qquad (5.3\text{-}20)$$

5.3.5.3 True of Date to Body-Fixed

The complete transformation between the true of epoch coordinate system and the body-fixed system is given by

$$\bar{r}_b = B_2 \, (x_p, y_p) \, B_1 \, (\alpha_g) \, \bar{r} \qquad (5.3\text{-}21)$$

where B_1 is presented in Equation (5.3-13) and B_2 in (5.3-20).

The time derivative of B_2 is negligibel, therefore the velocity is transformed as follows:

$$\dot{\bar{r}}_b = B_2 B_1 \, \dot{\bar{r}} + B_2 \dot{B}_1 \, \bar{r} \qquad (5.3\text{-}22)$$

where $\dot{B}_1$ is given by Equation (5.3-19).

5.3.5.4 Mean of 1950 to Body-Fixed

The total transformation from mean equinox and equator of 1950.0 coordinates to body-fixed coordinates is the product of the transformations in Equations (5-1), (5-10), (5-17), and (5-19)

$$\bar{r}_b = B_2 (x_p, y_p) \cdot B_1 (\alpha_g) \cdot N(\delta\epsilon, \delta\psi) \cdot A(\zeta_o, \theta_p, \xi_p) \, \bar{R}. \tag{5.3-23}$$

Hereafter this transformation is written

$$\bar{r}_b = H \cdot G \, \bar{R} \tag{5.3-24}$$

where

$$H = B_2 (x_p, y_p) \, B_1 (\alpha_g) \tag{5.3-25}$$

$$G = N (\delta\epsilon, \delta\psi) \, A (\zeta_o, \theta_p, \xi_p). \tag{5.3-26}$$

The matrices G and H depend only on time (not on satellite position). The matrices N, A, and B_1 vary so slowly with time that their rate of change can be neglected in velocity transformations. The matrix B_1 changes in proportion to the earth's spin rate; thus its time rate of change, given in Equation (5.3-19), must be accounted for. In GTDS the G matrix is synthesized during preprocessing computations using information from an ephemeris tape. Its elements are stroed as polynomial functions of time for use during problem execution. The H matrix is optionally computed either precisely as shown in Equation (5.3-20), or approximately by neglecting polar motion (e.g., $B_2 = 1$).

5.4 Utility Coordinate Systems

5.4.1 Introduction

Utility coordinate systems are those systems that are used internally in GMAS for the convenient computation of certain parameters. These systems are discussed in the order of the illustrated descriptions of Section 5.2. The transformations addressed are as follows:

1. Spherical-Cartesian
2. Geocentric-Orbit Plane
3. Earth-Fixed Geodetic
4. Earth-Fixed to Topocentric
5. Keplerian-Cartesian
6. Inertial-Vehicle Axes

Both the transformations and the Jacobians of the transformations are provided.

5.4.2 Spherical-Cartesian Transformations

5.4.2.1 Spherical to Cartesian

Using the spherical position coordinates, r, α, and δ, that are defined in Section 5.2-1, the transformation to Cartesian coordinates is seen from Figure 5.2-1 to be

$$\begin{bmatrix} x \\ y \\ z \end{bmatrix} = r \begin{bmatrix} \cos \delta \cos \alpha \\ \cos \delta \sin \alpha \\ \sin \delta \end{bmatrix}. \tag{5.4-1}$$

To transform the spherical velocity coordinates, V, γ, and A, described in Section 3.2.3, it is convenient to transform to the local plane coordinate system (see Figure 3-3) and then to the body-centered inertial Cartesian coordinate system. If the local plane coordinates, x_{lp}, y_{lp}, and z_{lp}, are fixed inertially (nonrotating), $\dot{r}_{lp}$ may be expressed as

$$\dot{\bar{r}}_{lp} = \begin{bmatrix} \dot{x}_{lp} \\ \dot{y}_{lp} \\ \dot{z}_{lp} \end{bmatrix} = V \begin{bmatrix} \cos \gamma \\ \sin A \sin \gamma \\ \cos A \sin \gamma \end{bmatrix}. \tag{5.4-2}$$

The transformation between the local plane and the body-centered inertial Cartesian coordinate systems is

$$\bar{r}_{lp} = C \, \bar{r} \tag{5.4-3}$$

where

$$C = \begin{bmatrix} \cos \delta \cos \alpha & \cos \delta \sin \alpha & \sin \delta \\ -\sin \alpha & \cos \alpha & 0 \\ -\sin \delta \cos \alpha & -\sin \delta \sin \alpha & \cos \delta \end{bmatrix}. \tag{5.4-4}$$

Since the local plane system is fixed inertiall the velocity vector in Equation (5.4-2) may be transformed to the body-centered inertial Cartesian axes by means of the transformation C as follows

$$\dot{\bar{r}} = C^{T} \, \dot{\bar{r}}_{lp}. \tag{5.4-5}$$

5.4.2.2 Spherical to Cartesian Partials

The partial derivatives of x, y, z, $\dot{x}$, $\dot{y}$, and $\dot{z}$ with respect to r, α, δ, V, A, and β are

$$\frac{\partial \bar{r}}{\partial r} = \frac{\bar{r}}{r} \tag{5.4-6}$$

$$\frac{\partial \bar{r}}{\partial \alpha} = \begin{bmatrix} -y \\ x \\ 0 \end{bmatrix} \tag{5.4-7}$$

$$\frac{\partial \bar{r}}{\partial \delta} = -r \begin{bmatrix} \sin \delta \cos \alpha \\ \sin \delta \sin \alpha \\ -\cos \delta \end{bmatrix} = \begin{bmatrix} -z \cos \alpha \\ -z \sin \alpha \\ \sqrt{x^2 + y^2} \end{bmatrix} \tag{5.4-8}$$

$$\frac{\partial \bar{r}}{\partial V} = \frac{\partial \bar{r}}{\partial A} = \frac{\partial \bar{r}}{\partial \beta} = \frac{\partial \dot{\bar{r}}}{\partial r} = 0 \tag{5.4-9}$$

$$\frac{\partial \dot{\bar{r}}}{\partial \alpha} = \begin{bmatrix} -\dot{y} \\ \dot{x} \\ 0 \end{bmatrix} \tag{5.4-10}$$

$$\frac{\partial \dot{\bar{r}}}{\partial \alpha} = \begin{bmatrix} -\dot{z} \cos \alpha \\ -\dot{z} \sin \alpha \\ V(\cos \beta \cos \delta - \cos A \sin \beta \sin \delta) \end{bmatrix} \tag{5.4-11}$$

$$\frac{\partial \dot{\bar{r}}}{\partial V} = \frac{\dot{\bar{r}}}{V} \tag{5.4-12}$$

$$\frac{\partial \dot{\bar{r}}}{\partial A} = V \begin{bmatrix} \sin \beta (\sin A \sin \delta \cos \alpha - \cos A \sin \alpha) \\ \sin \beta (\sin A \sin \delta \sin \alpha + \cos A \cos \alpha) \\ \sin A \cos \beta \cos \delta \end{bmatrix} \tag{5.4-13}$$

and

$$\frac{\partial \dot{\bar{r}}}{\partial \beta} = -V \begin{bmatrix} \cos \alpha (\cos \delta \sin \beta + \sin \delta \cos \beta \cos A) + \sin \alpha \cos \beta \sin A \\ \sin \alpha (\cos \delta \sin \beta + \sin \delta \cos \beta \cos A) - \cos \alpha \cos \beta \sin A \\ \sin \beta \sin \delta - \cos \delta \cos \beta \cos A \end{bmatrix} \tag{5.4-14}$$

5.4.2.3 Cartesian to Spherical

The inverse of the preceding transformations is described in the following text. The spherical radius, r, is given by

$$r = \sqrt{x^2 + y^2 + z^2}. \qquad (5.4\text{-}15)$$

From Figure 3-1 the right ascension, α, and declination, δ, of $\bar{r}$ are

$$\sin \delta = \frac{z}{r} \qquad \cos \delta = \frac{\sqrt{x^2 + y^2}}{r} \qquad -\frac{\pi}{2} \leq \delta \leq \frac{\pi}{2} \qquad (5.4\text{-}16)$$

and

$$\sin \alpha = \frac{y}{\sqrt{x^2 + y^2}} \qquad \cos \alpha = \frac{x}{\sqrt{x^2 + y^2}} \qquad 0 \leq \alpha \leq 2\pi. \qquad (5.4\text{-}17)$$

The right ascension is measured positive east from the inertial x-axis. The declination is measured positive north from the x-y plane.

The velocity vector's magnitude is

$$V = \sqrt{\dot{x}^2 + \dot{y}^2 + \dot{z}^2} \qquad (5.4\text{-}18)$$

and the azimuth, A, and flight path angle, β, are obtained from

$$\sin A = \frac{(x\dot{y} - y\dot{x})}{rV}, \quad \cos A = \frac{y(y\dot{z} - z\dot{y}) - x(x\dot{z} - \dot{x}z)}{r^2 V}. \qquad 0 \leq A \leq 2\pi. \qquad (5.4\text{-}19)$$

$$\sin \beta = \frac{|\bar{r} \times \dot{\bar{r}}|}{rV} \qquad \cos \beta = \frac{\bar{r} \cdot \dot{\bar{r}}}{rV} \qquad -\frac{\pi}{2} \leq \beta - \frac{\pi}{2} \qquad (5.4\text{-}20)$$

5.4.2.4 Cartesian to Spherical Partials

The partial derivatives of r, α, δ, V, Λ, and β with respect to x, y, z, $\dot{x}$, $\dot{y}$, and $\dot{z}$ are

$$\frac{\partial r}{\partial \bar{r}} = \frac{\bar{r}^T}{r} \tag{5.4-21}$$

$$\frac{\partial \alpha}{\partial \bar{r}} = \frac{1}{(x^2 + y^2)} \begin{bmatrix} -y \\ x \\ 0 \end{bmatrix}^T \tag{5.4-22}$$

$$\frac{\partial \delta}{\partial \bar{r}} = \frac{1}{r^2 \sqrt{x^2 + y^2}} \begin{bmatrix} -zx \\ -zy \\ (x^2 + y^2) \end{bmatrix}^T \tag{5.4-23}$$

$$\frac{\partial V}{\partial \bar{r}} = 0 \tag{5.4-24}$$

$$\frac{\partial \Lambda}{\partial \bar{r}} = \frac{1}{(V^2 - \dot{r}^2)(x^2 + y^2)} \begin{bmatrix} \dot{y}(r\dot{z} - z\dot{r}) - (x\dot{y} - y\dot{x})\left(x\dot{z} - z\dot{x} + \frac{xz\dot{r}}{r}\right)/r \\ -\dot{x}(r\dot{z} - z\dot{r}) + (x\dot{y} - y\dot{x})\left(y\dot{z} - z\dot{y} + \frac{yz\dot{r}}{r}\right)/r \\ (x\dot{y} - y\dot{x})(x^2 + y^2)\dot{r}/r^2 \end{bmatrix}^T \tag{5.4-25}$$

$$\frac{\partial \beta}{\partial \bar{r}} = \frac{1}{r^2 \sqrt{V^2 - \dot{r}^2}} \left(\frac{\bar{r}^T \dot{r}}{r} - \dot{\bar{r}}^T \right) \tag{5.4-26}$$

$$\frac{\partial r}{\partial \dot{\bar{r}}} = \frac{\partial \alpha}{\partial \dot{\bar{r}}} = \frac{\partial \delta}{\partial \dot{\bar{r}}} = 0 \tag{5.4-27}$$

$$\frac{\partial V}{\partial \dot{\bar{r}}} = \frac{\dot{\bar{r}}^T}{V} \tag{5.4-28}$$

$$\frac{\partial \Lambda}{\partial \dot{\bar{r}}} = \frac{1}{r(V^2 - \dot{r}^2)} \begin{bmatrix} (z\dot{y} - y\dot{z}) \\ (x\dot{z} - z\dot{x}) \\ (y\dot{x} - x\dot{y}) \end{bmatrix}^T \tag{5.4-29}$$

and

$$\frac{\partial \beta}{\partial \dot{\bar{r}}} = \frac{1}{r^2 \sqrt{V^2 - \dot{r}^2}} \left(\dot{r} \frac{\dot{\bar{r}}^T \bar{r}}{V^2} - \bar{r} \right)^T . \tag{5.4-30}$$

5.4.3 Geocentric to Orbit Plane

The unit vectors in the x_{op}, y_{op}, and z_{op} directions (see **Figure 5.2-5**) that are measured in the body-centered inertial Cartesian system are

$$\bar{U} = \frac{\bar{r}_o}{|\bar{r}_o|}$$

$$\bar{V} = \bar{W} \times \bar{U} \qquad\qquad (5.4\text{-}31)$$

$$\bar{W} = \frac{\bar{r}_o \times \dot{\bar{r}}_o}{|\bar{r}_o \times \dot{\bar{r}}_o|}$$

where $\bar{r}_o$ and $\dot{r}_o$ are the earth-centered position and velocity vectors used to determine the orbit plane coordinate system. If Equations (5.4-31) are expanded, they yield the following transformation relations between the orbit plane coordinates and the body-centered inertial Cartesian coordinates

$$\bar{r}_{op} = E\,\bar{r} \qquad\qquad (5.4\text{-}32)$$

where

$$E = \begin{bmatrix} U_x & U_y & U_z \\ V_x & V_y & V_z \\ W_x & W_y & W_z \end{bmatrix}. \qquad\qquad (5.4\text{-}33)$$

Regarding the orbit plane system as fixed inertially, the velocity transforms as follows

$$\dot{\bar{r}}_{op} = E\,\dot{\bar{r}} \qquad\qquad (5.4\text{-}34)$$

and the position and velocity partials are

$$\frac{\partial \bar{r}_{op}}{\partial \bar{r}} = \frac{\partial \dot{\bar{r}}_{op}}{\partial \dot{\bar{r}}} = E. \qquad\qquad (5.4\text{-}35)$$

5.4.4 Earth-Fixed Geodetic Transformations

The transformations between the body-centered inertial Cartesian system and the geodetic axes system (described in Section 5.2.2) involves modeling the earth's figure.

5.4.4.1 Geodetic to Earth-Fixed

Suppose (h, λ, ϕ) given. Then compute $N = \dfrac{R_e}{\sqrt{1 - e^2 \sin^2\phi}}$

where R_e is the equatorial radius of the earth and e is the eccentricity of the earth figure with $e^2 = 1 - \left(\dfrac{R_p}{R_e}\right)^2 = f(2 \cdot f)$ where R_p is the polar radius and f is the flattening of the earth.

$$
\begin{bmatrix} x_b \\ y_b \\ z_b \end{bmatrix} = \begin{bmatrix} (N + h)\cos\phi\cos\lambda \\ (N + h)\cos\phi\sin\lambda \\ (N + h - e^2 N)\sin\phi \end{bmatrix}
\tag{5.4-36}
$$

The partial derivatives of x_b, y_b, and z_b with respect to h, λ, and ϕ are

$$
\begin{bmatrix} \partial x_b/\partial h \\ \partial y_b/\partial h \\ \partial z_b/\partial h \end{bmatrix} = \begin{bmatrix} \cos\phi\cos\lambda \\ \cos\phi\sin\lambda \\ \sin\phi \end{bmatrix}
\tag{5.4-37}
$$

$$
\begin{bmatrix} \partial x_b/\partial\lambda \\ \partial y_b/\partial\lambda \\ \partial z_b/\partial\lambda \end{bmatrix} = \begin{bmatrix} -(N + h)\cos\phi\sin\lambda \\ (N + h)\cos\phi\cos\lambda \\ 0 \end{bmatrix}
\tag{5.4-38}
$$

$$
\begin{bmatrix} \partial x_b/\partial\phi \\ \partial y_b/\partial\phi \end{bmatrix} \left(N + h - \frac{N e^2 \cos^2\phi}{1 - e^2 \sin^2\phi}\right) \begin{bmatrix} -\sin\phi\cos\lambda \\ -\sin\phi\sin\lambda \end{bmatrix}
\tag{5.4-39}
$$

and

$$
[\partial z_b/\partial\phi] = \left(h + N(1 - e^2)\left(1 + \frac{e^2 \sin^2\phi}{1 - e^2 \sin^2\phi}\right)\right)\cos\phi
\tag{5.4-40}
$$

5.4.4.2 Earth-Fixed to Geodetic

In transforming geodetic coordinates to earth-fixed coordinates, the point of intersection of the height normal vector and the ellipsoid is given. In transforming from earth-fixed to geodetic, this point is not known a priori. This complicates the transformation. Since there is no set of equations in closed form giving this transformation.

Two solutions are presented. The first solution is iterative and can yield any required degree of accuracy. The second solution is a truncated binomial expansion that may be used when accuracy requirements are not so stringent.

The iterative technique is used primarily to determine geodetic tracking station positions where high accuracy is required. For this use (and for near earth satellites), the approximation $h \ll N$ is satisfied, and since the earth's figure is nearly spherical, $e^2 \ll 1$.

Introducing t, the z_b intercept of the normal vector, it can be shown that

$$t = e^2 z_b.$$ (5.4-41)

Using Equation (5.4-41) as an initial estimate for t, the following sequence of equations may be solved iteratively to yield a solution for h and ϕ.

$$z_t = z_b + t$$ (5.4-42)

$$N + h = \sqrt{x_b^2 + y_b^2 + z_t^2}$$ (5.4-43)

$$\sin \phi = \frac{z_t}{N + h}$$ (5.4-44)

$$N = \frac{R_c}{\sqrt{1 - e^2 \sin^2 \phi}}$$ (5.4-45)

$$t = N e^2 \sin \phi.$$ (5.4-46)

Upon convergence of t, ϕ and h are obtained from Equations (5.4-43) and (5.4-44). The longitude λ, is

$$\lambda = \tan^{-1} \left(\frac{y_b}{x_b} \right).$$ (5.4-47)

A second, computationally simpler, procedure for computing the values of ϕ and h to a specified point, P, is useful when accuracy requirements are less stringent. The latitude, ϕ, is

$$\tan \phi = \frac{z_b}{(1 - e^2) x_b} = \frac{z_b}{(1 - e^2) \sqrt{x_b^2 + y_b^2}}$$

The geocentric latitude is approximated by

$$\phi' = \sin^{-1}\left(\frac{z_b}{r_b}\right). \tag{5.4-48}$$

The (spheroid) light is

$$h = r_b - r_s. \tag{5.4-49}$$

where

$$r_s = \frac{R_e (1 - f)}{\sqrt{1 - (2 f - f^2) \cos^2 \phi'}} \tag{5.4-50}$$

The partial derivatives of h, ϕ, and λ with respect to x_b, y_b, and z_b are obtained

$$\begin{bmatrix} \partial h / \partial x_b \\ \partial h / \partial y_b \\ \partial h / \partial z_b \end{bmatrix} = -\left(\frac{e^2 a (1 - e^2) \sin \phi \cos \phi}{(1 - e^2 \sin^2 \phi)^{3/2}} + \frac{z_b \cos \phi}{\sin^2 \phi}\right) \begin{bmatrix} \partial \phi / \partial x_b \\ \partial \phi / \partial y_b \\ \partial \phi / \partial z_b \end{bmatrix} \tag{5.4-51}$$

$$\begin{bmatrix} \partial \lambda / \partial x_b \\ \partial \lambda / \partial y_b \\ \partial \lambda / \partial z_b \end{bmatrix} = \frac{1}{(x_b^2 + y_b^2)} \begin{bmatrix} -y_b \\ x_b \\ 0 \end{bmatrix} \tag{5.4-52}$$

and

$$\begin{bmatrix} \partial \phi / \partial x_b \\ \partial \phi / \partial y_b \\ \partial \phi / \partial z_b \end{bmatrix} = \frac{(1 - e^2)}{\sqrt{x_b^2 + y_b^2} \left[(1 - e^2)^2 (x_b^2 + y_b^2) + z_b^2\right]} \begin{bmatrix} -x_b z_b \\ -y_b z_b \\ (x_b^2 + y_b^2) \end{bmatrix}. \tag{5.4-53}$$

5.4.5 Earth-Fixed to Topocentric Local Tangent (East, North, Up)

The topocentric local tangent system, described in Section 3.2.3, is used in processing ground based observation data. The transformation from geocentric earth-fixed coordinates (x_b, y_b, z_b) to local tangent coordinates (x_{1t}, y_{1t}, z_{1t}) requires a translation along the geocentric radius vector to the station and a rotation of the axis through the station's longitude and latitude angles. The earth's shape and station identification parameters are defined as follows

$\bar{r}_s$ — the body-fixed coordinates of the station

ℓ_s — the geodetic latitude of the station (positive north)

ϕ_s' — the geocentric latitude of the station

λ_s — the longitude of the station (positive east)

h_s — the height of the station above the reference ellipsoid.

The local tangent coordinates of a point in space, x_b, y_b, and z_b, may be written as

$$\bar{r}_{1t} = M_{1t} (\bar{r}_b - \bar{r}_s). \qquad (5.4\text{-}54)$$

$$\dot{\bar{r}}_{1t} = M_{1t}\, \dot{\bar{r}}_b \qquad (5.4\text{-}55)$$

$$\begin{bmatrix} x_s \\ y_s \\ z_s \end{bmatrix} = \begin{bmatrix} (N_s + h_s)\cos \phi_s \cos \lambda_s \\ (N_s + h_s)\cos \phi_s \sin \lambda_s \\ (N_s + h_s - e^2 N_s)\sin \phi_s \end{bmatrix} \qquad (5.4\text{-}56)$$

$$N_s = \frac{R_e}{\sqrt{1 - (2f - f^2)\sin^2 \phi_s}}. \qquad (5.4\text{-}57)$$

$$M_{1t} = \begin{bmatrix} -\sin\lambda & \cos\lambda & 0 \\ -\sin\phi\cos\lambda & -\sin\phi\sin\lambda & \cos\phi \\ \cos\phi\cos\lambda & \cos\phi\sin\lambda & \sin\phi \end{bmatrix}. \qquad (5.4\text{-}58)$$

Since the local tangent system, determined only by the station parameters, is not a function of the coordinates of a given earth-fixed point, the partials of its components with respect to the earth-fixed components are the respective elements of the M_{1t} matrix given by

$$\frac{\partial \bar{r}_{1t}}{\partial \bar{r}_b} = \frac{\partial \dot{\bar{r}}_{1t}}{\partial \dot{\bar{r}}_b} = M_{1t}. \qquad (5.4\text{-}59)$$

5.4.6 Keplerian-Cartesian Transformations

5.4.6.1 Keplerian to Cartesian Coordinates

First consider the transformation from the orbital elements $(a, e, i, \Omega, \omega, M)$ to the orbital rectangular coordinate $(x_p, y_p, z_p, \dot{x}_p, \dot{y}_p, \dot{z}_p)$. The x_p axis is directed toward perigee, the y_p axis is in the plane of motion advanced $\pi/2$ from the x_p-axis in the direction of motion, and the z_p axis completes a right-handed system.

$$\begin{bmatrix} x_p \\ y_p \\ z_p \end{bmatrix} = a \begin{bmatrix} \cos E - e \\ \sqrt{1 - e^2}\, \sin E \\ 0 \end{bmatrix} \qquad (5.4\text{-}60)$$

and

$$\begin{bmatrix} \dot{x}_p \\ \dot{y}_p \\ \dot{z}_p \end{bmatrix} = \frac{\sqrt{\mu/a}}{(1 - e \cos E)} \begin{bmatrix} \sin E \\ \sqrt{1 - e^2}\, \cos E \\ 0 \end{bmatrix} \qquad (5.4\text{-}61)$$

where the eccentric anomaly E is computed from Kepler's equation $(M = E - e \sin E)$ by the following iteration scheme.

$$
\begin{aligned}
F_{ct}(E_n) &= E_n - e \sin E_n - M \\
D_n &= 1 - e \cos E_n - .5\, F_{ct}(E_n) \\
E_{n+1} &= E_n - D_n^{-1} F_{ct}(E_n) \qquad n = 0, 1, 2, \ldots \\
E_0 &= M - e \sin M
\end{aligned}
\qquad (5.4\text{-}62)
$$

The orbital rectangular coordinates are transformed to inertial Cartesian position and velocity coordinates as follows

$$\begin{bmatrix} x \\ y \\ z \end{bmatrix} = P \begin{bmatrix} x_p \\ y_p \end{bmatrix} \qquad\qquad \begin{bmatrix} \dot{x} \\ \dot{y} \\ \dot{z} \end{bmatrix} = P \begin{bmatrix} \dot{x}_p \\ \dot{y}_p \end{bmatrix} . \qquad (5.4\text{-}63)$$

The elements, P_{ij}, of the 3×2 rotation matrix, P, are

$$P_{11} = \cos \Omega \cos \omega - \sin \Omega \cos i \sin \omega$$

$$P_{12} = -\cos \Omega \sin \omega - \sin \Omega \cos i \cos \omega$$

$$P_{21} = \sin \Omega \cos \omega + \cos \Omega \cos i \sin \omega$$

$$P_{22} = -\sin \Omega \sin \omega + \cos \Omega \cos i \cos \omega \qquad (5.4\text{-}64)$$

$$P_{31} = \sin i \sin \omega$$

$$P_{32} = \sin i \cos \omega .$$

5.4.6.2 Keplerian to Cartesian Partials

Referring to equations (5.4-63a and 63b) of the previous section, the partials of the transformation may be written

$$\frac{\partial \overline{r}}{\partial(a,e,M)} = P \frac{\partial \overline{r}_p}{\partial(a,e,M)} \quad , \quad \frac{\partial \dot{\overline{r}}}{\partial(a,e,M)} = P \frac{\partial \dot{\overline{r}}_p}{\partial(a,e,M)} \tag{5.4-65}$$

$$\frac{\partial \overline{r}}{\partial(\Omega,\omega,i)} = \frac{\partial P}{\partial(\Omega,\omega,i)} \overline{r}_p, \quad \frac{\partial \dot{\overline{r}}}{\partial(\Omega,\omega,i)} = \frac{\partial P}{\partial(\Omega,\omega,i)} \overline{r}_p$$

where, if n denotes the mean motion $(n = \sqrt{\mu/a^3})$,

$$\frac{\partial \overline{r}_p}{\partial(a,e,i)} = \begin{bmatrix} \dfrac{x_p}{a} & \left(-a-\dfrac{y_p^2}{r(1-e^2)}\right) & \left(-\dfrac{a y_p}{r\sqrt{1-e^2}}\right) \\[3mm] \dfrac{y_p}{a} & \left(\dfrac{x_p y_p}{r(1-e^2)}\right) & \left(\dfrac{a\sqrt{1-e^2}(x_p+ae)}{r}\right) \\[3mm] 0 & 0 & 0 \end{bmatrix} \tag{5.4-66}$$

$$\frac{\partial \dot{\overline{r}}_p}{\partial(a,e,i)} = \begin{bmatrix} \dot{x}_p & \dot{x}_p\left(\dfrac{a}{r}\right)^2\left(\dots\right) & -n\left(\dfrac{a}{r}\right)^3 x_p \\[3mm] -\dfrac{\dot{y}_p}{2a} & \dfrac{n}{\sqrt{1-e^2}}\left(\dfrac{a}{r}\right)^2\left(\dfrac{x_p^2}{r}-\dfrac{y_p^2}{a(1-e^2)}\right) & -n\left(\dfrac{a}{r}\right)^3 y_p \\[3mm] 0 & 0 & 0 \end{bmatrix} \tag{5.4-67}$$

$$\frac{\partial P}{\partial \Omega} = \begin{bmatrix} (-\sin\Omega\cos\omega-\cos\Omega\cos i\sin\omega) & (-\sin\Omega\sin\omega-\cos\Omega\cos i\cos\omega) \\[2mm] (\cos\Omega\cos\omega-\sin\Omega\cos i\sin\omega) & (-\cos\Omega\sin\omega-\sin\Omega\cos i\cos\omega) \\[2mm] 0 & 0 \end{bmatrix} \tag{5.4-68}$$

$$\frac{\partial P}{\partial \omega} = \begin{bmatrix} (-\cos\Omega\sin\omega-\sin\Omega\cos i\cos\omega) & (-\cos\Omega\cos\omega+\sin\Omega\cos i\sin\omega) \\[2mm] (-\sin\Omega\sin\omega+\cos\Omega\cos i\cos\omega) & (-\sin\Omega\cos\omega-\cos\Omega\cos i\sin\omega) \\[2mm] (\sin i\cos\omega) & (-\sin i\sin\omega) \end{bmatrix} \tag{5.4-69}$$

$$\frac{\partial P}{\partial i} = \begin{bmatrix} \sin\Omega\sin i\sin\omega & \sin\Omega\sin i\cos\omega \\[2mm] -\cos\Omega\sin i\sin\omega & -\cos\Omega\sin i\cos\omega \\[2mm] \cos i\sin\omega & \cos i\cos\omega \end{bmatrix} . \tag{5.4-70}$$

5.4.6.3 Cartesian to Keplerian Transformation and Partials

Transformation

Radius	$r = \lvert \underline{r} \rvert$	(5.4-71)
Speed	$V = \lvert \underline{\dot{r}} \rvert$	(5.4-72)
Angular Momentum Vector	$\underline{h} = \underline{r} \times \underline{\dot{r}} = (h_x, h_y, h_z)$	(5.4-73)
Angular Momentum Magnitude	$h = \lvert h \rvert$	(5.4-74)
Semimajor Axis	$a = \mu r (2\mu - rV^2)^{-1}$	(5.4-75)
Similatus Rectum	$p = \mu^{-1}\left[(rV)^2 - (\underline{r} \cdot \underline{\dot{r}})^2 \right]$	(5.4-76)
Eccentricity	$e = (1 - p/a)^{\frac{1}{2}}$	(5.4-77)
Inclination	$\sin i = (h_x^2 + h_y^2)/(rV)$	(5.4-78)
	$\cos i = h_z/(rV)$	(5.4-79)
Eccentric Anomaly	$\sin E = e^{-1}(\underline{r} \cdot \underline{\dot{r}}/\sqrt{\mu a})$	(5.4-80)
	$\cos E = e^{-1}(1 - r/a)$	(5.4-81)
Mean Anomaly	$M = E - e \sin E$	(5.4-82)
Period	$P = 2\pi (a^3/\mu)^{\frac{1}{2}}$	(5.4-83)
Energy (per unit mass)	$\text{Energy} = -\mu/2a$	(5.4-84)
Longitude of Ascending Node	$\sin\Omega = h_y/h \qquad \cos\Omega = h_x/h$	(5.4-85)
True Anomaly	$\sin f = \sqrt{\mu p}\, \underline{r} \cdot \underline{\dot{r}}/(\mu re),$	(5.4-86)
	$\cos f = \mu(p - r)/\mu re$	(5.4-87)
Argument of Perfocus	$\sin(\omega + f) = \dfrac{\sqrt{\mu p}\, r_z}{hr},$	(5.4-88)
	$\cos(\omega + f) = \dfrac{r_y h_z - r_x h_y}{hr}$	(5.4-89)
Periapsis Radius	$r_p = a(1 - e)$	(5.4-90)
Apoapsis Radius	$r_a = a(1 + e)$	(5.4-91)

Partials: The Jacobian of the transformation is given by

$$
J = \begin{bmatrix} \dfrac{\alpha_X}{\alpha_a} & \cdots & \dfrac{\alpha_X}{\alpha_M} \\ \vdots & & \vdots \\ \dfrac{\alpha_Z}{\alpha_a} & & \dfrac{\alpha_Z}{\alpha_M} \end{bmatrix}^{-1} \tag{5.4-92}
$$

5.4-13

5.5 Vehicle Orientation Systems

5.5.1 Introduction

A critical part of mission analysis has to do with the attitude of the spacecraft. GMAS will permit the simulation of the nominal attitude during cruise segments by any of three reference systems: inertial, local vertical, and orbit plane. The attitude behavior to get into or from the required maneuver attitude may be modeled by any of three sets of attitude reference systems: inertial Euler angles, relative Euler angles, and body rates. No six-degree-of-freedom analysis will be made by GMAS. The prime transformation of attitude-related studies is defined by the $[IB]$ matrix which defines the conversion from the inertial system to the vehicle orientation frame. This section addresses the computation of the $[IB]$ matrix during cruise (non-maneuver) segments of the mission. The modeling of attitude behavior during maneuvers is discussed in Section 9.3.

5.5.2 Inertial to Cruise Attitude

The computation of the $[IB]$ matrix defining the transformation from the inertial coordinate system to the vehicle cruise orientation coordinate system will always be accomplished in two steps where the first rotation defines the transformation from inertial coordinates to the frame having the proper z_α-orientation and the second rotation "rolls" about that z_α-axis to align the x_α-axis as close as possible to the reference direction (See Figure 5-9).

Thus

$$[IB] = [IB_2] [IB_1] \qquad (5.5\text{-}1)$$

where $[IB]$ is defined by

$$\underline{r}_\alpha = [IB] \underline{R} \qquad (5.5\text{-}2)$$

where $\underline{R}$ is the position vector in the inertial frame and $\underline{r}_\alpha$ is the corresponding vector in the vehicle orientation frame.

5.5.2.1 Primary Axis and First Rotation

The first rotation transforms the inertial z-axis into direction of vehicle primary axis (spin-axis if applicable). This transformation is defined by the $\left[IB_1 \right]$ matrix defined by the different primary axis references as follows.

Inertial Reference

Under this option the user specifies the primary axis inertial right ascension α_p and declination δ_p. The primary axis is then held constant in this attitude throughout the desired trajectory segment. The IB_1 matrix is computed once per trajectory segment.

Local Vertical Reference

Under this option the primary axis is always directed along the local radius vector. Thus the inertial right ascension α_p and δ_p are determined at each computational event from the inertial position of the vehicle $\underline{R}$ as follows:

$$\underline{U} = \underline{R}/R = (U_x, U_y, U_z) \tag{5.5-3}$$

$$\sin\delta = U_z \qquad \cos\delta = + \sqrt{1 - U_z^2} \qquad 0 \leq \delta \leq 180 \tag{5.5-4}$$

$$\sin\alpha = U_y/\cos\alpha \quad \cos\alpha = U_x/\cos\alpha \qquad 0 \leq \alpha \leq 360 \tag{5.5-5}$$

Normal to Orbit Plane

Under this option the primary axis is always directed normal to the orbit plane. The inertial right ascension α_p and declination δ_p are computed from (5.5-4) and (5.5-5) after computing

$$\underline{U} = (\underline{R} \times \underline{V})/|\underline{R} \times \underline{V}| \tag{5.5-6}$$

After computing the inertial right ascension and declination the first rotation matrix is determined from

$$\left[IB_1 \right] = \begin{bmatrix} \cos\alpha \sin\delta & \sin\alpha \sin\delta & -\cos\delta \\ -\sin\alpha & \cos\alpha & 0 \\ \cos\alpha \sin\delta & \sin\alpha \cos\delta & \sin\delta \end{bmatrix} \tag{5.5-7}$$

5.5.2.2 Reference Direction and Second Rotation

The reference direction $\underline{U}_R$ locates the X_α axis in the vehicle orientation system (see Figure 5-8). It therefore defines the second transformation matrix $\left[IB_2\right]$. The reference direction may be computed according to the following options.

Inertial Reference (Star Sensor)

The $\underline{U}_R$ direction is specified by the user by defining its constant inertial right ascension α_R and declination δ_R. Then the $\underline{U}_R$ direction is defined by

$$\underline{U}_R = (\cos\alpha_R \cos\delta_R, \sin\alpha_R \cos\delta_R, \sin\delta_R) \tag{5.5-8}$$

Solar Reference (Sun Sensor)

The $\underline{U}_R$ direction is computed as the vector from the earth to the sun.

$$\underline{U}_R = -\underline{R}_E/R_E \tag{5.5-9}$$

Local Vertical (Center of Earth Disk)

The $\underline{U}_R$ direction is computed as the vector from the vehicle to the center of the earth or equivalently as the negative of the earth to vehicle position vector. Note that the user cannot specify a local vertical reference for both the primary axis and the reference direction.

$$\underline{U}_R = \underline{R}/R \tag{5.5-10}$$

The second rotation matrix $\left[IB_1\right]$ may now be computed. Write the first rotation matrix (5.5-7) as

$$\left[IB_1\right] = \left[X_1 \mid Y_1 \mid Z_1\right] \tag{5.5-11}$$

where the unit vectors $\underline{X}_1$, $\underline{Y}_1$, $\underline{Z}_1$ define the principle axes following the first rotation. The "roll" angle ρ necessary to align the X_α-direction properly is then given by

$$\cos\rho = \underline{X}_1 \cdot \underline{U}_R$$

$$\sin\rho = \frac{(\underline{X}_1 \times \underline{U}_R) \cdot \underline{Z}_1}{|(\underline{X}_1 \times \underline{U}_R) \cdot \underline{Z}_1|} \qquad 0 \leq \rho \leq 360 \tag{5.5-12}$$

The $[IB_2]$ matrix is then given by

$$IB_2 = \begin{bmatrix} \cos \varphi & -\sin \varphi & 0 \\ \sin \varphi & \cos \varphi & 0 \\ 0 & 0 & 1 \end{bmatrix} \qquad (5.5\text{-}8)$$

5.6 Time Systems

5.6.1 Introduction

The measure of time is a deceptively complex problem. Historically time measurements were based on the annual movement of planets about the sun or the daily rotation of the earth on its axis. Because of irregularities in these motions, these systems lead to non-uniform definitions of time. The desire to identify a uniform standard of time led to the use of high frequency atomic oscillations as the time standard. The other time systems are then related to this time reference. Thus the movement of time is considered uniform and the (irregular) motion of the earth is referenced to this uniform time standard.

Thus the standard time reference for the GMAS will be the atomic time system A.1 defined below. Other time systems will be used, however, including the ephemeris time system ET for the solar/lunar/planetary ephemerides, the universal time coordinated system UTC for tracking data, and universal time UT1 for computing Greenwich sideral time. Brief descriptions of various time systems and terms used in GMAS will be given in this section, most of which are taken directly from Reference 5-1. Section 5.6.2 addresses the uniform time systems of atomic and ephemeris times. Section 5.6.3 summarizes the universal time systems that relate the orientation of the earth to the vernal equinox. Section 5.6.4 will summarize the calendar date and Julian date conversions.

5.6.2   Standard Time Units

To eliminate the nonuniform time units discussed above, uniform time standards have been adopted. The two most common systems are atomic time and ephemeris time.

Atomic Time A.1

A.1 time is one of several types of atomic time. It is obtained from oscillations of the US Cesium Frequency Standard located at Boulder, Colorado. In 1958, the US Naval Observatory established the A.1 system based on an assumed frequency of 9,192,631,770 oscillations of the isotope 133 of cesium atom per A.1 second. The reference epoch of A.1 was established so that on January 1, 1958, $0^h0^m0^s$ UT2 the value of A.1 was $0^h0^m0^s$, January 1, 1958.

Ephemeris Time ET

This is the uniform measure of time, which is the independent variable of the equations of motion, and the argument for the ephem-erides of the planets, the moon, and the satellite. The unit of ET is the ephemeris second, which is defined as the fraction 1/31,556,925.9747 of the tropical year for 12^h ET of Jan 0^d, 1900. Ephemeris time is deter-mined from the instant near the beginning of the calendar year 1900 when the geometric mean longitude of the sun, L_M, was 279^h 41m 48.04 at which instant the measure of ephemeris time was 1900 Jan 0^d 12^h.

For most purposes, the difference between A.1 and ET may be con-sidered a constant. The suspected discrepancy is roughly two parts in 10^9. The actual transformation between A.1 and ET time is given by

$$(ET - A.1) = \Delta T_{1958} - \frac{(JD - 2,436,204.5)\ (86,400)}{9,192,631,770} \times \Delta f_{cesium}$$

$$(5.6-1)$$

$$+ \frac{2\ e\ (\mu a)\ 1/2\ \sin E}{c^2}$$

where

T_{1958} — the ET - UT2 on 01 January 1958, $0^h0^m0^s$ UT2 minus the periodic term in Equation (5.6-1) evaluated at this same epoch.

JD — the Julian date.

2,436,204.5 — the Julian date on 01 January 1958, $0^h0^m0^s$.

Δf_{cesium} — the correction to f_{cesium} = 9,192,631,770 cycles of cesium per ephemeris second.

μ — the gravitational constant of the sun, 1.327, 154,45 x 10^{11} km^3/sec^2.

a — the semimajor axis of the heliocentric orbit of the earth-moon barycenter, 149,599,000 km.

e — the eccentricity of the heliocentric orbit of the earth-moon barycenter .01672.

c — the speed of light at an infinite distance from the sun, 299,792.5 km/sec.

E — the eccentric anomaly of the heliocentric orbit of the earth-moon barycenter.

The first term of Equation (5.6-1) arises since A.1 was set equal to UT2 at the beginning of 1958. The second term accounts for the difference between the lengths of ET and A.1 seconds (if Δf_{cesium} is nonzero). The periodic term arises from general relativity. It accounts for the fact that A.1, UTC, and ST time is a measure of proper time observed on earth, and that ET is a measure of coordinate time in the heliocentric (strictly barycentric) space-time frame of reference. The contribution of the last two terms in Equation (5.6-1) is negligible for the range of applications currently contemplated for the GTDS program. Hence, the transformation between ET and A.1 is accomplished using the approximate formula,

$$ET - A.1 = 32\overset{s}{.}15 \tag{5.6-2}$$

5.6.2 Universal Time Systems

Universal time systems are used to determine the orientation of the earth relative to the vernal equinox at a specific instant.

In essence universal time is a measure of the angle between the Greenwich meridian and the sun at some instant with 12^h UT corresponding to the sun directly overhead. Because the rotation of the earth is irregular, the relations between uniform time and universal time are somewhat complicated and generally must be determined after the fact by observation. This irregularity is quite small and can generally be ignored in most mission analysis problems. However, in precise satellite tracking (where minor anomalies in the orbit are used to determine the parameters of the orbit, dynamic model, or measurement model) these rotational irregularities must be considered.

The differences between the universal time systems are essentially related to the manner in which the universal time is computed. The primary universal time systems are the universal time coordinated system (UTC) for the tracking data and the universal time UT1 for computing exact Greenwich sideral time. In practice, GMAS will determine the actual corrections from the time difference data A.1-UTC and A.1-UT1 supplied by the U.S. Naval Observatory. These data are supplied in the form

$$(A.1 - UTC)_i = a_{11} + a_{12} T + a_{13} T^2 \qquad (5.6-3)$$

$$(A.1 - UT1)_i = a_{14} + a_{15} T + a_{16} T^2 \qquad (5.6-4)$$

where

    A.1-UTC - the difference between A.1 and UTC time, in seconds.

    A.1-UT1 - the difference between A.1 and UT1 time, in seconds.

    T - the number of days from the beginning of the time span covered by the polynomial, T = 1, 2, ...

    i - the index of the time span.

The coefficients a_{ij} are given in Table 5.6-1, next to Modified Julian dates (mod 2,430,000) defining the time interval for which the coefficients are applicable. The table covers the time span from

Table 5.6-1.   Time Difference Coefficients

GREGORIAN DATE	MODIFIED JULIAN DATE	A.1-UTC			A.1-UT1		
		a_1	a_2	a_3	a_4	a_5	a_6
01/01/1958	6204	0.16180D 01	0.97450D-03	-0.39910D-06	0.18540D 01	0.20174D-02	-0.14030D-04
01/16/1958	6219	0.17545D 01	0.94021D-03	-0.72883D-05	0.45406D 01	0.16189D-02	0.17990D-06
02/06/1958	6240	0.56160D 01	0.83465D-03	-0.13736D-06	0.80117D 01	0.16625D-02	-0.26980D-05
02/20/1958	6254	0.87544D 01	0.83711D-03	0.45154D-06	0.10260D 00	0.16259D-02	0.21400D-05
04/10/1958	6303	0.14961D 00	0.94290D-03	-0.21316D-06	0.18746D 00	0.19994D-02	-0.60542D-06
05/31/1958	6354	0.19265D 00	0.66426D-03	0.20230D-05	0.27283D 00	0.12708D-02	-0.62937D-06
06/12/1958	6366	0.24111D 00	0.94086D-03	-0.14324D-05	0.28064D 00	0.10971D-02	-0.10284D-04
07/03/1958	6387	0.26262D 00	0.80819D-03	0.13736D-06	0.30501D 00	0.61508D-03	0.30861D-05
07/17/1958	6401	0.29520D 00	0.91009D-03	-0.18101D-06	0.31058D 00	0.79663D-03	0.66051D-05
10/23/1958	6499	0.40162D 00	0.84218D-03	-0.25981D-06	0.40965D 00	0.16710D-02	-0.13796D-06
11/27/1958	6534	0.45038D 00	0.76889D-03	0.22325D-05	0.40820D 00	0.16640D-02	-0.81837D-05
12/22/1958	6662	0.49406D 00	0.89040D-03	0.45974D-05	0.51426D 00	0.14992D-02	0.30561D-05
01/29/1959	6597	0.54583D 00	0.91691D-03	0.45577D-06	0.57006D 00	0.13938D-02	-0.13045D-05
02/26/1959	6625	0.59189D 00	0.94799D-03	-0.20740D-06	0.60282D 00	0.17060D-02	-0.32176D-06
04/02/1959	6702	0.73505D 00	0.11100D-02	-0.50000D-04	0.78856D 00	0.87143D-03	-0.28571D-04
05/06/1959	6706	0.75874D 00	0.07042D-03	-0.22186D-06	0.79189D 00	0.59155D-03	0.76140D-05
06/27/1959	6807	0.79597D 00	0.85812D-03	0.44598D-06	0.80767D 00	0.51800D-03	0.62997D-05
10/01/1959	6842	0.84726D 00	0.80073D-03	0.12137D-06	0.84928D 00	0.16958D-02	0.20480D-05
11/05/1959	6877	0.89834D 00	0.94247D-03	-0.3296D-06	0.90810D 00	0.17714D-02	0.26584D-05
11/19/1959	6891	0.93008D 00	0.81887D-03	0.40949D-06	0.93380D 00	0.17781D-02	0.45068D-05
12/17/1959	6919	0.97625D 00	0.67294D-03	0.13598D-04	0.97080D 00	0.14699D-02	-0.30766D-05
01/14/1960	6947	0.10058D 01	0.12703D-02	-0.26466D-07	0.10155D 01	0.14312D-02	0.69046D-05
05/30/1960	7084	0.11800D 01	0.12766D-02	-0.70583D-07	0.12238D 01	0.69186D-03	-0.17062D-05
09/07/1960	7184	0.13070D 01	0.12517D-02	0.20004D-08	0.12770D 01	0.12722D-02	0.10631D 00
01/01/1961	7300	0.14593D 01	0.12000D-02	-0.12594D-07	0.14424D 01	0.70022D-03	0.62074D-05
04/20/1961	7409	0.16004D 01	0.12887D-02	-0.46082D-07	0.15720D 01	0.14314D-02	-0.40660D-05
09/01/1961	7612	0.16027D 01	0.12976D-02	-0.16113D-07	0.16064D 01	0.60244D-03	0.42731D 00
12/17/1961	7650	0.18616D 01	0.13000D-02	-0.12627D-10	0.18265D 01	0.59200D-03	0.64505D-04
01/01/1962	7665	0.18815D 01	0.11213D-02	0.84592D-08	0.18437D 01	0.12372D-02	0.13325D-05
06/02/1962	7817	0.20518D 01	0.11164D-02	0.27764D-07	0.20706D 01	0.47241D-03	0.19611D-05
09/12/1962	7919	0.21059D 01	0.11206D-02	0.58281D-08	0.21415D 01	0.14008D-02	0.17563D-05
01/05/1963	8034	0.22948D 01	0.11102D-02	0.66207D-07	0.23369D 01	0.66111D-03	0.71013D-05
04/13/1963	8132	0.24044D 01	0.11232D-02	-0.42067D-09	0.24604D 01	0.70227D-03	-0.63169D-05
08/14/1963	8255	0.25420D 01	0.11180D-02	0.10362D-07	0.26032D 01	0.11400D-02	0.60660D-05
11/01/1963	8334	0.27312D 01	0.11120D-02	0.10421D-06	0.27506D 01	0.22533D-02	-0.10756D-05
01/06/1964	8400	0.28058D 01	0.12000D-02	-0.10445D-07	0.28918D 01	0.10026D-02	0.74760D-06
04/01/1964	8486	0.30173D 01	0.12930D-02	0.13042D-08	0.30035D 01	0.20842D-02	0.63261D-05
07/07/1964	8583	0.31429D 01	0.12946D-02	0.40200D-07	0.37544D 01	0.90044D-03	0.42367D-05
09/01/1964	8639	0.33153D 01	0.12876D-02	0.31036D-06	0.33218D 01	0.16453D-02	0.10561D-04
10/01/1964	8669	0.33552D 01	0.12051D-02	-0.12080D-08	0.33793D 01	0.27655D-02	-0.47032D 00
01/01/1965	8761	0.35743D 01	0.12934D-02	0.46089D-08	0.35876D 01	0.20301D-02	0.67042D 00
03/01/1965	8820	0.37607D 01	0.12974D-02	-0.11639D-07	0.37063D 01	0.20034D-02	-0.40227D 00
07/01/1965	8942	0.40098D 01	0.12062D-02	-0.86063D-08	0.39920D 01	0.16429D-02	0.12374D-05
09/01/1965	9004	0.41892D 01	0.12061D-02	-0.15623D-08	0.40898D 01	0.24052D-02	0.25459D-08
12/09/1965	9103	0.43174D 01	0.12980D-02	-0.13370D-10	0.43475D 01	0.24460D-02	-0.14892D-04
01/02/1966	9127	0.43445D 01	0.25916D-02	0.10584D-08	0.43906D 01	0.23429D-02	0.12215D-06
04/14/1966	9200	0.47710D 01	0.25941D-02	-0.18556D-07	0.40113D 01	0.10947D-02	0.32520D-05
08/25/1966	9333	0.50300D 01	0.25900D-02	0.19487D-07	0.50122D 01	0.28420D-02	0.59360D-06
12/01/1966	9460	0.52110D 01	0.25002D-02	-0.42063D-03	0.52113D 01	0.20906D-02	0.27519D-05
04/23/1967	9603	0.55817D 01	0.25933D-02	-0.88063D-03	0.55701D 01	0.20816D-02	-0.63680D-05
08/11/1967	9713	0.58669D 01	0.20854D-02	0.34789D-07	0.57930D 01	0.16062D-02	0.72409D-05
11/30/1967	9824	0.61543D 01	0.25901D-02	0.33990D-07	0.60640D 01	0.24730D-02	0.50221D-06
02/01/1968	9887	0.62170D 01	0.25930D-02	0.36377D-10	0.62773D 01	0.22505D-02	0.29557D-05
06/01/1968	10008	0.65313D 01	0.25920D-02	0.65706D-11	0.65594D 01	0.18464D-02	0.27527D-05
12/26/1968	10216	0.70704D 01	0.25920D-02	-0.61122D-10	0.70310D 01	0.23755D-02	0.34127D-05
05/18/1969	10359	0.74311D 01	0.25920D-02	0.12925D-03	0.74487D 01	0.23189D-02	0.17309D-05
09/01/1969	10471	0.77314D 01	0.25920D-02	-0.54770D-11	0.76939D 01	0.29856D-02	-0.72185D-07
04/14/1970	10690	0.82900D 01	0.25920D-02	0.79000D-11	0.83395D 01	0.33310D-02	0.75470D-05
08/17/1970	10815	0.86230D 01	0.25920D-02	-0.14950D-16	0.86399D 01	0.21509D-02	0.56553D-05
12/08/1970	10928	0.89160D 01	0.25920D-02	-0.26217D-11	0.89557D 01	0.23377D-02	0.20147D-05
04/17/1971	11058	0.92529D 01	0.25920D-02	0.22604D-16	0.96187D 01	0.31771D-02	-0.44673D-05
08/27/1971	11190	0.96990D 01	0.26920D-02	0.87452D-10	0.96634D 01	0.25250D-02	0.68343D-05
11/26/1971	11281	0.98309D 01	0.26922D-02	-0.48616D-08	0.99618D 01	0.33862D-02	-0.82477D-05
01/01/1972	11317	0.10034D 02	0 0	0 0	0.10066D 02	0.27600D-02	-0.44376D-14

5.6-5

January 1, 1958, and is updated once every month as current data from the U.S. Naval Observatory becomes available. The last row of coefficients in the table is used to obtain extrapolated values of the time-differences for a short time in the future. The table is used by finding the value of i such that the given date, MJD_j, is in the range

$$MJD_i \leq MJD_j < MJD_{i+1}$$

The argument of interpolation, T, is then computed from,

$$T = MJD_j - MJD_i + 1 \qquad\qquad (5.6-5)$$

Having given the computational transformations, we now proceed to give the rather lengthy definitions of the universal time systems.

Standard Universal Time, UT

This is the measure of time that is the theoretical basis for all civil time keeping. UT is related to the rotation of the earth on its axis. Compared to ephemeris time, which is uniform time, UT does not take into account the irregularities of the earth's rate of rotation.

The quantity UT is defined as 12 hours plus the Greenwich Hour Angle (GHA) of a point (representing a fictitious mean sun) on the mean equator of epoch whose right ascension measured from the mean equinox of epoch is

$$R_u = 18^h\, 38^m\, 45\overset{s}{.}836 + 8,640,184\overset{s}{.}542\, T_u + \overset{s}{.}0929\, T_u^2 \qquad (5.6-6)$$

where T is defined as the number of Julian centuries elapsed from 12^h UT1 January 0, 1900 (JD = 2415020.0) to the UT1 time of epoch.

The Greenwich hour angle of this point, denoted by a_s in Figure 5.6-1 is

$$\alpha_s = \alpha_{GM} - R_M \qquad\qquad (5.6-7)$$

where α_{GM} is the Greenwich mean sideral time; hence,

$$UT = 12^h + \alpha_{GM} - R_u.$$
<div align="right">(5.6-8)</div>
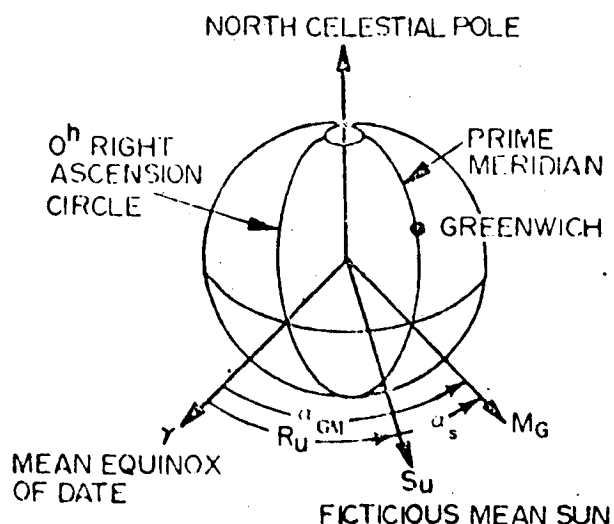
Figure 5.6-1. Greenwich Hour Angle

The practical determination of UT is obtained from meridian transits of stars by the U.S. Naval Observatory. At the instant of observation, the right ascension of the observing station is equal to the observed star, relative to the true equator and equinox of date. Subtracting the cast longitude of the observing station gives the true Greenwich sidereal time, α_g , at the instant of observation. α_g is also the Greenwich Hour Angle of the true equinox of date. Subtracting the nutation in right ascension gives the Greenwich Mean Sidereal Time, α_{GM} or GMST. UT is then determined from the above equation (5.6-8).

Uncorrected Universal Time, UTO

This measure of time is obtained from UT by assuming a nominal value of the longitude of each observing station. The resulting UT is labeled UTO. Actual determination of UTO is done by an instrument located at an observatory whose adopted conventional longitude is λ_A. When the longitude - λ_A is added to the observed _ocal hour angle of the point S_u, (See Figure 5.6-1), whose right ascension measured from the mean equator and equinox of date is R_u, then UTO is obtained (See Figure 5.6-2).

$$UTO = 12^h - \lambda_A + LHA\ of\ S_u.$$
<div align="right">(5.6-9)</div>
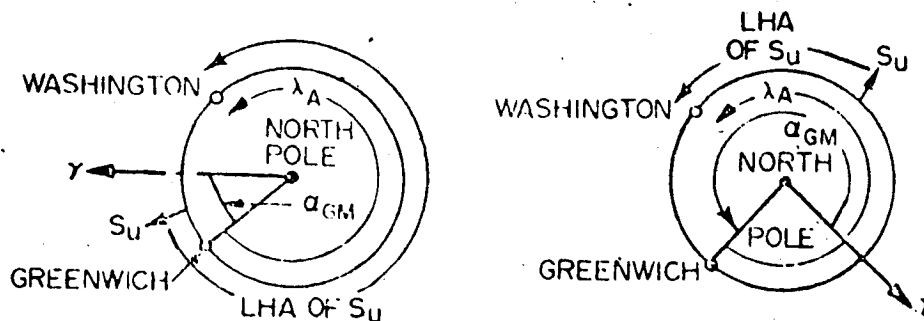
Figure 5.6-2. Universal Time References

Universal Time, UT1

This measure of time is defined in terms of UTO by applying an appropriate correction in longitude due to the motion of the pole. UT1 reflects the actual orientation of the earth with respect to the vernal equinox at that instant. UT1 will be the same for all observatories. In contrast, UTO time, as determined by different observatories using their adopted longitude in calculations, results in a different value of UTO for each observatory.

Then

$$UT1 = UTO - \qquad \qquad (5.6\text{-}10)$$

$$\Delta\lambda = \tan \phi_A \left[Xp \sin \lambda_A + Y_p \cos \lambda_A \right] \qquad (5.6\text{-}11)$$

where λ_A and ϕ_A are the adopted longitude and latitude and X_p, Y_p represent the polar motion (See Section 5.3.5). UT1 time is caused by GTDS to compute the a_{GM} as given in Equation (5.3-14).

Universal Time, UT2

If the extrapolated value of UT1 time is corrected for periodic seasonal variations, SV, in the earth's speed of rotation, the resulting time is UT2. UT2 does not represent the actual orientation of the earth with respect to the vernal equinox. UT1 should always be used when the actual orientation of the earth is required. UT2 is often referred to as GMT, Greenwich Mean Time, and ZULU time. The equations for UT2 are

$$UT2 = UT1 + SV \qquad\qquad (5.6\text{-}12)$$

where

$$SV = {}^s_.022 \sin 2t - {}^s_.017 \cos 2t - {}^s_.007 \sin 4t + {}^s_.006 \cos 4t$$

$$(5.6\text{-}13)$$

or

$$SV = {}^s_.022 \sin 2t - {}^s_.012 \cos 2t - {}^s_.006 \sin 4t + {}^s_.007 \cos 4t$$

$$(5.6\text{-}14)$$

Equation (5.6-13) was used prior to 1962 and Equation (5.6-14) has been in use since 1962. The quantity t equals the fraction of the tropical year elapsed from the beginning of the Besselian year for which the calculation is made. (One tropical year = 365.2422 days.) Since seasonal variations can be known precisely only after their occurrence, UT2 itself is rarely used. The Bureau International de l'Heure also issues corrections for   and SV.

Universal Time Coordinated, UTC

This is the standard time scale to which tracking stations are synchronized. UTC time is derived from atomic time, A.1, in a manner which makes it almost synchronous with Earth-rotation-derived time.

Up to January 1, 1972, the UTC time scale operated at a frequency offset from the atomic time scale. The value of the offset was period-ically changed by international agreement so that the UTC scale would correspond more closely to time derived from the rotation of the Earth.

On January 1, 1972, a new improved UTC system, adopted by the International Radio Consultative Committee (CCIR), was internationally implemented by the time-keeping laboratories and time-broadcast stations (References 10 and 11).

The new UTC system eliminates the frequency offset from atomic time, thus making the UTC second constant and equal in duration to the A.1 second. The new UTC time scale is now kept in synchronism with the rotation of the earth to within $\pm$ 0.7 second by step-time adjustments of exactly one second, when needed.

5.7 References

5-1. W. E. Wagner and C. E. Velez, "Goddard Trajectory
      Determination Subsystem Mathematical Specifications",
      March, 1972.

5-2. TRW Systems Group, "Houston Operations Predictor/Esti-
      mator (HOPE) Engineering Manual", TRW 70-FMT-792A.
      June 1970.

5-3. R. J. Haverkos, D. L. Beery and R. W. Herder, "Orbit
      Adjust Maneuver Program (OAMP) User's Information",
      CSC 3000-04800-05TM, March 1974.

5-4. A. Rochkind, "Synchronous Meteorological Satellite
      (SMS) Maneuver Control Program (SMSMAN) Task Speci-
      fication", CSC 3101-00800-02TN. July 1973.

5-5. Peabody, Scott, and Orozeo, "User's Description of
      JPL Ephemeric Tapes," JPL 32-580, 1964.

6.   State and State Transition Matrix Propagation

6.1 Introduction

This chapter will be devoted to the description and definition of
the dynamical models of spacecraft accelerations, the mathematical formu-
lation describing those models and the numerical or analytical techniques
used for solving those equations. GMAS will include the capability for
low, medium and high precision propagation but will access GTDS for the
latter capability.

The GMAS will be capable of simulating the motion of one or two ve-
hicles moving under some or all of the accelerations due to a non-spherical
central body, n-point masses, atmospheric drag, solar radiation pressure,
attitude control system corrections and finite thrust. The central body
asphericity will be modeled using the standard expansion in Legendre
polynomials. Drag calculations will include the vehicle characteristics
as modeled by effective cross-sectional area and drag coefficient and the
atmosphere as defined by a fairly accurate model such as the modified
Harris-Priester. Solar radiation pressure will include the vehicle char-
acteristics including luminosity, distance, and shadowing. The attitude
control system effects and finite thrust models will include polynomial
expansions for the accelerations.

GMAS will include the capability to propagate the vehicle trajecto-
ries at three levels of precision. The low level precision formulation
will be two-body motion and the Brouwer-Lyddane formulation. The medium
precision formulation will include both analytic and numerical averaging
techniques. To take advantage of existing capability, GMAS will be de-
signed to access the high precision propagation techniques available in
the GTDS.

All the propagators developed for GMAS will be built with complete
modularity to allow any combination of the models included, the mathe-
matical formulation, and the numerical scheme desired by the user. Pre-
vious studies have shown this can be done very efficiently.

6.2 Dynamical Models

The state of a spacecraft is a function of the many accelerations acting upon it. Some of these accelerations are due to the physical characteristics of the solar system, while others are generated by spacecraft systems. The dynamics of the situation are expressed by the equations of motion which provide the relationship between the spacecraft state at any instant and the state at the initial epoch. This section identifies the various sources of acceleration and gives the appropriate mathematical representation. The accelerations which are considered include:

1) the gravitational acceleration due to n-point masses,
2) the acceleration due to the central body gravity harmonics,
3) the acceleration due to atmospheric drag,
4) the acceleration due to solar radiation pressure,
5) the acceleration due to thrust.

6.2.1 N-Body Gravity Contribution

The equation of motion in an inertial frame of reference for a spacecraft of negligible mass under the influence of n-point masses is given by the summation of accelerations due to the point masses

$$\ddot{\bar{R}}_I = - \sum_{k=1}^{n} \frac{\mu_k}{R_{kp}^3} \bar{R}_{kp} \tag{6.2-1}$$

where $\bar{R}_I$ is the spacecraft position vector in the inertial frame, μ_k is the product of the universal gravitational constant and the mass of the kth body, and $\bar{R}_{kp}$ is the vector from the kth body to the spacecraft (R_{kp} denotes the magnitude of $\bar{R}_{kp}$).

It is normally more convenient to reference the motion of the spacecraft to one of the massive bodies. The equation of motion referenced to this "central" body is in an accelerated frame of reference and is given by:

$$\ddot{\bar{R}} = \frac{\mu}{R^3} \bar{R} + \sum_{k=2}^{n} \mu_k \left[\frac{\bar{R}_k - \bar{R}}{|\bar{R}_k - \bar{R}|^3} - \frac{\bar{R}_k}{|\bar{R}_k|^3} \right]$$

where $\bar{R}_k$ is the vector from the central body to the kth body and $\bar{R}$ is from the central body to the spacecraft.

In one case of practical application it is sometimes necessary to add an additional term to equation 6.2-2. This is the case of an orbit referenced to the Earth's moon where the indirect effect of the nonsphericity of the Earth on the lunar ephemeris is large enough to have an effect.

6.2.2 Gravitational Harmonics

The determination of the acceleration due to the nonsphericity of the central body is a classical problem and is well treated in the literature. A summary of the required mathematical formulae will be given below.

The central body gravity field is represented by a potential function which is an infinite sum of spherical harmonics. The sum is normally truncated at some appropriate level. The potential function is given in equation (6-3).

$$\psi(r, \varphi, \lambda) = \frac{\mu}{r} + \frac{\mu}{r} \sum_{n=1}^{\infty} C_n^0 \left(\frac{a_p}{r}\right)^n P_N^0 (\sin \varphi)$$

$$+ \frac{\mu}{r} \sum_{n=1}^{\infty} \sum_{m=1}^{n} \left(\frac{a_p}{r}\right)^n P_n^m (\sin \varphi) \left[S_n^m \sin m\lambda + C_n^m \cos m\lambda\right]$$

(6.2-3)

where

$\mu \sim$ the gravitational parameter of the central body

$a_p \sim$ the radius of the body (usually taken as the equatorial radius)

$P_n^m \sim$ the associated Legendre function

$S_n^m, C_n^m \sim$ harmonic coefficients.

The term $n = 1$ is usually not present when the origin of the coordinate system is placed at the center of mass.

The accelerations due to the nonspherical portion of this potential are obtained in the body-fixed, true of date coordinate system shown in Figure 6.2-1, where the coordinate directions are defined as follows:

x_b axis lies along the intersection of the central body's equatorial plane and the plane of the prime meridian

z_b axis lies along the axis to the adopted North Pole

y_b axis completes a right-handed coordinate system.

The acceleration due to nonsphericity in this coordinate system may be obtained as a vector r_b with components $\ddot{x}_b$, $\ddot{y}_b$, and $\ddot{z}_b$ where

$$\ddot{r}_b = \begin{bmatrix} \ddot{x}_b \\ \ddot{y}_b \\ \ddot{z}_b \end{bmatrix} = \frac{\partial \psi}{\partial r}\frac{\partial r}{\partial r_b} + \frac{\partial \psi}{\partial \varphi}\frac{\partial \varphi}{\partial r_b} + \frac{\partial \psi}{\partial \lambda}\frac{\partial \lambda}{\partial r_b} \qquad (6.2\text{-}4)$$
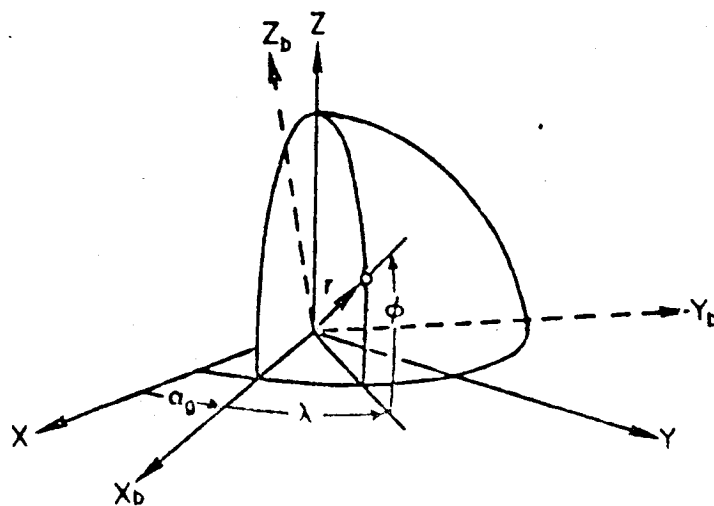
Figure 6.2-1.   Body Fixed System

The partial derivatives of the nonspherical portion of the potential with respect to r, φ, and λ are given by

$$\frac{\partial \psi}{\partial r} = -\frac{1}{r}\left(\frac{\mu}{r}\right)\sum_{n=2}^{N}\left(\frac{a_p}{r}\right)^n (n+1)\sum_{m=0}^{n}(C_n^m \cos m\lambda + S_n^m \sin m\lambda)P_n^m(\sin\varphi)$$

$$(6.2\text{-}5)$$

$$\frac{\partial \psi}{\partial \varphi} = \left(\frac{\mu}{r}\right)\sum_{n=2}^{N}\left(\frac{a_p}{r}\right)^n \sum_{m=0}^{n}(C_n^m \cos m\lambda + S_n^m \sin m\lambda)[P_n^{m+1}(\sin\varphi) - m\tan\varphi\, P_n^m(\sin\varphi)]$$

$$\frac{\partial \psi}{\partial \lambda} = \left(\frac{\mu}{r}\right)\sum_{n=2}^{N}\left(\frac{a_p}{r}\right)^n \sum_{m=0}^{n} m(S_n^m \cos m\lambda - C_n^m \sin m\lambda) P_n^m(\sin\varphi).$$

6.2-3

The Legendre functions and the terms $\cos m\lambda$, $\sin m\lambda$ and $m \tan\phi$ are computed via recursion formulae:

$$P_n^0 (\sin\phi) = [(2n-1) \sin\phi \, P_{n-1}^0 (\sin\phi) - (n-1) P_{n-2}^0 (\sin\phi)]/n \qquad (6.2-6)$$

$$P_n^m (\sin\phi) = P_{n-2}^m (\sin\phi) + (2n-1) \cos\phi \, P_{n-1}^{m-1} (\sin\phi) \quad m \neq 0, m < n \qquad (6.2-7)$$

$$P_n^n (\sin\phi) = (2n-1) \cos\phi \, P_{n-1}^{n-1} (\sin\phi) \quad m \neq 0, m = n \qquad (6.2-8)$$

where

$$P_0^0 (\sin\phi) = 1, \qquad P_1^0 (\sin\phi) = \sin\phi, \qquad P_1^1 (\sin\phi) = \cos\phi \qquad (6.2-9)$$

$$\sin m\lambda = 2 \cos\lambda \sin(m-1)\lambda - \sin(m-2)\lambda$$

$$(6.2-10)$$

$$\cos m\lambda = 2 \cos\lambda \cos(m-1)\lambda - \cos(m-2)\lambda$$

$$m \tan\phi = [(m-1) \tan\phi] + \tan\phi. \qquad (6.2-11)$$

The partial derivatives of r, ϕ, and λ with respect to x_b, y_b, and z_b are computed from the expressions

$$\frac{\partial r}{\partial r_b} = \frac{\bar{r}_b^T}{r} \qquad (6.2-12)$$

$$\frac{\partial \phi}{\partial r_b} = \frac{1}{\sqrt{x_b^2 + y_b^2}} \left[-\frac{z_b \bar{r}_b^T}{r^2} + \frac{\partial z_b}{\partial r_b} \right] \qquad (6.2-13)$$

$$\frac{\partial \lambda}{\partial r_b} = \frac{1}{(x_b^2 + y_b^2)} \left[x_b \frac{\partial y_b}{\partial r_b} - y_b \frac{\partial x_b}{\partial r_b} \right] \qquad (6.2-14)$$

where

$$\frac{\partial x_b}{\partial r_b}, \quad \frac{\partial y_b}{\partial r_b}, \quad \text{and} \quad \frac{\partial z_b}{\partial r_b} \qquad (6.2-15)$$

are the row vectors $(1, 0, 0)$, $(0, 1, 0)$, and $(0, 0, 1)$, respectively.

Substituting equations (6.2-12) through (6.2-14) into (6.2-4) yields

$$\ddot{x}_b = \left(\frac{1}{r}\frac{\partial \psi}{\partial r} - \frac{z_b}{r^2 \sqrt{x_b^2 + y_b^2}}\frac{\partial \psi}{\partial \phi}\right)x_b - \left(\frac{1}{(x_b^2 + y_b^2)}\frac{\partial \psi}{\partial \lambda}\right)y_b$$

$$\ddot{y}_b = \left(\frac{1}{r}\frac{\partial \psi}{\partial r} - \frac{z_b}{r^2 \sqrt{x_b^2 + y_b^2}}\frac{\partial \psi}{\partial \phi}\right)y_b + \left(\frac{1}{x_b^2 + y_b^2}\frac{\partial \psi}{\partial \lambda}\right)x_b \qquad (6.2\text{-}16)$$

$$\ddot{z}_b = \left(\frac{1}{r}\frac{\partial \psi}{\partial r}\right)z_b + \frac{\sqrt{x_b^2 + y_b^2}}{r^2}\frac{\partial \psi}{\partial \phi}.$$

The numerical computations related to spacecraft orbits are normally made in an inertial frame of reference (e.g. mean equator and equinox of 1950.0) so that the appropriate rotation of the acceleration vector from the body-fixed, true of date system must be made. This is discussed in Chapter 5.

The formulation given in equations (6.2-3) through (6.2-16) is taken from reference 6.1 and is necessary when the spacecraft orbit is being integrated in a Cartesian formulation; on the other hand, if a variation of parameters (VOP) formulation is being used, the planetary equations which express the rate of change of the Keplerian elements are given in terms of partials of the potential with respect to the elements. The potential must thus be expressed in terms of the elements.

In terms of Kepler elements, the equations of motion are:

$$\frac{da}{dt} = \frac{2}{na}\frac{\partial \psi}{\partial M},$$

$$\frac{de}{dt} = \frac{1-e^2}{na^2 e}\frac{\partial \psi}{\partial M} - \frac{(1-e^2)^{1/2}}{na^2 e}\cdot\frac{\partial \psi}{\partial \omega}, \qquad (6\text{-}16a) \qquad (6.2\text{-}17)$$

$$\frac{d\omega}{dt} = -\frac{\cos i}{na^2(1-e^2)^{1/2}\sin i}\frac{\partial \psi}{\partial i} + \frac{(1-e)^{1/2}}{na^2 e}\cdot\frac{\partial \psi}{\partial e},$$

$$\frac{di}{dt} = -\frac{\cos i}{na^2(1-e^2)^{1/2}\sin i}\frac{\partial \psi}{\partial \omega} - \frac{1}{na^2(1-e^2)^{1/2}\sin i}\frac{\partial \psi}{\partial \Omega} \; ,$$

$$\frac{d\Omega}{dt} = \frac{1}{na^2(1-e)^{1/2}\sin i}\frac{\partial \psi}{\partial i} \; , \qquad\qquad (6.2\text{-}18)$$

$$\frac{dM}{dt} = -\frac{1-e^2}{na^2e}\frac{\partial \psi}{\partial e} - \frac{2}{na}\frac{\partial \psi}{\partial a} + n \; ,$$

where ψ is the <u>disturbing</u> (non two-body) part of the potential. The expansion of the disturbing potentials (ψ_H and ψ_{TB} for gravitational harmonics and third body perturbations respectively) in terms of the Kepler elements of the spacecraft, the angular position of the Earth and the Kepler elements of the Sun and Moon are given by Kaula (reference 6.2) as

$$\psi_H = \sum_{\ell=2}^{\infty} \sum_{m=0}^{\ell} \psi_{\ell m}$$

$$\psi_{\ell m} = \frac{\mu a_e^{\ell}}{a^{\ell+1}} \sum_{p=0}^{\ell} \bar{F}_{\ell m p}(i) \sum_{q=-\infty}^{+\infty} G_{\ell p q}(e) \, S_{\ell m p q} \qquad (6.2\text{-}19)$$

$$S_{\ell m p q} = \begin{bmatrix} \cos \\ \\ \sin \end{bmatrix} \begin{matrix} \ell - m \text{ even} \\ \\ \ell - m \text{ odd} \end{matrix} \; [(\ell - 2p)\omega + (\ell - 2p + q)M + m(\Omega - \theta)]$$

where

μ = earth gravitational constant

a_e = earth equatorial radius

r = radial distance to vehicle

a = semi-major axis

e = eccentricity

i = inclination

M = mean anomaly

ω = argument of perigee

Ω = right ascension of ascending node

θ = right ascension of Greenwich

$G_{\ell pq}(e)$ and $F_{\ell mp}(i)$ are functions arising from the Harmonic analysis of the potential field and transformation to functions of Kepler elements. Both $G_{\ell pq}(e)$ and $F_{\ell mp}(i)$ are available as computer subroutines.

The third body disturbing function is given by

$$\psi_2^* = m^* \frac{a^2}{a^{*3}} \sum_{m=0}^{2} \kappa_m \frac{(2-m)!}{(2+m)!} F_{nmp}(i) \cdot$$

$$\sum_{h=0}^{2} F_{nmh}(i^*) \sum_{q=\infty}^{+\infty} H_{npq}(e) \qquad (6.2\text{-}20)$$

$$\sum_{j=\infty}^{+\infty} G_{nhj}(e^*) \cos [2-2p)\omega + (2-2p+q) M - (2-2h)\omega^*$$

$$- (2-2h+j)M^* + m(\Omega - \Omega^*)]$$

where a "star" refers to the Kepler element of the disturbing body.

$$K_1 = 1$$

$$K_m = 2 \cdot m \neq 0$$

$H_{npq}(e)$ is available as part of the computer subroutine which calculates $G_{\ell pq}(e)$.

6.2.3 Atmospheric Drag

One of the more complicated forces acting on the satellite is aerodynamic drag. The complications arise because of the presence in the mathematical model of the atmospheric density, a parameter whose properties and characteristics are not well known. The model for this force is only as good as the model for the atmospheric density and if consideration is given to the hourly, daily, monthly, and even yearly variations of atmospheric constituents, then the complexity begins to become more evident.

The braking effect of this force is characterized by a deceleration of the satellite which, in turn, tends to secularly decrease the energy and lower the altitude.

The direction of the force is opposite to the direction of motion and is dependent upon the shape, size, orientation and velocity of the satellite as well as the density of the atmosphere. The atmosphere is rotating; consequently, the velocity referred to above is not the inertial velocity of the satellite but rather the velocity relative to the rotating atmosphere. The consequence of using a rotating atmosphere is that the force is no longer in the plane of undisturbed motion.

The force is defined in terms of these factors to be

$$\bar{F} = - \frac{AC_D}{2} \rho \, V_{REL} \, \bar{V}_{REL} \tag{6.2-21}$$

where

$A \sim$ the effective cross-sectional area

$C_D \sim$ the aerodynamic drag coefficient

$\rho \sim$ the density of the atmosphere

$\bar{V}_{REL} \sim$ the velocity vector of the satellite relative to the atmosphere.

In the 1950.0 coordinate system, the relative velocity vector is given by

$$\bar{V}_{REL} = \dot{\bar{R}} - (\bar{\omega} \times \bar{R})$$

(6.2-22)

where

$\bar{\omega} \sim$ the angular rotation vector of the earth expressed in 1950.0 coordinates

$\bar{R}, \dot{\bar{R}} \sim$ the earth-centered 1950.0 position and velocity vectors of the satellite.

The required acceleration is given by

$$\ddot{\bar{R}}_D = \frac{-C_D \Lambda}{2 m_0} \rho \, V_{REL} \, \bar{V}_{REL}$$

(6.2-23)

where m_0 is the mass of the spacecraft. Equations (6.2-21) through (6.2-23) are taken from reference 6.1.

6.2.4 Solar Radiation Pressure

The force due to solar radiation pressure on a vehicle's surface is proportional to the effective area A of the surface normal to the incident radiation, to the surface reflectivity, η, to the luminosity, L_s, of the Sun, and inversely proportional to the square of the distance R_{vs} from the Sun, and to the speed of light, c.

The magnitude of the force due to direct solar radiation pressure on an area A is therefore given by

$$F = \frac{L_s \gamma \Lambda}{4 \pi R_{vs}^2 c}$$

(6.2-24)

where $\gamma = 1 + \eta$ (e.g. $\gamma = 1.95$ for aluminum) (6.2-25)

The magnitude of the acceleration on a spacecraft of mass, m_0, and area, A, due to direct solar radiation pressure at one astronomical unit from the Sun is

$$\frac{F}{m_0} = \frac{S}{c} \frac{\gamma A}{m_0}$$

(6.2-26)

6.2-9

where S denotes the mean solar flux at one astronomical unit. The quantities γ, A and m_0 are grouped together since they are spacecraft properties and can be determined prior to flight. The magnitude of the acceleration on a spacecraft due to direct solar radiation at the actual distance R_{vs} from the Sun is given by

$$\frac{F}{m_0} = \frac{S}{c} \frac{R_{sun}^2}{R_{vs}^2} \frac{\gamma A}{m_0} \tag{6.2-27}$$

where R_{sun} designates one astronomical unit, i.e., the semimajor axis of the Earth's orbit.

All of the above factors except R_{vs} are constant for a given spacecraft and mission. For computational convenience, P_s replaces S/c. P_s is defined as the force on a perfectly absorbing surface ($\eta = 0$) due to solar radiation pressure at one astronomical unit.

The acceleration due to direct solar radiation is away from the Sun; that is, in the direction of

$$\overline{R}_{vs} = \overline{R} - \overline{R}_s \tag{6.2-28}$$

where

$\overline{R} \sim$ the position vector of the vehicle in the inertial mean of 1950.0 coordinate system

$\overline{R}_s \sim$ the position vector of the Sun in the inertial mean of 1950.0 coordinate system.

The model for the acceleration $\ddot{\overline{R}}_{SR}$ due to direct solar radiation is

$$\ddot{\overline{R}}_{SR} = \nu P_s R_{sun}^2 \frac{\gamma A}{m_0} \frac{\overline{R}_{vs}}{R_{vs}^3} \tag{6.2-29}$$

where

ν – eclipse factor such that =
$\begin{matrix} 0 \text{ if the satellite is in shadow (umbra)} \\ 1 \text{ if the satellite is in sunlight and} \\ 0 < \nu < 1 \text{ if the satellite is in penumbra.} \end{matrix}$

Equations (6.2-24) through (6.2-29) are taken from reference 6.1.

6.2.5 Finite Thrust

The model used to describe the spacecraft acceleration during propulsive maneuvers is an empirical representation based on the reduction of data taken during the motor burn testing procedures. It is represented in an inertial true of date systems as

$$\ddot{\bar{r}}_T = a \{ u(t - T_0) - u(t - T_f) \} \, U_T \qquad (6.2\text{-}30)$$

where

$a \sim$ the magnitude of the thrust acceleration

$U_T \sim$ the direction of the thrust acceleration

$T_0 \sim$ the effective initiation time of the motor burn (ET)

$T_f \sim$ the effective termination time of the motor burn (ET)

and

$$u(t - \tau) = \begin{cases} 1, & t \geqslant \tau \\ 0, & t < \tau \end{cases} \qquad (6.2\text{-}31)$$

The motor's effective burn time is

$$T_b = T_f - T_0. \qquad (6.2\text{-}32)$$

The propulsive acceleration is modeled as follows

$$a = a_0 + a_1 \tau + a_2 \tau^2 + a_3 \tau^3 + a_4 \tau^4 \qquad (6.2\text{-}33)$$

where $\quad \tau = t - T_0 \qquad (6.2\text{-}34)$

Equation (6.2-33) characterizes the thrust acceleration as a fourth degree polynomial in τ, the time from effective thrust initiation, to represent the effective thrust to mass ratio as a function of time.

The unit vector $\overline{U}_T$ is assumed to be directed along the spacecraft's thrust axis direction. The true epoch components of the thrust axis are

$$U_T = \begin{bmatrix} \cos \alpha_T \cos \delta_T \\ \sin \alpha_T \cos \delta_T \\ \sin \delta_T \end{bmatrix} \qquad (6.2\text{-}35)$$

where

$\alpha_T \sim$ the right ascension of the spacecraft's thrust axis relative to the true equinox and equator of epoch

$\delta_T \sim$ the declination of the spacecraft's thrust axis relative to the true equinox and equator of epoch.

The thrust axis orientation is also represented by fourth-degree polynomials in τ

$$\alpha_T = \alpha_0 + \alpha_1 \tau + a_2 \tau^2 + a_3 \tau^3 + a_4 \tau^4 \tag{6.2-36}$$

$$\delta_T = \delta_0 + \delta_1 \tau + \delta_2 \tau^2 + \delta_3 \tau^3 + \delta_4 \tau^4 \tag{6.2-37}$$

The thrust acceleration is expressed in the true earth equator and equinox of epoch coordinate system (via the unit vector $\overline{U}_T$). This is then rotated to the inertial mean equinox and equator of 1950.0. Equations (6.2-30) through (6.2-37) are taken from reference 6-1.

6.3 Low Precision Propagation

Many of the functions of GMAS such as mission assessment and profile generation, maneuver analysis and error analysis will require the availability of extremely fast propagation methods. A consequence of the fast computation time will be low precision, since analytic techniques cannot include a complicated force model. Two basic analytic methods will be sufficient for most applications. The salient equations for a very efficient formulation of basic two body motion by Goodyear (Reference 6.3) and the Brouwer-Lyddane theory (Reference 6.4) which includes effects of the first few zonal harmonics will be given below.

6.3.1 Two Body Motion

The Goodyear formulation of the two body problem uses a change of variables that permits a very concise set of equations to be used that are the same whether the motion is hyperbolic, parabolic or elliptic. A consequence of this is the introduction of several new transcendental functions replacing the standard trigonometric and hyperbolic functions. With this formulation, the propagation of a two body orbit is accomplished very quickly.

The change of variables is made by defining

$$\dot{\psi} = 1/r \tag{6.3-1}$$

which leads to the relationship of ψ to the eccentric (E) and hyperbolic (F) anomalies in standard two body formulations as

$$= \frac{E-E_0}{\sqrt{\mu/a}} = \frac{F-F_0}{\sqrt{-\mu/a}} \tag{6.3-2}$$

The equations necessary for propagating a two body orbit as taken from reference 6.3 are given below, where $\bar{r}_0$ and $\dot{r}_0$ are the position and velocity at time t_0 and $\bar{r}$ and $\dot{r}$ are the position and velocity at time t and the gravitational parameter is μ. First

$$r_0 = \sqrt{\vec{r}_0 \cdot \vec{r}_0}$$

$$\sigma_0 = \vec{r}_0 \cdot \dot{\vec{r}}_0 \tag{6.3-3}$$

$$\alpha = \dot{\vec{r}}_0 \cdot \dot{\vec{r}}_0 - 2\mu/r_0$$

are determined. Then the parameter ϕ and its transcendental functions

$$s_0 = 1 + \alpha\,\phi^2/2! + \alpha^2\,\phi^4/4! + \alpha^3\,\phi^6/6! + \ldots$$

$$s_1 = \phi + \alpha\,\phi^3/3! + \alpha^2\,\phi^5/5! + \alpha^3\,\phi^7/7! + \ldots$$

$$s_2 = \phi^2/2! + \alpha\,\phi^4/4! + \alpha^2\,\phi^6/6! + \alpha^3\,\phi^8/8! + \ldots$$

$$s_3 = \phi^3/3! + \alpha\,\phi^5/5! + \alpha^2\,\phi^7/7! + \alpha^3\,\phi^9/9! + \ldots$$

(6.3-4)

are obtained by solving the equation

$$t = t_0 + r_0 s_1 + \sigma_0 s_2 + \mu s_3 \tag{6.3-5}$$

for ϕ. Then

$$r = r_0 s_0 + \sigma_0 s_1 + \mu s_2 \tag{6.3-6}$$

and

$$f = 1 - \mu s_2/r_0 \qquad\qquad g = (t - t_0) - \mu s_3$$

$$\dot{f} = -\mu s_1/(r\,r_0) \qquad\quad \dot{g} = 1 - \mu s_2/r$$

(6.3-7)

give the final solution for the coordinates.

$$\vec{r} = f\,\vec{r}_0 + g\,\dot{\vec{r}}_0$$

$$\dot{\vec{r}} = \dot{f}\,\vec{r}_0 + \dot{g}\,\dot{\vec{r}}_0$$

(6.3-8)

The state transition matrices are given in terms of the initial and final coordinates and the initial and final accelerations. The auxillary parameter U is defined in terms of two additional transcendental functions S_4 and S_5 where

$$U = S_2(t - t_0) + \mu(7 S_4 - 3 S_5) \tag{6.3-9}$$

where

$$s_4 = \phi^4/4! + \alpha\,\phi^6/6! + \alpha^2\,\phi^8/8! + \alpha^3\,\phi^{10}/10! + \ldots \tag{6.3-10}$$

$$s_5 = \phi^5/5! + \alpha\,\phi^7/7! + \alpha^2\,\phi^9/9! + \alpha^3\,\phi^{11}/11! + \ldots \tag{6.3-11}$$

The state transition matrices are given on the following page.

$$
\begin{bmatrix} \partial x/\partial x_0 & \partial x/\partial y_0 & \partial x/\partial z_0 \\ \partial y/\partial x_0 & \partial y/\partial y_0 & \partial y/\partial z_0 \\ \partial z/\partial x_0 & \partial z/\partial y_0 & \partial z/\partial z_0 \end{bmatrix} = \begin{bmatrix} f & 0 & 0 \\ 0 & f & 0 \\ 0 & 0 & f \end{bmatrix} + U \begin{bmatrix} \dot{x} \\ \dot{y} \\ \dot{z} \end{bmatrix} \begin{bmatrix} \ddot{x}_0 & \ddot{y}_0 & \ddot{z}_0 \end{bmatrix}
$$

$$(6.3\text{-}12)$$

$$
+ \begin{bmatrix} x & \dot{x} \\ y & \dot{y} \\ z & \dot{z} \end{bmatrix} \begin{bmatrix} -\dfrac{\dot{f}\,s_1 + (f-1)/r_0}{r_0} & -\dot{f}\,s_2 \\[2ex] \dfrac{(f-1)\,s_1}{r_0} & (f-1)s_2 \end{bmatrix} \begin{bmatrix} x_0 & y_0 & z_0 \\ \dot{x}_0 & \dot{y}_0 & \dot{z}_0 \end{bmatrix}
$$

$$
\begin{bmatrix} \partial x/\partial \dot{x}_0 & \partial x/\partial \dot{y}_0 & \partial x/\partial \dot{z}_0 \\ \partial y/\partial \dot{x}_0 & \partial y/\partial \dot{y}_0 & \partial y/\partial \dot{z}_0 \\ \partial z/\partial \dot{x}_0 & \partial z/\partial \dot{y}_0 & \partial z/\partial \dot{z}_0 \end{bmatrix} = \begin{bmatrix} g & 0 & 0 \\ 0 & g & 0 \\ 0 & 0 & g \end{bmatrix} - U \begin{bmatrix} \dot{x} \\ \dot{y} \\ \dot{z} \end{bmatrix} \begin{bmatrix} \dot{x}_0 & \dot{y}_0 & \dot{z}_0 \end{bmatrix} -
$$

$$(6.3\text{-}13)$$

$$
+ \begin{bmatrix} x & \dot{x} \\ y & \dot{y} \\ z & \dot{z} \end{bmatrix} \begin{bmatrix} -\dot{f}\,s_2 & -(\dot{g}-1)s_2 \\[1ex] (f-1)\,s_2 & g\,s_2 \end{bmatrix} \begin{bmatrix} x_0 & y_0 & z_0 \\ \dot{x}_0 & \dot{y}_0 & \dot{z}_0 \end{bmatrix}
$$

$$
\begin{bmatrix} \partial \dot{x}/\partial x_0 & \partial \dot{x}/\partial y_0 & \partial \dot{x}/\partial z_0 \\ \partial \dot{y}/\partial x_0 & \partial \dot{y}/\partial y_0 & \partial \dot{y}/\partial z_0 \\ \partial \dot{z}/\partial x_0 & \partial \dot{z}/\partial y_0 & \partial \dot{z}/\partial z_0 \end{bmatrix} = \begin{bmatrix} \dot{f} & 0 & 0 \\ 0 & \dot{f} & 0 \\ 0 & 0 & \dot{f} \end{bmatrix} + U \begin{bmatrix} \ddot{x} \\ \ddot{y} \\ \ddot{z} \end{bmatrix} \begin{bmatrix} \ddot{x}_0 & \ddot{y}_0 & \ddot{z}_0 \end{bmatrix}
$$

$$(6.3\text{-}14)$$

$$
+ \begin{bmatrix} x & \dot{x} \\ y & \dot{y} \\ z & \dot{z} \end{bmatrix} \begin{bmatrix} -\dot{f}\left(\dfrac{s_0}{r\,r_0} + \dfrac{1}{r^2} + \dfrac{1}{r_0^2}\right) & -\dfrac{\dot{f}\,s_1 + (\dot{g}-1)/r}{r} \\[2ex] \dfrac{\dot{f}\,s_1 + (f-1)/r_0}{r_0} & \dot{f}\,s_2 \end{bmatrix} \begin{bmatrix} x_0 & y_0 & z_0 \\ \dot{x}_0 & \dot{y}_0 & \dot{z}_0 \end{bmatrix}
$$

$$
\begin{bmatrix} \partial \dot{x}/\partial \dot{x}_0 & \partial \dot{x}/\partial \dot{y}_0 & \partial \dot{x}/\partial \dot{z}_0 \\ \partial \dot{y}/\partial \dot{x}_0 & \partial \dot{y}/\partial \dot{y}_0 & \partial \dot{y}/\partial \dot{z}_0 \\ \partial \dot{z}/\partial \dot{x}_0 & \partial \dot{z}/\partial \dot{y}_0 & \partial \dot{z}/\partial \dot{z}_0 \end{bmatrix} = \begin{bmatrix} \dot{g} & 0 & 0 \\ 0 & \dot{g} & 0 \\ 0 & 0 & \dot{g} \end{bmatrix} - U \begin{bmatrix} \ddot{x} \\ \ddot{y} \\ \ddot{z} \end{bmatrix} \begin{bmatrix} \dot{x}_0 & \dot{y}_0 & \dot{z}_0 \end{bmatrix}
$$

$$(6.3\text{-}15)$$

$$
+ \begin{bmatrix} x & \dot{x} \\ y & \dot{y} \\ z & \dot{z} \end{bmatrix} \begin{bmatrix} -\dfrac{\dot{f}\,s_1 + (\dot{g}-1)/r}{r} & -\dfrac{(\dot{g}-1)\,s_1}{r} \\[2ex] \dot{f}\,s_2 & (\dot{g}-1)\,s_2 \end{bmatrix} \begin{bmatrix} x_0 & y_0 & z_0 \\ \dot{x}_0 & \dot{y}_0 & \dot{z}_0 \end{bmatrix}
$$

The partials with respect to the gravitational constant are given by

$$
\begin{bmatrix} \partial x / \partial \mu \\ \partial y / \partial \mu \\ \partial z / \partial \mu \end{bmatrix} = \begin{bmatrix} x & \dot{x} \\ y & \dot{y} \\ z & \dot{z} \end{bmatrix} \begin{bmatrix} -s_2 / r_0 \\ U / r_0 - s_3 \end{bmatrix} \tag{6.3-16}
$$

$$
\begin{bmatrix} \partial \dot{x} / \partial \mu \\ \partial \dot{y} / \partial \mu \\ \partial \dot{z} / \partial \mu \end{bmatrix} = \begin{bmatrix} x & \dot{x} & \ddot{x} \\ y & \dot{y} & \ddot{y} \\ z & \dot{z} & \ddot{z} \end{bmatrix} \begin{bmatrix} -s_1 / (r \, r_0) \\ s_2 / r_0 \\ U / r_0 - s_3 \end{bmatrix} \tag{6.3-17}
$$

6.3.2 Brouwer-Lyddane

The Brouwer theory for the motion of a satellite moving around a central body including the effect of the first five zonal harmonics develops the solution in canonical variables using the von Zeipel method. It is applicable to elliptical drag-free orbits but has singularities for zero eccentricity and inclination and the critical inclination of 63° 26'. Lyddane improved upon the Brouwer theory by obtaining improved algorithms applicable for zero eccentricity and inclination. This section presents the equations required for the Brouwer-Lyddane formulation.

In these formulas, the osculating orbit is divided into secular terms and long and short period periodic terms. Delaunay variable notation is used, i.e.,

$$
\begin{aligned}
l'' &= M'' \\
g'' &= \omega'' \\
h'' &= \Omega''
\end{aligned}
\qquad (6.3\text{-}9)
$$

The double prime will be used on a variable to indicate secular or mean motion, single prime will indicate secular plus long period terms, and unprimed variables will include all effects and are used for the osculating elements. The semi-major axis, eccentricity and inclination, will be represented by a, e, and i, respectively. The radius of the central body is given by R_e.

Propagating only secular terms to time t yields

$$
\begin{aligned}
a'' &= a_o'' \\
e'' &= e_o'' \\
i'' &= i_o''
\end{aligned}
\qquad (6.3\text{-}10)
$$

$$
\begin{aligned}
l'' &= n_o \Delta t + \dot{l} \Delta t + l_o'' & 0 &\le l'' < 2\pi \\
g'' &= \dot{g} \Delta t + g_o'' & 0 &\le g'' < 2\pi \\
h'' &= \dot{h} \Delta t + h_o'' & 0 &\le h'' < 2\pi
\end{aligned}
$$

where

$$\dot{\ell} = n_0\eta\left\{\gamma_2'\left[\frac{3}{2}(3\theta^2-1)+\frac{3}{32}\gamma_2'\left(25\eta^2+16\eta-15+(30-96\eta-90\eta^2)\theta^2\right.\right.\right.$$
$$\left.\left.\left.+(105+144\eta+25\eta^2)\theta^4\right)\right]+\frac{15}{16}\gamma_4'e''^2(3-30\theta^2+35\theta^4)\right\}$$

$$\dot{g} = n_0\left\{\gamma_2'\left[\frac{3}{2}(5\theta^2-1)+\frac{3}{32}\gamma_2'\left(25\eta^2+24\eta-35+(90-192\eta-126\eta^2)\theta^2\right.\right.\right.$$

(6.3-11)

$$\left.\left.+(385+360\eta+45\eta^2)\theta^4\right)\right]+\frac{5}{16}\gamma_4'\left[21-9\eta^2+(126\eta^2-270)\theta^2\right.$$
$$\left.\left.+(385-189\eta^2)\theta^4\right]\right\}$$

$$\dot{h} = n_0\left\{\gamma_2'\left[\frac{3}{8}\gamma_2'\left((9\eta^2+12\eta-5)\theta-(35+36\eta+5\eta^2)\theta^3\right)-3\theta\right]\right.$$
$$\left.+\frac{5}{4}\gamma_4'\theta(5-3\eta^2)(3-7\theta^2)\right\}$$

and the abbreviations are

$$n_0 = \sqrt{\frac{\mu}{a''^3}}, \qquad \eta = \sqrt{1-e''^2} \qquad \theta = \cos i$$

$$k_2 = \frac{J_2 R_e^2}{2} \qquad \gamma_2 = \frac{k_2}{a''^2} \qquad \gamma_2' = \frac{\gamma_2}{\eta^4}$$

$$k_3 = -J_3 R_e^3 \qquad \gamma_3 = \frac{k_3}{a''^3} \qquad \gamma_3' = \frac{\gamma_3}{\eta^6}$$

(6.3-12)

$$k_4 = -\frac{3J_4 R_e^4}{8} \qquad \gamma_4 = \frac{k_4}{a''^4} \qquad \gamma_4' = \frac{\gamma_4}{\eta^8}$$

$$k_4 = -J_5 R_e^5 \qquad \gamma_5 = \frac{k_5}{a''^5} \qquad \gamma_5' = \frac{\gamma_5}{\eta^{10}}$$

Note that the secular terms depend only on the second and fourth harmonics, J_2 and J_4.

6.3-6

The mean value of the eccentric anomaly, E", is obtained iteratively from Kepler's equation

$$E'' - e'' \sin E'' = \ell''$$ (6.3-13)

The mean true anomaly, f', mean radial distance, r", and the differential of the mean semimajor axis with respect to the mean radial distance, da"/dr", are

$$f'' = \tan^{-1}\left[\frac{\sqrt{1-e''^2}\,\sin E''}{\cos E'' - e''}\right]$$ (6.3-14)

$$r'' = a''(1 - e'' \cos E'')$$ (6.3-15)

$$\frac{da''}{dr''} = \frac{1}{(1 - e'' \cos E'')}$$ (6.3-16)

Since the periodic terms are somewhat lengthy, the following abbreviations are introduced to shorten the computations.

$$A_1' = \frac{1}{(1-5\theta^2)}$$

$$A_1 = \frac{1}{8}\gamma_2' \eta^2 (1 - 11\theta^2 - 40\theta^4 A_1')$$

$$A_2' = 3\theta^2 + 8\theta^4 A_1'$$

$$A_2 = \frac{5}{12}\frac{\gamma_4'}{\gamma_2'}\eta^2 (1 - A_2')$$

$$A_3 = \frac{\gamma_5'}{\gamma_2'}(3e''^2 + 4)$$

$$A_4 = \frac{\gamma_5'}{\gamma_2'}(1 - 3A_2')$$

$$A_5 = A_3(1 - 3A_2')$$

$$A_6 = \frac{1}{4}\frac{\gamma_3'}{\gamma_2'}$$

$$A_7 = A_6 \eta^2 \sin i''$$

$$A_8 = \frac{\gamma_5'}{\gamma_2'}e''^2 (1 - 5\theta^2 - 16\theta^4 A_1')$$

$$A_9 = \eta^2 \sin i''$$

$$A_{10} = 2 + e''^2$$

$$A_{11} = 3e''^2 + 2$$

$$A_{12} = A_{11}\theta^2$$

$$A_{13} = (5e''^2 + 2)\theta^4 A_1'$$

$$A_{14} = e''^2 \theta^6 A_1'^2$$

$$A_{15} = \theta^2 A_1'$$

$$A_{16} = A_{15}^2$$

$$A_{17} = e'' \sin i''$$

$$A_{18} = \frac{A_7}{1+\eta}$$

$$A_{19} = (1+\theta)\sin i''$$ (6.3-17)

$$A_{20} = e'' \theta$$

$$A_{21} = e'' A_{20}$$

$$A_{22} = A_{20} \tan\left(\frac{i''}{2}\right)$$

$$A_{23} = \eta^2 A_{17}$$

$$A_{24} = A_{11} + 2$$

$$A_{25} = 16 A_{15} + 40 A_{16} + 3$$

$$A_{26} = \frac{1}{8}A_{21}(11 + 200 A_{16} + 80 A_{15})$$

and

$$B_1 = \eta(A_1 - A_2) \cdot \left[\frac{1}{16}(A_{10} - 400 A_{14} - 40 A_{13} - 11 A_{12})\right.$$
$$\left. + \frac{1}{8} A_{21}(11 + 200 A_{16} + 80 A_{15})\right] \gamma_2'$$
$$+ \left[\frac{5}{24}(-80 A_{14} - 8 A_{13} - 3 A_{12} + \quad + \frac{5}{12} A_{25} A_{21}\right] \frac{\gamma_4'}{\gamma_2'}$$

$$B_2 = A_6 A_{10}(2 + \eta - e''^2) + \frac{5}{64} A_5 A_{19} \eta^2 - \frac{15}{32} A_4 A_{17} \eta^3 \cdot$$
$$+ A_{20} \tan\left(\frac{i''}{2}\right)\left[\frac{5}{64} A_5 + A_6\right] + \frac{5}{64} A_4 A_{17}\left[9 e''^2 + 26\right]$$
$$+ \frac{15}{32} A_3 A_{20} A_{25} \sin i''(1-\theta)$$

$$B_3 = \frac{35}{576} \frac{\gamma_5'}{\gamma_2'} e'' \sin i''(\theta - 1) A_{21}\left[80 A_{16} + 5 + 32 A_{15}\right]$$
$$- \frac{35}{52} \frac{A_8}{e''}\left\{A_{21}\tan\left(\frac{i''}{2}\right) + \left[2 e''^2 + 3(1 - \eta^3)\right]\sin i''\right\}$$

$$B_4 = \eta e''(A_1 - A_2)$$

$$B_5 = \eta\left[\frac{5}{64} A_4 A_9(9 e''^2 + 4) + A_7\right] \qquad\qquad (6.3\text{-}18)$$

$$B_6 = \frac{35}{384} \eta^3 A_8 \sin i''$$

$$B_7 = \eta^2 A_{17} A_1'\left[\frac{1}{8}\gamma_2'(1 - 15\theta^2) - \frac{5}{12}\frac{\gamma_4'}{\gamma_2'}(1 - 7\theta^2)\right]$$

$$B_8 = \frac{5}{64} A_3 \eta^2(1 - 9\theta^2 - 24\theta^4 A_1') + \eta^2 A_6$$

$$B_9 = \frac{315}{384} \eta^2 A_8$$

$$B_{10} = \sin i''\left[\frac{5}{12}\frac{\gamma_4'}{\gamma_2'} A_{21} A_{25} - A_{26}\gamma_2'\right]$$

$$B_{11} = A_{21}\left[\frac{5}{64} A_5 + A_6 + \frac{15}{32} A_3 A_{25}\sin^2 i''\right]$$

$$B_{12} = -\left[(80 A_{16} + 32 A_{15} + 5)(\frac{35}{576}\frac{\gamma_5'}{\gamma_2'} e'' \sin^2 i'' A_{21}) + \frac{35}{52} A_8 A_{20}\right]$$

$$B_{13} = e''(A_1 - A_2)$$

$$B_{14} = \frac{5}{64} A_3 \eta^2 \sin i'' + A_7$$

$$B_{15} = \frac{35}{384} A_8 \eta^2 \sin i''$$

The following formulas give the osculating elements at time t.

Semimajor Axis

$$a = a''\left\{1 + \gamma_2\left[(3\theta^2 - 1)\frac{e''}{\eta^6}\left(e''\eta + \frac{e''}{1+\eta} + \cos f''(3 + 3 e'' \cos f'' + e''^2 \cos^2 f'')\right)\right.\right.$$
$$\left.\left. + 3(1 - \theta^2)\left(\frac{da''}{dr''}\right)^3 \cos(2 f'' + 2 g'')\right]\right\} \qquad (6.3\text{-}19)$$

Eccentricity

$$\delta_1 e = B_{13} \cos 2g'' + B_{14} \sin g'' - B_{15} \sin 3g''$$

$$(6.3\text{-}20)$$

$$
\begin{aligned}
\delta e = \delta_1 e \; - \; \frac{\eta^2}{2} \Big\{ &\gamma_2'(1-\theta^2)\big[3\cos(2g''+f'') + \cos(3f''+2g'')\big] \\
&- 3\gamma_2 \frac{1}{\eta^6}(1-\theta^2)\cos(2g''+2f'')(3e''\cos^2 f'' + 3\cos f'' + e''^2\cos^3 f'' + e'') \\
&- \gamma_2 \frac{1}{\eta^6}(3\theta^2-1)\big[e''\eta - \frac{e''}{1+\eta} + 3e''\cos^2 f'' + 3\cos f'' + e''^2\cos^3 f''\big]\Big\}
\end{aligned}
$$

$$(6.3\text{-}21)$$

$$
\begin{aligned}
e''\delta\ell = B_4 \sin 2g'' - &B_5 \cos g'' + B_6 \cos 3g'' \\
- \frac{1}{4}\eta^3\gamma_2' \Big\{ &2(3\theta^2-1)\big[\eta^2(\tfrac{da''}{dr''})^2 + \tfrac{da''}{dr''} + 1\big]\sin f'' \\
&+ 3(1-\theta^2)\big[\big(-\eta^2(\tfrac{da''}{dr''})^2 - \tfrac{da''}{dr''} - 1\big)\sin(2g''+f'') \\
&+ \big(\eta^2(\tfrac{da''}{dr''})^2 + \tfrac{da''}{dr''} + \tfrac{1}{3}\big)\sin(3f''+2g'')\big]\Big\}
\end{aligned}
$$

$$(6.3\text{-}22)$$

$$e = \sqrt{(e'' + \delta e)^2 + (e''\delta\ell)^2}$$

$$(6.3\text{-}23)$$

Inclination

$$
\begin{aligned}
\delta i = \; \frac{1}{2}\theta\gamma_2'\sin i''\big[&e''\cos(3f''+2g'') \\
&+ 3\big(e''\cos(2g''+f'') + \cos(2f''+2g'')\big)\big] \\
&- \frac{A_{20}}{\eta^2}\big[B_7 \cos 2g'' + B_8 \sin g'' - B_9 \sin 3g''\big]
\end{aligned}
$$

$$(6.3\text{-}24)$$

$$\sin\left(\tfrac{i}{2}\right)\delta h = \frac{1}{2\cos\left(\tfrac{i'}{2}\right)}\left\{ B_{10}\sin 2g'' + B_{11}\cos g'' + B_{12}\cos 3g'' \right.$$
$$- \tfrac{1}{2}\gamma_2'\theta \sin i''\left[6\left(e''\sin f'' - \ell'' + f''\right)\right.$$
$$- 3\left(\sin(2g''+2f'') + e''\sin(2g''+f'')\right)$$
$$\left.\left. - e''\sin(3f''+2g'')\right]\right\} \qquad (6.3\text{-}25)$$

$$i = 2\sin^{-1}\left\{\left[\sin\left(\tfrac{i}{2}\right)\delta h\right]^2 + \left[\tfrac{1}{2}\delta i \cos\left(\tfrac{i''}{2}\right) + \sin\left(\tfrac{i''}{2}\right)\right]^2\right\}^{1/2} \qquad (6.3\text{-}26)$$

Mean Anomaly, ℓ , Argument of Perigee, g , and Right Ascension of Ascending Node, h

$$\ell' + g' + h' = (\ell'' + g'' + h'') + B_1\sin 2g'' + B_2\cos g'' + B_3\cos 3g'' \qquad (6.3\text{-}27)$$

$$\ell + g + h = (\ell' + g' + h') + \left\{\tfrac{1}{4}\left(\tfrac{\eta^2}{\eta+1}\right)e''\gamma_2'\left[3(1-\theta^2)\left(\sin(3f''+2g'')\right)\right.\right.$$
$$\times\left(\tfrac{1}{3} + \left(\tfrac{d\alpha''}{dr''}\right)^2\eta^2 + \tfrac{d\alpha''}{dr''}\right) + \sin(2g''+f'')\left(1 - \left(\tfrac{d\alpha''}{dr''}\right)^2\eta^2 - \tfrac{d\alpha''}{dr''}\right)$$
$$\left.\left. + 2\sin f''(3\theta^2-1)\left(1 + \left(\tfrac{d\alpha''}{dr''}\right)^2\eta^2 + \tfrac{d\alpha''}{dr''}\right)\right]\right\}$$
$$+ \tfrac{3}{2}\gamma_2'\left[(5\theta^2-2\theta-1)(e''\sin f + f''-\ell'')\right]$$
$$+ (3+2\theta-5\theta^2)\left\{\tfrac{1}{4}\gamma_2'\left[e''\sin(3f''+2g'') + 3\left(\sin(2g''+2f'') + e''\sin(2g''+f'')\right)\right]\right\} \qquad (6.3\text{-}28)$$

$$\ell = \tan^{-1}\left\{\frac{e''\delta\ell\cos\ell'' + (e''+\delta e)\sin\ell''}{(e''+\delta e)\cos\ell'' - e''\delta\ell\sin\ell''}\right\} \quad \text{if} \quad e \neq 0$$
$$\ell = 0 \qquad\qquad\qquad\qquad\qquad \text{if} \quad e = 0 \qquad (6.3\text{-}29)$$

$$h = \tan^{-1}\left\{\frac{\sin\left(\tfrac{i}{2}\right)\delta h\cos h'' + \sin h''\left[\tfrac{1}{2}\delta i\cos\left(\tfrac{i}{2}\right) + \sin\left(\tfrac{i}{2}\right)\right]}{\cos h''\left[\tfrac{1}{2}\delta i\cos\left(\tfrac{i}{2}\right) + \sin\left(\tfrac{i}{2}\right)\right] - \sin\left(\tfrac{i}{2}\right)\delta h\sin h''}\right\} \quad \text{if} \quad i \neq 0$$
$$h = 0 \qquad\qquad\qquad\qquad\qquad\qquad \text{if} \quad i = 0 \qquad (6.3\text{-}30)$$

$$g = (\ell + g + h) - \ell - h \qquad (6.3\text{-}31)$$

The eccentric anomaly is iteratively determined from Kepler's equation

$$E - e \sin E = \ell \qquad (6.3\text{-}32)$$

The true anomaly and radial distance are

$$f = \tan^{-1}\left[\frac{\sqrt{1-e^2}\,\sin E}{\cos E - e}\right] \qquad (6.3\text{-}33)$$

$$r = a(1 - e\cos E) \qquad (6.3\text{-}34)$$

The Brouwer-Lyddane theory was developed for drag-free orbits
However, the primary influence of drag on high altitude, small eccentricity
orbits is to cause a secular effect in the mean anomaly. The effect is relatively
small and noticeable only over a long period of time. Therefore, a first order
correction to the mean anomaly is optionally included of the form

$$\Delta\ell_{DRAG} = \sum_{q=0}^{m} \sum_{p=2}^{3} N_{pq} (t - t_q)^p \qquad (6.3\text{-}35)$$

$$m = 0, 1, 2, \ldots, 19$$

where

N_{pq} ~ Brouwer drag parameters

t_q ~ Brouwer drag parameters reference time

The correction is applied to the mean motion in Equation (6.3-10) as follows

$$\ell'' = n_o \Delta t + \dot{\ell}\,\Delta t + \ell_o'' + \Delta\ell_{DRAG} \qquad (6.3\text{-}36)$$

The Brouwer-Lyddane theory, presented previously, requires the Brouwer mean elements a'', e'', i'', l'', g'' and h'' to commence the procedure. Usually, however, the osculating orbital elements a_0, e_0, l_0, g_0 and h_0 are provided at initial epoch time t_0.

To transform the osculating elements to mean elements, a successive approximation scheme is utilized which involves the Brouwer-Lyddane algorithm. Given an initial estimate of the mean elements, a_0'', e_0'', . . ., the osculating elements at time t_0 are computed from Equations (6.3-10) thru (6.6-31). If these computed elements differ from the specified osculating elements a_0, e_0, . . . then the mean elements are differentially corrected by means of a Newton Raphsen successive approximation procedure so as to cause the computed osculating elements to agree with the a priori specified elements. To commence the successive approximation procedure, the mean elements a_0'', e_0'', . . . are approximated by the a priori specified osculating elements a_0, e_0, ... It should be noted that since Δt is zero in Equation (6.6-10) (i.e., $t = t_0$), the secular terms $\dot{l}$, $\dot{g}$ and $\dot{h}$ in Equation (6.3-11) need not be calculated.

6.4 Medium Precision Propagation

Since almost every type of mission considered at GSFC requires pre-mission analysis for long periods of time (i.e., months or years) full high precision integration of the equation of motion is untenable. A method of approximating the motion while retaining the important long term characteristics must be used. The method used in various forms involves the use of averaged equations of motion.

In general, averaged equations of motion are useful only when the dominant characteristic of the motion is periodicity and all perturbative forces have characteristic frequencies significantly lower than that of the basic motion. Thus, the motion of a satellite whose basic orbit is elliptical about a central body can be investigated with averaging techniques, whereas the motion of a probe traveling on a hyperbola departing or arriving at a planet or on an arc of an heliocentric conic cannot be usefully investigated with these techniques.

The basis for averaging is the technique of variation of parameters (VOP). The VOP technique formulates the equations of motion in terms of parameters which are constants in the unperturbed problem (i.e., conic elements). Under the influence of perturbations, these parameters will then be relatively slowly varying functions of time. The VOP formulation can be used for full high precision integration of the motion since no approximation is made.

The VOP form of the equations of motion (planetary equations) can be represented by

$$\dot{E}_i = F_i(E_j, t) \qquad i = 1,6; \quad j = 1,6 \qquad (6.4\text{-}1)$$

where the E_i represent some set of six orbital elements. The full form of these equations for the classical orbital elements was given previously in equations (6.2-17 & 18). The form of the equations for the set of elements defined by

$$p = a(1-e^2)$$
$$h = e \sin\omega$$
$$k = e \cos\omega$$
$$u = \omega + f$$
$$i = i$$
$$\Omega = \Omega$$

$$(6.4\text{-}2)$$

is given in reference 6.6 as

$$\dot{p} = \left(2 r \sqrt{\frac{p}{\mu}}\right) S$$

$$\dot{h} = \sqrt{\frac{p}{\mu}} \left\{ -\cos(\omega + f) R + \left[\left(1 - \frac{r}{p}\right) \sin(\omega + f) + \frac{r}{p} e \sin \omega \right] S \right.$$
$$\left. - e \cos \omega \frac{r}{p} \sin(\omega + f) \cot i\ W \right\}$$

$$\dot{k} = \sqrt{\frac{p}{\mu}} \left\{ \sin(\omega + f) R + \left[\left(1 + \frac{r}{p}\right) \cos(\omega + f) + \frac{r}{p} e \cos \omega \right] S \right.$$
$$\left. + \frac{r}{p} e \sin \omega \sin(\omega + f) \cot i\ W \right\} \qquad (6.4\text{-}3)$$

$$\dot{u} = \sqrt{p\mu}/r^2 - \left(r\sqrt{\frac{1}{\mu p}} \sin(\omega + f) \cot i\right) W$$

$$\dot{i} = r \cos(\omega + f)\ W\ /\ \sqrt{p\mu}$$
$$\dot{\Omega} = r \sin(\omega + f)\ W\ /\ (\sin i\ \sqrt{p\mu})$$

where R, S, and W are the components of the inertial perturbing acceleration resolved along the radial, tangential and normal directions.

The general characteristics of the integrals of the above equations is that they contain short, medium and long periodic variations as well as secular variations. The short period variations are of the order of the orbital period or less and are directly related to the motion of the spacecraft around a single orbit. The other variations are related to longer frequency parameters affecting the motion such as the rotation of the central body or the motion of third bodies.

The objective of averaging techniques is to remove the short period variations by transforming the set of ordinary differential equations describing the osculating or instantaneous orbital elements to a set of ordinary differential equations describing the mean values of the orbital elements.

The result of the averaging procedure is that to first order in the small quantity characterizing the perturbation the set of ordinary differential equations in the mean elements is given by

$$\dot{\overline{E}}_i = \frac{1}{\tau} \int_{t-\tau/2}^{t+\tau/2} F_i(\overline{E}_i, t)dt \qquad i = 1,6; \ j = 1,5 \qquad (6.4\text{-}4)$$

where it should be noted that the orbital elements are treated as constant at their mean values $\overline{E}_j(t)$ during the averaging integration. The period τ must be defined in terms of the <u>mean</u> value of the semimajor axis at time t. It should also be noted that explicit dependence on the fast variable E_6 (e.g., true or mean anomaly) has been removed.

There are two methods of performing the averaging quadrature. Analytic averaging refers to processes in which the integrals in (6.4-4) are taken analytically. One great advantage of analytical averaging is that when the perturbing forces are derivable from a potential then only the potential need be averaged and not all six force equations as indicated by (6.4-3). This is valid since the order of the partial differentiation and the averaging integration may be reversed. The equations given in section 6.2.2 for the perturbing potential in terms of the Keplerian elements are written so that the short period contributions may be specifically excluded.

For perturbations of a complex nature or for time dependent forces such as atmospheric drag or tesseral harmonics, the averaging in equation (6.4-4) is most conveniently performed by numerical quadrature. Reference 6.7 has found for most applications that 6-point Gaussian quadrature applied to the averaging interval broken into one to three subintervals yields excellent accuracy for almost any application.

The principal advantages of analytic averaging are speed and precision with respect to the averaged rates—it should be used whenever possible. On the other hand, numerical averaging offers high flexibility in perturbation modeling. Although slightly more expensive, Reference 6.8 indicates that such flexibility is highly desirable and useful. Numerical averaging also offers the basis for improved averaging schemes, which are impossible with analytical averaging.

By whatever method the averaged rates are obtained, the differential equations are then solved numerically using standard numerical integration schemes which are discussed in section 6.6. Step sizes on the order of the orbital period may be used.

6.5 High Precision Propagation

GMAS will include the capability for high precision propagation but will access GTDS for this capability. The various propagation options in this mode will include Cowell and VOP formulations of the equations of motion. The Cowell equations of motion can be integrated with either a fixed or variable step size with the use of time regularized variables available for elliptical motion. The VOP formulation can be in terms of Keplerian or equinoctial elements as well as the Kustaanheimo-Stiefel set of variables.

6.6 Integration Methods

The classical integration problem involved in orbital dynamics is solving the initial value problem specified by

$$\ddot{y} = f(y, \dot{y}, x)$$
$$y(x_o) = y_o$$
$$\dot{y}(x_o) = \dot{y}_o$$

(6.6-1)

where y and f are three-vectors defining the position and acceleration respectively of a spacecraft. Defining the six component state vector $W^T = (y^T, \dot{y}^T)$ equation (6.6-1) can be reduced to a class I first order differential equation by defining $g^T = (\dot{y}, f)$ and thus

$$\dot{W} = g(W, x)$$
$$W(x_o) = W_o$$

(6.6-2)

In addition to class I problems, of frequent interest are class II problems whereby the acceleration is a function of only the position and possibly time (i.e., in equation (6.6-1) $\ddot{y} = f(y,x)$). Such problems occur quite frequently in dynamics and are usually handled by special class II methods in lieu of reducing it to a class I problem. Such methods avoid the artificial introduction of first order derivatives, which may not be of interest, and the possible introduction of undesirable error propagation properties.

Classical class I and II integration methods approximate y at a sequence of time points ($x_i = x_o + ih \quad i = 1, 2, \ldots$) where the stepsize h, is assumed to be a constant. An approximate solution at x_i is denoted y_i.

Among the many classical methods available for solving initial value problems one can distinguish between single-step and multi-step methods. In a single-step method, the value of y_{n+1} can be found if only y_n is known. In a multi-step method, the calculation of y_{n+1} depends on explicit knowledge of y_n and certain "back" values y_{n-1}, $y_{n-2}, \ldots$ A method is called a k-step method if k such back values are required. Another distinction between these two types of methods is that in multi-step methods the function $f(y,x)$ is evaluated only at the points x_i whereas most single-step methods require the evaluation of f at intermediate points.

Although multi-step methods are in general more complex than single-step methods in that special starting and "memory maintenance" procedures are required, they offer the advantage of high accuracy at minimum number of evaluations of f. If this function is very complex, as is frequently the case, this results in multi-step methods being much more efficient than single-step methods and, therefore, of more general use.

6.6.1 Single-Step Techniques

Single-step integration schemes require the evaluation of the function to be integrated f at intermediate points between x_n and x_{n+1}. The equations for the commonly used four-cycle Runge-Kutta technique are

$$Y\left(X_0 + h\right) = Y_0 + \frac{1}{6}\left(K_1 + 2K_2 + 2K_3 + K_4\right) \qquad (6.6\text{-}3)$$

where

$$K_1 = hf\left(X_0, Y_0\right)$$

$$K_2 = hf\left(X_0 + \frac{1}{2}h, Y_0 + \frac{1}{2}K_1\right)$$

$$K_3 = hf\left(X_0 + \frac{1}{2}h, Y_0 + \frac{1}{2}K_2\right)$$

$$K_4 = hf\left(X_0 + h, Y_0 + K_3\right)$$

The equations for a seventh-order ten-cycle Runge-Kutta scheme are given as

$$Y\left(X_0 + h\right) = Y_0 + \frac{1}{840}\left(41\left(K_0 + K_9\right) + 216\left(K_4 + K_8\right) + 27\left(K_5 + K_7\right) + 272\ K_6\right)$$

where $(6.6\text{-}4)$

$$K_0 = hf\left(X_0, Y_0\right)$$

$$K_1 = hf\left(X_0 + \frac{1}{3}h, Y_0 + \frac{1}{3}K_0\right)$$

$$K_2 = hf\left(X_0 + \frac{1}{2}h, Y_0 + \frac{1}{8}\left[K_0 + 3K_1\right]\right)$$

$$K_3 = hf\left(X_0 + h, Y_0 + \frac{1}{2}\left[K_0 - 3K_1 + 4K_2\right]\right)$$

$$K_4 = hf\left(X_0 + \frac{1}{6}h, \; Y_0 + \frac{1}{648}\left[83K_0 + 32K_2 - 7K_3\right]\right)$$

$$K_5 = hf\left(X_0 + \frac{1}{3}h, \; Y_0 + \frac{1}{54}\left[-3K_0 - 4K_2 + K_3 + 24K_4\right]\right)$$

$$K_6 = hf\left(X_0 + \frac{1}{2}h, \; Y_0 + \frac{1}{5088}\left[-290K_0 - 524K_2 + 145K_3 \right.\right.$$
$$\left.\left. + 1908K_4 + 1305K_5\right]\right)$$

$$K_7 = hf\left(X_0 + \frac{2}{3}h, \; Y_0 + \frac{1}{1431}\left[292K_0 + 108K_2 + 13K_3 - 318K_4 \right.\right.$$
$$\left.\left. + 753K_5 + 106K_6\right]\right)$$

$$K_8 = hf\left(X_0 + \frac{5}{6}h, \; Y_0 + \frac{1}{68688}\left[14042K_0 + 11012K_2 - 4477K_3 \right.\right.$$
$$\left.\left. + 5724K_4 - 6903K_5 + 6360K_6 + 31482K_7\right]\right)$$

$$K_9 = hf\left(X_0 + h, \; Y_0 + \frac{1}{4346}\left[-2049K_0 - 18306K_2 + 839K_3 + 5724K_4 \right.\right.$$
$$\left.\left. - 4692K_5 + 12084K_6 - 9540K_7 + 3846K_8\right]\right)$$

The above equations are taken from reference 6-9 .

6.6.2 Multi-Step Techniques

The multi-step technique of interest for GMAS will be the same as for GTDS, namely the Adams-Cowell ordinate second sum. These formulas are of the Newtonian type and define the predictor-corrector Adams method for first-order equations and the Cowell method for second-order systems.

The Adams-Cowell predictor formulas as taken from reference 6.1 are

$$\dot{x}_{n+1} = h\left[{}^IS_n + \sum_{i=0}^{k} \beta_i \, \ddot{x}_{n-i}\right]$$

$$\tag{6.6-5}$$

$$x_{n+1} = h^2\left[{}^{II}S_n + \sum_{i=0}^{k} \alpha_i \, \ddot{x}_{n-i}\right]$$

where

$$^{I}S_n = \nabla^{-1}\ddot{x}_n$$

(6.6-6)

$$^{II}S_n = \nabla^{-2}\ddot{x}_n.$$

The quantities $\nabla^{-1}x(t)$ and $\nabla^{-2}x(t)$ are called the first and second sums of $x(t)$ and satisfy the relationships

$$\nabla^{-1}\ddot{x}(t) - \nabla^{-1}\ddot{x}(t-h) = \ddot{x}(t)$$

(6.6-7)

and

$$\nabla^{-2}\ddot{x}(t) - \nabla^{-2}\ddot{x}(t-h) = \nabla^{-1}\ddot{x}(t).$$

(6.6-8)

The Adams-Cowell corrector formulas are given in reference 6.1 as

$$\dot{x}_{n+1} = h\left[{}^{I}S_n + \sum_{i=0}^{k}\beta_i^{*}\,\ddot{x}_{n+1-i}\right]$$

(6.6-9)

$$x_{n+1} = h^2\left[{}^{II}S_n + \sum_{i=0}^{k}\alpha_i^{*}\,\ddot{x}_{n+1-i}\right]$$

The β_i and β_i^{*} are called the summed ordinate Adams-Moulton predicator-corrector coefficients and the α_i and α_i^{*} are the corresponding Stormer-Cowell coefficients. These coefficients are tabulated in reference 6.5 for formulas of order 4 through 15.

6.7   Attitude Model

The modeling of vehicle attitude in GMAS will not include any six-degree-of-freedom analysis since the detailed analysis of the attitude system is not the responsibility of GMAS. However, simple analytic models for attitude maneuvers from nominal cruse to nominal Δ V attitude and back again are discussed in Section 9.3. The vehicle attitude during various cruse segments will be stored for use in mission parameter computations that may involve the attitude.

6.8 References

6.1 W. E. Wagner and C. E. Velez. "Goddard Trajectory Determination Subsystem Mathematical Specifications." March, 1972.

6.2 W. Kaula. "Theory of Satellite Geodesy." Waltham, Mass. 1966.

6.3 W. H. Goodyear. "A General Method for the Computation of Cartesian Coordinates and Partial Derivatives of the Two-Body Problem." NASA CR-522. September, 1966.

6.4 Unknown. "Brouwer-Lyddane Analytic Orbit Theory." Excerpt from personal communication with A. Fuchs (GSFC).

6.5 J. L. Maury and G. P. Brodsky. "Cowell Type Numerical Integration as Applied to Satellite Orbit Computation." Goddard Space Flight Center 553-69-46. December, 1969.

6.6 D. A. Lutzky, W. S. Bjorkman and C. Uphoff. Final Report for Radio Astronomy Explorer-B In-Flight Mission Control System Development Effort. Analytic Mechanics Associates, Inc. Report No. 73-8 under Contract No. NAS5-11900. March, 1973.

6.7 C. Uphoff. Numerical Averaging in Orbit Prediction. AIAA Paper 72-934. September, 1972.

6.8 C. E. Velez and A. J. Fuchs. "A Review of Averaging Techniques and Their Application to Orbit Determination Systems." AIAA Paper 74-117. January, 1974.

6.9 D. A. Lutzky and C. Uphoff. Final Report for In-Flight Mission Control System Design Study. Analytic Mechanics Associates, Inc. Report No. 71-23 under Contract No. NAS5-11796. April, 1971.

$$C_{\mu}(t) = -\frac{\bar{R}}{R^3} \qquad (6.8\text{-}4)$$

$$C_{\mu_k}(t) = \frac{(\bar{R}_k - \bar{R})}{|\bar{R}_k - \bar{R}|^3} - \frac{\bar{R}_k}{R_k^3} \qquad (6.8\text{-}5)$$

6.8.2 Gravitational Harmonics

As was the case in Section 6.2.2, a central body-fixed coordinate frame is used, with the final result being rotated to inertial system for integration. The notation a(t), b(t), and c(t) will be used for the body-fixed frame. The matrix a(t) is given by

$$a(t) = \frac{\partial}{\partial \bar{r}_b}\left(\frac{\partial \psi}{\partial r}\right)\frac{\partial r}{\partial \bar{r}_b} + \frac{\partial}{\partial \bar{r}_b}\left(\frac{\partial \psi}{\partial \phi}\right)\frac{\partial \phi}{\partial \bar{r}_b} + \frac{\partial}{\partial \bar{r}_b}\left(\frac{\partial \psi}{\partial \lambda}\right)\frac{\partial \lambda}{\partial \bar{r}_b}$$

$$ \qquad (6.8\text{-}6)$$

$$+ \frac{\partial \psi}{\partial r}\frac{\partial^2 r}{\partial \bar{r}_b^2} + \frac{\partial \psi}{\partial \phi}\frac{\partial^2 \phi}{\partial \bar{r}_b^2} + \frac{\partial \psi}{\partial \lambda}\frac{\partial^2 \lambda}{\partial \bar{r}_b^2} \ .$$

where the partials for the first three terms are given by

$$\frac{\partial}{\partial \bar{r}_b}\begin{bmatrix} \partial \psi/\partial r \\[6pt] \partial \psi/\partial \phi \\[6pt] \partial \psi/\partial \lambda \end{bmatrix} = \begin{bmatrix} \dfrac{\partial^2 \psi}{\partial r^2} & \dfrac{\partial^2 \psi}{\partial r \partial \phi} & \dfrac{\partial^2 \psi}{\partial r \partial \lambda} \\[10pt] \dfrac{\partial^2 \psi}{\partial \phi \partial r} & \dfrac{\partial^2 \psi}{\partial \phi^2} & \dfrac{\partial^2 \psi}{\partial \phi \partial \lambda} \\[10pt] \dfrac{\partial^2 \psi}{\partial \lambda \partial r} & \dfrac{\partial^2 \psi}{\partial \lambda \partial \phi} & \dfrac{\partial^2 \psi}{\partial \lambda^2} \end{bmatrix}\begin{bmatrix} \partial r/\partial \bar{r}_b \\[6pt] \partial \phi/\partial \bar{r}_b \\[6pt] \partial \lambda/\partial \bar{r}_b \end{bmatrix} \qquad (6.8\text{-}7)$$

and the terms of the second partial matrix are given by

$$\frac{\partial^2 \psi}{\partial r^2} = \frac{\mu}{r^3}\sum_{n=2}^{N}\left(\frac{a_p}{r}\right)^n (n+2)(n+1)\sum_{m=0}^{n}(C_n^m \cos m\lambda + S_n^m \sin m\lambda)\,\Gamma_n^m(\sin \phi)$$

$$ \qquad (6.8\text{-}8)$$

$$\frac{\partial^2 \psi}{\partial r \partial \phi} = \frac{\partial^2 \psi}{\partial \phi \partial r} = -\frac{\mu}{r^3}\sum_{n=2}^{N}\left(\frac{a_p}{r}\right)^n (n+1)\sum_{m=0}^{n}(C_n^m \cos m\lambda + S_n^m \sin m\lambda)\times$$

$$ \qquad (6.8\text{-}9)$$

$$[\Gamma_n^{m+1}(\sin \phi) - m \tan \phi \, \Gamma_n^m(\sin \phi)]$$

$$\frac{\partial^2 \psi}{\partial r \, \partial \lambda} = \frac{\partial^2 \psi}{\partial \lambda \, \partial r} = -\frac{\mu}{r^3} \sum_{n=2}^{N} \left(\frac{a_p}{r}\right)^n (n+1) \sum_{m=0}^{n} m \left(S_n^m \cos m\lambda - C_n^m \sin m\lambda\right) P_n^m (\sin\phi)$$

$$(6.8\text{-}10)$$

$$\frac{\partial^2 \psi}{\partial \phi^2} = \frac{\mu}{r} \sum_{n=2}^{N} \left(\frac{a_p}{r}\right)^n \sum_{m=0}^{n} \left(C_n^m \cos m\lambda + S_n^m \sin m\lambda\right) \{ \tan\phi \, P_n^{m+1} (\sin\phi)$$

$$(6.8\text{-}11)$$

$$+ \left[m^2 \sec^2 \phi - m \tan^2 \phi - n(n+1)\right] P_n^m (\sin\phi)\}$$

$$\frac{\partial^2 \psi}{\partial \phi \, \partial \lambda} = \frac{\partial^2 \psi}{\partial \lambda \, \partial \phi} = \frac{\mu}{r} \sum_{n=2}^{N} \left(\frac{a_p}{r}\right)^n \sum_{m=0}^{n} m \left(S_n^m \cos m\lambda - C_n^m \sin m\lambda\right) (P_n^{m+1} (\sin\phi)$$

$$(6.8\text{-}12)$$

$$- m \tan\phi \, P_n^m (\sin\phi))$$

$$\frac{\partial^2 \psi}{\partial \lambda^2} = -\frac{\mu}{r} \sum_{n=2}^{N} \left(\frac{a_p}{r}\right)^n \sum_{m=0}^{n} m^2 \left(C_n^m \cos m\lambda + S_n^m \sin m\lambda\right) P_n^m (\sin\phi) \qquad (6.8\text{-}13)$$

The partials of ψ in the last three terms of equation (6.8-6) were given in equation (6.2-5), the second partials with respect to $\bar{r}_b$ are given by

$$\frac{\partial^2 r}{\partial \bar{r}_b^2} = \frac{1}{r} \left[I - \frac{\bar{r}_b \, \bar{r}_b^T}{r^2} \right] \qquad (6.8\text{-}14)$$

$$\frac{\partial^2 \phi}{\partial \bar{r}_b^2} = -\frac{1}{(x_b^2 + y_b^2)^{3/2}} \left[\left(\frac{\partial z_b}{\partial \bar{r}_b}\right)^T - \frac{z_b \bar{r}_b}{r^2} \right] \left[x_b \left(\frac{\partial x_b}{\partial \bar{r}_b}\right) + y_b \left(\frac{\partial y_b}{\partial \bar{r}_b}\right) \right]$$

$$(6.8\text{-}15)$$

$$- \frac{1}{r^2 \sqrt{x_b^2 + y_b^2}} \left[\bar{r}_b \left(\frac{\partial z_b}{\partial \bar{r}_b}\right) + z_b I - \frac{2 z_b}{r^2} \bar{r}_b \, \bar{r}_b^T \right]$$

$$\frac{\partial^2 \lambda}{\partial \bar{r}_b^2} = -\frac{2}{(x_b^2 + y_b^2)} \begin{bmatrix} -y_b \\ x_b \\ 0 \end{bmatrix} \left[x_b \left(\frac{\partial x_b}{\partial \bar{r}_b}\right) + y_b \left(\frac{\partial y_b}{\partial \bar{r}_b}\right) \right] + \frac{1}{(x_b^2 + y_b^2)} \begin{bmatrix} 0 & -1 & 0 \\ 1 & 0 & 0 \\ 0 & 0 & 0 \end{bmatrix} \quad (6.8\text{-}16)$$

where $\partial x_b / \partial \bar{r}_b$, $\partial y_b / \partial \bar{r}_b$, and $\partial z_b / \partial \bar{r}_b$ are (1, 0, 0), (0, 1, 0), and (0, 0, 1), respectively.

The $c(t)$ matrix is partitioned into c_C and c_S corresponding to the two types of harmonics and is given by

$$c_C = \frac{\partial}{\partial C_n^m}\left(\frac{\partial \psi}{\partial r}\right)\frac{\partial r}{\partial \bar{r}_b} + \frac{\partial}{\partial C_n^m}\left(\frac{\partial \psi}{\partial \phi}\right)\frac{\partial \phi}{\partial \bar{r}_b} + \frac{\partial}{\partial C_n^m}\left(\frac{\partial \psi}{\partial \lambda}\right)\frac{\partial \lambda}{\partial \bar{r}_b} \qquad (6.8\text{-}17)$$

$$c_S = \frac{\partial}{\partial S_n^m}\left(\frac{\partial \psi}{\partial r}\right)\frac{\partial r}{\partial \bar{r}_b} + \frac{\partial}{\partial S_n^m}\left(\frac{\partial \psi}{\partial \phi}\right)\frac{\partial \phi}{\partial \bar{r}_b} + \frac{\partial}{\partial S_n^m}\left(\frac{\partial \psi}{\partial \lambda}\right)\frac{\partial \lambda}{\partial \bar{r}_b} \qquad (6.8\text{-}18)$$

where the necessary second partials are given by

$$\frac{\partial}{\partial C_n^m}\begin{bmatrix}\partial\psi/\partial r \\ \partial\psi/\partial \phi \\ \partial\psi/\partial \lambda\end{bmatrix} = \left(\frac{\mu}{r}\right)\left(\frac{a_p}{r}\right)^n \begin{bmatrix} -\frac{1}{r}(n+1)\cos m\lambda\, P_n^m(\sin\phi) \\ \cos m\lambda\,[P_n^{m+1}(\sin\phi) - m\tan\phi\, P_n^m(\sin\phi)] \\ -m\sin m\lambda\, P_n^m(\sin\phi) \end{bmatrix} \qquad (6.8\text{-}19)$$

$$\frac{\partial}{\partial S_n^m}\begin{bmatrix}\partial\psi/\partial r \\ \partial\psi/\partial \phi \\ \partial\psi/\partial \lambda\end{bmatrix} = \left(\frac{\mu}{r}\right)\left(\frac{a_p}{r}\right)^n \begin{bmatrix} -\frac{1}{r}(n+1)\sin m\lambda\, P_n^m(\sin\phi) \\ \sin m\lambda\,[P_n^{m+1}(\sin\phi) - m\tan\phi\, P_n^m(\sin\phi)] \\ m\cos m\lambda\, P_n^m(\sin\phi) \end{bmatrix} \qquad (6.8\text{-}20)$$

6.8.3 Atomspheric Drag

The matrices for drag are given by

$$B(t) = -\frac{C_D A}{2 m_0}\, \rho \left\{ \frac{\bar{V}_{REL}\, \bar{V}_{REL}^T}{V_{REL}} + V_{REL}\, I \right\} \qquad (6.8\text{-}21)$$

$$A(t) = \frac{\ddot{\bar{R}}_D}{\rho}\left(\frac{\partial \rho}{\partial \bar{R}}\right) - \frac{\partial \ddot{\bar{R}}_D}{\partial \bar{R}}\, \Omega_\omega . \qquad (6.8\text{-}22)$$

where the notation was defined in Section 6.2.3. The relative velocity $\overline{V}_{REL}$ has been re-written as

$$\overline{V}_{REL} = \dot{\overline{R}} - \Omega_\omega \overline{R}$$

(6.8-23)

where Ω_ω is given by

$$\Omega_\omega = \begin{bmatrix} 0 & -\omega_z & \omega_y \\ \omega_z & 0 & -\omega_x \\ -\omega_y & \omega_x & 0 \end{bmatrix}$$

(6.8-24)

The partial of ρ necessary in equation (6.8-22) is given by

$$\frac{\partial \rho}{\partial \overline{R}} = \left(\frac{\partial \rho}{\partial \rho_m} \frac{\partial \rho_m}{\partial h} + \frac{\partial \rho}{\partial \rho_M} \frac{\partial \rho_M}{\partial h} \right) \frac{\partial h}{\partial \overline{R}} + \frac{\partial \rho}{\partial \psi} \frac{\partial \psi}{\partial R}$$

(6.8-25)

where

$$\frac{\partial \rho}{\partial \rho_m} = \left(1 - \cos^n \frac{\psi}{2} \right) \left(1 + \rho_3 \cos^n \frac{\psi}{2} \right)$$

(6.8-26)

$$\frac{\partial \rho}{\partial \rho_M} = \cos^n \frac{\psi}{2} \left(1 + \rho_3 \cos^n \frac{\psi}{2} \right)$$

(6.8-27)

$$\frac{\partial \rho_m}{\partial h} = - \frac{\rho_m}{H_m}$$

(6.8-28)

$$\frac{\partial \rho_M}{\partial h} = - \frac{\rho_M}{H_M}$$

(6.8-29)

The partial derivative of density with respect to ψ and the partial of ψ with respect to $\bar{R}$ are

$$\frac{\partial \rho}{\partial \psi} = -\frac{n}{2} \cos^{n-1}\frac{\psi}{2} \sin\frac{\psi}{2} \left\{ (\rho_M - \rho_m) \left(1 + \rho_3 \cos^n\frac{\psi}{2}\right) \right.$$

$$\left. + \rho_3 \left[\rho_m + (\rho_M - \rho_m) \cos^n\frac{\psi}{2}\right] \right\} \tag{6.8-30}$$

$$\frac{\partial \psi}{\partial \bar{R}} = \frac{1}{\sin\psi} \left[\left(\frac{\bar{R}\cdot\bar{U}_B}{R^3}\right) \bar{R} - \frac{\bar{U}_B}{R}\right]. \tag{6.8-31}$$

The partial of h in equation (6.8-25) is given by

$$\frac{\partial h}{\partial \bar{R}} = \frac{\bar{R}}{R} - R_e \left\{ \frac{(1-f)(2f-f^2)\cos\delta}{[1-(2f-f^2)\cos^2\delta]^{3/2}} \right\} \frac{\partial(\cos\delta)}{\partial \bar{R}} \tag{6.8-32}$$

where

$$\frac{\partial(\cos\delta)}{\partial \bar{R}} = \frac{1}{R^4 \cos\delta} \begin{bmatrix} X\,Z^2 \\ Y\,Z^2 \\ -Z\,(X^2+Y^2) \end{bmatrix}. \tag{6.8-33}$$

The quantities ρ, ρ_m, ρ_M, H_m, H_M, h, ρ_1, ρ_2, ρ_3 and $\bar{U}_B$ are related to the drag co-efficient and atmospheric density model as described in Reference 6.1. The latitude of the sub-satellite point is δ and the angle ψ is given by

$$\psi = \cos^{-1}\left(\frac{\bar{R}\cdot\bar{U}_B}{R}\right) \tag{6.8-34}$$

The C matrix component relating to the model parameter ρ_1, is given by

$$C(t) = \frac{R_{DRAG}}{(1+\rho_1)} \qquad (6.8\text{-}35)$$

6.8.4 Solar Radiation Power

The $A(t)$ matrix is given by

$$A(t) = \nu \frac{P_s \, R_{sun}^2 \, \gamma \, A}{m_0 \, |\bar{R} - \bar{R}_s|^3} \left[I - \frac{3 \, [\bar{R} - \bar{R}_s] \, [\bar{R} - \bar{R}_s]^T}{|\bar{R} - \bar{R}_s|^2} \right] \qquad (6.8\text{-}36)$$

where the notation is the same as in Section 6.2.4.. The component of the C matrix for the model parameter k defined by

$$k = \frac{P_s \, A}{m_0} \qquad (6.8\text{-}37)$$

is given by

$$C(t) = \nu \, R_{sun}^2 \, \gamma \, \frac{[\bar{R} - \bar{R}_s]}{|\bar{R} - \bar{R}_s|^3} \qquad (6.8\text{-}38)$$

6.8.5 Finite Thrust

Since acceleration due to thrust engines is independent of the spacecraft state both $A(t)$ and $B(t)$ are zero. The C matrix components for the model parameters a_0, ..., a_4 defined in Section 6.2.5 are

$$C_a(t) = \frac{\ddot{R}_{THRUST}}{a} \, \Gamma^T \qquad (6.8\text{-}39)$$

and for the parameters $\alpha_0, \ldots, \alpha_4$ and $\delta_0, \ldots, \delta_4$

$$C_\alpha(t) = a\left\{u(t-T_0)-u(t-T_f)\right\} G^T U_\alpha \Gamma^T \qquad (6.8-40)$$

$$C_\delta(t) = a\left\{u(t-T_0)-u(t-T_f)\right\} G^T U_\delta \Gamma^T \qquad (6.8-41)$$

where G^T is the transformation from the true of epoch to the mean of 1950.0 system. The matrices Γ^T, U_α and U_δ are defined by

$$\Gamma^T = \left[1, \gamma, \gamma^2, \gamma^3, \gamma^4\right] \qquad (6.8-42)$$

$$U_\alpha = \begin{bmatrix} -\sin\alpha_T\cos\delta_T \\ \cos\alpha_T\cos\delta_T \\ 0 \end{bmatrix} \qquad (6.8-43)$$

$$U_\delta = \begin{bmatrix} -\cos\alpha_T\sin\delta_T \\ -\sin\alpha_T\sin\delta_T \\ \cos\delta_T \end{bmatrix} \cdot \qquad (6.8-44)$$

The results of integrating the variational equations to obtain the state transition matrices under certain simplifying assumptions are discussed in Section 13.3.

7. MISSION ANALYSIS PARAMETERS

7.1 Introduction

Mission analysis parameters are used for both mission design and mission control. When used in mission design they are most usefully made functions of the orbital elements and can usually be evaluated through analytical methods. When the mission analysis parameters are used for mission control, a requirement is levied for recognition of changes in the parameters as the mission progresses. Because mission control parameters are usually computed from instantaneous numerical values of position and velocity, numerical analysis methods are indicated. This distinction between analytical and numerical analysis methods has generally been preserved in the following discussions.

7.2 Geodetic Data and Ground Tracks

The geodetic data and ground track data are calculated from the position vector (x, y, z) in Earth-referenced coordinates and the flattening of the Earth. The calculations (Ref. 7-1) are in closed form and are used in both the numerical analysis methods and the approximate analytical solutions.

Geodetic latitude $\phi*$ is

$$\phi* = \tan^{-1} \frac{z}{(x^2 + y^2)^{\frac{1}{2}}(1 - f)^2} \qquad (7.2-1)$$

Geocentric latitude ϕ is

$$\phi = \tan^{-1} \frac{z}{(x^2 + y^2)^{\frac{1}{2}}} \qquad (7.2-2)$$

Subvehicle latitude ϕ_v and longitude ℓ are

$$\phi_v = \delta + \sin^{-1}\left[\frac{f \sin 2\delta}{r} + \left(\frac{f^2}{4r}\right)\left(\frac{4}{r} - 1\right) \sin 4\delta \right] \qquad (7.2-3)$$

$$\ell = \alpha - \alpha_g - \omega_E(t - t_g) \qquad (7.2.4)$$

Altitude h is

$$h = r - \frac{R_E (1 - f)}{\left[1 - (2f - f^2) \frac{x^2 + y^2}{r^2}\right]^{\frac{1}{2}}} \qquad (7.2-5)$$

In the above equations

Right ascension α: $\quad \alpha = \tan^{-1}\left(\frac{y_I}{x_I}\right) \qquad (7.2-6)$

Declination δ: $\quad \delta = \tan^{-1} \frac{z_I}{(x_I^2 + y_I^2)^{\frac{1}{2}}} \qquad (7.2-7)$

Epoch time: t_g

Greenwich mean sidereal time: α_g

Earth rotation rate: ω_E

Earth radius: R_E

Radius of satellite r: $\quad r = (x_I^2 + y_I^2 + z_I^2)^{\frac{1}{2}} \qquad (7.2-8)$

Flattening f: $\quad f = \frac{R_{EQ} - R_P}{R_{EQ}} \qquad (7.2-9)$

For the subscripts, I indicates inertial coordinates, EQ indicates equatorial and P indicates polar.

7.3 Tracking

The tracking problem of calculating the rise and set times of a satellite from a ground station has two aspects: (1) the degree of sophistication of the types of problems solved, and (2) the methods used. The problems are, in a generally increasing order of complexity:

o appearance above the horizon,

o appearance above a given elevation angle for the entire azimuth range,

o appearance above an elevation angle which is dependent on azimuth, thus posing a realistic radar masking situation,

o computation of critical radar parameters at the times of certain events (such as azimuth, elevation, Doppler rate, range, range rates and aspect angles at times of acquisition, loss, zenith, etc.),

o computation of rises, sets and radar parameters relative to an Earth-synchronous communication satellite, and

o generalization of the circular area of tracking to an area of any ground shape, such as states and Earth-resources targets.

Secondly, the methods may vary: (1) continual checking of a rise-set function throughout the ephemeris of the satellite, (2) evaluating a closed-form analytical expression only a few times during an ephemeris. The first method is referred to as a numerical analysis method while the second is an analytical method.

7.3.1 Numerical Analysis Method

The trajectory is computed point by point to obtain the position vector $\underline{r}$ of the satellite which is used in the following expression along with $\underline{R}$, the position vector of the tracking

station. Both vectors are in inertial coordinates. When the fol-
lowing equation (Ref. 7-1) is true the satellite is rising above or
setting below a given elevation angle E_m.

$$\underline{r} \cdot \underline{R} - rR \cos(\pi/2 - E_m - \sin^{-1} \frac{R}{r} \cos E_m) = 0 \qquad (7.3-1)$$

When the left-hand expression goes from negative to positive, a
rise is indicated; from positive to negative, a set. If E_m is set
to zero, as is the case for a rise or set with respect to the hor-
izon, the equation becomes:

$$\underline{r} \cdot \underline{R} - R^2 = 0 \qquad (7.3-2)$$

That this is true is seen from the following figure.
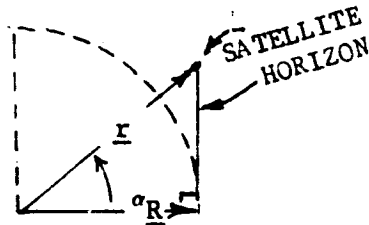
$$\underline{r} \cdot \underline{R} = rR \cos \alpha \qquad (7.3-3)$$

$$\cos \alpha = R/r \qquad (7.3-4)$$

$$\underline{r} \cdot \underline{R} = rR\left(\frac{R}{r}\right) = R^2 \qquad (7.3-5)$$

$$\underline{r} \cdot \underline{R} - R^2 = 0 \qquad (7.3-6)$$

The radar masking situation can be solved by evaluating az-
imuth and elevation pairs as the satellite passes over a station.
This gives a numerically-defined function E(Az). This function
minus an input function of the mask E_m(Az) gives another function

$$F(Az) = E_L(Az) - E_m(Az) \qquad (7.3-7)$$

The zeros of this function F give the azimuths and elevations of
the rising and setting points.

Azimuth Az and elevation E are found from:

$$Az = \tan^{-1} \frac{x_T}{y_T} \qquad (7.3-8)$$

$$E_L = \sin^{-1} \frac{z_T}{(x_T^2 + y_T^2 + z_T^2)^{\frac{1}{2}}} \qquad (7.3-9)$$

where (x_T, y_T, z_T) are the coordinates of the satellite in a top-
ocentric system at the station, x_T being to the East, y_T to the
North and z_T along the geodetic vertical.

Doppler rate Δf is found from

$$\Delta f = -K_D \, \dot{r} \, (1 - \frac{\dot{r}}{c}) \qquad (7.3-10)$$

where $\dot{r}$ is the range rate, K_D is a constant and c is the speed of light.

Attenuation A_t is

$$A_t = -40 \, \log_{10} r \qquad (7.3-11)$$

Aspect angles to the tracking station are given in terms of θ and ϕ. Theta (θ) is the angle between the roll axis and the line-of-sight to the ground station; phi (ϕ) is the angle between the negative "yaw" axis and the projection of the line-of-sight into the "roll" plane.

$$\tan \phi = - \frac{T_{yB}}{T_{zB}} \qquad (7.3-12)$$

$$\cos \theta = \frac{T_{xB}}{(T_{xB}^2 + T_{yB}^2 + T_{zB}^2)^{\frac{1}{2}}} \qquad (7.3-13)$$

Phi and theta depend on the attitude of the satellite (see matrix D below) and the position of the tracking station (T_{xI}, T_{yI}, T_{zI}) in inertial coordinates with respect to the satellite. T_{xI}, T_{yI}, and T_{zI} are components of the vector $\underline{T}_I$ which is found from

$$\underline{T}_I = \underline{R} - \underline{r} \qquad (7.3-14)$$

The vector (T_{xB}, T_{yB}, T_{zB}) is calculated from (Ref. 7-2)

$$\begin{bmatrix} T_{xB} \\ T_{yB} \\ T_{zB} \end{bmatrix} = [D][K] \begin{bmatrix} T_{xI} \\ T_{yI} \\ T_{zI} \end{bmatrix} \qquad (7.3-15)$$

D is the direction cosine matrix of the body-axis system with respect to an orbital reference system,

$$[D] = \begin{bmatrix} \cos(x_B, x_0) & \cos(x_B, y_0) & \cos(x_B, z_0) \\ \cos(y_B, x_0) & \cos(y_B, y_0) & \cos(z_B, z_0) \\ \cos(z_B, x_0) & \cos(z_B, y_0) & \cos(z_B, z_0) \end{bmatrix} \qquad (7.3-16)$$

The orbital reference system (ORS) is defined (Ref. 7-2) as centered at the satellite with x_0 along the radius vector, z_0 is the direction of the orbit pole and y_0 forming a dextral system. (NOTE: For a circular orbit, these axes are up, left and forward, respectively). The transformation matrix K takes the vector from the inertial to the ORS system and is a function of inclination i, right ascension Ω of the ascending node and θ, the sum of the argument of perigee ω_0 and true anomaly v.

$$[K] = \begin{bmatrix} \cos\theta\cos\Omega + \sin\theta\cos i \cos\Omega - \sin\theta\sin i \sin\Omega & \cos\theta\sin\Omega + \sin\theta\cos i & \cos\Omega\sin\theta\sin i \\ -\sin\theta\cos\Omega + \cos\theta\cos i \cos\Omega - \cos\theta\sin i \sin\Omega & -\sin\theta\sin\Omega + \sin\theta\cos i & \cos\Omega\cos\theta\sin i \\ \sin i \sin\Omega & -\sin i \cos\Omega & \cos i \end{bmatrix}$$

(7.3-17)

In case the attitude of the satellite is more easily expressed in inertial coordinates, D should be relative to the inertial system and K should be the identity matrix.

Tracking problems from an orbiting Earth-synchronous satellite can be solved in the same way as they were for ground-based stations. The position vector of the tracking satellite is used instead of the ground station. Computational time will be about the same as for ground stations, the major difference being that the radius vector of the tracking station is longer. Also, the value of the elevation angle E_m of acquisition will be approximately -80 degrees instead of the +5 or +10 used for ground stations.

The fact that the projection of a truncated tracking cone onto the surface of the Earth describes a circle suggests that the rise-set problems might also be solved by checking latitude and longitude of a satellite in circular orbit to see if the geodetic position falls within the circle. Thus passage over circular areas could easily be determined. Without any changes in the mathematics but at some cost in computer checking, these areas can be easily

extended to graticules (whose boundaries are lines of latitude and longitude) or even, with added mathematical sophistication, to irregularly shaped areas. Such extension (which has been programmed for Skylab) would be extremely valuable for Earth resources studies.

7.3.2 Analytical Method

The tracking problem can be attacked analytically by solving the following equation for the eccentric anomaly E at which the equation holds and then transforming to time (Ref. 7-3).

$$F(E) = a(\cos E - e)\underline{P} \cdot \underline{Z} + (a\sqrt{1-e^2}\sin E)\underline{Q} \cdot \underline{Z} - G - \rho(E)\sin E_m = 0 \quad (7.3\text{-}18)$$

(see Note next page)

This equation can be solved for E by using Newton's method:

$$E_{n+1} = E_n - \frac{F(E_n)}{F'(E_n)} \quad (7.3\text{-}19)$$

which is a quickly converging iterative method.

The derivative $F'(E_n)$ is given by

$$F'(E) = \left[a(\cos E - 1)(P_y Z_x + P_x Z_y) + \right.$$

$$\left. a\sqrt{1-e^2}\sin E(Q_y Z_x - Q_x Z_y) \right] \frac{1 - e\cos E}{n}\dot\theta +$$

$$\underline{Q} \cdot \underline{Z} \, a\sqrt{1-e^2}\cos E - \underline{P} \cdot \underline{Z} \, a\sin E \quad (7.3\text{-}20)$$

with the initial value of E on the right-hand side being evaluated by using an approximate value of E given by

$$E \cong \beta - \cos^{-1}\left[\frac{G + \underline{P} \cdot \underline{Z}\, ae}{a\sqrt{(\underline{P} \cdot \underline{Z})^2 + (\underline{Q} \cdot \underline{Z})^2(1-e^2)}} \right] \quad (7.3\text{-}21)$$

The starting value for $\rho(E)$, the slant range, in (7.3-18) is

$$\rho(E) = \left\{ \left[a^2(1 - e\cos E)^2 + G_0^2 \right] \right.$$

$$-2G_1 Z_x \left[a(\cos E - e)P_x + a\sqrt{1-e^2}\sin E\, Q_x \right]$$

$$-2G_1 Z_y \left[a(\cos E - e)P_y + a\sqrt{1-e^2}\sin E\, Q_y \right]$$

$$\left. -2G_1 Z_z \left[a(\cos E - e)P_z + a\sqrt{1-e^2}\sin E\, Q_z \right] \right\}^{\frac{1}{2}} \quad (7.3\text{-}22)$$

NOTE: The vectors in equation (7.3-18) are:

$$\underline{P} = \begin{bmatrix} P_x \\ P_y \\ P_z \end{bmatrix} \begin{bmatrix} \cos\omega\cos\Omega - \sin\omega\sin\Omega\cos i \\ \sin\omega\sin\Omega + \sin\omega\cos\Omega\cos i \\ \sin\omega\sin i \end{bmatrix} \qquad (7.3-23)$$

$$\underline{Z} = \begin{bmatrix} Z_x \\ Z_y \\ Z_z \end{bmatrix} = \begin{bmatrix} \cos\phi\cos(\theta_0 + \omega_E[\frac{E - e\ \sin E}{n} + T - t_0]) \\ \cos\phi\sin(\theta_0 + \omega_E[\frac{E - e\ \sin E}{n} + T - t_0]) \\ \sin\phi \end{bmatrix} \qquad (7.3-24)$$

$$\underline{Q} = \begin{bmatrix} Q_x \\ Q_y \\ Q_z \end{bmatrix} = \begin{bmatrix} -\sin\omega\cos\Omega - \cos\omega\sin\Omega\cos i \\ -\sin\omega\sin\Omega + \cos\omega\cos\Omega\cos i \\ \cos\omega\sin i \end{bmatrix} \qquad (7.3-25)$$

where $\omega \sim$ argument of perigee

$\Omega \sim$ right ascension of ascending node

$i \sim$ inclination

$\phi \sim$ station geodetic latitude

$\theta_0 \sim$ epoch station sidereal time in radius

$\omega_E \sim$ sidereal rate of change (Earth rotation rate)

$T \sim$ time of latest perigee passage

$n \sim$ mean motion $\qquad n = \dfrac{\sqrt{\mu}}{a^{3/2}}$ $\qquad\qquad$ (7.3-26)

$\mu \sim$ Earth gravitational constant, $\mu = GM_E$ $\qquad$ (7.3-27)

$G \sim$ universal gravitational constant

$M_E \sim$ mass of earth

$a \sim$ semi-major axis of orbit

$t_0 \sim$ epoch universal time

The variables in equation (7-27) not defined above are:

$$G = G_1 \cos^2\phi + G_2 \sin^2\phi \qquad (7.3-28)$$

$$G_1 = \frac{R_{EQ}}{\sqrt{1 - (2f - f^2)\sin^2\phi}} + h \qquad (7.3-29)$$

$$G_2 = \frac{(1-f)^2 R_{EQ}}{\sqrt{1 - (2f - f^2)\sin^2\phi}} + h \qquad (7.3-30)$$

where $f \sim$ flattening of Earth ellipsoid

$h \sim$ geodetic altitude of station above ellipsoid

$$\beta = \tan^{-1}\left[\frac{\underline{Q} \cdot \underline{Z}\sqrt{1 - e^2}}{\underline{P} \cdot \underline{Z}}\right] \text{and} \qquad (7.3-31)$$

$\rho \sim$ slant range from station to satellite

When E in (7.3-19) stops converging within a certain limit, the iterations are stopped and the time of rise or set can be found from

$$t = \frac{E - e \, \sin E}{n} + T \qquad (7.3-32)$$

If $F'(E)$ from (7.3-20) is positive, the satellite is rising; if negative, the satellite is setting.

After finding the rise and set times, future rise and set times can be found by adding multiples of the period. Then, using the value of the eccentric anomaly, the state vector in terms of orbital elements can be determined from well-known classical equations. Transformation from the orbital elements to Cartesian coordinates in both inertial and rotating Earth systems provide data with which to compute radar parameters given in equation (7.3-8) through (7.3-13).

7.4 Solar Geometry

The required parameters that depend on solar geometry are beta angle, aspect angles and times of shadowing. The beta angle is the angle between the Earth-Sun line and the orbit plane. Aside from being a variable that is useful in other calculations, it is a key parameter in satellite heating, solar power and surface lighting. Aspect angles relate the direction of the Sun's rays to the body-axis system of the satellite. Shadowing times are the times of sunset and sunrise on the satellite, related to both the penumbra and unbra of the Earth.

These are both analytical and numerical analysis methods for calculating shadowing; the methods of computing beta angle and aspect angles are analytical.

7.4.1 Analytical Methods

Beta Angle

The beta angle is computed from the following equations:

$$N_z = \sin i \, \sin \Omega \qquad (7.4\text{-}1)$$

$$N_y = \sin i \, \cos \Omega \qquad (7.4\text{-}2)$$

$$N_z = \cos i \qquad (7.4\text{-}3)$$

$$\underline{N} = (N_x, N_y, N_z) \qquad (7.4\text{-}4)$$

$$S_x = \cos \delta \, \cos \alpha \qquad (7.4\text{-}5)$$

$$S_y = \cos \delta \, \sin \alpha \qquad (7.4\text{-}6)$$

$$S_z = \sin \delta \qquad (7.4\text{-}7)$$

$$\underline{S} = (S_x, S_y, S_z) \qquad (7.4\text{-}8)$$

$$\beta = \sin^{-1}(\underline{N} \cdot \underline{S}) \qquad (7.4\text{-}9)$$

where i is the orbit inclination, Ω is the right ascension of the ascending node of the orbit, δ is the declination of the Sun and α is the right ascension of the Sun.

Beta can be expanded in terms of the orbital elements i and Ω by

$$\sin \beta = \sin i \, \sin \Omega \cos \delta \cos \alpha - \sin i \cos \Omega \cos \delta \sin \alpha + \cos i \, \sin \delta \qquad (7.4\text{-}10)$$

This equation is convenient for finding sensitivities to the orbital elements i and Ω by differentiating it.

Aspect Angles

Aspect angles give the relation of the rays of the sun to the body axes of the satellite. One of these angles (θ) is the angle between the "roll" axis and the rays; the other angle (ϕ) is between the negative "yaw" axis and the projection of the rays into the "roll" plane. In an attitude control mode where the roll (spin) axis is perpendicular to the orbit plane, the beta angle itself gives the total aspect angle.

In a local vertical attitude control mode (with the "yaw" axis along the vertical), the angle α gives the total aspect angle where

$$\cos\alpha = \cos\nu\cos\beta \tag{7.4-11}$$

with ν being the central angle at the central body between the satellite and the point in its orbit where the Sun is closest to its zenith (i.e., "orbital noon"). The aspect angles θ and ϕ are found from:

$$\begin{bmatrix} S_x \\ S_y \\ S_z \end{bmatrix}_B = \begin{bmatrix} -\sin\nu & \cos\nu & 0 \\ 0 & 0 & -1 \\ -\cos\nu & -\sin\nu & 0 \end{bmatrix} \begin{bmatrix} \cos\beta \\ 0 \\ \sin\beta \end{bmatrix} \tag{7.4-12}$$

with subscript B indicating that the Sun vector is in the body axis system. Then θ and ϕ are calculated from (Ref. 7-1).

$$\cos\theta = \frac{S_x}{(S_x^2 + S_y^2 + S_z^2)^{\frac{1}{2}}} \tag{7.4-13}$$

$$\tan\phi = \frac{-S_y}{S_z} \tag{7.4-14}$$

In the inertial attitude control mode, with the attitude of the satellite given by a 3 x 3 matrix M of direction cosines of the body axes relative to the inertial axes and the Sun position given by (S_x, S_y, S_z) in the inertial system, the components of the Sun in the body axis system are:

$$\begin{bmatrix} S_x \\ S_y \\ S_z \end{bmatrix}_B = [M] \begin{bmatrix} S_x \\ S_y \\ S_z \end{bmatrix}_I \tag{7.4-15}$$

with the I subscript indicating the inertial system and

$$[M] = \begin{bmatrix} \cos(x_B, x_I) & \cos(x_B, y_I) & \cos(x_B, z_I) \\ \cos(y_B, y_I) & \cos(y_B, y_I) & \cos(y_B, z_I) \\ \cos(z_B, z_I) & \cos(z_B, z_I) & \cos(z_B, z_I) \end{bmatrix} \tag{7.4-16}$$

Then θ and ϕ are calculated as in (7.4-13 and 14 above).

Shadowing

To obtain the times of shadowing, we equate (Ref. 7-4) the radius vector at entrance (sunset) or exit (sunrise) of the shadow to the analytical expression of the radius vector,

$$\rho = \frac{R}{\sin(\alpha + \psi)} \qquad (7.4\text{-}17)$$

and

$$r = \frac{p}{1 + e \cos(\theta + \gamma_i)} \qquad (7.4\text{-}18)$$

that is,

$$\frac{R}{\sin(\alpha + \psi)} = \frac{p}{1 + e \cos(\theta + \gamma_i)} \qquad (7.4\text{-}19)$$

with ψ related to θ through the pseudo-beta angle by

$$\cos\psi = \cos\beta \cos\theta. \qquad (7.4\text{-}20)$$

Here $d_i \sim$ cone angle of the penumbra or umbra,

$$i = u \text{ or } p \qquad (7.4\text{-}21)$$

for umbra or penumbra and

$$\alpha_u = \frac{r_\theta - R_E}{d} \qquad (7.4\text{-}22)$$

$$\alpha_p = \frac{r_\theta - R_E}{d} \qquad (7.4\text{-}23)$$

$d \sim$ distance from Earth to Sun

$R_r \sim$ radius of Earth

$r_\theta \sim$ radius of sun

$\psi \sim$ angle between anti-solar point α_p and spacecraft at entrance or exit,

$\beta \sim$ pseudo-beta angle, measured between orbit plane and anti-solar point,

$\theta \sim$ Central angle measured from entrance or exit to the orbit midnight point,

$\gamma_i \sim$ argument of perigee measured from the orbital midnight point (point on orbit where spacecraft is closest to anti-solar point or projection of anti-solar line on orbit plane),

$p \sim$ semi-latus rectum, $p = a(1-e)$ (7.4-24)

NOTE: $\gamma_p = \gamma_u - \pi$

There are two methods for finding θ. The first is to step around the orbit in values of θ until P from (7-53) is equal to r from (7-54). Since θ moves in discrete steps and the point of equality will not in general be exactly found, a simple Bolzano interval-halving scheme will find values of θ.

The second method (Ref. 7-5) is to solve the equality (3) of P and r which gives a quartic in $\cos\theta$:

$$(C_4 \cos^4\theta + C_3 \cos^3\theta + C_2 \cos^2\theta + C_1 \cos\theta + C_0 = 0 \qquad (7.4\text{-}25)$$

where

$$C_4 = c^2 - d^2 \qquad (7.4\text{-}26)$$

$$C_3 = -2bc \qquad (7.4\text{-}27)$$

$$C_2 = b^2 + 2ac + d^2(1 + \cos^2\beta) \qquad (7.4\text{-}28)$$

$$C_1 = -2ab \qquad (7.4\text{-}29)$$

$$C_0 = a^2 - d^2 \cos^2\beta \qquad (7.4\text{-}30)$$

with

$$a = (p \sin\alpha\cos\beta - Re\cos\gamma)^2 + (Re\sin\gamma)^2 + (p \cos\alpha\cos\delta)^2 \qquad (7.4\text{-}31)$$

$$b = 2R(p \sin\alpha\cos\delta - Re\cos\gamma) \qquad (7.4\text{-}32)$$

$$c = R^2(1-e^2 \sin^2\gamma) - p^2 \cos^2\alpha \qquad (7.4\text{-}33)$$

$$d = 2p \, Re \sin\gamma\cos\alpha \qquad (7.4\text{-}34)$$

Quadrant checks will place θ in the correct quadrant.

Once θ is found, the time relative to the perigee point can be found from $\theta + \gamma = v$ (the true anomaly by (Ref. 7-6).

$$\Delta t = \frac{a^{3/2}}{\sqrt{\mu_E}} \left\{ 2 \tan^{-1} \sqrt{\frac{1-e}{1+e}} \tan \tfrac{1}{2}v - e \frac{\sqrt{1-e^2} \sin v}{1+e \cos v} \right\} * \qquad (7.4\text{-}35)$$

μ_E being the gravitational constant (GM) for the Earth. Here G is the universal gravitational constant and M is the mass of the Earth.

Since the semi-latus rectum p appearing in (7.4-18) is a function of a and e, the sensitivity of Δt with respect to a or e can be found by numerical differencing.

7.4.2 Numerical Analysis Method

Beta Angle

The beta angle is computed using the instantaneous state vector from equations (7.4-8) and (7.4-9) on beta angle. However, the vector components in (7.4-4) of the orbit normal vector N must be generated by x, y, z, $\dot{x}$, $\dot{y}$, and $\dot{z}$.

The equations then become

$$\underline{P} = (x, y, z) \tag{7.4-36}$$

$$\underline{V} = (\dot{x}, \dot{y}, \dot{z}) \tag{7.4-37}$$

$$\underline{N} = \frac{\vec{P} \times \vec{V}}{|\vec{P}| \times |\vec{V}|} \tag{7.4-38}$$

$$\underline{S} = (S_x, S_y, S_z)/|\underline{S}| \tag{7.4-39}$$

$$\beta = \sin^{-1}(\vec{N} \cdot \vec{S}) \tag{7.4-40}$$

where $\underline{S}$ is the vector from Earth to Sun. $\underline{N}$ and $\underline{S}$ must be put in the same coordinate system.

Shadowing

Shadowing data are calculated in essentially the same way as the first analytical method; using the step-by-step integrated values from an ephemeris to find a function indicative of passing through the shadow cone (Ref. 7-5). In calculating the shadowing from an ephemeris, the stepping is done in terms of the position vector $\underline{r}$.

$$\underline{r} = (x, y, z) \tag{7.4-41}$$

$$\theta = \cos^{-1}(\underline{r} \cdot \underline{B})/|\underline{r}||\underline{S}| \tag{7.4-42}$$

$$D_u = \left\{ |\underline{r}| \sin\theta + (|\underline{r}| \cos\theta - \frac{R_E}{\sin\alpha}) \tan d_u \right\} \left\{ \cos\alpha_u \right\} \tag{7.4-43}$$

$$D_p = \left\{ |\underline{r}| \sin\theta - (|\underline{r}| \cos\theta - \frac{R_E}{\sin\alpha}) \tan d_p \right\} \left\{ \cos\alpha_p \right\} \tag{7.4-44}$$

α_p and α_u are defined by (7-58) and (7-59) of the previous section. D_u and D_p are the distance functions to the umbra and penumbra cones respectively.

When the shadow function D_u or D_p passes through zero, a sunset or sunrise is indicated and exactly determined by a Newton-Raphson iteration. The sign of the derivative determines sunset or sunrise - sunset if negative, sunrise if positive. The derivative is calculated by

$$\frac{dD}{dt} = \underline{V} \cdot \hat{Z} \tag{7.4-45}$$

$$\underline{N} = \frac{(\underline{P} \times \underline{S})}{\underline{P} \times \underline{S}} = (N_x, N_y, N_z) \tag{7.4-46}$$

$$\left[\hat{Z}' \right] = \begin{bmatrix} -\sin\alpha \\ \cos\alpha \\ 0 \end{bmatrix} \tag{7.4-47}$$

$$\underline{2} = (\underline{N} \times -\underline{P})/|-\underline{P}| = (2_x, 2_y, 2_z) \tag{7.4-48}$$

$$\hat{2} = \begin{bmatrix} -X/S & 2_x & N_x \\ -Y/S & 2_y & N_y \\ -Z/S & 2_z & N_z \end{bmatrix} \left[\hat{2}' \right] \tag{7.4-49}$$

7.5 Sensor Coverage and Resolution

Optical, radar, infrared and ultraviolet sensors operate on similar principles as far as coverage is concerned, i.e., they all operate within the electromagnetic theory, have a field of view, a resolving power, etc. Here the emphasis is on optical sensors with later extensions to be made to the longer radar and infrared wave lengths and the shorter ultraviolet wave lengths. Optical sensors are discussed with respect to both astronomy and Earth-viewing missions.

7.5.1 Astronomy

Given a sensor pointing program that directs the sensor at a point on the celestial sphere defined by right ascension α_0 and declination δ_0 with a half-angle field of view of ρ, the boundaries of the coverage circle on the celestial sphere are given by (Ref. 7-7).

$$\sin\delta = \sin\delta_0 \cos\rho + \cos\delta_0 \sin\rho \cos\theta \qquad (7.5-1)$$

$$\sin\Delta\alpha = \frac{\sin\rho \sin\theta}{\cos\delta} \qquad (7.5-2)$$

where θ is an azimuth parameter and

$$\Delta\alpha = \left| \alpha - \alpha_0 \right| \qquad (7.5-3)$$

Various scanning patterns, such as toruses, can be based on these equations.

Given a table of astronomy objectives in terms of right ascension and declination, an opportunity program can be written to determine when the objectives fall within the coverage circle. This scheme is especially adaptable for graphical display.

A first-order approach at resolution is based on a diffraction-limited (perfect) telescope and using the Rayleigh criterion. The resolution between two point sources is given as the angular separation γ; given the wave length of the light of interest and the decimeter D of other aperture this is:

$$\gamma = \frac{1.22}{D} \tag{7.5-4}$$

The image tube resolution is given as d, the separation in millimeters between lines on the image tube, with γ in arc seconds as

$$d = \frac{C_1 \gamma}{P_s} \tag{7.5-5}$$

where C_1 is a multiplying factor resulting from energy lost by secondary obscuration, wave front errors and pointing errors (C_1 is often as 1.5). P_s in (7-83) is the plate scale in arc sec/mm and is given by

$$P_s = \frac{2 \tan^{-1} \frac{1}{2F}}{D} \tag{7.5-6}$$

where F is the ratio of camera focal length to telescope aperture D in millimeters.

Knowing the line separation d, the bit rate of transmission k, the bits/pixel b, the square image tube dimension x in mm and the required sampling rate s in samples/cycle, the time required to transmit one x X x picture is

$$t = \frac{\left[\left(\frac{1}{d}\right) sx\right]^2}{k} b \tag{7.5-7}$$

Typical values used are d = 26 mm, s = 3 samples/cycle, x = 50 mm, k = 500 kilobits/second and b = 8 bits/pixel. Transmission times are important for deciding whether to transmit in real time or dump to tape.

7.5.2 Earth-viewing

The coverage area on the Earth, unlike on the celestial sphere, is not bounded by a circle because of the generally varying distances to the points of the boundary. The input variables are:

$d \sim$ depression angle of the instrument centerline

$y \sim$ yaw angle of the instrument centerline, measured from the forward direction of the satellite

$\rho \sim$ half-angle field of view

$\alpha_0 \sim$ longitude of sub-satellite point

$\lambda_0 \sim$ longitude of sub-satellite point

$\alpha_{AN} \sim$ longitude of the ascending node

$r \sim$ total regression rate of the ascending node

$h \sim$ altitude of satellite

$i \sim$ inclination of orbit

The elements of the cone are computed by stepping around the apex of the cone, in say, 10 degree increments of θ. The central angle ϕ_H at the center of the Earth is computed from

$$\phi_H = \cos^{-1} \frac{R_E}{R_E + h} \tag{7.5-8}$$

R_E being the radius of the Earth. Then the angle d_E is computed from

$$d_E = \sin^{-1} \left[\cos\rho\sin d + \sin\rho\cos d\cos\theta \right] \tag{7.5-9}$$

If d_E is greater than ϕ_H, the cone element does not intercept the Earth and boundary points lie on the horizon circle. These boundary points are denoted by α_H, λ_H. If d_E is less than ϕ_H, the cone elements do intercept the Earth and the boundary points α_I, λ_I on the interception boundary are located.

The azimuth A_z for each θ is computed from

$$A_z = \sin^{-1}(\cos i/\cos\lambda_0) + y + \sin^{-1} \left(\frac{\sin\rho \, \sin\theta}{\cos\phi}\right) \tag{7.5-10}$$

For the interception case, the central angle ϕ_I is

7.5-3

$$\phi_I = \sin^{-1}\left[\frac{R_E + h}{R_E}\sqrt{1 - (\cos\rho\sin d + \sin\rho\cos d\cos\theta)^2}\right] \quad (7.5\text{-}11)$$

Then the coordinates of the boundary points whether it lie on the horizon or in the intercept and located by:

$$\lambda_k = \sin^{-1}(\cos\phi_k \sin\lambda_0 + \sin\phi_k \cos\lambda_0 \cos A_z) \quad (7.5\text{-}12)$$

$$\alpha_k = \alpha_0 + \sin^{-1}\frac{\sin\phi_k \sin A_z}{\cos\lambda_k} \quad (7.5\text{-}13)$$

$$k = H, I \quad (7.5\text{-}14)$$

Resolution of Earth-directed sensors has some similarities to stellar-directed sensors.

7.6 Relative Vehicle Geometry

The relative position $\underline{P}_R$ and relative velocity $\underline{V}_R$ of satellite 2 with respect to satellite 1 are given by

$$\underline{P}_R = \underline{P}_2 - \underline{P}_1 \tag{7.6-1}$$

$$\underline{V}_R = \underline{V}_2 - \underline{V}_1 \tag{7.6-2}$$

Aspect angles of satellite 2 with respect to satellite 1 are given by the generally similar equations as for computation of Sun aspect angles and tracking station aspect angles. Thus,

$$x_i = x_2 - x_1 \tag{7.6-3}$$

$$y_i = y_2 - y_1 \tag{7.6-4}$$

$$z_i = z_2 - z_1 \tag{7.6-5}$$

$$\begin{bmatrix} x_B \\ y_B \\ z_B \end{bmatrix} = \begin{bmatrix} M \end{bmatrix} \begin{bmatrix} x_i \\ y_i \\ z_i \end{bmatrix} \tag{7.6-6}$$

with M given by (7.4-16). The aspect angles and are

$$\cos\theta = \frac{x_B}{\sqrt{x_B^2 + y_B^2 + z_B^2}} \tag{7.6-7}$$

$$\tan\phi = \frac{-y_B}{z_B} \tag{7.6-8}$$

The mutual visibility can be determined by evaluating the visibility function between satellite 2 and satellite 1 (Ref. 7-):

$$R = (\underline{P}_2 \cdot \underline{P}_1)^2 - P_2^2 P_1^2 + (P_2^2 + P_1^2)S^2 - 2S^2 \underline{P}_2 \cdot \underline{P}_1 \tag{7.6-9}$$

where

$$S = R_E + h_{ATM} \tag{7.6-10}$$

R_E being the Earth radius and h_{ATM} being the height of the atmosphere. When R is negative, mutual visibility is implied; a positive value denotes non-visibility. R must be evaluated on a point-by-point check of the two ephemerides.

7.6 Orbit Stability

7.6.1 General Formulation

A basic problem in highly-eccentric earth orbital analysis is that of orbit stability. Orbit stability refers to the characteristic of orbits whose time-varying periapsis radius remains over its initial value while under the perturbative influence of lunar and solar gravity.

The relevant equations describing orbit stability may be derived from writing the third body gravitational force as the perturbating acceleration in the planetary equations (Reference 7-12). Then the time derivative of the perigee radius $q = a(1-e)$ to first order in (r/a_D) is

$$\dot{q} = -\frac{\sqrt{1-e^2}}{nae}\left[(ae \sin f) R + \left(\frac{a^2(1-e^2)}{r} - r\right)S\right] \qquad (7.6-1)$$

$$R = \frac{\mu_D r}{2a_D^3}(1 + 3 \cos 2 \phi)$$

$$S = \frac{-3\mu_D r}{a_D^3}\left[\cos\gamma \sin(\omega+f) - \sin\gamma \cos(\omega+f) \cos i\right]\cos\phi \qquad (7.6-2)$$

where r is the satellite radius from the earth and a_D is the semimajor axis of the disturbing body relative to the earth, and where the non-standard parameters are illustrated in Figure 7.6-1. In writing equation (7.6-1) we have anticipated the result that $\Delta a = 0$ for third body accelerations.
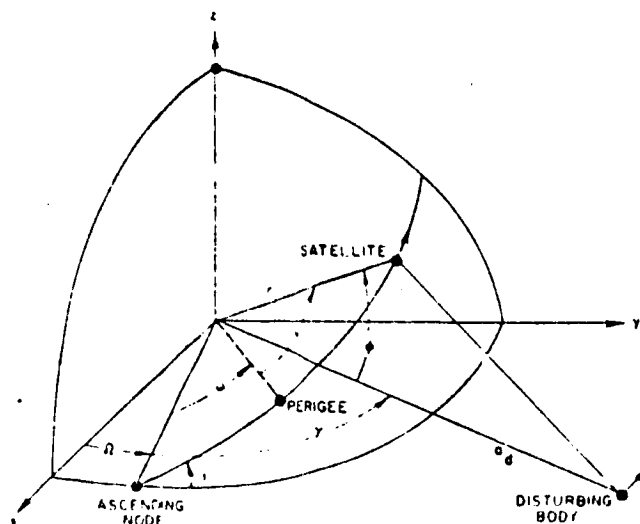
Figure 7.6-1. Definition of Variables

The singly averaged form of equation (7.6-1) is obtained by assuming the disturbing body does not move during one orbit of the satellite. Then equation (7.6-1) may be integrated over one period of the true anomaly f, yielding the change in perigee per orbit Δq where

$$\Delta q = B(a,e) \quad g(\gamma,\omega,i) \qquad\qquad (7.6-3)$$

where

$$B(a,e) = \frac{15\pi}{2}\left(\frac{T}{T_D}\right)^2 \quad ae(1-e^2)^{1/2} \qquad\qquad (7.6-4)$$

$$T = 2\pi\sqrt{a^3/\mu}$$

$$g(\gamma,\omega,i) = \sin 2\gamma \cos 2\omega \cos i - (\cos^2\gamma - \sin^2\gamma\cos^2 i) - \sin 2\omega$$

The doubly-averaged equations describing the long term periapsis radius evolution are generated by averaging the singly-averaged equation over the period of the disturbing body. Then the formal integration indicated by the equation

$$\Delta Q = \sum_{i=1}^{N} \Delta q_i \sim \int_0^{T_D} \Delta q(t)\,dt \qquad\qquad (7.6-5)$$

is carried out with the motion of the disturbing body γ represented by γ

$$\gamma = \gamma_0 + \dot{\gamma}t = \gamma_0 + n_D t \qquad\qquad (7.6-6)$$

The result can be written

$$\Delta q = K_0\left[K_1 \sin(2n_D t + K_2) + K_3 t + K_4\right] \qquad\qquad (7.6-7)$$

where

$$K_0 = \frac{15}{8}\sqrt{\frac{\mu_d}{\mu_{r_d}^3}}\sqrt{a^5 e^2(1-e^2)}$$

$$K_1 = -\sqrt{K_5^2 + K_6^2}$$

$$K_2 = \tan^{-1}(K_5/K_6) + \pi + \gamma_{D0}$$

$$K_3 = -\sqrt{\frac{\mu_d}{r_d^3}}(\sin 2\omega \sin^2 i) \qquad\qquad (7.6-8)$$

$$K_4 = \text{initialize } \Delta q = 0 \text{ at } t = 0$$

$$K_5 = \cos 2\omega \cos i$$

$$K_6 = \frac{1}{2}\sin 2\omega(1 + \cos^2 i)$$

7.6.2 SABAC Technique

The general formulation of the third body perturbative effect on the perigee evolution was presented in the previous subsection to motivate the following summary of the techniques used in program SABAC - Stability Analysis by Approximate Criteria (Reference 7-13). The normal SABAC documentation is quite difficult to follow. Therefore the SABAC equations will be summarized but reference will be made to the above general formulation.

The SABAC approach evaluates a candidate orbit for a series of approximate criteria until the first criteria violation. It then immediately proceeds to the next orbit. The criteria are as follows

1) Long term stability:

$$(\Delta e)_{LR} = \frac{e \, \epsilon^{1/2}}{4} (A_s \sin^2 i_s \sin 2\omega_s + A_M \sin^2 i_M \sin 2\omega_M) \leqslant 0 \qquad (7.6-9)$$

with

$$A_d = 15\pi(\mu_D/\mu_E)(a/P_D)^3 \, \epsilon_D^{3/2} \qquad (7.6-10)$$

$$\epsilon = 1-e^2$$

This corresponds to requiring the linear term of (7.6-7) to be positive (i.e., $(K_0 K_3)_s + (K_0 K_3)_M \geqslant 0$)

2) Short term stability:

$$(\Delta e)_{sR} = -e \, \epsilon^{1/2} \left\{ (A_M/\epsilon_M^{3/2})\beta_{3,M} + (A_s/\epsilon_s^{3/2})\beta_{3,s} \right\} \leqslant 0 \qquad (7.6-11)$$

where $\beta_{3,D} = \xi_{1,D}\xi_{2,D}(P_D/r_D)^3$ and ξ_1, ξ_2 are the projections of the unit vector to the disturbing body on the line of apsides and semilatus rectum, respectively. This corresponds to keeping the perigee altitude from decreasing during the first orbit, i.e., from equation (7.6-3)

$$B_s \, g(\gamma_s, \omega_s, i_s) + B_M \, g(\gamma_M, \omega_M, i_M) \geqslant 0 \qquad (7.6-12)$$

3) Intermediate range stability:

$$(\Delta e)_{INT} = (\Delta e)_{<sR,s>,M} + (\Delta e)_{LR,M} \leqslant 0 \qquad (7.6-13)$$

in which $<sR,s>,M$ means the short range effect of the sun averaged over the lunar period. This corresponds to determining that the averaged effects of the sun and moon for the first month result in increased perigee radius.

4) Lunar Ripple:

$$\Delta e_j^* = -e \, \epsilon^{1/2} \sum_{K=1}^{j} \frac{A_M}{\epsilon_M^{3/2}} \beta_{3,M}^{(k)} + \frac{A_s}{\epsilon_s^{3/2}} \beta_{3,s}^{(k)} \leqslant 0 \qquad (7.6-14)$$

in which j is the number of passages at perigee over half a lunar month.

This criterion corresponds to restricting the lunar sinusoidal term of Equation (7.6-7) from causing perigee to decrease below its initial value when the sin term reaches its minimum (negative) value during the first half-month.

5) Solar Ripple:

$$\Delta e_{<sR,s>,M} > \Delta e_{LR} \qquad \text{or, if not satisified,} \qquad (7.6\text{-}15)$$

$$\Delta e_{LR} < \frac{4}{9\sqrt{3}} \left[\Delta e_{<sR,s>,M} - \Delta e_{LR} \right] \qquad (7.6\text{-}16)$$

This criterion supposedly corresponds to insuring that the solar sinusoidal term does not cause perigee to be lower than its initial value (equivalently, eccentricity to be higher than its initial value). The derivation of (7.6-16) is uncertain; an approximation to it can be found in the following manner. Let the change in eccentricity due to the sun be written

$$\Delta e = at + b\sin 4\pi t \qquad (7.6\text{-}17)$$

where t is measured in years. For stability, the constant a is assumed to be negative leading to a long term decreasing trend. However the sinusoidal term could cause a local maximum near $t = 3/8$. To insure stability even in this "worst" period we require

$$\Delta e(t = \frac{3}{8}) = \frac{3a}{8} - b < 0 \qquad (7.6\text{-}18)$$

The constants a and b may be approximated by setting

$$\Delta e_{LR} = a$$
$$\Delta e_{<sR,s>,M} = \frac{d\,\Delta e}{dt}(t = 0) = a + 4\pi b \qquad (7.6\text{-}19)$$

Combining the two previous cases results in the condition

$$\Delta e_{LR} < \frac{2}{3\pi}(\Delta e_{<sR,s>,M} - \Delta e_{LR}) \qquad (7.6\text{-}20)$$

which is a general approximation to the SABAC result stated in (7.6-16). An alternate approach which appears to be preferrable would be to use the full equation (7.6-7) to estimate both the lunar and solar effects directly and avoid the numerous and unnecessary approximations indicated above.

6) Very Long Range Stability:

There are two versions of SABAC corresponding to two methods of computing the very-long-term stability. Both methods essentially use the constants of Lidov's theory

$$C_1 = \epsilon \cos^2 i$$

$$C_2 = (1-\epsilon)(\frac{2}{5} - \sin^2 i \ \sin^2 \omega) \tag{7.6-21}$$

6.a) In the first method the extremal values of $\epsilon = 1-e^2$ are determined as follows. If $C_2 > 0$

$$\epsilon_{max} = 1 - \frac{5}{2} C_2$$

$$\epsilon_{min} = \frac{1}{2} \left\{ 1 + \frac{5}{3}(C_1 + C_2) - \left[(1 + \frac{5}{3}(C_1 + C_2))^2 - \frac{20}{3} C_1 \right]^{1/2} \right\} \tag{7.6-22}$$

If $C_2 < 0$ they are computed as the roots of

$$\epsilon^2 - \left[1 + \frac{5}{3}(C_1 + C_2) \right] \epsilon + \frac{5}{3} C_1 = 0 \tag{7.6-23}$$

In the above two sets of equations the parameters are computed as though the moon were acting alone. Then

$$\sin E_0 = \frac{e_{max} - e_0}{e_{max} - e_{min}} \qquad\qquad 0 \leqslant E_0 \leqslant \frac{\pi}{2} \tag{7.6-24}$$

$$T_{VLR} = \pi(e_{max} - e_{min}) \ \cos E_0 \ T_{SAT} \ |\Delta e_{INT}| \tag{7.6-25}$$

where Δe_{INT} is computed by (7.6-13). The very-long-term stability is assumed satisfied if

$$T^* = T_{VLR} \ (1 - \frac{2E_0}{\pi}) \ \geqslant L \tag{7.6-26}$$

6.b) In the improved version of SABAC for near-polar orbits the very-long-term stability is computed differently. An auxiliary plane, denoted P_A is constructed by rotating the ecliptic by i_A about the nodal line of the moon where

$$i_A = \left(\frac{A_M}{A_M + A_s} \right) \ i_M \tag{7.6-27}$$

The predicted lifetime L is then computed from

$$L = 2(\pi - \omega_A) \ \frac{\Delta\omega}{\Delta t} \tag{7.6-28}$$

where ω_A is the satellite argument of perigee referred to the auxiliary plane P_A. The last term is computed from

$$\left(\frac{\Delta\omega}{\Delta t} \right) = \left(\frac{\Delta\omega}{\Delta t} \right)_{LR,M} + \left(\frac{\Delta\omega}{\Delta t} \right)_{LR,s} (1 + w) \tag{7.6-29}$$

where

$$\left(\frac{\Delta\omega}{\Delta t}\right)_{LR,D} = A_D \left[(\cos^2 i_D - \epsilon)\sin^2\omega_D + \frac{2\epsilon}{5}\right] / 2\epsilon^{1/2} \qquad (7.6\text{-}30)$$

The documentation does not detail how the factor w is computed.

7.6.3 Alternate Approach

An alternate approach to that of SABAC should be considered which could be as accurate, more efficient, and much clearer than SABAC. This would involve the direct use of equation (7.6-7), possibly in conjunction with the proceed-until-condition-violated approach of SABAC. The SABAC technique appears especially questionable in the analysis of the so-called lunar and solar "ripple" effects. Significant improvement in this area could be made with equation (7.6-7) in this respect.

7.7 Lifetime

The equation for the approximate lifetime L is given as a function of initial perigee altitude hp in km, initial apogee altitude h_A in km, ballistic coefficient B and date of launch t_L in years (Ref. 7-9).

$$L_n = L_3 \times f_D \left(h_p, \ t_L + L_{n-1} \right) \Big]_{t_L}^{t_L + L_{n-1}} \tag{7.7-1}$$

where $]$ indicates that f_D is averaged over the period from t_L to $t_L + L_{n-1}$. The iterative process indicated in (7.7-1) is carried out until

$$\left| L_{n-1} - L_n \right| < \epsilon \tag{7.7-2}$$

where ϵ is a preset small lifetime tolerance figure set by the user. L_3 in equation (7-101) is

$$L_3 = L_1(h_p, h_A) \cdot B \cdot f_{i\omega}(i, \omega) \tag{7.7-3}$$

B is given by

$$B = \frac{M}{C_D A} \tag{7.7-4}$$

where M is the mass of the satellite in kg, C_D is the drag coefficient and A is the reference area in square meters.

The functions $f_D(h_p, \ t_L + L_{n-1})$, $L_1(h_p, h_A)$ and $f_{i\omega}(i, \omega)$ have been precalculated and can be stored as tables.

The function f_D is conveniently expanded in a polynomial in h_p (Ref. 7-10) as

$$f_D = f_{D1}(t) + f_{D2}(t)h_p + f_{D3}(t)h_p^2 + f_{D4}(t)h_p^3 \tag{7.7-5}$$

where

$$t = 4(t_L - 1974.00) + 1 \tag{7.7-6}$$

t_L being in fractional years to the nearest 1/4 year. Table 7.7-I gives f_D for a nominal density 1962 U.S. Standard atmosphere and for a +2σ density atmosphere over the period from 1974.00 through 1984.75.

The function L_1 polynomial has been made an exponential in a polynomial power in circular altitude h_c (Ref. 7-5):

$$L_1 = e^{L_1 + L_2 h_c + L_3 h_c^2 + L_4 h_c^3 + L_5 h_c^4} \qquad (7.7-7)$$

with

$$L_1 = -.135 \times 10^2 \qquad (7.7-8)$$
$$L_2 = .713 \times 10^{-1} \qquad (7.7-9)$$
$$L_3 = -.143 \times 10^{-3} \qquad (7.7-10)$$
$$L_4 = 1.0 + .167 \times 10^{-6} \qquad (7.7-11)$$
$$L_5 = -.778 \times 10^{-10} \qquad (7.7-12)$$

The function $f_{i\omega}$ is a function of i only when circular orbits are considered (Ref. 7-5):

$$f_{i\omega} = f_{i\omega 1} + f_{i\omega 2} i + f_{i\omega 3} i^2 + f_{i\omega 4} i^3 \qquad (7.7-13)$$

with

$$f_{i\omega 1} = 0.934 \times 10^0 \qquad (7.7-14)$$
$$f_{i\omega 2} = -0.486 \times 10^{-3} \qquad (7.7-15)$$
$$f_{i\omega 3} = 0.120 \times 10^{-3} \qquad (7.7-16)$$
$$f_{i\omega 4} = 1 - 0.992 \times 10^{-6} \qquad (7.7-17)$$

TABLE 7.7-I

Coefficients of Density Function f_D

YEAR	f_{D1} NOMINAL	f_{D1} +2σ	f_{D2} NOMINAL	f_{D2} +2σ	f_{D3} NOMINAL	f_{D3} +2σ	f_{D4} NOMINAL	f_{D4} +2σ
1974.00	.152(1)	.861(1)	-.926(-2)	-.237(-2)	.510(-4)	.283(-4)	-.166(-7)	-.127(-7)
.25	.129(1)	.866(0)	-.625(-2)	-.140(-2)	.409(-4)	.227(-4)	-.195(-7)	-.131(-7)
.50	.208(1)	.132(1)	-.148(-1)	-.723(-2)	.666(-4)	.447(-4)	-.148(-7)	-.162(-7)
.75	.178(1)	.103(1)	-.113(-1)	-.333(-2)	.574(-4)	.304(-4)	-.227(-7)	-.161(-7)
1975.00	.216(1)	.117(1)	-.155(-1)	-.575(-2)	.686(-4)	.400(-4)	-.141(-7)	-.154(-7)
.25	.171(1)	.920(0)	-.106(-1)	-.206(-2)	.552(-4)	.255(-4)	-.224(-7)	-.142(-7)
.50	.254(1)	.996(0)	-.190(-1)	-.388(-2)	.772(-4)	.337(-4)	-.100(-7)	-.141(-7)
.75	.414(1)	.889(1)	-.746(-2)	.655(-2)	.449(-4)	-.513(-5)	-.207(-7)	.629(-8)
1976.00	.145(1)	.460(1)	-.875(-2)	.312(-2)	.495(-4)	.188(-5)	-.164(-7)	-.149(-8)
.25	.108(1)	.774(0)	-.384(-2)	.141(-2)	.323(-4)	-.601(-6)	-.168(-7)	-.327(-10)
.50	.201(1)	.545(0)	-.119(-1)	.288(-2)	.549(-4)	-.227(-5)	-.283(-7)	.117(-8)
.75	.808(0)	.957(0)	-.676(-3)	-.104(-3)	.196(-4)	-.356(-6)	-.117(-7)	.363(-9)
1977.00	.639(0)	.778(0)	.220(-3)	.110(-2)	.181(-4)	-.276(-5)	-.921(-8)	.207(-8)
.25	.651(0)	.112(1)	.161(-2)	-.166(-2)	.769(-5)	.139(-5)	-.561(-8)	-.369(-9)
.50	.564(0)	.815(0)	.117(-2)	.783(-3)	.139(-4)	-.244(-5)	-.750(-8)	.194(-8)
.75	.661(0)	.117(1)	.204(-2)	-.220(-2)	.211(-5)	.219(-5)	-.215(-6)	-.796(-9)
1978.00	.466(0)	.980(0)	.317(-2)	-.761(-3)	.923(-6)	-.560(-6)	-.913(-9)	.104(-8)
.25	.732(0)	.127(1)	.171(-2)	-.328(-2)	-.192(-6)	.397(-5)	-.430(-9)	-.179(-8)
.50	.472(0)	.985(0)	.361(-2)	-.808(-3)	.572(-6)	-.506(-6)	-.713(-9)	.102(-8)
.75	.764(0)	.129(1)	.148(-2)	-.341(-2)	-.532(-6)	.425(-5)	-.108(-9)	-.198(-8)
1979.00	.534(0)	.106(1)	.281(-2)	-.151(-2)	-.124(-5)	.615(-6)	.333(-9)	.378(-9)
.25	.788(0)	.127(1)	.131(-2)	-.329(-2)	-.744(-6)	.400(-5)	.115(-9)	-.182(-8)

NOTE: Numbers within parentheses denote exponents of 10; e.g. .461(-8) = .461·10^{-8}

7.7-3

TABLE 7.7-I

(Continued)

YEAR	f_{D1}		f_{D2}		f_{D3}		f_{D4}	
	NOMINAL	+2	NOMINAL	+2	NOMINAL	+2	NOMINAL	+2
1979.50	.484(0)	.938(0)	.317(-1)	-.354(-3)	-.404(-6)	-.113(-5)	-.103(-9)	-.133(-8)
.75	.756(0)	.121(1)	.155(-2)	-.263(-2)	-.556(-6)	.291(-5)	-.108(-9)	-.120(-8)
1980.00	.493(0)	.917(0)	.317(-2)	-.160(-3)	-.124(-5)	-.143(-5)	.451(-9)	.152(-8)
.25	.729(0)	.113(1)	.713(-2)	-.173(-2)	-.230(-6)	.147(-5)	-.405(-9)	-.396(-9)
.50	.455(0)	.720(0)	.306(-2)	.159(-2)	.276(-5)	-.312(-5)	-.199(-9)	.219(-8)
.75	.819(0)	.100(1)	.772(-3)	-.516(-3)	.415(-5)	-.340(-7)	-.416(-8)	.300(-9)
1981.00	.462(0)	.689(0)	.312(-2)	.185(-2)	.179(-5)	-.312(-5)	-.144(-8)	.208(-8)
.25	.644(0)	.917(0)	.206(-2)	.250(-3)	.337(-5)	-.664(-6)	-.298(-8)	.476(-9)
.50	.572(0)	.412(0)	.109(-2)	.397(-2)	.142(-4)	-.436(-5)	-.764(-8)	.288(-8)
.75	.619(0)	.769(0)	.142(-2)	.145(-2)	.909(-5)	-.610(-6)	-.637(-8)	-.383(-10)
1982.00	.822(0)	.658(0)	-.879(-3)	.205(-2)	.206(-4)	.232(-5)	-.121(-7)	-.230(-8)
.25	.708(0)	.701(0)	.653(-3)	.188(-2)	.133(-4)	.636(-6)	-.867(-8)	-.110(-8)
.50	.115(1)	.655(0)	-.474(-2)	.147(-2)	.356(-4)	.872(-5)	-.179(-7)	-.619(-8)
.75	.813(0)	.644(0)	-.779(-3)	.190(-2)	.201(-4)	.512(-5)	-.119(-7)	-.410(-8)
1983.00	.116(1)	.715(0)	-.480(-2)	.592(-3)	.358(-4)	.135(-4)	-.180(-7)	-.880(-8)
.25	.903(0)	.652(0)	-.186(-2)	.158(-2)	.247(-4)	.782(-5)	-.139(-7)	-.570(-8)
.50	.169(1)	.916(0)	-.104(-1)	-.202(-2)	.546(-4)	.253(-4)	-.224(-7)	-.142(-7)
.75	.110(1)	.698(0)	-.423(-2)	.806(-3)	.334(-4)	.125(-4)	-.172(-7)	-.826(-8)
1948.00	.156(1)	.853(0)	-.907(-2)	-.124(-2)	.503(-2)	.220(-4)	-.216(-7)	-.128(-7)
.25	.114(1)	.694(0)	-.460(-2)	.840(-3)	.351(-4)	.124(-4)	-.177(-7)	-.817(-8)
.50	.212(1)	.104(1)	-.147(-1)	-.345(-2)	.673(-4)	.309(-4)	-.231(-7)	-.163(-6)
.75	.132(1)	.684(0)	-.648(-2)	.102(-2)	.417(-4)	.113(-4)	-.197(-7)	-.764(-7)

NOTE: Numbers within parentheses denote exponents of 10; e.g. $.461(-8) = .461 \cdot 10^{-8}$.

7.8 REFERENCES

7-1   Tonies, C. C., "Trace Orbit Determination Program,"
       Version D, Aerospace Corp., E. Segundo, California.
       September, 1966.

7-2   McCollough, R. R., "Computation of Spacecraft
       Orientation Angles," Apollo Applications Program,
       Martin Marietta Aerospace, July, 1968.

7-3   Escobal, P. R., "Methods of Orbit Determination,"
       John Wiley and Sons, Inc., 1965.

7-4   Lutzky, D. and Uphoff, C., "In-Flight Mission
       Control System (IFMCS) Design Study," Contract
       No. NAS5-11796, Report No. 71-23, Analytical
       Mechanics Associates, Inc., Los Angeles,
       22 April 1971.

7-5   Lutzky, D., et al, "Programmer's Manual for Mission
       Analysis Evaluation and Space Trajectory Operations
       Program," MAESTRO, Analytical Mechanics Associates,
       Los Angeles, March, 1973.

7-6   Thomson, W. T., "Introduction to Space Dynamics,"
       John Wiley and Sons, 1963.

7-7   McCollough, R. R., "Graphical Analysis of Celestial
       Field of View," Contract NAS8-24000, Martin Marietta
       Aerospace, 10 March 1971.

7-8   McCollough, R. R., "Footprint," unpublished FORTRAN
       Program for Skylab, Contract NAS8-24000, Martin
       Marietta Aerospace, 1972.

7-9   Escobal, P. R., "Methods of Astrodynamics," John
       Wiley and Sons, Inc., 1968.

7-10   Hausler, J. b., "A Graphic Method for the Prediction
       of Satellite Lifetime Based on a Time-Dependent
       Atmosphere Density Model," NASA, MSFC, Alabama;
       S&E-AERO-MM-59-71, 03 September 1971.

7-11   Tuttle, J. C., et al, "Optimum Mission Profile
       Design-Documentation of Program Pops," Contract
       NAS8-28146, Martin Marietta Aerospace, Denver,
       Colorado. 10 January 1973.

8. LAUNCH PHASE ANALYSIS

8.1 Introduction

This chapter summarizes the mathematical details of launch phase analysis. Launch phase analysis determines the trajectory and maneuver sequence from launch to insertion onto some target orbit. The orbits encountered are the parking orbit, the transfer or intermediate orbit, and the target orbit. The maneuvers are insertion into the parking orbit, injection into the transfer orbit, and insertion into the target orbit. The timing of the launch (both in terms of calendar date and time-of-day) is a critical element in launch phase analysis because of the constraints to launch from specified launch sites in a general direction (launch azimuth).

This chapter attempts to provide a unified discussion of launch phase analysis. Launch is quite different from the usual orbital analysis because of the special parameters used to describe launch. Thus frequent references are made to other sections of this report for the detailed formulation of general parameters.

Section 8.2 descusses the determination of the launch profile from a standard set of launch parameters. Section 8.3 describes how this profile is used in a launch period/window analysis. Section 8.4 summarizes the techniques and models used in detailed launch phase trageting. Section 8.5 discusses launch phases error analysis.

8.2 Launch Profile Determination

8.2.1 Definition of Standard Profile

The standard launch profile will be assumed to consist of a circular parking orbit, a coplanar (Hohman) transfer orbit, and a circular target orbit. Instantaneous, impulsive maneuvers will be assumed throughout. Variations to this "standard" profile will be discussed in Section 8.2.4.

This standard profile is as simple a model possible yet yields very useful data in a first-cut launch opportunity assessment study. It is an excellent approximation to the synchronous orbit profile (Ref. 8-1, 8-2). The profile is defined by specification of the parameters listed in Table 8.2-1.

> Launch date D_L
> Launch site latitude ϕ_L, longitude θ_L, azimuth Σ_L
> Launch time-of-day t_L or parking orbit ascending node Ω_p
> Parking orbit radius R_p
> Target orbit radius R_T, right ascension Ω_T, inclination i_T
> Long or short coast flag, k (see 9-15)
> Integer number of parking orbits N_p or transfer orbits N_I

Table 8.2-1. Standard Launch Profile Input Parameters

8.2.2 Launch Timing and Orbit Plane

Two possibilities exist for the specification of the launch time-of-day and the resultant parking orbit plane. The required input parameters are the launch date, D_L, the launch site latitude ϕ_L and longitude θ_L, and the launch azimuth Σ_L. Then with the specification of the launch time-of-day t_L, the (inertial) right ascension at launch Θ_L and the equatorial inclination i_p, ascending node longitude Ω_p, and normal vector $\hat{N}$ of the launch plane may be computed. Equivalently if the ascending node Ω_p is specified, the launch time-of-day and the other parameters may be computed. A clear concise development of these calculations is provided below with most variables defined in Fig. 8.2-1 and formulation derived from spherical trigonometry.

Launch Time-of-Day Input:

$$\Theta_L = (GHA + \theta_L + \omega\, t_L) \bmod 360 \tag{8.2-1}$$

$$\hat{N} = \begin{bmatrix} \sin\Theta_L\cos\Sigma_L - \cos\Theta_L\sin\phi_L\sin\Sigma_L \\ -\cos\Theta_L\cos\Sigma_L - \sin\Theta_L\sin\phi_L\sin\Sigma_L \\ \cos\phi_L\sin\Sigma_L \end{bmatrix} \tag{8.2-2}$$

Figure 8.2-1. Launch Geometry

Figure 8.2-2. Transfer Orbit Geometry

$$i_p = \cos^{-1}(N_z) \qquad 0 \le i_p \le 90 \qquad\qquad (8.2\text{-}3)$$

$$\Omega_p = \tan^{-1}(-N_x/N_y) \qquad 0 \le \Omega_p < 360 \qquad\qquad (8.2\text{-}4)$$

Longitude of Ascending Node Input:

$$i_p = \cos^{-1}(\cos \phi_L \sin \Sigma_L) \qquad 0 \le i \le 90^{\circ} \qquad\qquad (8.2\text{-}5)$$

$$\hat{N} = (\sin \Omega_p \sin i_p, \ -\cos \Omega_p \sin i_p, \ \cos i_p) \qquad\qquad (8.2\text{-}6)$$

$$\theta_L = (\Omega_p + \Delta\theta) \bmod 360 \qquad\qquad (8.2\text{-}7)$$

$$\text{where } \Delta\theta = \ \begin{array}{l} 90^{\circ}, \text{ if } \Sigma_L = 90^{\circ} \\ 90^{\circ} - \cos^{-1}(\tan \phi_L/\tan i), \text{ if } \Sigma_L < 90^{\circ} \\ 90^{\circ} + \cos^{-1}(\tan \phi_L/\tan i_p), \text{ if } \Sigma_L > 90^{\circ} \end{array} \qquad (8.2\text{-}8)$$

$$t_L = \frac{(\theta_L - \theta_L - \text{GHA}) \bmod 360}{\omega} \qquad\qquad (8.2\text{-}9)$$

In equations (8.2-1 and -9), GHA is the Greenwich hour angle at 0^h UT on the launch date, given by

$$\text{GHA} = 100\overset{\circ}{.}07554260 + 0\overset{\circ}{.}9856473460 \ T_d + 2.9015 \times 10^{-13} \ T_d^{\ 2} \qquad (8.2\text{-}10)$$

where T_d = days past 0^h January 1, 1950. In those equations θ_L is the input launch site longitude and ω is the rotation rate of the earth.

In either case the definition of RTN coordinate system defining the launch plane (Figure 8-1 or 8-2) can now be completed

$$\hat{R} = (\cos \theta_L \cos \phi_L, \ \sin \theta_L \cos \phi_L, \ \sin \phi_L) \qquad\qquad (8.2\text{-}11)$$

$$\hat{T} = \hat{N} \times \hat{R} \qquad\qquad (8.2\text{-}12)$$

8.2.3 Trajectory and Maneuver Sequence

Having determined the launch plane and timing, the next step is to compute the trajectory and maneuver sequence for the standard launch profile. The intersection of the launch plane (containing both the parking orbit and the transfer orbit) and the target orbit plane is first computed. The target plane normal N_T is given by

$$\hat{N}_T = (\sin \Omega_T \sin i_T, \ -\cos \Omega_T \sin i_T, \ \cos i_T) \qquad\qquad (8.2\text{-}13)$$

Define the auxiliary vector $\hat{I}_o$ as the quantity

$$\hat{I}_o = \frac{\hat{N}_T \times \hat{N}}{|\hat{N}_T \times \hat{N}|} \qquad\qquad (8.2\text{-}14)$$

$\hat{I}_o$ then defines the intersection of the launch plane and the target plane.

Let $\hat{I}$ represent the vector to the point of injection from the parking orbit to the transfer orbit. Then assume the user states his preference for short or long coast by specifying the flag

$$k = +1, \text{ short coast}$$
$$\quad\quad -1, \text{ long coast}$$

(8.2-15)

The geometry discriminator K is computed from

$$K = (\hat{R} \times \hat{I}_o) \cdot \hat{N}$$

(8.2-16)

K is then ± 1 with the positive sign corresponding to $\hat{I}_o$ lying in the first or second quadrant of Figure 8.2-2; the negative sign corresponding to the third or fourth quadrant. To force I to point to the injection point $\bar{I}$ must be set to

$$\hat{I} = k \cdot K \cdot \hat{I}_o$$

(8.2-17)

With these definitions the trajectory and maneuver sequences are determined. The conic descriptions of the three phases are summarized in Table 8.2-2. The parameters R_p, R_T, i_T and Ω_T are input variables. The parameter Ω_p is either input or computed from Equation (8.2-4). The parameter i_p is computed from either Equation (8.2-3) or 8.2-5). The parameter ω_I is computed as follows. The unit vector to the ascending node of the parking orbit is $\hat{A}_p$ where

$$\hat{A}_p = (\cos \Omega_p, \sin \Omega_p, 0)$$

(8.2-18)

Then ω_I $(0 \leq \omega_I < 360)$ is defined by

$$\sin \omega_I = (\hat{A} \times \hat{I}) \cdot \hat{N}$$
$$\cos \omega_I = \hat{A} \cdot \hat{I}$$

(8.2-19)

	Parking Orbit	Intermediate Orbit	Target Orbit
Semimajor axis, a	R_p	$\frac{1}{2}(R_p + R_T)$	R_T
Eccentricity, e	0	$(R_T - R_p)/2a_I$	0
Argument of Perigee ω	-	ω_I	-
Inclination, i	i_p	i_p	i_T
Longitude of ASC Node, Ω	Ω_p	Ω_p	Ω_T
Entrance True Anomaly, f	-	0	-

Table 8.2-2. Launch Phase Trajectory Description

The computation of the critical points within the sequence are summarized in Table 8.2-3. The basic directions in the inertial equatorial system are those of the launch site at launch $\hat{R}$ (8.2-11), the velocity at launch $\hat{m}$ (8.2-12), the injection and anti-insertion position $\hat{I}$ (8.2-17), the injection and anti-insertion velocities $\hat{S}$ and the post-insertion velocity direction P where

$$\hat{S} = \hat{N} \times \hat{I} \qquad (8.2\text{-}20)$$

$$\hat{P} = \hat{N}_T \times \hat{I} \qquad (8.2\text{-}21)$$

	Insertion into Parking Orbit	Injection into Transfer Orbit	Insertion into Target Orbit
Position Vector	$R_p \, \hat{R}$	$R_p \, \hat{I}$	$-R_T \, \hat{I}$
Pre-maneuver Velocity	-	$\left(\dfrac{\mu}{R_p}\right)^{\frac{1}{2}} \hat{S}$	$-\left(\dfrac{\mu \, R_p}{\varepsilon_I R_T}\right)^{\frac{1}{2}} \hat{S}$
Post-maneuver Velocity	$\left(\dfrac{\mu}{R_p}\right)^{\frac{1}{2}} \hat{T}$	$\left(\dfrac{\mu \, R_T}{a_I R_p}\right)^{\frac{1}{2}} \hat{S}$	$\left(\dfrac{\mu}{R_T}\right)^{\frac{1}{2}} \hat{P}$

Table 8.2-3. Launch Phase Maneuvers

Finally the times of the maneuvers must be computed. Some generality is permitted here by allowing waiting several periods before performing the injection or insertion maneuvers. Let N_p be the integer number of "waiting" parking orbits and N_I be the integer number of "waiting" transfer orbits. The angle between the launch and the first opportunity for injection is θ_c ($0 \le \theta_c < 360$) where

$$\sin \theta_c = (\hat{R} \times \hat{I}) \cdot \hat{N}$$
$$\cos \theta_c = \hat{R} \cdot \hat{I} \qquad (8.2\text{-}22)$$

The total coast time in parking orbit is then

$$T_c = (\theta_c + N_p \cdot 360) \, (R_p{}^3/\mu)^{\frac{1}{2}} \left(\frac{2\pi}{360}\right) \qquad (8.2\text{-}23)$$

The total coast time in the transfer orbit is

$$T_I = (N_I + \tfrac{1}{2}) \, 2\pi \, (a_I{}^3/\mu)^{\frac{1}{2}} \qquad (8.2\text{-}24)$$

8.2.4 Variations to Standard Profile

The standard profile described in the previous three subsections is effective because it can be generated very quickly for each use over a wide range of launch dates D_L and launch times t_L (or ascending nodes Ω_L). The standard

profile provides a generally adequate simulation of the launch phase for most missions. However, closed-form analytical solutions may also be computed for other variations of the launch profile. These variations include eccentric target orbits and non-coplanar transfer orbits.

Eccentric Target Orbits

The standard formulation may be easily adapted to eccentric target orbits. It is possible that eccentric drift orbits might be desirable for eccentric synchronous missions such as the International Ultraviolet Explorer (IUE) mission. The additional input required to describe the target orbit includes the eccentricity e_T, and the argument of periapsis ω_T, while the semimajor axis a_T is substituted for the radius of the target orbit x R_T.

In this variation the transfer orbit is still assumed to be a Hohman transfer lying in the parking orbit plane. The calculations are identical to the standard profile through Equation (8.2-19). However, the intermediate transfer orbit must now be computed in terms of the elliptical input elements (a_T, e_T, ω_T) instead of the radius R_T.

The vector to the ascending node of the target orbit is given by

$$\hat{A}_T = (\cos \Omega_T, \sin \Omega_T, 0) \tag{8.2-25}$$

An auxiliary vector $\hat{B}_T$ may be constructed in the target orbit plane as

$$\hat{B}_T = \hat{N}_T \times \hat{A}_T \tag{8.2-26}$$

The vector to perigee, $\hat{P}_T$, is then given by

$$\hat{P}_T = \cos \omega_T \, \hat{A}_T + \sin \omega_T \, \hat{B}_T \tag{8.2-27}$$

The true anomaly at insertion f_I $(0 \le f_I < 360)$ is then computed from the known direction of the insertion point $(-\hat{I})$ as follows:

$$\begin{aligned} \sin f_I &= (\hat{I} \times \hat{P}_T) \cdot \hat{N}_T \\ \cos f_I &= - \hat{P}_T \cdot \hat{I} \end{aligned} \tag{8.2-28}$$

The radius to the insertion point is then given by

$$R_I = \frac{a_T \, (1-e_T^2)}{1+e_T \cos f_I} \tag{8.2-29}$$

The radius R_I then replaces the variable R_T in Table 8.2-2 describing the intermediate orbit. The input variables (a_T, e_T, ω_T) are of course entered into the target orbit parameters.

The only other parameters affected in standard launch sequence is the position and velocity following insertion into the target orbit. The speed at that point is given by

$$V_I = \mu\left(\frac{2}{R_I} - \frac{1}{a_T}\right)^{\frac{1}{2}} \tag{8.2-30}$$

The flight path angle γ ($-90° \leq \gamma \leq 90°$) is given by

$$\tan = \frac{e_T \sin f}{1 + e_T \cos f} \tag{8.2-31}$$

The position and velocity following insertion into the target orbit are then

$$\underline{R}_T(t_T) = -R_I \, \hat{I} \tag{8.2-32}$$

$$\underline{V}_T(t_T) = V_I \, \hat{P} \tag{8.2-33}$$

$$\hat{P} = -\sin \gamma \, \hat{I} + \cos \hat{\gamma} \, (\hat{I} \times \hat{N}_T) \tag{8.2-34}$$

Inclined Transfer Orbits

The ability to specify the longitude of the ascending node of the parking orbit as an initial condition (Section 8.2.2) permits the evaluation of Hohman transfers involving inclined intermediate orbits. The inclusion of such transfers may be necessary at some time to meet peculiar mission requirements while satisfying mission constraints.

The critical feature of such a transfer is that the nodes of all three phases are collinear, resulting in a 180 deg Hohman transfer. Note that if this assumption were removed a unique solution could still be determined via Lambert's theorem if the transfer orbit transit time were specified. However, the intuitive feeling is that the Hohman transfer would be near optimal and numerical techniques (see Chapter 11) would be required to determine and prove the global optimal solution.

This extended possibility for launch analysis could be easily developed using the Sun technique (Reference 8-3) implemented in the post injection trim analysis in MAESTRO (Reference 8-4). The Sun technique generates analytically the optimal two-impulse $180°$ transfer between non-coplanar orbits. The mathematical details of this method are supplied in Chapter 10. The method, however, results in the specification of the trajectories and maneuvers of the launch sequence defined in Tables 8-2 and 8-3. The Sun technique is a powerful technique and recommended for use in the launch phase analysis.

8.3 Launch Window Analysis

The previous section discussed the construction of an analytic launch profile. This section addresses the evaluation of such a launch profile in launch window analysis.

Launch window analyses determine the optimal launch dates (or equivalently the launch period) during which time adequate daily launch windows exist. A daily launch window is defined as a continuous interval of time on a single day that a launch may be made which with the ensuing transfer satisfies all mission and system constraints.

8.3.1 Method of Analysis

The launch window analysis generally has two principal independent parameters: the candidate calendar dates and the ascending node or time-of-day of launch on each date. Critical parameter constraint contours are then plotted on the grid whose principal axes correspond to these time-variables. An example is given in Figure 8.3-1 taken from Reference 8-2. The contour plot is of a launch period-launch window analysis made for the Synchronous Meteorological Satellite (SMS) mission. The critical mission-system constraints for this mission were those on shadowing in the parking and transfer orbits and solar aspect angle at insertion into transfer orbit and synchronous orbit. The hatched lines represent regions that violate the solar aspect angle constraint; the light solid lines define contours of constant (acceptable) transfer orbit shadow duration. The two open belts define the time-varying launch windows during the given launch period. Other studies demonstrated that optimal fuel requirements occurred at ascending node values at $\Omega = 225$ and 305°. The final launch time strategy as a function of launch date is then demonstrated by the heavy solid line of the figure. Such a plot is extremely useful in launch window analyses and should be the primary output of those studies.

8.3.2 Computational Flow

The general computational flow for launch window studies is illustrated in Figure 8.3-2. The structure is essentially the same as that of FLAP (Reference 8-1) but with the launch time and launch date loops reversed. This revised structure permits the one-time computation of launch date peculiar data such as the Earth-Sun direction or the Greenwich Hour Angle for the range of launch times. The launch time or ascending node computation was given in
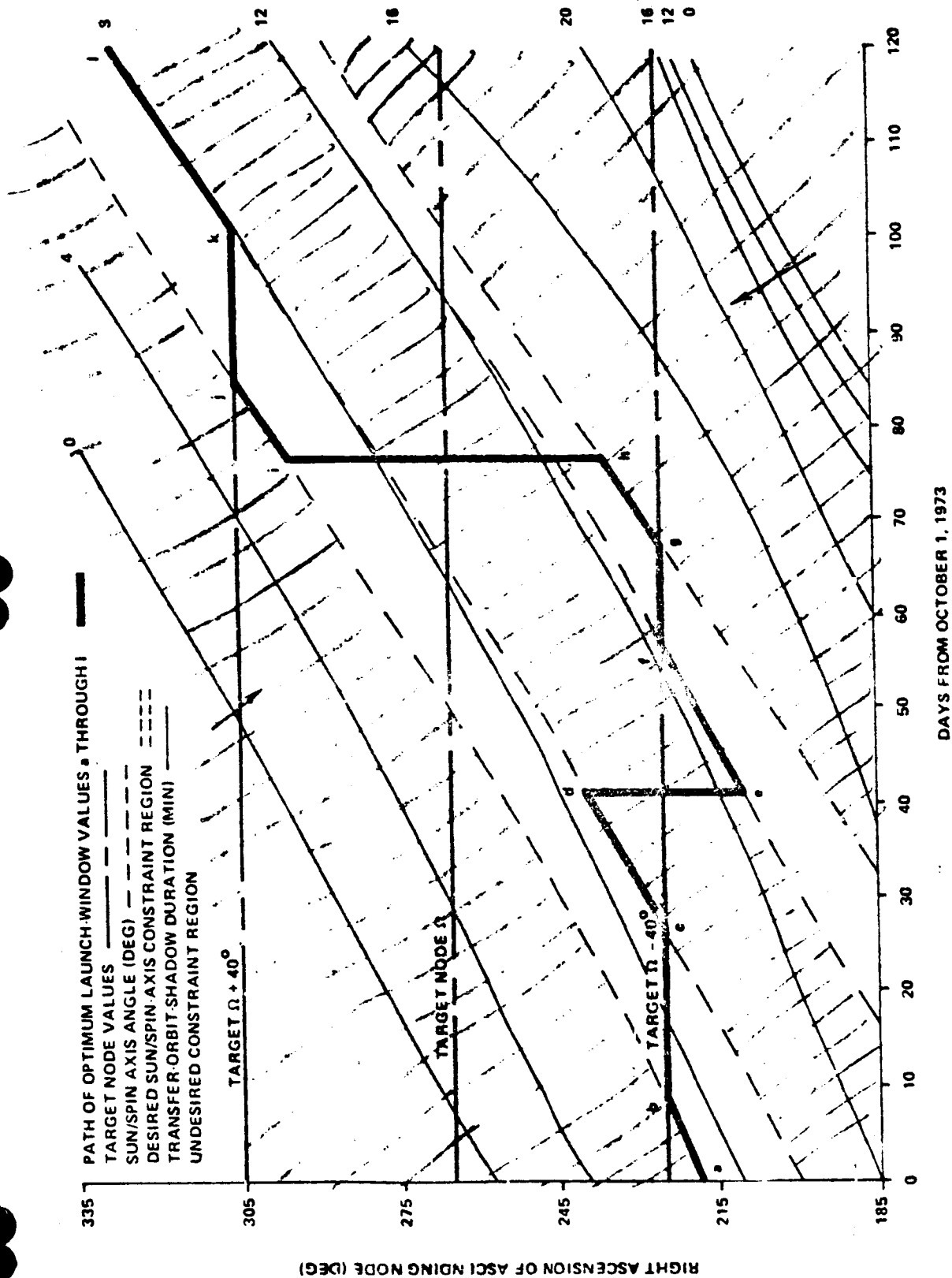
Figure 8.3-1.   Figure 9-3.   Launch Window Analysis for SMS

Section 8.2.2. The trajectory/maneuver sequence computations were presented in Sections 8.2.3 and 8.2.4. The computation of the mission/systems constraints is discussed in Section 8.3.3 below.
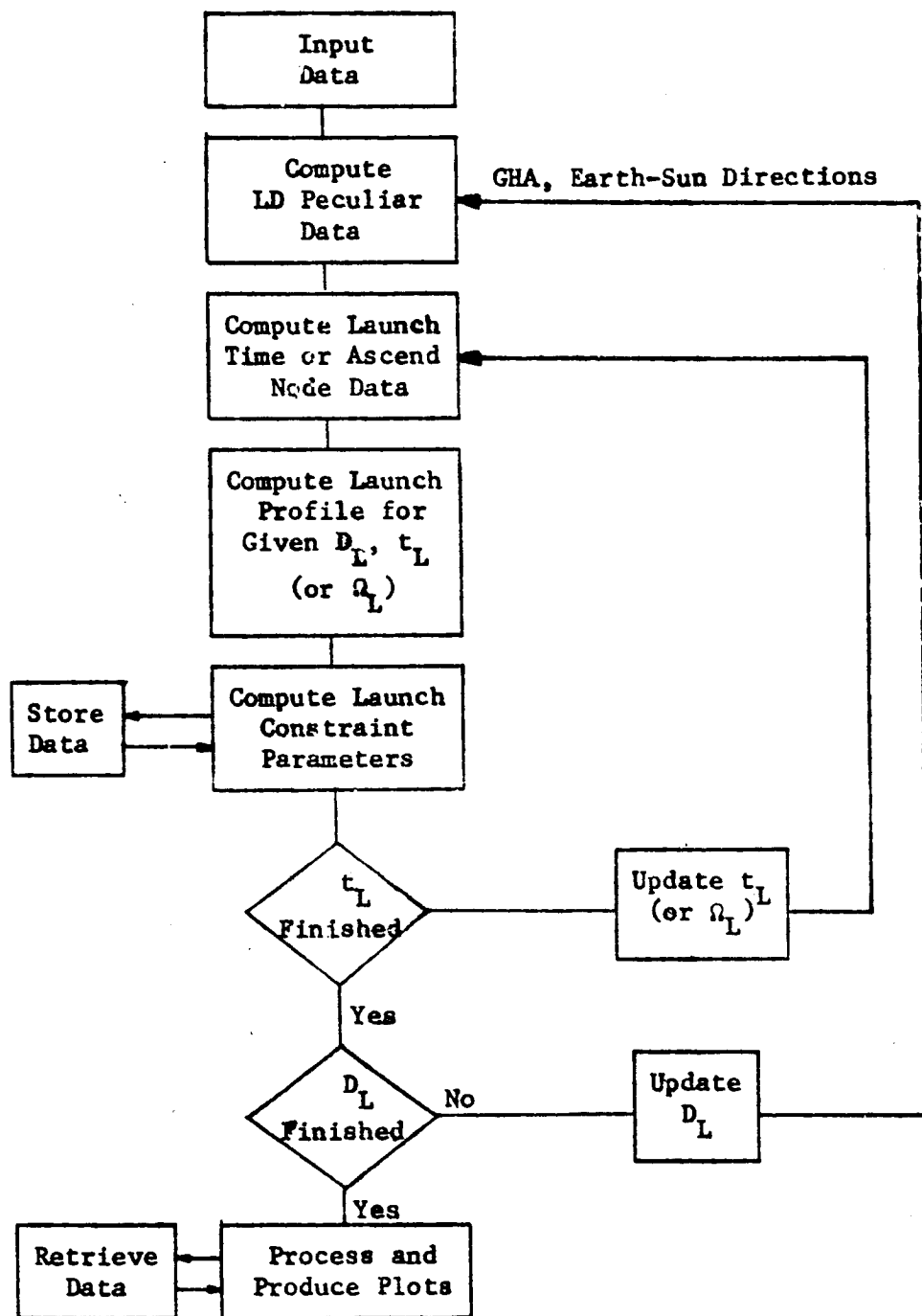
Figure 8.3-2. Launch Window Analysis

8.3.3 Launch Phase Constraints

Constraints are imposed on the launch and transfer phases of a mission by the mission objectives and spacecraft systems requirements. The parameters considered in the launch window analysis are generally amenable to simple formulation and efficient computation to facilitate the necessary wide scans in launch date and daily launch time. After identifying attractive dates and orbits more detailed studies may be made (Section 8.4). Candidate launch phase parameters are given in Table 8.3-3 below.

Shadowing

Earth Site Passages

Orbit Lifetime

Orbit Stability

Solar Aspect Angles at Maneuvers

Station Visibility at Maneuvers

Table 8.3-3. Critical Launch Parameters

The first four parameters are based on the orbits of the transfer phases as given in Table 8.2-2; the latter two on the critical states at maneuvers as given in Table 8.2-3.

The shadowing data needed includes the start time and duration of each shadow within each of the orbits encountered along with the total time-in-shadow encountered. The earth site passage data includes the time of entrance and the duration over specific earth sites, (e.g., science target sites or tracking sites) and the total time over sites. The orbit lifetime computations are analytic expressions for gross estimates of the lifetime for low-altitude drag-affected orbits. The orbit stability approximations determine the life-expectancy of high-altitude orbits affected by third-body gravitation. Either of these computations if efficiently formulated is appropriate for launch window studies. The solar aspect angle at maneuvers is critical because it defines the vehicle maneuver attitude relative to the sun which may expose sensitive instruments to sunlight or violate solar array requirements. The station visibility at maneuvers may be necessary for maneuver implementation.

The mathematical formulation of each of these parameters is detailed in Chapter 7.

8.4 Detailed Launch Targeting

A slightly different kind of launch phase analysis capability
is represented by the routine START of Reference 8-5. This is the
capability to target to desired conditions using realistic launch para-
meters as the control parameters. This targeting capability uses the
results of the launch window analysis to narrow the range of appropriate
launch dates initially. The START capability provides a refined and
extended analysis of the launch phase for a specific date and approxi-
mate time of launch. Suggested extensions to the START capability in
Section 8.4.2 would appear to be extremely useful.

8.4.1 Detailed Launch Profile

The detailed launch profile input parameters are defined in
Table 8.4-1 and illustrated in Figure 8.4-1. The detailed model permits
the boost or ascent arc and the injection arc to be modeled as finite
duration in both angle and time. Furthermore, the injection burn it-
self can be modeled as a finite thrust maneuver. The parameters defining
the parking orbit allow its modeling as either a circle $[\Gamma_p = 0, V_p = (\mu/R_p)^{\frac{1}{2}}]$
or ellipse ($\Gamma_p \neq 0$).

The conversion of these parameters into a post-injection state
suitable for targeting closely parallels the development of the standard
profile defined in Section 8.2. The launch time-of-day input option is
required for this application so equations (8.2-1) through (8.2-4) are used
to compute the normal $\hat{N}$, the inclination i_p and node Ω_p of the parking
orbit. The RTN coordinate system is then established at the launch site
(at the launch time-of-day) via Equations (8.2-11) and (8.2-12).

The state at the burnout point following the insertion into park-
ing orbit. This state is computed as

$$\underline{R}_B = R_p \ (\hat{R} \cos \psi_L + \hat{T} \sin \psi_L) \tag{8.4-1}$$

$$\underline{V}_B = V_p \ (-\hat{R} \sin(\psi_L + \Gamma_p) + \hat{T} \cos (\psi_L + \Gamma_p) \tag{8.4-2}$$

$$t_B = t_L + \Delta t_L \tag{8.4-3}$$
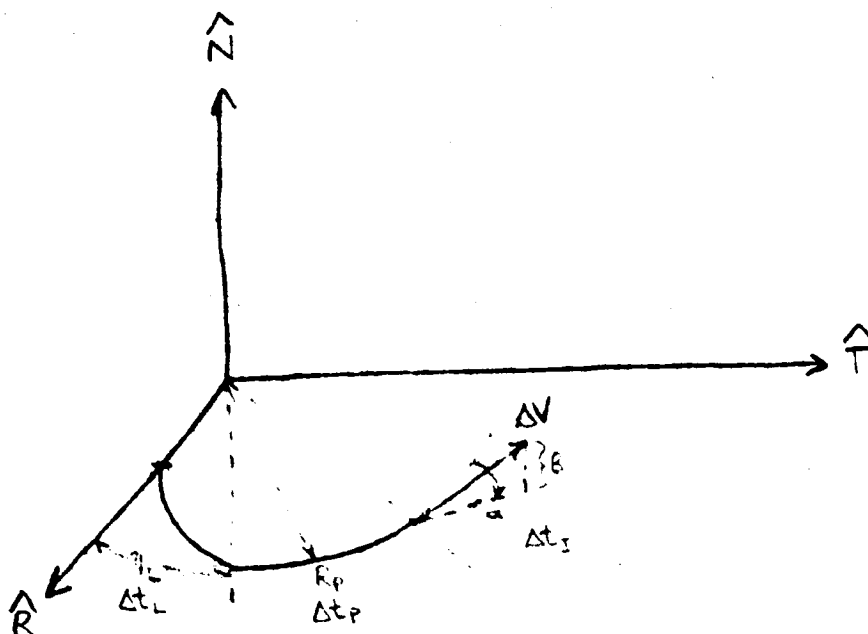
Figure   Figure 8.4-1.   Detailed Targeting Profile

Phase	Fixed Parameters	Control Parameters
Boost	Launch site longitude θ_L	Launch azimuth Σ_L
	Launch site latitude Φ_L	Launch time t_L
	Central angle of burn ψ_{L}	
	Time interval of burn Δt_L	
Parking Orbit	Burnout radius R_p	Parking orbit coast time Δt_p
	Burnout velocity V_p	
	Burnout flight path angle Γ_p	
Injection (Impulsive)	Central Angle of Burn ψ_I	Injection in-plane angle α
	Time interval of burn Δt_I	Injection out-of-plane angle β
		Injection magnitude ΔV
Injection (Finite thrust)	Vehicle mass before burn M_o	α
	Mass flow rate in	β
	Thrust magnitude T	Burn time t_B

Table 8.4-1.   Detailed Targeting Parameters

8.4-2

The preinjection state (R_I, V_I, t_I) is then computed. With the assumption of a circular parking orbit the state is given by

$$\underline{R}_I' = R_P (\hat{R} \cos \chi + \hat{T} \sin \chi) \tag{8.4-4}$$

$$\underline{V}_I' = V_P (-\hat{R} \sin \chi + \hat{T} \sin \chi) \tag{8.4-5}$$

$$t_I' = t_B + \Delta t_P \tag{8.4-6}$$

where

$$\chi = \chi_L + \omega_P \Delta t_P \tag{8.4-7}$$

$$\omega_P = (\mu / R_P^3)^{\frac{1}{2}} \tag{8.4-8}$$

and where Δt_P is the control parameter of parking orbit coast time. In the case of elliptic motion and/or a more accurate propagator, the state at the end of insertion burnout is propagated forward over the time interval Δt_P to generate $(\underline{R}_I', \underline{V}_I')$.

The post-injection state depends directly on the parameters defining the injection maneuver. The current model (Ref. 8-5) is based on a fixed attitude maneuver using either impulsive or finite thrust. The direction in either case is specified by the in-plane (elevation) angle α from the premaneuver velocity vector V_I and the out-of-plane angle β described in Figure 8.4-1. The right ascension of the premaneuver velocity vector in the RTN System is

$$\delta = \tan^{-1}(V_T/V_R) \qquad 0 \leq \delta < 360 \tag{8.4-9}$$

Then the direction of the injection burn is given by

$$\Delta V = \cos \cos (\alpha + \delta)\hat{R} + \cos\beta\sin (\alpha + \delta)\hat{T} + \sin\beta\hat{N} \tag{8.4-10}$$

The post injection state for the impulsive model is then given as

$$\underline{R}_I^+ = R_I^- \tag{8.4-11}$$

$$\underline{V}_I^+ = V_I' + \Delta V_I \quad \Delta V \tag{8.4-12}$$

$$t_I^+ = t_I + \Delta t_I \tag{8.4-13}$$

The post injection state for the finite thrust model is given in Section 9.2.

8.4.2 Targeting and Optimization

The six controls defined in Table 8.4-1 may be varied to satisfy up to six target parameters. If the number of controls exceeds the number of targets some quantity may be minimized as well.

For general earth orbital targeting it is reasonable to define the target or performance variables in terms of the state following the post-insertion burn (8.4-11, 12, 13). This permits a standard formulation of the general targeting process. Assume that the target parameters are the six conic elements denoted by the vector $\underline{\tau}$. Let the desired values of these parameters be denoted τ^*. Then let the K-th iterate of the control parameters be denoted α_K and the corresponding value of the target parameters be denoted τ_K. The (K+1)th iterate value of the control parameters is then formally given by

$$\alpha_{K+1} = \underline{\alpha}_K + f[\tau - \tau_K, \frac{\partial \tau}{\partial \underline{\alpha}} \Big|_K]$$

(8.4-14)

where the details of this targeting is given in Chapter 11. The zero iterate needed to start the process may be computed from the standard launch profile described in Section 8.2. The sensitivity matrix may be computed by numerical differencing or the analytic equations given in the state transition matrix computations provided in Chapter 6.

It would be desirable to extend the targeting and optimization process through a second maneuver at injection into a third orbit. This would then allow the automated and integrated targeting of the parking, trans-fer and target orbits for preflight analysis.

8.5   Launch Phase Error Analysis

The preflight error analysis of the launch phase is generally
performed by the launch vehicle personnel up to and including the in-
jection maneuver. The results of this analysis is an injection covari-
ance which defines the errors at the injection point based on errors in
the boost maneuver, the parking orbit and the injection maneuver itself.
GMAS must be able to accept such an injection covariance and propagate
it along the transfer orbit to the injection point for the inclusion of
the insertion maneuver errors. This, however, is the purpose of the
maneuver error analysis addressed in Chapter 13. It is necessary to
transform the injection covariance from any of the injection peculiar
coordinate systems to a standard system for the use by the linear or
Monte Carlo analyses.

8.6 References

8-1 K. G. Nickerson and S. Rosenberg: FORTRAN LAUNCH ANALYSIS PROGRAM (FLAP), CSC Report No. 5035-26600-01TR, October, 1972

8-2 S. Rosenberg: SYNCHRONOUS METEOROLOGICAL SATELLITE (SMS) LAUNCH WINDOW ANALYSIS, CSC Report No. 9101-13500-02TR, November 1972

8-3 F. T. Sun: ANALYSIS SOLUTION FOR OPTIMAL TWO IMPULSE 180° TRANSFER BETWEEN NONCOPLANAR ORBITS AND THE OPTIMAL ORIENTATION OF THE TRANSFER PLANE, AIAA Journal, Vol. 7, No. 10, October 1969

8-4 D. A. Lutzky, W. S. Bjorkman, C. Uphoff: FINAL REPORT FOR RADIO ASTRONOMY EXPLORER-B IN FLIGHT MISSION CONTROL DEVELOPMENT EFFORT; AMA Report No. 73-8, March 1973

8-5 W. S. Bjorkman and M. J. Brooks: PROGRAMMER'S MANUAL FOR THE ADVANCED MISSION ANALYSIS PROGRAMS, Philco-Ford Report TR-DA1622, January 1968.

8-6 B. Kaufman and D. P. Muhover: IMP-I LAUNCH WINDOW ANALYSIS, GSFC X-551-71-5, January 1971

9. MANEUVER MODELING

9.1 Introduction

The next three chapters consider directly a primary problem addressed by GMAS: maneuver analysis. This chapter discusses the general mathematical modeling of maneuvers. Chapter 10 addresses the deterministic targeting of impulsive maneuvers. Chapter 11 considers the refinement of maneuvers by numerical techniques to permit more detailed implementation models, targeting of more complicated maneuvers or sequences, or optimization of maneuvers when possible.

As stated, this chapter is intended to provide the mathematical models used in general maneuver analysis. Section 9.2 defines the mathematical models available for maneuver simulation. Section 9.3 addresses the modeling of vehicle attitude at maneuvers. Section 9.4 discusses the propulsion system characteristics.

The consideration of maneuver command generation and processing in the operational Flight Dynamics System was beyond the scope of this effort but would be considered for possible inclusion as a separate chapter in GMAS at some later date.

9.2 Maneuver Simulation

Three options for simulating burn maneuvers will provide the user with the capability to simulate a given maneuver with three levels of accuracy. The three options are described as follows:

1) Impulsive delta velocity maneuver,

2) Analytical finite burn maneuver,

3) Numerically integrated finite burn maneuver.

Each option will be selected by user input.

The equations for these models and the underlying assumptions for each model will now be described.

9.2.1 Impulsive Delta Velocity Maneuver

This frequently-used model (Ref. 9-1) will instantaneously apply a delta inertial velocity in the direction of the positive roll axis of the vehicle. The vehicle roll axis orientation and delta velocity can be user specified or internally calculated to produce a specified maneuver, i.e., plane change apogee raising, etc. The equations for this model are

$$\underline{r}_2 = \underline{r}_1 \tag{9.2-1}$$

$$\underline{V}_2 = \underline{V}_1 + [IB]^{-1} \begin{bmatrix} \Delta V \\ 0 \\ 0 \end{bmatrix} \tag{9.2-2}$$

where:

$\underline{r}_2$ is the final radius vector

$\underline{r}_1$ is the initial radius vector

$\underline{V}_2$ is the inertial velocity vector after the impulsive maneuver

$\underline{V}_1$ is the inertial velocity vector before the impulsive maneuver

ΔV is the delta velocity magnitude, and

$[IB]$ is the transformation from the geocentric inertial system to the vehicle body coordinate system.

9.2.2 Analytical Finite Burn Maneuver

This model (Ref. 9-2) will propagate the vehicle state vector through a burn maneuver by analytically solving the equations of motion under certain simplifying assumptions. These assumptions are:

a) Constant vehicle attitude during the burn maneuver,

b) Constant thrust and flowrate during the burn maneuver,

c) Spherical planet model with constant gravity during the burn maneuver.

The equations of motion for these conditions are given by

$$\underline{a}_I = \frac{-\mu \, \underline{\gamma}_1}{\gamma_1^{\,3}} + \left[IB\right]^{-1} \frac{T}{m} \hat{T} \qquad (9.2\text{-}3)$$

The acceleration vector is integrated to yield the velocity vector after the burn maneuver

$$\underline{V}_2 = \underline{V}_1 - \frac{\mu \underline{\gamma}_1 \, \Delta t}{\gamma_1^{\,3}} + \left[IB\right]^{-1} \frac{T}{\dot{m}} \hat{T} \ell n \left(\frac{m_1 + \dot{m}\Delta t}{m_1} \right) \qquad (9.2\text{-}4)$$

The velocity vector is integrated to yield the radius vector after the burn maneuver

$$\underline{\gamma}_2 = \underline{\gamma}_1 + \underline{V}_1 \Delta t - \frac{\mu \underline{\gamma}_1 \Delta t^2}{2\gamma_1} + \left[IB\right]^{-1} \frac{T}{\dot{m}} \hat{T} \Delta t^2 \left[\frac{m_1 + \dot{m}\Delta t}{\dot{m}\Delta t} \ell n \left(\frac{m_1 + \dot{m}\Delta t}{m_1} \right) - 1 \right] \qquad (9.2\text{-}5)$$

where:

$\underline{a}_I$ is the acceleration vector

T is the thrust magnitude

m is the current vehicle mass

$\dot{m}$ is the vehicle mass rate of change

m_1 is the vehicle mass before the burn maneuver

Δt is the maneuver burn time

$\hat{T}$ is the unit thrust vector in the body system

9.2.3 Numerically Integrated Finite Burn Maneuver

This model (Ref. 9-3) will simulate the burn maneuver by numerically integrating the burn. The thrust and flowrate for this model are user specified as time history tables. The thrust vector is assumed to be coincident with the vehicle roll axis, with the

vehicle roll axis being oriented via user input or by the target-
ing algorithm based on user input. The equations of motion for this
model are given by

$$\underline{a}_I = \underline{a}_G + \left[\, IB\,\right]^{-1} \left(\frac{T(t)}{m_1 + \dot{m}(t)\Delta t} \right) \hat{T} \qquad\qquad (9.2\text{-}6)$$

where:

$\underline{a}_G$ is the gravity acceleration

$T(t)$ is the current table look-up value of thrust

$\dot{m}(t)$ is the current table look-up value of mass flowrate

$\hat{T}$ is the unit thrust vector in the body system

9.3 Attitude Modeling

9.3.1 Introduction

Attitude modeling plays a critical role in maneuver analysis and design. The vehicle has a nominal attitude (for example, inertially fixed or local vertical) during periods of cruise. It generally must be reoriented prior to each maneuver to align the engines in the direction of the desired burn. Following the maneuver the vehicle is generally reoriented to its cruise attitude.

The detailed analysis of attitude maneuvers and the attitude control system are not the responsibility of the GMAS; six-degree-of-freedom analyses at this time are groundruled out of the study. However much instructive information defining the size and direction of attitude maneuvers can be computed from analytic equations.

There are two approaches possible in attitude maneuver modeling. The standard approach as used in a program such as POST (Ref. 9-4) develops a general targeting structure that includes attitude system parameters directly as control parameters within the trageting process. This is an extremely effective means of simulating a wide variety of steering laws and simulation models. Such an approach permits convenient simulation and targeting of maneuvers in which thrusting occurs during attitude maneuvers. This capability may eventually be necessary for shuttle era missions which require repeated satellite transfers to shuttle-accessible orbits.

The significant orbital maneuvers might occur over long enough time intervals to require vehicle pitching during the thrusting to reduce velocity losses.

The approach used in this section addresses the problem somewhat differently. It assumes that the thrust direction has been computed by some means (analytic targeting, parametric scan, numerical targeting) and the cruise attitude is known (input). The approach then computes the Euler angles, angle rates or body rates and the attitude behavior during the orientation maneuvers. The

computations can then be performed in an independent module to the standard maneuver analysis and available on request. The formulation still allows the reader to see the computational flow for the more standard POST approach by reversing the computations and proceding from the attitude control parameters to the definition of the ΔV direction.

The attitude of the spacecraft is conventionally specified in terms of an appropriate set of Euler angles. Distinct combinations of such Euler angles best simulate various attitude reference systems. The difference between these various Euler angle combinations are the initial reference frame and the ordered sequence of rotations. A good range of attitude modeling capability is represented by the following attitude models:

    1)   Inertial Euler angles

    2)   Relative Euler angles

    3)   Velocity relative angles

    4)   Vehicle body rates

These models are discussed in the following subsections.

9.3.2 Inertial Euler Angles

The inertial system is most convenient when considering spacecraft employing inertial reference systems. The ordered inertial Euler angles with respect to the inertial attitude reference frame are defined below:

ϕ_I - Inertial roll angle. The roll angle about the inertial x-axis (1st rotation).

ψ_I - Inertial yaw angle. The yaw angle about the z-axis that resulted from the ϕ_I rotation (2nd rotation).

θ_I - Inertial pitch angle. The pitch angle about the y-axis that resulted from the ϕ_I & ψ_I rotations (3rd rotation).
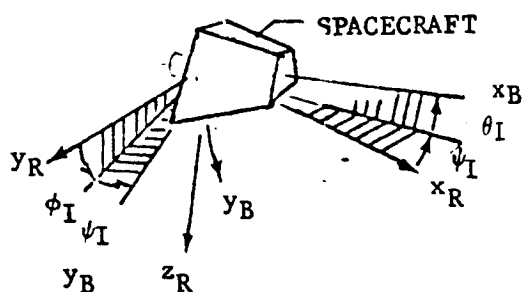
Figure 9.3-1
Inertial Euler Angles

Denote the unit vectors defining the inertial reference frame by (x_R, y_R, z_R) and those defining the desired maneuver direction by (x_B, y_B, z_B) with reference to the geocentric inertial coordinates. Then the angles ϕ_I, ψ_I, and θ_I are defined by

$$\phi_I = \tan^{-1}(RB_{23}/RB_{22})$$

$$\psi_I = -\sin^{-1}(RB_{21})$$ (9.3-1)

$$\theta_I = \tan^{-1}(RB_{31}/RB_{11})$$

where $[RB]$ is the matrix defining the rotation from the reference frame to the body frame computed from

$$RB = \begin{bmatrix} X_B \\ \hline Y_B \\ \hline Z_B \end{bmatrix} \begin{bmatrix} X_R \\ \hline Y_R \\ \hline Z_R \end{bmatrix}^T$$ (9.3-2)

9.3.3 Relative Euler Angles

The relative system is most convenient when analyzing vehicles using local horizontal reference systems. The relative Euler angles with respect to the geographic frame are given by:
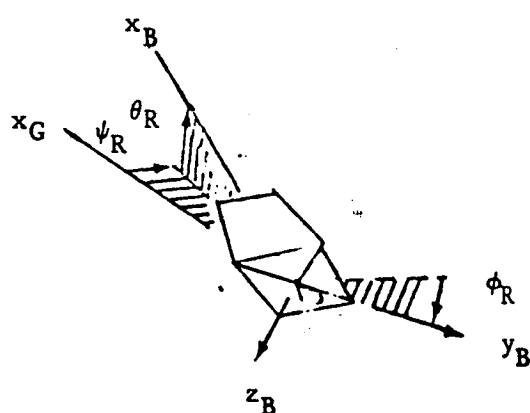
ψ_R – Relative yaw angle. The azimuth angle of x_B axis measured clockwise from the reference direction (1st rotation).

θ_R – Relative pitch angle. The elevation angle of x_B axis above the local horizon frame (2nd rotation).

ϕ_R – Relative roll angle. The roll angle about the x_B axis (3rd rotation).

Figure 9.3-2   Relative Euler Angle

The geographic frame is defined with respect to the inertial geocentric system by (X_G, Y_G, Z_G) where X_G is in the local horizontal plane and points north, the Y_G axis is in the local horizontal plane and points east and Z_G completes the right hand system.

Then the angles (ψ_R, θ_R, ϕ_R) are defined as

$$\psi_R = \tan^{-1}(GB_{12}/GB_{11})$$
$$\theta_R = -\sin^{-1}(GB_{13})$$
$$\phi_R = \tan^{-1}(GB_{23}/GB_{33})$$

(9.3-3)

where $[GB]$ is the matrix defining the rotation from the geographic frame to the body frame defined by

$$[GB] = \begin{bmatrix} X_B \\ \hline Y_B \\ \hline Z_B \end{bmatrix} \begin{bmatrix} X_G \\ \hline Y_G \\ \hline Z_G \end{bmatrix}'$$

(9.3-4)

where (X_G, Y_G, Z_G) are the unit vectors defining the geographic axes relative to the inertial system.

9.3.4 Velocity Relative Angles

The velocity relative system is useful in developing intuition about the geometry of the required maneuvers. The Euler angles in this system are computed from:

σ_I - Velocity relative roll angle. This angle is a rotation about the inertial velocity vector (1st rotation).

β_I - Out of plane yaw angle. This angle is a negative rotation about the intermediate z-axis resulting from the roll angle I (2nd rotation).

α_I - Velocity relative pitch angle. This angle is a positive rotation (nose-up) when the vehicle is in an upright attitude (3rd rotation).
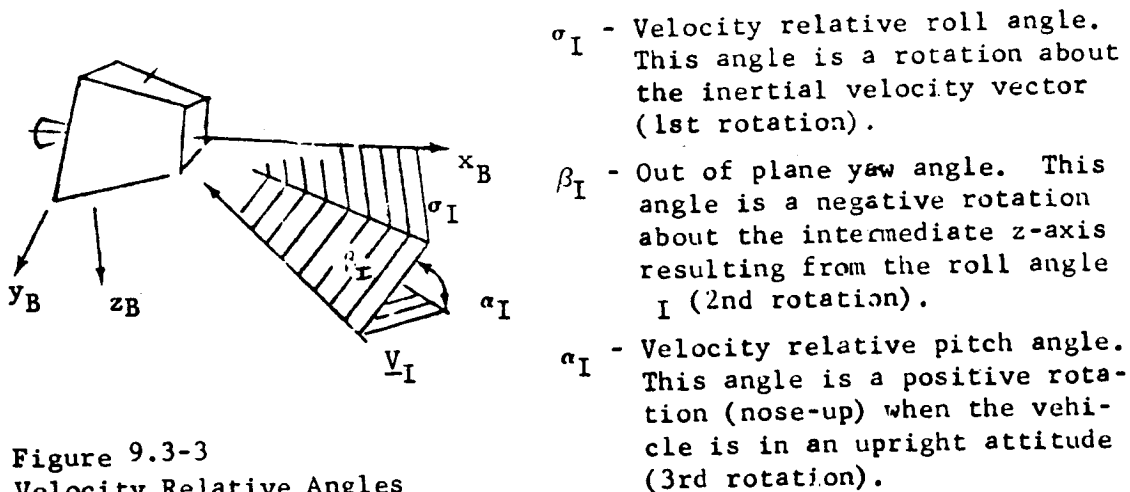
Figure 9.3-3
Velocity Relative Angles

These angles amy be computed from

$$\alpha = \tan^{-1}(V_{IXB}/V_{IZB})$$
$$\beta = \tan^{-1}(V_{IYB}/\sqrt{V_{IXB}^2 + V_{IYB}^2})$$
$$\sigma = \tan^{-1}\left(\frac{GB_{23} + \sin\beta \sin\gamma_I}{GB_{22}\cos A_{ZI} - GB_{21}\sin A_{ZI}\cos\gamma_I}\right)$$

(9.3-5)

where $[GB]$ is the matrix transformation from the geographic frame to the body frame, $\underline{V}_{IB}$ is the inertial velocity in the body frame, and A_{ZI} and γ_I are the inertial velocity azimuth and flight path angle.

9.3.5 Angle Rates

The actual reorientation of the spacecraft attitude from the initial to the final orientation can be modeled by an appropriate set of piecewise linear attitude polynomials. In this type of model the attitude rates are computed to satisfy the desired change in each attitude angle.

The calculation of the attitude rates ($\dot{\psi}$, $\dot{\theta}$, $\dot{\phi}$) required to change the attitude from the initial orientation (ψ_i, θ_i, ϕ_i) to the desired orientation (ψ_f, θ_f, ϕ_f) in the (input) time periods (Δt_ψ, Δt_θ, Δt_ϕ) are given by

$$\dot{\psi} = \frac{\psi_f - \psi_i}{\Delta t_\psi}, \qquad \dot{\theta} = \frac{\theta_f - \theta_i}{\Delta t_\theta}, \qquad \dot{\phi} = \frac{\phi_f - \phi_i}{\Delta t_\phi} \qquad (9.3\text{-}6)$$

The attitude during the maneuver is then computed as indicated in Figure 9-4 and equations (9-13).

$$\psi = \begin{cases} \psi_i + \dot{\psi}(t-t_i) & : t_i \leq t \leq t_i + \Delta t_\psi \\ \psi_f & : t > t_i + \Delta t_\psi \end{cases}$$

$$\theta = \begin{cases} \theta_i + \dot{\theta}(t-t_i) & : t_i \leq t \leq t_i + \Delta t_\theta \\ \theta_f & : t > t_i + \Delta t_\theta \end{cases} \qquad (9.3\text{-}7)$$

$$= \begin{cases} \phi_i + \dot{\phi}(t-t_i) & : t_i \leq t \leq t_i + \Delta t_\phi \\ \phi_f & : t_i > t_i + \Delta t_\phi \end{cases}$$

Figure 9.3-4. Linear Attitude Reorientation Model

9.3.6 Vehicle Body Rates

Any of the above-described Euler rotations may be described in terms of equivalent body rates. These rates are defined as

ω_x — Roll body rate. The angular rate about the x_B-axis in deg/sec.

ω_y — Pitch body rate. The angular rate about the y_B-axis in deg/sec.

ω_z — Yaw body rate. The angular rate about the z_B-axis in deg/sec.
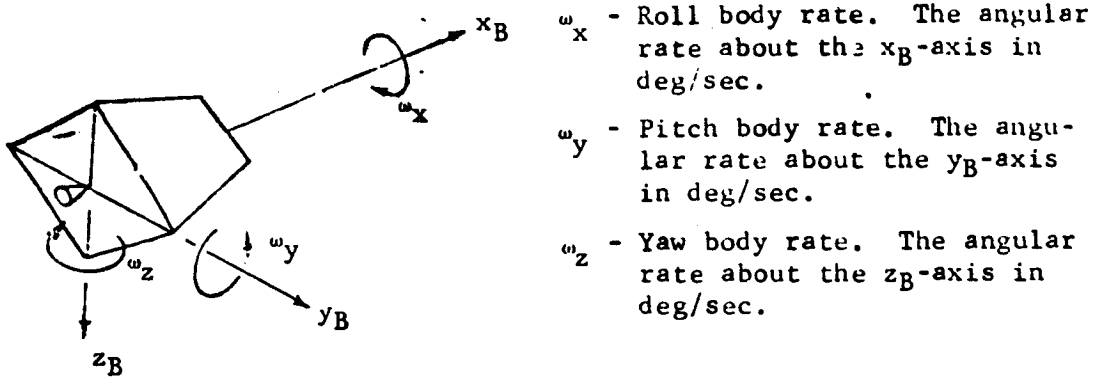
Figure 9.3-5. Body Rates

These rates may be computed from each of the referenced angular systems as follows:

<u>Inertial Euler Angle Rates</u>:

$$\begin{bmatrix} \omega_x \\ \omega_y \\ \omega_z \end{bmatrix} = \begin{bmatrix} \dot{\phi}_I \cos\psi_I \cos\theta_I - \dot{\psi}_I \sin\theta_I \\ \dot{\theta}_I - \dot{\phi}_I \sin\psi_I \\ \dot{\phi}_I \cos\psi_I \sin\theta_I + \dot{\psi}_I \cos\theta_I \end{bmatrix} \qquad (9.3\text{-}8)$$

<u>Relative Euler Angle Rates</u>:

$$\begin{bmatrix} \omega_x \\ \omega_y \\ \omega_z \end{bmatrix} = \begin{bmatrix} \dot{\phi}_R - \dot{\psi}_R \sin\theta_R \\ \dot{\theta}_R \cos\phi_R + \dot{\psi}_R \sin\phi_R \cos\theta_R \\ \dot{\psi}_R \cos\phi_R \cos\theta_R - \dot{\theta}_R \sin\phi_R \end{bmatrix} + \begin{bmatrix} GB \end{bmatrix} \begin{bmatrix} v/r \\ -u/r \\ -\dfrac{v}{r} \tan\phi_c \end{bmatrix}_1 \qquad (9.3\text{-}9)$$

where $\begin{bmatrix} GB \end{bmatrix}$ is the transformation matrix between the geographic and the body frame; u and v are the north and east components of the inertial velocity vector; r is the current geocentric radius vector to the vehicle; and ϕ_c is the current geocentric latitude of the vehicle.

Velocity Relative Angles:

$$\begin{bmatrix} \omega_x \\ \omega_y \\ \omega_z \end{bmatrix} = \begin{bmatrix} a_1 + d_1\dot{\sigma} + (\sin\alpha)\,\dot{\beta} \\ a_2 + d_2\sigma + \\ a_3 + d_3\dot{\sigma} + (\cos\alpha)\,\dot{\beta} \end{bmatrix} \quad ; \tag{9.3-10}$$

where

$$\begin{bmatrix} u \\ v \\ \omega \end{bmatrix} = \begin{bmatrix} IG \end{bmatrix} \underline{V}_I, \tag{9.3-11}$$

$$\begin{bmatrix} a_1 \\ a_2 \\ a_3 \end{bmatrix} = \begin{bmatrix} GB \end{bmatrix} \begin{bmatrix} v/r_I - \dot{\gamma}_I \sin\pi_I \\ -u/r_I + \dot{\gamma}_I \cos\pi_I \\ -\dfrac{v\tan\phi}{r_I} + \dot{\pi}_I \end{bmatrix} \tag{9.3-12}$$

$$\begin{bmatrix} d_1 \\ d_2 \\ d_3 \end{bmatrix} = \begin{bmatrix} GB \end{bmatrix} \begin{bmatrix} \cos\pi_I \cos\gamma_I \\ \sin\pi_I \cos\gamma_I \\ -\sin\gamma_I \end{bmatrix} \tag{9.3-13}$$

$$\dot{\pi}_I = (u\dot{v} - v\dot{\omega})/(u^2 + v^2) \tag{9.3-14}$$

$$\dot{\gamma}_I = (-V_I\dot{\omega} + \omega\dot{V}_I)/V_I\sqrt{V_I^2 - \omega^2}$$

Having computed the body rates the attitude kinematics during the orientation maneuver may be computed. Define the quaternion as

$$\underline{q} = e_0 + e_1 i + e_2 j + e_3 k = (e_0, e_1, e_2, e_3) \tag{9.3-15}$$

The quaternion rate equation is given by

$$\dot{\underline{q}} = \frac{1}{2} Q \underline{\omega} \tag{9.3-16}$$

where

$$Q = \begin{bmatrix} -e_1 & e_2 & e_3 \\ e_0 & e_2 & -e_3 \\ e_0 & -e_1 & e_3 \\ e_0 & e_1 & -e_2 \end{bmatrix} \tag{9.3-17}$$

The initial value of $\underline{q}$ for (9.3-16) is given by

$$\underline{q}_0 = \underline{q}(\phi_I)* \ \underline{q}(\psi_I)* \ \underline{q}(\theta_I) \tag{9.3-18}$$

where

$$\underline{q}(\phi_I) = \cos\frac{\phi_I}{2} + \sin\frac{\phi_I}{2} \, i$$

$$\underline{q}(\psi_I) = \cos\frac{\psi_I}{2} + \sin\frac{\psi_I}{2} \, k \tag{9.3-19}$$

$$\underline{q}(\theta_I) = \cos\frac{\theta_I}{2} + \sin\frac{\theta_I}{2} \, j$$

The solution to (9.3-16) through 9.3-19) then yields the instantaneous orientation of the body reference frame with respect to the inertial frame:

$$\begin{bmatrix} RB \end{bmatrix} = \begin{bmatrix} e_0^2+e_1^2-e_2^2-e_3^2 & 2(e_1e_2+e_0e_3) & 2(e_1e_3-e_0e_2) \\ 2(e_1e_2-e_0e_3) & e_0^2-e_1^2+e_2^2-e_3^2 & 2(e_0e_1+e_2e_3) \\ 2(e_1e_3+e_0e_2) & 2(e_2e_3-e_0e_1) & e_0^2-e_1^2-e_2^2+e_3^2 \end{bmatrix} \tag{9.3-20}$$

9.3.7 Translational Effects of Attitude Maneuvers

The effect of the Attitude Control System (ACS) maneuvers on the vehicle state vector can be estimated in point mass trajectory simulations by including a translational delta velocity per maneuver along each axis in the vehicle body system. The calculation of the amount of translational delta velocity along each axis requires the use of a program which can simulate the maneuver in six degrees-of-freedom. Once the translational delta velocity values are known, these delta velocities can be added along each vehicle axes at the time of each orientation maneuver. This procedure requires that the trajectory be interrupted the time of each orientation maneuver in order to add the estimated delta velocities due to the maneuver.

The translational delta velocities are a function of the net thrust along each axis and the amount of time each thruster is on during a maneuver, and the orientation of the vehicle before and after the maneuver.

Neglecting thruster misalignment angles, the relationships between the type of thruster and the delta velocity direction would be as follows:

THRUSTER TYPE	ΔV DIRECTION ALONG
ROLL	VEHICLE PITCH AND/OR YAW AXES
PITCH	VEHICLE ROLL AXIS
YAW	VEHICLE ROLL AXIS

Given the initial vehicle orientation, final orientation, the time required to reorient, and the net thrust for each type of thruster over the reorientation time, the translational acceleration can be approximated by

$$\underline{a}_I = \underline{a}_G + \begin{bmatrix} IB \end{bmatrix}^{-1} \frac{1}{m} \begin{bmatrix} T_{NRP} + T_{NRY} \\ T_{NPR} \\ T_{NYR} \end{bmatrix} \qquad (9.3-21)$$

where:

T_{NRP} is the net thrust along the roll axis due to a pitch maneuver

T_{NRY} is the net thrust along the roll axis due to a yaw maneuver

T_{NPR} is the net thrust along the pitch axis due to a roll maneuver

T_{NYR} is the net thrust along the yaw axis due to a roll maneuver

The reorientation maneuver would then be simulated by specifying the start and end times of the maneuver, the initial and final vehicle orientation angles and the appropriate net thrust values for the maneuver. The maneuver would then be numerically integrated to obtain the approximate translational effect of the reorientation maneuver.

9.4 Propulsion System Modeling

The problem of monitoring vehicle center of gravity shifts due to propellant usage in certain tanks requires knowledge of the spacecraft geometry and propulsion characteristics. The number, location and orientation of tanks must be defined as well as the center of gravity shift versus propellant usage. In certain systems, half of the tanks are inverted to produce cancelling center of gravity shifts. If the tanks are the pressurized, diaphram type, then the center of gravity shift in the tank can be assumed to be along the centerline of the tank. If the propulsion system is a blow-down type system, the tank pressure is a function of the gas volume in the tank.

9.4.1 Thrust Modeling

One method of modelling such a system is the orbit adjust propulsion subsystem OAPS (Ref. 9-3). The following analysis is taken from that reference.

The rate of change in gas volume V_G and gas pressure $\dot{P}_G$ are given by the ideal gas low as follows

$$\dot{V}_G = \frac{F}{\rho} g_0 ISP \tag{9.4-1}$$

$$\dot{P}_G = -k \frac{P_G}{V_G} \frac{F}{\rho g_0 ISP} \tag{9.4-2}$$

where

ρ is the propellant density

k is the ratio of specific heats for the pressurant gas

P_G is the gas pressure

V_G is the gas volume

The propellant density can be described as a polynomial function of propellant temperature by

$$\rho = \sum_{i=1}^{3} d_i T_F^{i-1} \tag{9.4-3}$$

where d_i is the ith coefficient of the polynomial

T_F is the propellant temperature in degrees Rankine

The thrust (F) and specific impulse (I_{SP}) are given as polynomial functions of propellant pressure (P_P)

$$F = \sum_{i=1}^{5} a_i P_P^{i-1} \qquad (9.4-4)$$

$$I_{SP} = \sum_{i=1}^{5} C_i P_P^{i-1} \qquad (9.4-5)$$

where

a_i are the thrust polynomial coefficients

C_i are the specific impulse polynomial coefficients

the propellant pressure in the thrust chamber is computed as

$$P_P = (1 - \delta P_V)(P_G - \delta P_D) \qquad (9.4-6)$$

where

δP_V is a percentage pressure drop due to valves in the propellant line between the tank and the thrust chamber

δP_D is the pressure difference across the tank diaphram.

The pressure difference δP_D is given as a constant or as a polynomial function of propellant mass depending on the percentage of propellant usage as

$$\delta P_D = \sum_{i=1}^{2} C_i \left(1 - \frac{M_{P\eta}}{M_{P\eta_0}}\right)^{i-1} \qquad (9.4-7)$$

where

C_i are polynomial coefficients which are a function of ΔMP

$M_{P\eta}$ is the current propellant mass in the nth tank

$M_{P\eta_0}$ is the initial propellant mass in the nth tank

The acceleration due to the orbit adjust propulsion subsystem is given by

$$\underline{a} = \frac{F}{M} \hat{F} \qquad (9.4-8)$$

where

> M is the total spacecraft mass
>
> $\hat{F}$ is the unit vector defining the thrust axis in the vehicle body system.

9.4.2 Mass Properties Modeling

The center of mass of the spacecraft is calculated based on the summation of the individual centers of mass of each tank and the spacecraft with no propellant as follows (Ref. 9-5):

$$\underline{C} = \frac{\sum_{i=1}^{6} M_{P_\eta} \underline{C}_\eta}{M} + \frac{M_0}{M} \underline{C}_0 \qquad (9.4-9)$$

where

> M_{P_η} is the propellant mass in the nth tank
>
> M_0 is the spacecraft weight with no propellant
>
> M is the current total mass of the spacecraft
>
> $\underline{C}_0$ is the spacecraft center of mass with no propellant

The individual tank center of mass is assumed to lie on the tank centerline. The tank centerline orientation with respect to the body axis is given by the tank mounting angles θ_n and α_n.

The individual tank center of mass is then given by

$$\underline{C}_m = \underline{C}_{n0} + C_{L_n} \begin{pmatrix} \cos\theta_n \cdot \cos\alpha_n \\ \cos\theta_n \sin\alpha_n \\ \sin\theta_n \end{pmatrix} \qquad (9.4-10)$$

where

> $\underline{C}_{n0}$ is the origin of the tank coordinate system in vehicle body coordinates
>
> C_{L_n} is the tank center of mass in the tank coordinates

The tank mounting angles are illustrated as follows

X_B

α

θ

Y_B

CL_n

$\underline{C}_{n_0}$ X_T

Z_B
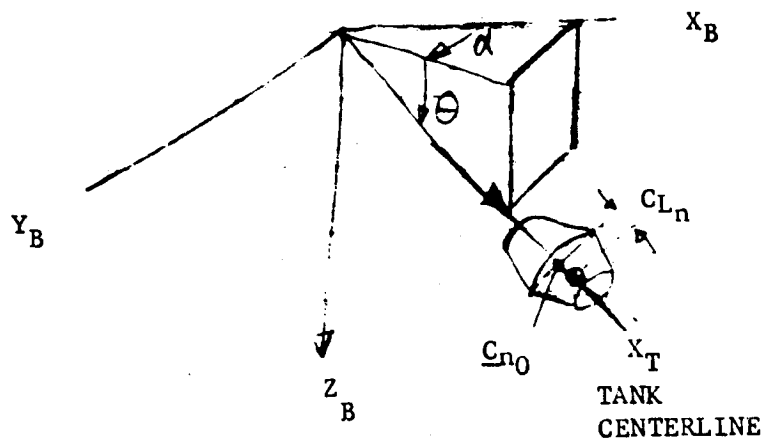
TANK
CENTERLINE

Given the composite center of mass of the spacecraft as a function of the propellant used in each tank, center of mass control logic can be implemented. This implementation consists of investigating the center of mass shift of the spacecraft assuming each tank is to be used for the maneuver in turn. The center of mass is then controlled by selecting the tank for the maneuver which minimizes the center of mass shift. The tank selection logic also has certain back-up options. For example, if more than one tank would satisfy the center of mass shift requirements, the tank with the most propellant is selected. If no tanks satisfy the requirement, the tank which minimizes the center of mass shift is selected. Tanks that have depleted all of their propellant or tanks that have valve failures are not considered for a given maneuver.

References

7-1 IBM Federal Systems Division. "Applications Technology Satellite Programming System." Vol II, May, 1969.

7-2 W.S. Bjorkman and M. J. Brooks. "Programmer's Manual for the Advanced Mission Analysis Program". Philco-Ford TR-DA16221 January, 1965.

7-3 R.J. Hanakos, D.L. Beery and R.W. Herder. "Orbit Adjust Maneuver Program (OAMP) User's Information." CSC 3000-04800-05TM. March, 1974.

7-4 G.L. Brauer, D.E Cornick, R.T. Steinhoff and R. Stevenson. "Program to Optimize Simulated Trajectories (POST) Programmer's Manual." MMC Report MCR-73-206. October, 1973.

9.5 REFERENCES

9-1   IBM Federal Systems Division. "Applications Technology
      Satellite Programming System." Vol. II, May, 1969.

9-2   W. S. Bjorkman and M. J. Brooks. "Programmer's Manual
      for the Advanced Mission Analysis Programs." Philco-
      Ford TR-DA1622. January, 1968.

9-3   R. J. Haverkos, D. L. Beery and R. W. Herder. "Orbit
      Adjust Maneuver Program (OAMP) User's Information."
      CSC 3000-04800-05TM. March, 1974.

9-4   G. L. Brauer, D. E. Cornick, R. T. Steinhoff and
      R. Stevenson. "Program to Optimize Simulated Trajectories
      (POST) Programmer's Manual." MMC Report MCR-73-206.
      October, 1973.

10. ANALYTIC TARGETING

10.1 Introduction

Analytic targeting refers to the computation of closed-form solutions for maneuvers satisfying desired orbital changes using an impulsive approximation for the maneuver itself. The closed form solution thereby generated yeilds a simple and reliable approximation for most orbital maneuvers. As a result, impulsive modeling has received widespread application in preflight mission planning as well as real-time mission support. In thise applications, the impulsive models are typically used to provide rapid estimates of maneuver parametrics. They also furnish effective initial iterates for parametric scan or numerical targeting and optimization for more detailed simulation of the maneuver.

Orbital maneuvers are conveniently categorized into two classes of maneuvers. Orbit change maneuvers will refer to programmed or scheduled orbit changes such as orbit insertion, orbit transfer, or routine plane change maneuvers. Orbitkeeping maneuvers will refer to maneuvers required to maintain some orbital characteristic in the presence of perturbations. Orbitkeeping maneuvers include such maneuvers as synchronous or sun-synchronous orbit stationkeeping.

This chapter describes the analytic targeting of both kinds of orbital maneuvers. A section is devoted to each specific maneuver within the two general classes so that later additions, deletions, or modifications to this chapter may be easily implemented. A listing of these maneuvers is provided below:

Orbit Change Maneuvers

(10.2) Injection from Parking Orbit
(10.3) Insertion from Transfer Orbit (Apogee Maneuver)
(10.4) Station Acquisition
(10.5) Single Impulse Plane Change
(10.6) Two Impulse Plane Change
(10.7) Fixed Location In-Plane Maneuvers
(10.8) Variable Location In-Plane Maneuvers

Orbitkeeping Maneuvers

(10.9)   Orbit Trims

(10.10)   Synchronous Stationkeeping

(10.11)   Sun-Synchronous Stationkeeping

(10.12)   Perigee Altitude Maintenance

Two coordinate systems will be used repeatedly in this chapter.
These coordinate systems were described in detail in Section 5.2.5.
Both are based on the satellite orbit plane.

The X_{OP}-Y_{OP}-Z_{OP} frame will be denoted by its briefer and more
descriptive title, the RTN system where

  $\underline{R}$ is directed along the satellite position vector (X_{OP})

  $\underline{T}$ is directed in the orbit plane normal to $\underline{R}$ (Y_{OP})

  $\underline{N}$ is defined by $\underline{r} \times \underline{\dot{r}}$ (Z_{OP})

The second frame is the X_P-Y_P-Z_P which for simplicity will be
called the PQN frame where

  $\underline{P}$ is directed toward perigee (X_P)

  $\underline{Q}$ is in the orbit plane normal to $\underline{P}$ (Y_P)

  $\underline{N}$ is defined by $\underline{r} \times \underline{\dot{r}}$ (Z_P

These frames are illustrated in Figure 10.1-1 below.

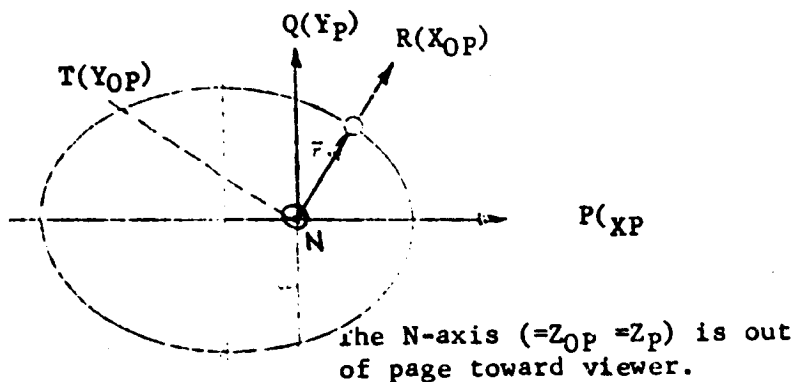The N-axis ($=Z_{OP} = Z_P$) is out
of page toward viewer.

Figure 10.1-1.   Description of RTN
and PQN Frames

10.2 Injection from Parking Orbit

The injection from the parking orbit to the target or transfer orbit is discussed in detail in Chapter 8 because this maneuver is intimately tied to the launch phase of the mission. Generally the launch time and azimuth is selected on the basis of optimizing the transfer orbit injection and target orbit insertion. Apparently the operational targeting and implementation of this maneuver is not the responsibility of the Mission Support Computing and Analysis Division. For completeness however the impulsive targeting of this maneuver will be briefly summarized here.

The parking orbit is characterized by the inclination i_p, the longitude of the ascending mode Ω_p, and the circular radius R_p. Define the radius vector to the desired transfer orbit apogee by $\underline{R}_A$. It is assumed that the launch analysis phase has selected the launch time and azimuth to insure that $\underline{R}_A$ lies in the parking orbit plane. Then the argument of the latitude of the injection point (angle in the parking orbit from the ascending node to the injection point) is given by

$$\cos U_I = -\hat{L} \cdot \underline{R}_A/R_A$$
$$\sin U_I = (-\hat{L} \times \underline{R}_A) \cdot \hat{N}/\underline{R}_A \qquad 0 \leq U_I < 360 \qquad (10.2\text{-}1)$$

where $\hat{N} = (\sin \Omega_p \sin i_p, \; -\cos \Omega_p \sin i_p, \; \cos i_p)$ $\qquad (10.2\text{-}2)$

$\qquad \hat{L} = (\cos \Omega_p, \; \sin \Omega_p, \; 0)$

The ΔV is given by

$$\underline{\Delta V} = \sqrt{\frac{\mu}{R_P}} \left[\sqrt{\frac{2R_A}{R_A + R_P}} - 1 \right] \hat{Q} \qquad (10.2\text{-}3)$$

where Q is defined by Figure 10.1-1.

10.3 Apogee Maneuver

The analysis of the apogee maneuver has been the subject of much repeated effort at GSFC. Programs for the analysis of the targeting of this maneuver have included FUS1T2, FUS1T5, and FUS1T6 (Reference 10.3-1), FUS1T7 (Reference 10.3-2), RAEMOT (Reference 10.3-1) and CAMPO1 (Reference 10.3-3). Currently, investigations are underway for the CTS (Reference 10.3-4) and it may be necessary to update this section when those analyses are completed.

The mathematical description of the apogee maneuver targeting problem is as follows. The elements of the transfer orbit are known and designated by $(a_T, e_T, i_T, \Omega_T, \omega_T)$. The elements of the desired near-synchronous orbit are given as $(a_S, e_S, i_S, \Omega_S, \omega_S)$. The solid rocket motor has a fixed ΔV capability denoted as ΔV_B. The problem is to determine the ΔV direction $\underline{U}$ so that when the engine is fired the resulting orbit is acceptable and as close to the desired orbit as possible.

Acceptability in this context is a somewhat vague term as it may mean some complicated combination of constraints including drift time, observability by certain stations at certain times, shadowing, etc. Thus the actual targeting of the apogee maneuver will undoubtedly involve some post-analytic targeting refinement by either the parametric scan or optimization modules. Therefore the approach described below should generate an acceptable solution but need not consider all the constraints involved in those later refinements. The approach discussed was suggested by the approach taken by Novak of Reference 10.3-4 but differs substantially from the solution. Figure 10.3-1, taken from Reference 10.3-4, is an extremely effective illustration of the apogee maneuver problem.

The algorithm presented below determines in closed form the direction of the solid rocket motor burn to

(1) Acquire the desired plane and drift rate and minimize eccentricity error.

(2) If (1) is not possible, acquire the desired plane and min-imize drift rate error.

(3) If (2) is not possible, minimize the plane error.

The input therefore is the desired drift orbit inclination i, longitude of ascending node Ω, semimajor axis a and eccentricity e; the solid rocket motor fixed capability ΔV; and the transfer orbit defined by a position $\underline{r}_t$ and velocity $\underline{V}_t$. The output is the optimal burn direction $\underline{U}_{\Delta V}$.

The transfer orbit is defined by computing the angular momentum and eccentricity vectors

$$\underline{H}_t = \underline{r}_t \times \underline{V}_t \qquad (10.3\text{-}1)$$

$$\underline{e}_t = -\underline{r}_t/r_t - \underline{H}_t \times \underline{V}_t/\mu \qquad (10.3\text{-}2)$$

The normal to the desired drift orbit plane is given by

$$\underline{n} = (\sin i \ \sin\Omega, \ -\sin i \ \cos\Omega, \ \cos i) \qquad (10.3\text{-}3)$$

The line of relative modes between the transfer plane and the drift orbit plane is given by

$$\underline{U}_r = \underline{H}_t \times \underline{n}/|\underline{H}_t \times \underline{n}| \qquad (10.3\text{-}4)$$

Then the radius at the intersection point is

$$r = \frac{H_t^2}{\mu(1+\underline{e}_t \cdot \underline{U}_r)} \qquad (10.3\text{-}5)$$

The velocity vector on the transfer orbit at the intersection point is

$$\underline{V} = \left(\frac{\mu}{H_t^2}\right) \underline{H}_t \times (\underline{e}_t + \underline{U}_r) \qquad (10.3\text{-}6)$$

The RTN system is established in the initial orbit plane with the R axis coincident with the $\underline{U}_r$ axis.

$$\begin{aligned} \hat{R} &= \underline{U}_r \\ \hat{N} &= \underline{n} \qquad\qquad (10.3\text{-}7) \\ \hat{T} &= \hat{N} \times \hat{R} \end{aligned}$$

The transformation from the inertial to the RTN frame is then given by

10.3-2

Figure 10.3-1.   Illustration of Apogee Maneuver Burr Geometry
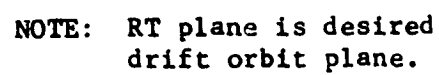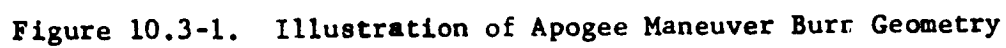

NOTE: RT plane is desired
        drift orbit plane.

Figure 10.3-2.   Construction of RTN System for Problem
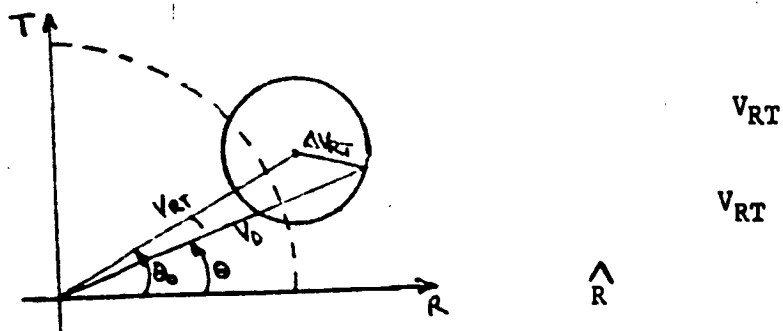
Figure 10.3-3.   Velocity Parameters in RT Plane

$$\Phi_{RTN} = \begin{bmatrix} \hat{R} \\ \hline \hat{T} \\ \hline \hat{N} \end{bmatrix} \qquad (10.3-8)$$

The out-of-plane component of the velocity vector at the injection point is given by

$$V_N = \underline{V} \cdot \hat{N} \qquad (10.3-9)$$

The first logical branch point depends on the relative size of V_N and V. If $|V_n| > \Delta V$ the sphere of possible velocities following the solid rocket motor burn does not intersect the desired orbit plane. In this case the ΔV direction should be directed toward the plane to minimize the planar error. Mathematically

$$\text{If} \quad \Delta V \leqslant |V_N| \qquad (10.3-10)$$

$$\underline{U}_{\Delta V} = (-\text{sign } V_N)\, \hat{N} \qquad (10.3-11)$$

If $\Delta V > |V_N|$ the sphere does intersect the desired plane in a circle (Figure 10.3-3). The radius of that circle is given by

$$\Delta V_{RT} = (\Delta V^2 - V_N^2)^{\frac{1}{2}} > 0 \qquad (10.3-12)$$

Denote the length of the projection of $\underline{V}$ in the RT plane by V_{RT}, and its polar angle by θ_0 where

$$V_{RT} = (V_R^2 + V_T^2)^{\frac{1}{2}} \qquad (10.3-13)$$

$$\cos\theta_0 = V_R \qquad \qquad \sin\theta_0 = V_T$$

Then the equation of the circle defining possible drift orbit velocities lying in the desired plane is given by (r,θ) where

$$r^2 - 2r\, V_{RT}\, \cos(\theta - \theta_0) + (V_{RT}^2 - \Delta V_{RT}^2) = 0 \qquad (10.3-14)$$

Now the desired velocity magnitude can be computed from the desired semimajor axis (equivalently, the drift rate) from the energy

equation

$$V^* = \left[\mu \left(\frac{2}{r} - \frac{1}{a} \right) \right]^{\frac{1}{2}}$$ (10.3-15)

The intersection of the circle $r = V^*$ with the desired plane circle (10.3-14) then defines velocity orientations that acquire both the desired plane and drift rate.

If there are single or no intersections, the velocity directions in the RT frame are given as follows

$$V_{RT} > \Delta V_{RT}: \qquad V^* > V_{RT} + \Delta V_{RT} \qquad \theta = \theta_o$$
$$V^* < V_{RT} - \Delta V_{RT} \qquad \theta = \theta_o$$ (10.3-16)

$$V_{RT} < \Delta V_{RT}: \qquad V^* > V_{RT} + \Delta V_{RT} \qquad \theta = \theta_o$$
$$\Delta V^* < V_{RT} - V_{RT} \qquad \theta = \theta_o + 180^\circ$$

Then the optimal ΔV direction is given by

$$\underline{U}_{\Delta V} = \Phi_{RTN}^T \quad \underline{\Delta V}_{RTN} / \Delta V$$ (10.3-17)

where

$$\Delta V_{RTN} = \begin{bmatrix} \Delta V_{RT} \cos\theta \\ \Delta V_{RT} \sin\theta \\ (\Delta V^2 - V_N^2)^{\frac{1}{2}} \end{bmatrix}$$ (10.3-18)

If the conditions (10.3-16) are not satisfied there are two solutions which acquire the proper plane and the correct drift rate. In this case the solution is chosen which minimizes the eccentricity error.

The two solutions of the simultaneous equations $r = V^*$ (10.3-15) and (10.3-14) can be written as

$$V^{*2} - 2V^* V_{RT} \cos(\theta - \theta_o) + (V_{RT}^2 - \Delta V_{RT}^2) = 0$$ (10.3-19)

Solving for the values of θ,

$$\theta = \theta_o \pm \cos^{-1} \left[\frac{V^{*2} + (V_{RT}^2 - \Delta V_{RT}^2)}{2 V_{RT} V^*} \right]$$ (10.3-20)

Then $\left| \cos(\theta - \theta_o) \right| < 1$ since the exclusion of conditions (10.3-16) requires

$$\left| V_{RT} - \Delta V_{RT} \right| < V^* < V_{RT} + \Delta V_{RT}$$ (10.3-21)

Then the ambiguity in sign may be resolved by selecting the solution

that lies closest to the desired eccentricity. Note that θ represents the complement of the flight path angle at $\underline{r}$. The desired flight path angle is a function of the desired eccentricity by the relation

$$\gamma = \cos^{-1} \left(\frac{\sqrt{\mu a \ (1-e^2)}}{r \ v_{RT}} \right) \qquad (10.3-22)$$

Thus the sign of (10.3-20) is selected to minimize the error $\left| \gamma - \theta \right|$.

10.5 Plane Change

The plane change maneuver described below involves simply a plane change so that no other elements but inclination i and longitude of ascending node are affected. The analysis of a single maneuver that obtains a plane change and affects other elements can be made by computing the plane change impulse ΔV_P and the subsequent in-plane impulse ΔV_I (see next section) and adding them together.

Let the elements of the initial orbit be denoted $(a_I, e_I, i_I, \Omega_I, \omega_I)$ and the desired planar orientation by (i_f, Ω_f). The normals to the two planes are then given by

$$\hat{N}_i = (\sin\Omega_i \, \sin i_i, \, -\cos\Omega_i \, \sin i_i, \, \cos i_i) \qquad (10.5\text{-}1)$$

$$\hat{N}_f = (\sin\Omega_f \, \sin i_f, \, -\cos\Omega_f \, \sin i_f, \, \cos i_f) \qquad (10.5\text{-}2)$$

Define the line of relative nodes by

$$\hat{L} = \pm(\hat{N}_i \times \hat{N}_f)/\left|\hat{N}_i \times \hat{N}_f\right| \qquad (10.5\text{-}3)$$

where the sign is chosen to force $L_z > 0$. If $L_z = 0$ as computed from (10.5-3), then $\hat{L}$ is set equal to

$$\hat{L} = (\cos\Omega_i, \, \sin\Omega_i, \, 0) \qquad (10.5\text{-}4)$$

The true anomaly of the first intersection point (there are obviously two points of intersection) on the initial orbit is given by

$$\begin{aligned}\cos f_1 &= \hat{P} \cdot \hat{L} \\ \sin f_1 &= \hat{Q} \cdot \hat{L}\end{aligned} \qquad 0 \leqslant f_1 < 360° \qquad (10.5\text{-}5)$$

where $\hat{P}$ and $\hat{Q}$ are computed from the elements of the initial orbit as discussed in Section 10.1.

The RTN system is established in the initial orbital plane with the R axis coincident with the L-axis:

$$\begin{aligned}\hat{R} &= \hat{L} \\ \hat{N} &= \hat{N}_i \\ \hat{T} &= \hat{N} \times \hat{R}\end{aligned} \qquad (10.5\text{-}6)$$

The initial velocity in the RTN system is given by

10.5-1

$$\underline{v}_i^{RTN} = (v_i \sin\gamma, \ v_i \cos\gamma, \ 0) \tag{10.5-7}$$

where

$$r_i = \frac{a(1-e^2)}{1+e \cos f_i} \tag{10.5-8}$$

$$v_i = \sqrt{\mu(2r_i^{-1} - a^{-1})} \tag{10.5-9}$$

$$\gamma_i = \tan^{-1}\left(\frac{e \sin f}{1+e \cos f}\right) \tag{10.5-10}$$

The final velocity in the RTN system is then

$$\underline{v}_f^{RTN} = \Phi_R \ \underline{v}_i^{RTN} \tag{10.5-11}$$

where

$$\Phi_R = \begin{bmatrix} 1 & 0 & 0 \\ 0 & \cos\Delta_i & -\sin\Delta_i \\ 0 & \sin\Delta_i & \cos\Delta_i \end{bmatrix} \tag{10.5-12}$$

and where as indicated by Figure 10.5-1 the following conditions are imposed

$$\begin{aligned} \Delta_i &= i_f - i_i && \text{if} \quad (v_i^I)_z > 0 \\ &= i_i - i_f && \text{if} \quad (v_i^I)_z < 0 \end{aligned} \tag{10.5-13}$$

Figure 10.5-1.   Geometry for First Solution

The velocity increment in the RTN frame is then

$$\underline{\Delta v}^{RTN} = \underline{v}_f^{RTN} - \underline{v}_i^{RTN} = (\Phi_R - I) \ \underline{v}_i^{RTN} \tag{10.5-14}$$

This may be simplified to yield

$$\underline{\Delta v}^{RTN} = \begin{bmatrix} 0 \\ v_i \cos\gamma (\cos\Delta_i - 1) \\ v_i \sin\gamma \sin\Delta_i \end{bmatrix} \tag{10.5-15}$$

The inertial velocity increment is then given by

$$\underline{\Delta v}^I = \Phi_{RTN}^T \underline{\Delta v}^{RTN} \qquad (10.5\text{-}16)$$

The second solution which occurs in the southern hemisphere is determined by reversing the sign of $\hat{L}$ in (10.5-4). The true anomaly of the intersection point is given by

$$f_2 = f_1 + 180^\circ \qquad (10.5\text{-}17)$$

The computation of the $\underline{\Delta v}$ for this solution then proceeds as above.

Figure 10.5-2. Geometry of Second Solution

10.6 Two-Impulse Plane Change

The MAESTRO program development (Reference 10.6-1) identified an excellent technique for the closed-form optimal solution to the two-impulse 180° nonplanar transfer. This capability, originally derived by T. Sun (Reference 10.6-2) should be available in the GMAS. Sun's method determines the optimal two impulse 180° transfer between non-coplanar orbits. Since a 180° transfer is specified, the first impulse must be applied at the intersection of the initial and final orbit planes. Thus, the angle between the initial and final orbit planes and the position on the initial orbit where the maneuver is made can be obtained from the spherical trigometric relationships, See Figure below. The following development is taken directly from Reference 10.6-1.
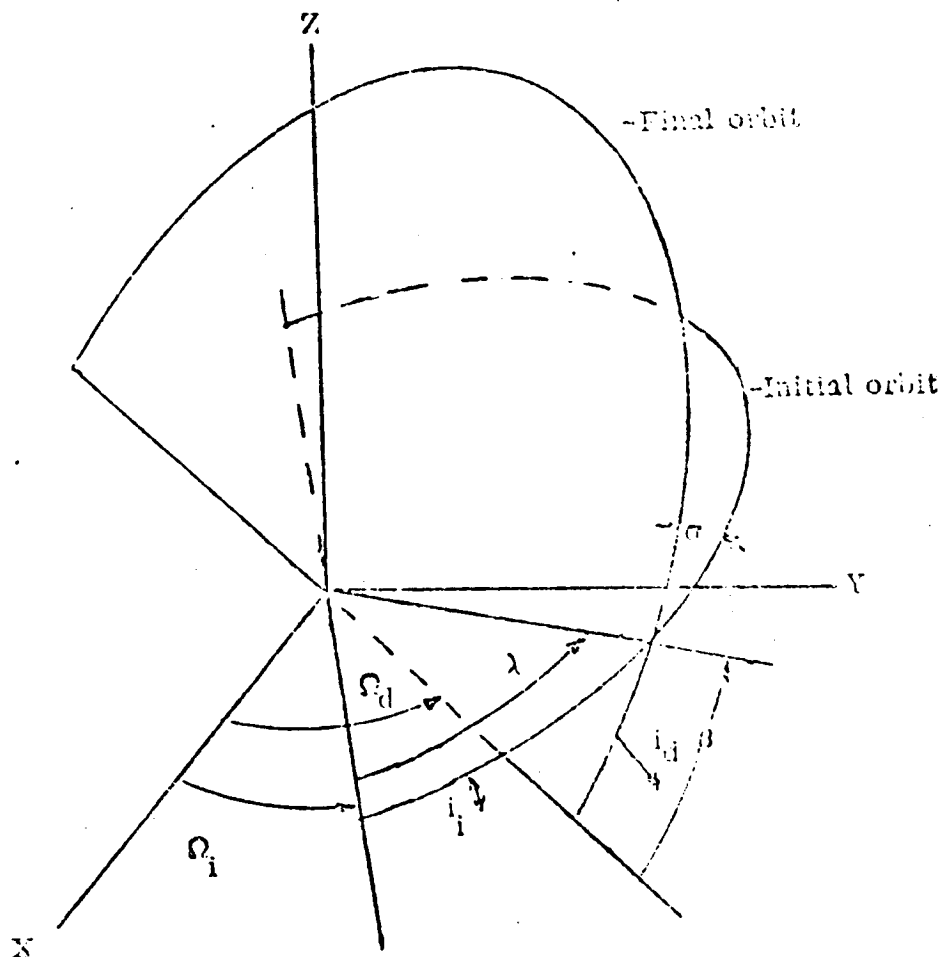
The angle from the reference plane to the common line of nodes in the initial orbit, λ , can be determined from the input initial true anamoly, f, and the argument of the ascending node of the initial orbit as,

$$\lambda = f + \omega$$

(10.6-1)

Then, the angle between the two orbit planes, σ, can be determined from,

$$\sin \beta = \sin i_i \sin i_d / \sin \lambda \qquad (10.6-2)$$

$$\tan \frac{\sigma}{2} = \frac{\sin (\frac{\lambda - \beta}{2})}{\sin (\frac{\lambda + \beta}{2}) \tan (\frac{i_d - i_i}{2})}$$

where i is the inclination

β is the angle from the reference plane to the common line of nodes in the final orbit plane.

and the subscripts i and d refer to the initial and desired orbits, respectively.

The radius and velocity components can be determined from standard orbital relationships at the initial true anomaly, f.

The orientation of the transfer plane with respect to the initial and final orbit planes is described in the figure below:
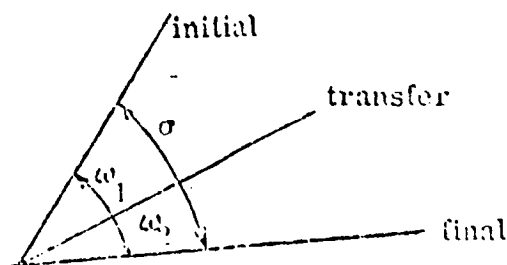
The angles ω_1 and ω_2 describe the orientation of the transfer plane with respect to the initial and final orbit planes, respectively.

If the inclination of the transfer plane with respect to the initial plane is specified, then the optimal velocity can now be determined using Sun's equation 10.

$$\Delta V = \sqrt{\frac{\mu}{r_1}} \left\{ V_{r1}^2 + \left[\left(V_{T1}^2 - \sqrt{\frac{2n}{n+1}} \, V_{T1} \cos \omega_1 + \frac{2n}{n+1} \right)^{1/2} + \left(1 - 2\sqrt{\frac{2}{n+1}} \cos \omega_2 + \frac{n}{n+1} \right)^{1/2} \right]^2 \right\}^{1/2} \qquad (10.6-3)$$

where μ is the gravitational constant

r_i is the radius at λ

V_{ri}, V_{Ti} are the radial and transverse velocity components on the

initial orbit relative to local velocity ($V = \sqrt{\mu/r}$)

n is r_d/r_i

The equation above is somewhat simplified from Sun's equation since the final orbit is circular. Thus,

$$V_{r2} = 0$$
$$V_{T2} = 1. \tag{10.6-4}$$

If the velocity of each trim maneuver is desired, then

$$\frac{\Delta V_1}{\Delta V} = 1 + \frac{1}{\sqrt{n}} \left[\frac{1 - 2\sqrt{\frac{2}{n+1}} \cos \omega_2 + \frac{2}{n+1}}{V_{T1}^2 - \sqrt{\frac{2n}{n+1}} V_{T1} \cos \omega_1 + \frac{2n}{n+1}} \right]$$

$$\frac{\Delta V_2}{\Delta V} = 1 + \sqrt{n} \left[\frac{V_{T1}^2 - 2\sqrt{\frac{2n}{n+1}} V_{T1} \cos \omega_1 + \frac{2n}{n+1}}{1 - 2\sqrt{\frac{2}{n+1}} \cos \omega_2 + \frac{2}{n+1}} \right] \tag{10.6-5}$$

where ΔV_1 and ΔV_2 denote the magnitudes of the first and second trim maneuvers.

The direction these impulses are applied can be determined by noting the following relationships.

$$\Delta V_{R1} = V_{RT1} - V_{R1}$$
$$\Delta V_{N1} = -V_{T1} \sin \omega_1 \tag{10.6-6}$$
$$\Delta V_{T1} = V_{TT1} - V_{T1} \cos \omega_1$$

The second trim is determined in a similar manner as

$$\Delta V_{r2} = V_{R2} - V_{RT2}$$
$$\Delta V_{N2} = -V_{T2} \sin \omega_2 \tag{10.6-7}$$
$$\Delta V_{T2} = V_{T2} \cos \omega_2 - V_{TT2}$$

In the above equations the components of velocity are defined as follows,

$V_{R1,2}$ radial component of velocity of the initial or final orbit.

$V_{T1,2}$ Transversal component of velocity of the initial or final orbit, in the initial or final orbit plane.

$V_{TT1,2}$ Transversal component of velocity of the initial or final orbit written in the transfer plane.

$V_{RT1,2}$ Radial component of velocity of the transfer orbit at initial and final orbit crossings.

All components of velocity except the radial components of the transfer orbit in eqns (10.6-6 and 7) are fixed by specifying the initial and final orbits. The radial component of velocity is determined from the condition that the total trim velocity is to be minimized. The total trim velocity is

$$\Delta V = \Delta V_1 + \Delta V_2 = \sqrt{\Delta V_{T1}^2 + \Delta V_N^2 + (V_{rT1} - V_{r1})^2}$$
$$+ \sqrt{\Delta V_{T2}^2 + \Delta V_{N2}^2 + (V_{r2} - V_{rT2})^2} \quad . \tag{10.6-8}$$

Also,

$$V_{rT1} = -V_{rT2}$$
$$\tag{10.6-9}$$
$$V_{r2} = 0$$

since a $180°$ transfer is specified and the final orbit is to be circular. Now, the partial derivative of the trim velocity with respect to V_{rT1} can be written as,

$$\frac{\partial \Delta V}{\partial V_{rT1}} = \frac{V_{rT1} - V_{r1}}{\Delta V_1} + \frac{V_{rT1}}{\Delta V_2} = 0$$

or

$$V_{rT1} = \frac{\Delta V_2 \, V_{r1}}{\Delta V_1} \tag{10.6-10}$$

The components of the trim velocity obtained from eqns (10.6-6, 7, & 10) describe the trim velocity with respect to the transfer plane. The trim velocity vector in the same coordinate system of the initial orbit is obtained through a three Euler angle rotation pictured in the figure below.
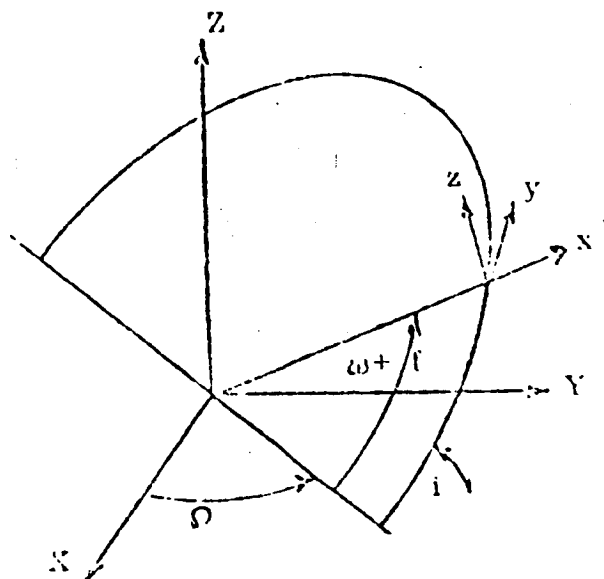
In the figure above, x corresponds to the radial direction, y to the transversal direction and z to the normal direction.

The angular elements of the reference orbit define the Euler angles. Thus the transformation from the x, y, z system to the X, Y, Z system is

$$
\begin{Bmatrix} X \\ Y \\ Z \end{Bmatrix} = \begin{bmatrix} \cos \psi \cos \Omega & -\sin \psi \cos \Omega & \sin i \sin \Omega \\ -\cos i \sin \Omega \sin \psi & -\cos i \sin \Omega \cos \psi & \\ \cos \psi \sin \Omega & -\sin \psi \sin \Omega & -\sin i \cos \Omega \\ +\cos i \cos \Omega \sin \psi & +\cos i \cos \Omega \cos \psi & \\ \sin i \cos \psi & \sin i \sin \psi & \cos i \end{bmatrix} \begin{Bmatrix} x \\ y \\ z \end{Bmatrix} \quad (10.6\text{-}11)
$$

where $\psi = f + \omega$

The above equation is used to transform the trim velocity components from an orbit plane coordinate system to the system of the reference orbit.

Optimum Inclination of the Transfer Plane

The condition for the optimal orientation of the transfer plane is expressed by

$$
\frac{\sin \omega_2}{\sin \omega_1} = - n \left(\frac{1 - 2 \rho_2 \cos \psi_2 + \rho_2^2}{1 - 2\rho_1 \cos \psi_1 + \rho_1^2} \right)^{1/2}
$$

10.6-5

where
$$\rho_1 = \left(\frac{2 \, r_d / r_1}{r_d + r_1} \right)^{1/2} \frac{1}{V_{T1}}$$

$$\rho_2 = \left(\frac{2 \, r_1 / r_d}{r_d + r_1} \right)^{1/2}$$

Equation 12 along with the condition

$$\omega_2 = \sigma + \omega_1$$

yields a set of equations which can be solved for ω_1 or ω_2 to yield the optimum orientation of the transfer plane. The solutions to eqn (10.6-12) resulted in a sixth order polynomial in $\sin \omega$. The equation was solved numerically in order to avoid the cumbersome task of solving a sixth order equation. A Newton-Raphson procedure was employed to determine the solution to eqn (10.6-13). Sun, in the reference states that the solution is unique. Thus, the task of finding multiple solutions with the Newton-Raphson method is not required.

The optimum 180° transfer solution discussed above determines the maneuver to go from a fixed point on the initial orbit to the final orbit. We are not constrained to any specific point on the initial orbit.

Thus, it is necessary to determine the position on the initial orbit to make the first maneuver that results in the lowest trim requirement. The optimum position on the initial orbit is determined by a search of the entire orbit. A half-interval iteration is used to find the local minimum and the position used is the minimum of all the local minimums.

10.7 Fixed Location In-Plane Maneuvers

Fixed location maneuvers refer to maneuvers that are performed at a specific point within the initial orbit. Such maneuvers as perigee altitude adjustment performed at the apogee point or apogee altitude adjustment performed at perigee are included in this classification. These maneuvers are computationally much simpler than the in-plane maneuvers having unknown locations discussed in the next section (10.8).

10.7.1 Apogee Maneuvers

The primary in-plane apogee maneuvers involve perigee raising or lowering illustrated in Figure 10.7-1. The most convenient form
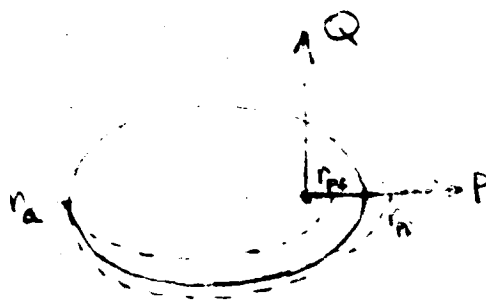
Figure 10.7-1. Perigee Adjustment at Apogee

of the ΔV equations employs directly the initial perigee radius r_{pi}, the desired final perigee altitude r_{pf}, and the initial apogee radius r_a. The ΔV magnitude is then given by

$$\Delta V_a = \sqrt{\frac{2}{r_a}} \left| \sqrt{\frac{r_{pf}}{r_{pf} + r_a}} - \sqrt{\frac{r_{pi}}{r_{pi} + r_a}} \right| \qquad (10.7\text{-}1)$$

The direction is given by

$$\hat{\Delta V} = \pm \hat{Q} \qquad (10.7\text{-}2)$$

where the negative sign is used for perigee raising and the positive sign for perigee lowering.

10.7.2 Perigee Maneuvers

The principle in-plane plane perigee maneuvers involve apogee altitude adjustment. The equations for this maneuver are as follows.
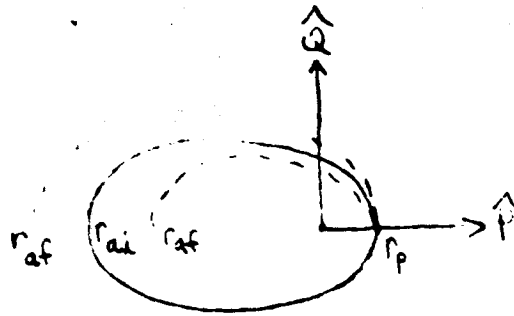
Figure 10.7-2. Apogee Adjustment at Perigee

The ΔV magnitude is given by

$$\Delta V_p = \sqrt{\frac{2}{r_p}} \left| \sqrt{\frac{r_{ai}}{r_{ai} + r_p}} - \sqrt{\frac{r_{af}}{r_{af} + r_p}} \right| \qquad (10.7\text{-}3)$$

The direction is given by

$$\Delta \hat{V} = \pm \hat{Q}$$

where the positive sign is used for apogee raising and the negative sign is used for apogee lowering.

10.9 Orbit Trims

Small single impulsive maneuvers are those that allow the use of perturbation approximations. These small impulse models are generally quite useful for maneuvers such as minor orbit adjustment or orbitkeeping. The strategies used to determine the desired orbit changes are discussed in more detail in Sections 10.10 and following.

The most useful form of the planetary equations for impulsive maneuver analysis is the Gauss form (Reference 10.9). For maneuver analysis the force components F_R, F_T, F_N in the radial, tangential (normal to radius), and normal directions are replaced by the approximations $\frac{1}{\Delta t}(\Delta V_R, \Delta V_T, \Delta V_N)$ yielding the equations

$$\Delta a = \frac{2}{n\sqrt{1-e^2}}\left(e\sin f\, \Delta V_R + \frac{p}{r}\Delta V_T\right)$$

$$\Delta e = \frac{\sqrt{1-e^2}}{na}\left[\sin f\, \Delta V_R + (\cos E + \cos f)\,\Delta V_T\right]$$

$$\Delta i = \frac{r\cos U}{na^2\sqrt{1-e^2}}\Delta V_N \qquad\qquad (10.9\text{-}1)$$

$$\Delta \Omega = \frac{r\sin U}{na^2\sqrt{1-e^2}\sin i}\Delta V_N$$

$$\Delta \varpi = \frac{\sqrt{1-e^2}}{nae}\left[-\cos f\, \Delta V_R + \left(1+\frac{r}{p}\right)\sin f\, \Delta V_T\right] + 2\sin^2\frac{i}{2}\Delta\Omega$$

$$\Delta \epsilon = \frac{e^2}{1+\sqrt{1-e^2}}\Delta\varpi + 2\sqrt{1-e^2}\sin^2\frac{i}{2}\Delta\Omega - \frac{2r}{na^2}\Delta V_R$$

where f and E are the true and eccentric anomalies respectively,

$n = \sqrt{\mu/a^3}$,

$p = a(1-e^2)$,

$u = f + \varpi - \Omega = f + \omega$, and

ϵ is the planets mean longitude at the instant from which time is measured given by

$$\epsilon = \widetilde{\omega} - n\tau \qquad\qquad (10.9\text{-}2)$$

Ref. 10.9: A. E. Roy, "The Foundations of Astrodynamics," The McMillan Co., New York, 1965.

The equation (10.9-1) can be used to compute combination orbital corrections as well as single element corrections. Thus writing the vector of elements as $\underline{E}$ the equation (10.9-1) can be written as

$$\Delta \underline{E} = \left[M \right] \underline{\Delta V}_{RTN} \qquad (10.9\text{-}3)$$

This equation then allows the exact targeting of up to three components of $\underline{E}$ or the least-squares solution for more than three components of $\underline{E}$.

10.10   Synchronous Stationkeeping

It is normally desired that synchronous satellites be kept "on-station" at a given longitude. Even if an equatorial synchronous satellite is placed perfectly at the desired longitude with no initial drift rate, the action of various perturbations upon the satellite orbit will eventually cause it to drift away from that station. The normal method of stationkeeping is to choose two bounding longitudes, one on either side of the desired station longitude, and then to use maneuvers whenever it is necessary to remain between the boundaries. Due to the accelerations of the tesseral harmonics and the luni-solar perturbations, the satellite is allowed to drift until it reaches the boundary toward which the net perturbative acceleration is directed. At this point a maneuver is performed which changes the semi-major axis of the orbit so that the drift rate is in the opposite direction, toward the other bound. The maneuver is sized so that the drift rate will decrease to zero just as the other bound is reached. The continued perturbative acceleration will then reverse the drift and eventually return the satellite to the first bound, whereupon another maneuver is performed to begin the cycle again.

By only considering a simple approximation to the tesseral accelerations, an analytic technique of calculating stationkeeping maneuvers is described in the RQUEST program documentation (Reference 10-AA). This program was written to provide a "quick-look" program for calculations connected with controlling the ATS-1 and ATS-3 satellites, to be used as an aid in planning and to provide weekly status reports for the satellites. The equations of this method are given below in Section 10.10.1. A much more complete analytic theory including the accelerations of both the tesseral harmonics and the luni-solar effects has been published recently by Kamel (Reference 10-BB). The equations required for this method are summarized in Section 10.10.2 below.

10.10.1   Approximate Tesseral Method

The RQUEST program (Reference 10-AA) models the effect of the tesseral accelerations as a simple drift in longitude of the form

$$\ddot{\lambda} = -A \sin 2\lambda \qquad\qquad (10.10\text{-}1)$$

where λ is the station longitude measured in radians from the nearest minor axis, and A is given as $(-72 \pi^2)$ $(1/6.61)^2$ (1.81×10^{-6}) = -2.944×10^{-5} radians/day^2. The minor axes or stable equilibrium points (from which the satellite will not drift if placed there with no drift rate) are located according to Reference 10-AA at 108 degrees W and 288 degrees W. The points of unstable equilibrium are at 18 degrees W and 198 degrees W. The location of these four equilibrium points as determined by Kamel in Reference 10-BB are different by as much as seven degrees and are not exactly symmetrically located.

The four equilibrium points form the boundaries of four zones in each of which the direction of the drift acceleration is opposite that of the zones on either side of it. It is assumed that in the stationkeeping mode all of the satellite motion (i.e., both boundaries) will be within one zone. A stationkeeping maneuver is calculated given a time, the satellite initial longitude and drift rate and the bounding longitudes. It is assumed that if the initial drift is opposite to the tesseral acceleration, that the satellite drift rate will be reduced to zero approximately at the boundary toward which it is drifting. For this case, the following calculations are made

$$\lambda_f = 1/2 \cos^{-1} (\cos 2\lambda_i - \dot{\lambda}_i^2/A) \qquad\qquad (10.10\text{-}2)$$

$$\Delta t_1 = \left| \frac{2(\lambda_f - \lambda_i)}{\dot{\lambda}_i} \right| \qquad\qquad (10.10\text{-}3)$$

$$\dot{\lambda}_1 = \sqrt{2 \ddot{\lambda}_1 \Delta\lambda_f} \qquad\qquad (10.10\text{-}4)$$

$$\Delta t_2 = \left| \frac{2 \Delta\lambda_f}{\dot{\lambda}_1} \right| \qquad\qquad (10.10\text{-}5)$$

$$\Delta T = \Delta t_1 + \Delta t_2 \qquad (10.10\text{-}6)$$

$$M = -(\dot{\lambda}_1 + \sqrt{2\,\ddot{\lambda}_2 \Delta \lambda}\,) \qquad (10.10\text{-}7)$$

where

λ_f is the longitude at which the drift rate becomes zero.

λ_i is the input satellite longitude.

$\dot{\lambda}_i$ is the input drift rate.

Δt_1 is the time taken to reach λ_f.

$\dot{\lambda}_1$ is the drift rate at BOUND1.

$\ddot{\lambda}_1$ is the average acceleration between BOUND1 and λ_f.

$\Delta \lambda_f$ is the distance between BOUND1 and λ_f.

Δt_2 is the time taken to drift from λ_f to BOUND1.

ΔT is the time from the initial time to BOUND1.

ΔM is the change in drift rate which the maneuver must produce.

$\ddot{\lambda}_2$ is the average acceleration between BOUND1 and BOUND2.

$\Delta \lambda$ is the distance between BOUND1 and BOUND2.

If the initial drift rate is in the same direction as the tesseral acceleration and the satellite is between BOUND1 and BOUND2, the following calculations are made

$$\Delta \dot{\lambda} = 1/2 \sqrt{2\,\ddot{\lambda}_3\,\Delta \lambda_S} \qquad (10.10\text{-}8)$$

$$\dot{\lambda}_A = \dot{\lambda}_i + \Delta\dot{\lambda} \qquad\qquad (10.10\text{-}9)$$

$$\Delta t = \Delta\lambda_S / \dot{\lambda}_A \qquad\qquad (10.10\text{-}10)$$

$$\dot{\lambda}_M = \dot{\lambda}_A + \Delta\dot{\lambda} \qquad\qquad (10.10\text{-}11)$$

where

> $\ddot{\lambda}_3$ is the average acceleration between λ_i and BOUND1.
>
> $\Delta\lambda_S$ is the distance between λ_i and BOUND1.
>
> $\dot{\lambda}_A$ is the average velocity between λ_i and BOUND1.
>
> Δt is the time it takes to drift to BOUND1.
>
> $\dot{\lambda}_M$ is the drift rate of BOUND1.

If the satellite has drifted past BOUND1 in the direction of the
tesseral acceleration, a maneuver can be performed at the initial time.
In both this case and the previous case where the satellite drifts to
BOUND1 before performing the maneuver, the maneuver is calculated by

$$\Delta M = -(\dot{\lambda}_M + \sqrt{2\,\ddot{\lambda}_4\,\Delta\lambda_M}) \qquad\qquad (10.10\text{-}12)$$

where

> $\dot{\lambda}_M$ is the drift rate at the maneuver (either BOUND1
> or λ_i).
>
> $\ddot{\lambda}_4$ is the average acceleration between the maneuver a
> and BOUND2.
>
> $\Delta\lambda_M$ is the distance between BOUND2 and the maneuver
> point.

Since ΔM is calculated in radians/day, it is converted to ft/sec by

$$\Delta V = (9.34) \ (180/\pi) \ \Delta M \hspace{3cm} (10.10\text{-}13)$$

where ΔV is the velocity change in ft/sec.

10.10.2

In reference 10-BB, Kamil develops the equations of motion of the synchronous satellite in terms of the deviation in longitude around the nominal satellite station λ_S. The solution for the drift cycle initial conditions and stationkeeping requirements is found first due to tesseral harmonics only and then due to the inclusion of luni-solar effects.

10.10.2.1 Solution Due to Tesseral Harmonics

As noted in Section 10.10.1, the equilibrium points as determined by Kamel are located at slightly different points than in Reference 10-AA. The stable points are located at 76 degrees and 258 degrees (or 102 degrees W and 284 degrees W) and the unstable equilibrium points are at 164 degrees and 349 degrees (or 11 degrees W and 196 degrees W). These points are defined by the zeros of the G_1 function given below and will of course be functions of the values used for the various harmonics.

In the presence of only harmonic accelerations the drift cycle is independent of epoch and repeats itself when a maneuver is performed once each cycle. In this case, it is normally termed the limit cycle. To maintain the satellite within the required tolerance $(\pm \lambda_o)$ around the nominal station longitude λ_S, the optimal stationkeeping strategy locates the satellite at one boundary of the tolerance band ($\lambda = \lambda_o$ or BOUND1 in the nomenclature of Section 10.10.1) with the initial drift rate $\dot{\lambda}_o$ which causes the satellite to drift to the other boundary and back again. Upon reaching $\lambda = \lambda_o$ again the drift rate is $-\dot{\lambda}_o$ and a maneuver must be performed to prevent violation of the constraints. In theory, since we are concerned with circular orbits,

this maneuver is actually a two-maneuver Hohmann transfer between the
two circular orbits (the differing drift rates are caused by the
change in semi-major axis due to the perturbations). In practice the
eccentricity of this "transfer orbit" is smaller than normal residual
eccentricities usually involved with synchronous orbits, so that in
practice only a single maneuver need be made to change the semi-major
axis to the value giving the desired drift rate. The required initial
drift rate is given by

$$\dot{\lambda}_o = \mp 2\sqrt{3 \, G_1 \, \lambda_o} \qquad\qquad (10.10\text{-}14)$$

where λ_o should have the same sign as G_1 and the upper sign is used
when $G_1 > 0$. This is equivalent to the convention of Section 10.10.1
that the drift cycle starts at the boundary closest to the nearest
minor axis (BOUND1) with the initial drift towards the other boundary
and opposite to the direction of the acceleration. The function G_1
and its derivative with respect to longitude, G_2 are given by

$$G_1 = 6 \, J_{22} \, (R_e/a_s)^2 \, \sin 2 \, (\lambda_s - \lambda_{22})$$

$$- \frac{3}{2} \, J_{31} \, (R_e/a_s)^3 \, \sin \, (\lambda_s - \lambda_{31})$$

$$+ 45 \, J_{33} \, (R_e/a_s)^3 \, \sin 3 \, (\lambda_s - \lambda_{33}) \qquad (10.10\text{-}15)$$

and

$$G_2 = 12 \, J_{22} \, (R_e/a_s)^2 \, \cos 2 \, (\lambda_s - \lambda_{22})$$

$$- \frac{3}{2} \, J_{31} \, (R_e/a_s)^3 \, \cos \, (\lambda_s - \lambda_{31})$$

$$+ 135 \, J_{33} \, (R_e/a_s)^3 \, \cos 3 \, (\lambda_s - \lambda_{33}) \qquad (10.10\text{-}16)$$

where R_e is the Earth equatorial radius, a_s is the reference synchronous semi-major axis, J_{ij} is the ij coefficient in the Earth's potential function, and λ_{ij} is the ij angle in the Earth's potential function. Numerical values are given in Reference 10-BB as

$$J_{22} = 1.7208 \times 10^{-6}$$

$$J_{31} = 2.005 \times 10^{-6}$$

$$J_{33} = 0.16456 \times 10^{-6}$$

$$\lambda_{22} = -0.2331601 \text{ radians}$$

$$\lambda_{31} = 0.1154309 \text{ radians}$$

$$\lambda_{33} = 0.32571 \text{ radians.}$$

The period of the drift cycle is given as

$$P = 2\,\bar{\mathcal{T}}_1/\omega_e \qquad\qquad (10.10\text{-}17)$$

where

$$\bar{\mathcal{T}}_1 = \frac{1}{\sqrt{3}\,G_2}\,\ln\left[\,S + C\,\right] \qquad\qquad (10.10\text{-}18)$$

and

$$S = 2\,\frac{\sqrt{G_1 G_2\,\lambda_o}}{\left|G_1 - G_2\lambda_o\right|} \qquad\qquad (10.10\text{-}19)$$

$$C = \frac{G_1 + G_2\lambda_o}{G_1 - G_2\lambda_o} \qquad\qquad (10.10\text{-}20)$$

The rotation rate of the earth, ω_e, is given as 6.300388 radians/day. The velocity increment necessary per cycle is given by

$$V = \frac{1}{3} \dot{\lambda}_o V_s \qquad (10.10\text{-}21)$$

where V_s is the synchronous orbit velocity. A typical optimal drift cycle with only tesseral harmonics is shown in Figure 10.10-1 taken from Reference 10-BB.
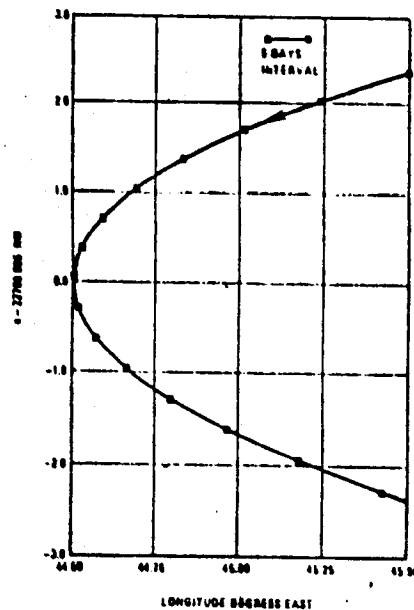
Figure 10.10-1. Optimal Drift Cycle in the Absence of Luni-Solar Perturbations

10.10.2.2 Luni-Solar Effects

After including the effects of the Sun and Moon, the equations for $\dot{\lambda}_o$ and τ_1 corresponding to equations (10.10-14) and (10.10-18) are given by

$$\tau_1 = \bar{\tau}_1 + \frac{\varepsilon}{2(\overline{G_1 - G_2 \bar{\lambda}_o})}\left[C_2(\tau_1) - \frac{3\left|\overline{G_1 + G_2 \bar{\lambda}_o}\right|}{2\sqrt{3G_1 \bar{\lambda}_o}} \ (S_2(\tau_1) + S_2(0))\right] \qquad (10.10\text{-}22)$$

$$\dot{\lambda}_o = \mp 2\sqrt{3G_1 \bar{\lambda}_o} + \frac{9}{4}\varepsilon \frac{\left|\overline{G_1 - G_2 \bar{\lambda}_o}\right|}{\sqrt{3G_1 \bar{\lambda}_o}} \ (S_2(\tau_1) + S_2(0)) \qquad (10.10\text{-}23)$$

where

$$\bar{\lambda}_o = \lambda_o + \frac{3}{2} \, \mathcal{E} \, S_2(0) \qquad (10.10\text{-}24)$$

Again the upper sign is used for $G_1 > 0$ and λ_o has the same sign as G_1. Equation (10.10-22) must be solved iteratively for τ_1'. A suitable starting value is $\tau_1 = \bar{\tau}_1$ as given in equation (10.10-18). The required initial semi-major axis to start the drift cycle is given by

$$a_o = a_s \, (1 + \eta_0) \qquad (10.10\text{-}25)$$

$$\eta_0 = \pm \frac{4}{3} \sqrt{3G_1 \bar{\lambda}_0} - \frac{3 \, \mathcal{E} \, |G_1 - G_2 \, \bar{\lambda}_0|}{2 \sqrt{3G_1 \, \bar{\lambda}_0}} \, (S_2(\tau_1) + S_2(0))$$

$$+ \frac{3}{2} \, \mathcal{E} \, (C_1(0) - 2S_1(0) \, \bar{\lambda}_0) \qquad (10.10\text{-}26)$$

where a_s is the synchronous semi-major axis after accounting for oblateness and luni-solar effects. The unitless quantity $\mathcal{E}$ is related to the lunar mass and mean motion and is given as $\mathcal{E} = 1.628157 \times 10^{-5}$. The functions S_1, C_1, S_2 and C_2 are related to the luni-solar geometry and are given as

$$S_1 = 0.941\,480 \left[\sin(2x_m) + 0.460\,488 \sin(2x_s) \right] +$$
$$+ 0.016\,601 \sin x_m + 0.121\,571 \sin(3x_m) + 0.188\,300 \sin(2x_m - M_m)$$

$$C_1 = \cos^4(i_m/2) \left[1.030\,076 \cos(2x_m) + 0.201\,935 \cos(2x_m - M_m) - \right.$$
$$- 0.027\,949 \cos(2x_m + M_m) + 0.026\,454 \cos(2x_m - 2M_m) \left] + \right.$$
$$+ \sin^2(i_m) \left[0.502\,270 \cos(2x_m + 2y_m) + \right.$$
$$+ 0.040\,570 \cos(2x_m + 2y_m + M_m) +$$
$$+ 0.042\,080 \cos(2x_m + 2y_m - M_m) \left] + \right.$$
$$+ 0.424\,255 \cos(2x_s) + 0.024\,867 \cos(2x_s - M_s) -$$
$$- 0.003\,545 \cos(2x_s + M_s) + 0.036\,332 \cos(2x_s + 2y_s) +$$
$$+ 0.011\,39 \cos(x_m + 2y_m) + 0.0018 \cos(x_m + 2y_m + M_m) +$$
$$+ 0.033\,783 \cos x_m + 0.001\,776 \cos(x_m + M_m) +$$
$$+ 0.005\,750 \cos(x_m - M_m) + 0.011\,924 \cos(x_m - 2y_m) +$$
$$+ 0.011\,013 \cos(3x_m + 2y_m) + 0.082\,131 \cos(3x_m) +$$

$$+ 0.023\,254 \cos(3x_m - M_m) - 0.00454 \cos(3x_m + M_m) +$$
$$+ 0.004\,106 \cos(3x_m - 2M_m) + 0.0073 \cos(4x_m) +$$
$$+ 0.0042 \cos(2x_m) + 0.001\,69 \cos(2x_m + 4y_m)$$
$$S_2 = 2.169\,035 [\sin(2y_m) + 6.156\,11 \sin(2y_s)] +$$
$$+ 1.526\,84 [1.503\,78 \sin M_m + 2.819\,51 \sin M_s] +$$
$$+ 0.416\,777 \sin(2y_m + M_m) + 0.8000 \sin(2y_s + M_s)$$
$$C_2 = 0.158\,736 [\cos(2y_m) + 0.460\,488 \cos(2y_s)] +$$
$$+ 1.526\,84 [0.0549 \cos M_m + 0.0077 \cos M_s].$$

where

λ = satellite longitude measured along the equator, then along the orbital plane;
$\quad = \Omega + \omega + M - \theta$;
Ω = right ascension of ascending node;
ω = argument of perigee;
M = mean anomaly;
θ = Greenwich hour angle;
a = osculating semimajor axis;
n_m = Moon's mean motion = 0.23 rad day^{-1};
n_s = Sun's mean motion = 0.017203 rad day^{-1};
i_m = Moon's orbit inclination to the equatorial plane, $18.3° \leqslant i_m \leqslant 28.59°$;
i_s = Sun's apparent orbit inclination to the equatorial plane = 23.445°;
M_m = Moon's orbit mean anomaly = $n_m t + M_m(0)$;
M_s = Sun's apparent orbit mean anomaly = $n_s t + M_s(0)$;
$y_m = \omega_m + M_m$;
$y_s = \omega_s + M_s$;
ω_m = Moon's orbit argument of perigee measured from its equatorial ascending node;
ω_s = Sun's apparent orbit argument of perigee;
$x_m = \lambda + \theta - y_m - \Omega_m$;
$x_s = \lambda + \theta - y_s$;
Ω_m = right ascension of Moon's orbit ascending node measured along the equator.

A typical optimal drift cycle which includes luni-solar effects is shown in Figure 10.10-2. The results using the equations summarized above from Reference 10-BB are given along with numerical integration of the equations of motion. The agreement is very good and is substantially different from the result which ignores the luni-solar effects. The computer time necessary for the numerical integration is about 150 times as much as for the analytical result.
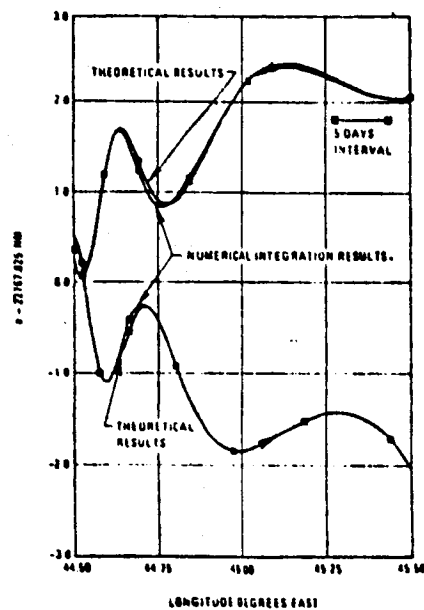
Figure 10.10-2. Typical Optimal Drift Cycle. Epoch Time
is 19th May 1972 8^h 49^m.

11. NUMERICAL TARGETING AND OPTIMIZATION

11.1 Introduction

Targeting and optimization in mission analysis is the problem of selecting certain mission control parameters to optimize some mission objective while satisfying all mission constraints. Examples are numerous and diverse. Among the areas giving rise to such problems in orbital mission analysis are:

1) Orbital selection (e.g., choose orbital parameters to maximize the science return while meeting all other mission requirements).

2) Maneuver selection (e.g., select a maneuver strategy and set of control variables to minimize required propellant while achieving the desired orbital transfer).

Two basic approaches to the targeting and optimization problem can be identified: 1) numerical and 2) analytical. The numerical method consists of building a complete numerical simulation of the system to be optimized and then using some numerical procedure to determine the optimal control parameters. The analytical approach, on the other hand, involves constructing an analytical model of the system and manipulating it mathematically to obtain the optimal control parameters. Which of the approaches is superior for a particular application depends upon the users relative requirements for solution efficiency and flexibility.

In comparing the efficiencies of the two approaches analytical as well as numerical effort must be accurately assessed. In general analytical solutions utilize problem-specific analytical techniques to express the answer in the most computationally efficient form. Numerical solutions by contrast use general numerical procedures to iteratively converge upon the answer. Thus numerical solutions trade computation for analysis. Although a numerical solution may place heavier demands upon computer resources, its analytical counterpart may lay even heavier claims upon analytical and programming manpower. Generalized numerical optimization procedures used in conjunction with generalized system simulators can enable users to solve difficult optimization problems without writing

11-1

a single simulation equation or implementing a line of code. Further, certain analytical solutions may require the evaluation of transcendental functions or the solution of nonlinear equations which are computationally more onerous than a direct solution by numerical means. Finally, problems which possess simple analytical solutions usually yield with commensurate ease to numerical solution.

In comparing the flexibility of the two approaches, numerical techniques have a clear cut advantage. First, only numerical techniques permit the level of model sophistication necessary to accurately model operational systems. Only the simplest of analytical models yield a solution through mere mathematical manipulation. Nonetheless if analytical technique yield sufficiently accurate results in the context of data, modeling, and execution uncertainties, they should be judged on other more relevant considerations. Second, numerical solutions generally require a shorter lead time from problem statement to answer. By merely building a data deck for a generalized simulation and optimization program a relatively unsophisticated user can bring to bear on his problem state-of-the-art simulation and optimization techniques. The usual lengthy processes of education, derivation, implementation, and checkout are circumvented.

11.2 Mathematical Structure of Problem

From the vast diversity of optimization and targeting problems in orbital mission analysis a common mathematical structure can be distilled. First, there is a vector $\underline{u}$ of control parameters which must be selected to define a trajectory. Second, for each trajectory as defined by the vector of control parameters, $\underline{u}$, there is a vector of constraint parameters $\underline{g}(\underline{u})$ together with a vector of constraint limiting values, $\underline{b}$. The number of such parameters can be less than, equal to, or greater than the number control parameters. The constraint parameters may have upper bounds, lower bounds, or both. In fact, the upper bound may equal the lower bound; that is the parameter may have an equality constraint. Finally, of each trajectory as characterized by its control parameters, there is an objective function $F(\underline{u})$. The object of the problem is then to determine the control parameters, $\underline{u}$, which are feasible in that all of the constraint parameters fall within their acceptable ranges and optimal in the sense that objective is minimized. It suffices to consider the case of minimization since maximization can be handled as a minimization of the negative of the desired objective.

The general targeting problem is then the well known nonlinear programming problem. Symbolically it is expressed as

$$
\begin{aligned}
&\text{minimize:} \quad && F(\underline{u}) \\
&\text{subject to:} \quad && \underline{g}(\underline{u}) \; \underline{\alpha} \; \underline{b} \\
&\text{where:} \quad && \underline{u} \text{ is the } m{\times}1 \text{ column matrix of control parameters,} \\
& && F \text{ is the scalar objective function of the vector of} \\
& && \quad \text{control parameters,} \\
& && \underline{g} \text{ is the } n{\times}1 \text{ column matrix of constraint parameters,} \\
& && \underline{b} \text{ is the } n{\times}1 \text{ column matrix of constraint parameter limits,} \\
& && \underline{\alpha} \text{ is the } n{\times}1 \text{ column matrix of constraint parameter relations} \\
& && \quad \text{(each element is the appropriate relation of the triple} \\
& && \quad <, =, \text{ or } >).
\end{aligned}
\tag{11-1}
$$

Note that if a trajectory variable has both an upper and lower bound, both it and its negative must be identified as constraint parameters in this formulation.

Virtually all orbital mission analysis targeting problems can be cast into this structure. Tables 11-1 and 11-3 provide nonlinear-programming

formulations of maneuver targeting problems for the Synchronous Meteorological Satellite and the Tug/Shuttle Rendezvous, respectively. Table 11-2 is a nonlinear programming formulation of an orbit selection problem for an Earth Resources Technology Satellite.

Numerical solution of the nonlinear programming problem (11-1) presupposses that the objective function F and the constraint function g be computable from the control parameters, u. Further, all practical algorithms for solving the general nonlinear minimization problem require the gradient of the objective function and the Jacobian sensitivity matrix of the constraint function. These quantities can be obtained in two basic ways. First, the user can supply computer code to calculate the necessary function values. The required sensitivities can then either be obtained indirectly from the function values by numerical differencing or directly from additional user-supplied computer code. Such an approach could best be taken in solving the orbit selection problem of Table 11-2. Brouwer propagation theory would provide the necessary functional relations among the mean Keplerian orbital elements. Second, the user can obtain the necessary functional values from a generalized numerical simulator simply by selecting the appropriate simulation options in a data deck. The required sensitivities must then be obtained by numerical differencing. The burden of modeling analysis and computer coding is thus removed from the user. Further, sophisticated state-of-the-art simulation procedures are placed at his disposal. This second approach would probably be preferable in solving the maneuver targeting problems of Tables 11-1 and 11-3. The simulation could then be performed at any level of refinement from impulsive transfer with conic coasting arcs to high precision numerically integrated trajectories with accurate representation of all relevant forces.

PROBLEM STATEMENT

Perform synchronous noncoplanar, fixed duration, fixed thrust maneuver at apogee to minimize attitude-control-system propellant required on subsequent prescheduled coplanar phasing maneuver.

NONLINEAR PROGRAMMING FORMULATION

Minimize: $t_p(t_p)$

subject to:

$$360\left[\frac{P_p(\theta_A, \alpha_A, \delta_A, t_p) - 1}{.24} - 1\right] = \dot{\lambda}_D$$

$$i_A(\theta_A, \alpha_A, \delta_A) = i_D$$

$$t_p \geq 1$$

where:

t_p is the duration of the ACS phasing maneuver (sec)

θ_A is true anomaly of apogee motor ignition (deg)

α_A is fixed right ascension of the apogee motor thrust (deg)

δ_A is fixed declination of the apogee motor thrust (deg)

$\dot{\lambda}_D$ is desired westward longitudinal drift rate (deg/sec)

P_p period of orbit after ACS phasing maneuver (hr)

i_A inclination after apogee maneuver (deg)

i_D desired final inclination (deg).

TABLE 11-1

Representation of <u>Synchronous</u> <u>Meteorological</u> <u>Satellite</u>
Maneuver Targeting Problems as a Nonlinear Program

PROBLEM STATEMENT

Construct an earth orbit with the following properties:

1. Daily westward progression of ground swaths with at least 10 percent overlap;

2. Ground swath repeat cycle of 18 days;

3. Sun synchronous orbit;

4. Eccentricity less than .006;

5. North-to-south equator crossings at approximately 10:00 AM local time.

Minimize:	No minimization is possible since constraint parameters uniquely determine control parameters.
subject to:	$\bar{e}(\bar{e}) < .006$
	$\dot{\Omega}(\bar{a}, \bar{e}, \bar{i}) = .9856122624$
	$N\lambda_R(\bar{a}, \bar{e}, \bar{i}) > 360$
	$N\lambda_R(\bar{a}, \bar{e}, \bar{i}) - 360 \leq .9\,S$
	$18N\lambda_R(\bar{a}, \bar{e}, \bar{i}) \geq 360.$
	$t_D(t_D) = 10.$
where:	$\bar{e}$ is the mean orbital eccentricity
	$\dot{\Omega}$ is rate of change of right ascension of ascending node (deg/day)
	N is the nearest integral number of orbits per day (rev/day)
	λ_R westward longitudinal progression of the orbit between consecutive nodal passages (deg/rev)
	S is the longitudinal width of the ground swath at the equator (deg)
	t_D is mean local time at passage of mean descending node on first orbit (hrs)
	$\bar{a}$ is the mean orbital semi-major axis (km)
	$\bar{i}$ is the mean orbital inclination (deg).

TABLE 11-2

Representation of Earth-Resources Technology Satellite Orbit
Selection Problem as a Nonlinear Program

PROBLEM STATEMENT

Assume the elements of a tug transfer orbit to geosynchronous radius are available from tracking information just subsequent to the jettisoning of the synchronous equatorial payload. Determine the tug maneuver controls to rendezvous the tug with the shuttle orbiter while maximizing the tug propellant margin when the maneuver strategy is as follows:

1. Perform approximately retro-thrust near tug apogee to correct perigee altitude.

2. Perform approximately normal thrust near maximum declination to correct longitude of ascending node and inclination errors between tug and shuttle orbits.

3. Perform approximately retro-thrust near tug perigee to secure a low eccentricity intermediate orbit for time phasing for rendezvous at next perigee passage.

4. Perform approximately retro-thrust near tug perigee for final convergence of tug orbit to shuttle orbit.

Minimize: $P(t_1, \psi_1, \theta_1, d_1, \ldots, t_4, \psi_4, \theta_4, d_4)$

subject to: $t_4 + d_4 = t_D$

$$\underline{r}_T^* = \underline{r}_S^*$$

$$\underline{v}_T^* = \underline{v}_S^*$$

where: t_i = thrust ignition time for ith maneuver as defined in the PROBLEM STATEMENT.

ψ_i = angle from vertical plane containing tug velocity vector to vertical plane containing tug thrust vector for ith maneuver

θ_i = angle of tug thrust vector above horizontal plane for ith maneuver

d_i = duration of ith maneuver

t_D = desired time of rendezvous

$\underline{r}_T^*$ = position vector of tug at time $t_4 + d_4$

$\underline{r}_S^*$ = position vector of shuttle-orbiter at time $t_4 + d_4$

$\underline{v}_T^*$ = position vector of tug at time $t_4 + d_4$

$\underline{v}_S^*$ = position vector of shuttle at time $t_4 + d_4$

P = total tug propellant used in the four maneuver sequence

Table 11-3

Representation of Tug/Shuttle Rendezvous Problem as a Nonlinear Program

11.3 Numerical Targeting and Optimization Algorithms

11.3.1 Introduction

The range of algorithms designed to solve the nonlinear programming problem (11-1) is so vast as to make a survey of even the most important ones beyond the scope of this document. Reference [11-1] and [11-2] serve this purpose well. The objective of this section is rather to mathematically specify a nonlinear programming algorithm which the authors extensive experience on trajectory shaping and maneuver targeting has proven vastly superior to all others. For problems in which the objective and constraint functions are specified numerically it converges faster than any other of the well-known procedures.

Two other well known nonlinear programming techniques are described in later sections. These are respectively the well-known quality constraint methods and a special-purpose inhibited least-squares algorithm in use at GSFC. The authors do not, however, recommend their implementation. Computational experience here reveals that any problem that can be solved by these specialized methods can be solved at least as easily by the accelerated projected gradient technique. The presence of ary other targeting and optimization modules in the GMAS would only serve to confuse the user without adding any additional problem solving capability.

11.3.2 Accelerated Projected Gradient Algorithm

The accelerated projected gradient algorithm is based on five intuitive working principles. The first is one-dimensional search. Using cost and constraint function gradient information a direction of search is established. Then a one-dimensional minimization is performed in this direction upon an appropriate function. In this manner, a difficult multidimensional optimization problem is replaced by a sequence of simple one dimensional minimizations. The second working principle is linearized constraint correction. Assume that the current vector of control parameters is outside the feasible region. This correction scheme approximates the contours of constant constraints as uniformly spaced parallel hyperplanes based on their respective gradients and values for the current control parameter vector. Using this approximation the

smallest correction to the control parameters is computed which would satis-
fy all of the active constraints or that failing minimize the sum of the
squares of their violations. One-dimensional minimization of the sum of
squares of the constraint errors is then performed along the direction of
this correction to obtain the next iterate of control parameters. The
third principle is gradient projection. Once a feasible vector of con-
trol parameters is obtained the negative gradient is resolved into two
components - one parallel to and one normal to the hyperplane tangent to
the boundary to the feasible region at the current point. A minimization
is then performed along the direction of the parallel negative gradient
component to obtain the next control parameter iterate. The function
to be minimized in this one dimensional search is the fourth basic prin-
ciple of the algorithm - the estimated net cost function. Since the con-
straints are nonlinear, the tangent plane only coincides with the bound-
ary of the feasible region at the point of tangency. Hence a search
along the component of the gradient lying in the tangent plane will
probably terminate at a point external to the feasible region. Hence
the real object of the search should not merely be to find the minimum
value of the cost function in the search direction. Rather it should be
that unique point along the search ray which yields upon correction back
to the feasible region a new feasible point with the smallest value of
the cost function. This point is approximately determined by minimizing
along the parallel component of the gradient the cost function less an
estimate of the deterioration of the cost function occasioned by correct-
ing back to the feasible region. The estimate is based upon the linear-
ized constraint-correction formulae. The fifth and final working prin-
ciple is gradient acceleration. It is well known that the convergence of
unconstrained gradient algorithms can be drastically improved by using
gradient information from several iterations to estimate the inverse of
the Hessian matrix of a quadratic form approximating the cost function.
In fact for a cost function of m control parameters it can be shown
that a Hessian-inverse estimating accelerated gradient scheme converges
in m iterations while a conventional steepest descent algorithm converges
only asymptotically (see Reference [6]). To similarly accelerate the
projected gradient algorithm for constrained problems, it is assumed

that the cost function is a quadratic in m-q variables over the constraint boundary. Here q is the number of active constraints defining the boundary. Thus covergence should be accelerated to m-q iterations after the set of active constraints determining the feasible region stabilizes.

For the well known special cases of the general nonlinear programming problem the accelerated projected gradient algorithm degenerates to the appropriate special purpose state-of-the-art programming procedures. For example, if no constraints are present, the algorithm degenerates to the Davidon deflected gradient procedure. This procedure has long been considered the method of choice for solving unconstrained parameter minimization problems. At the other extreme, if the problem has more active constraints than controls, the algorithm reduces to the Gauss' least squares procedure for minimizing constraint violation. This technique is generally conceded to be the best available for solving over-determined systems of equations. Similarly, if the number of constraints is precisely equal to the number of controls, the algorithm becomes the well known Newton-Raphson procedure for solving systems of nonlinear equations. This scheme is certainly the simplest of the efficient methods for solving fully determined systems of equations.

In order to conveniently specify mathematically the accelerated projected gradient algorithm it is necessary first to attend to two matters. The constraints in the nonlinear program must be reformulated so that the constraint limits are all zero. Thus problem (11-1) beccmes

minimize: $F(\underline{u})$

subject to: $\underline{c}(\underline{u}) \ \alpha \ \underline{0}$

where: $\underline{u}$ is the mx1 column matrix of control parameters

F is the scalar objective or cost function

$\underline{c}$ is the nx1 constraint matrix equal to $\underline{g}(\underline{u})-\underline{b}$ in problem (11-1)

$\underline{\alpha}$ is the nx1 column matrix of constraint relations (each element is the appropriate relation to the triple $<, =, >$).

(11-2)

Next the algorithm must be divided into logically self-contained components each of which can best be described separately. This is particularly true of components such as the one-dimensional minimization logic which is used in more than one context in the algorithm. The precise operation of

the overall method can then be presented as simple macrologic relating these basic comporents.

11.3.2.1 Sensitivity Information

The entire algorithm is based upon first order sensitivity information concerning the cost function and gradient vector. The cost function gradient with respect to the control vector evaluated at $\underline{u}$ is denoted $\underline{\nabla}F(\underline{u})$ and is defined as the 1xm row matrix

$$[\underline{\nabla}F(\underline{u})]_j = \left.\frac{\partial F}{\partial u_j}\right|_{\underline{u}} \quad \text{for } j = 1,\ldots, m. \tag{11-3}$$

The Jacobian matrix of the constraint vector with respect to the control vector evaluated at $\underline{u}$ is denoted by $J(\underline{u})$ and is defined as the nxm matrix

$$J(\underline{u}) = \left.\frac{\partial c_i}{\partial u_j}\right|_{\underline{u}} \quad \text{for } \begin{matrix} i = 1,\ldots, n \\ j = 1,\ldots, m \end{matrix}. \tag{11-4}$$

These quantities can either be supplied by the user in the form of computer code or generated autonomously by the algorithm through numerical differencing.

11.3.2.2 Constraint Information

The algorithm functions by manipulating the sensitivity information according to logic based on the status of the constraints. To define this logic certain fundamental definitions must be made and basic relations stated.

The definition process is best begun by defining the error vector and its sensitivity matrix. Let $K(\underline{u})$ denote the set of active constraints at the point $\underline{u}$, and let k be its cardinality. The term active will be defined later. For now suffice it to say that the term refers to constraints which may be violated in the next one-dimensional search. Let $\sigma(\ell)$ be the index of the ℓth constraint in $K(\underline{u})$. Then the error vector at point $\underline{u}$ is defined as the kx1 column matrix

$$e_\ell(\underline{u}) = \underline{c}_{\sigma(\ell)}(\underline{u}) \quad \text{for } \ell = 1,\ldots, k. \tag{11-5}$$

Similarly the error sensitivity matrix at point $\underline{u}$ is defined to be the kxm matrix

$$[S(\underline{u})]_{\ell j} = \left.\frac{\partial e_{\sigma(\ell)}}{\partial u_j}\right|_{\underline{u}} \tag{11-6}$$

$$\left.\right\} \text{ for } \begin{array}{l} \ell = 1,\ldots,k \\ j = 1,\ldots, m \end{array}$$

$$= [J(\underline{u})]_{\sigma(\ell)j} \tag{11-7}$$

To motivate the gradient projection formulae, certain geometrical concepts and relations must be stated. Corresponding to each constraint function c_i is a boundary hypersurface, B_i, defined by

$$B_i = \{\underline{u}:c_i(\underline{u}) = 0\} \qquad \text{for } i = 1,\ldots, m. \tag{11-8}$$

B_i is an $(m-1)$-dimensional nonlinear manifold. It can, however, be approximated as an $(m-1)$-dimensional hyperplane at any point, $\hat{\underline{u}}$, in the control space based upon the value of the constraint and its gradient there. The approximating hyperplane is simply

$$c_i(\hat{\underline{u}}) = \{\underline{u}:-\nabla c_i(\underline{u})\ (\underline{u}-\hat{\underline{u}}) + c_i(\hat{\underline{u}}) = 0\} \qquad \text{for } i=1,\ldots, m. \tag{11-9}$$

The feasible region for the ith inequality constraint is that half space of the control parameter space defined by

$$R_i = \{\underline{u}:\ c_i(\underline{u}) \geq 0\} \qquad \text{for } i = 1,\ldots, m. \tag{11-10}$$

The complete feasible region for all of the constraints is then

$$R = \bigcap_{i=1}^{n} R_i. \tag{11-11}$$

The boundary of the complete feasible region is then

$$B(R) = \bigcup_{i=1}^{n} (B_i \cap R). \tag{11-12}$$

The intersection in the preceding definition is required to select from the unbounded boundary, B_i, of the feasible half space of the ith constraint that portion which is adjacent to the common feasible region, R, for all constraints.

The fundamental concept in the gradient projection method of constrained optimization is a local boundary hypersurface, $B(\hat{\underline{u}})$, defined at each point in the control space.

$$B(\hat{\underline{u}}) = \bigcap_{\ell \in K(\hat{\underline{u}})} B_\ell. \tag{11-13}$$

The local boundary hypersurface contains the nearest adjacent boundary face of the feasible region. If $\hat{u}$ is infeasible, it can be made feasible by proceeding in a normal direction toward $B(\hat{u})$. If $\underline{u}$ is feasible it can be improved by following the projection in $B(\hat{u})$ of the cost function gradient.

Although analytic expressions for the above constraint correction and optimization directions relative to the local boundary hypersurface can not be developed for arbitrary constraint functions c_i, formulas can be derived for the approximating linear manifold $C(\hat{u})$. Let

$$C(\hat{u}) = \bigcap_{\ell \in K(\underline{u})} C_\ell(\hat{u}) \tag{11-14}$$

$$= \{\underline{u}: \{S(\hat{u})\ (\underline{u}-\hat{u}) + \underline{e}(\hat{u}) = \underline{0}\}. \tag{11-15}$$

Let $\tilde{Q}(\hat{u})$ denote the linear space spanned by the gradients to the active constraints; that is

$$\tilde{Q}(\hat{u}) = \{\underline{u}: \underline{u} = \sum_{\ell=1}^{k} \alpha_\ell \nabla c_\ell^T\} \tag{11-16}$$

and let $Q(\hat{u})$ denote the orthogonal complement to $\tilde{Q}(\hat{u})$; that is

$$R^m = Q(\hat{u}) \oplus \tilde{Q}(\hat{u}). \tag{11-17}$$

It can be shown that $Q(\hat{u})$ is the unique linear space that can be translated to obtain the linear manifold $C(\hat{u})$ and hence whose unique orthogonal projection operators $P(\hat{u})$ and $\tilde{P}(\hat{u})$ are sought. These projections are defined by the relations for any $\underline{u}$ in the control parameter space that

$$\underline{u} = P(\hat{u})\underline{u} + \tilde{P}(\hat{u})\underline{u} \tag{11-18}$$

where

$$P(\hat{u})\underline{u} \in Q(\hat{u}) \tag{11-19}$$

and

$$\tilde{P}(\hat{u})\underline{u} \in \tilde{Q}(\hat{u}). \tag{11-20}$$

The numerical formula for the operators can be shown to be

$$\tilde{P}(\hat{u}) = [S^T(SS^T)^{-1}S](\hat{u}) \tag{11-21}$$

and

$$P(\underline{u}) = I - \tilde{P}(\hat{u}). \tag{11-22}$$

With these fundamental concepts described and formulated, it is now possible to define an active constraint. The ith constraint is said to be tight at control vector $\underline{u}$ when

$$\alpha_i \neq "=" \text{ and } c_i(\underline{u}) \leq 0 \qquad (11\text{-}23)$$

or

$$\alpha_i = "=" .$$

This condition implies that constraint i is either violated or on the verge of being so. A tight constraint i is said to be unconstraining at $\underline{u}$ for the active constraint set $K(\underline{u})$ when

$$\alpha_i \neq "=", \qquad c_i(\underline{u}) = 0, \qquad (11\text{-}24)$$

and

$$r_i = \left[(SS^T)^{-1} S \right] (\underline{u}) \, \underline{\nabla} \, F(\underline{u}) \leq 0 \qquad (11\text{-}25)$$

Here the sensitivity matrix $S(\underline{u})$ is based upon the candidate active-constraint set $K(\underline{u})$. The condition implied by relations (11-24) and (11-25) is that constraint i is on the verge of violation; but that if a one-dimensional minimization is conducted along a direction parallel to the linearized boundary hypersurface $C'(\underline{u})$ corresponding to a new active constraint set $K'(\underline{u})$ obtained from $K(\underline{u})$ by deleting the ith constraint, constraint i will remain unviolated. The concepts of tight and unconstraining constraints give rise to the following inductive definition of the active constraint set $K(\underline{u})$ at $\underline{u}$:

1) Take the initial candidate active constraint set $K(\underline{u})$ at $\underline{u}$ to be the set of tight constraints there;

2) Form the sensitivity matrix $S(\underline{u})$ corresponding to $K(\underline{u})$;

3) If any of the constraints in $K(\underline{u})$ are unconstraining remove that one, constraint i, with the smallest value of r_i return to step 2).

4) Take the existing candidate set $K(\underline{u})$ as the desired active constraint set.

11.3.2.2 Directions of Search

The accelerated projected gradient method conducts its one dimensional minimizations in two basic search directions termed the constraint and optimization directions respectively. The formulas for computing these directions at an arbitrary point $\hat{\underline{u}}$ in the control parameter space are readily written in terms of the sensitivity matrix $S(\hat{\underline{u}})$ based on the active constraint set, $K(\hat{\underline{u}})$, there. Let the cardiality of this set be denoted by k.

Consider first the constraint direction, $s^C(\underline{u})$. The error function to be minimized along the constraint direction is the squared length of the error vector. Three cases can be distinguished depending on the number of active constraints, k, relative to the number of controls, m. Nonetheless, in all cases an analytical exact correction, $\Delta\hat{\underline{u}}$, can be derived for the case of linear constraints. This linear exact correction is then used in the case of nonlinear constraints to provide not only a search direction, $s^C(\hat{\underline{u}})$, but also an initial trial step length $\gamma_o^C(\hat{\underline{u}})$; namely

$$s^C(\hat{\underline{u}}) = \frac{\Delta\hat{\underline{u}}}{||\Delta\hat{\underline{u}}||} \tag{11-26}$$

and

$$\gamma_o^C(\hat{\underline{u}}) = ||\Delta\hat{\underline{u}}|| . \tag{11-27}$$

(CASE 1: $k < m$) That unique control correction, $\Delta\hat{\underline{u}}$, is sought which solves the linearized constraint equation

$$S(\hat{\underline{u}}) \Delta\underline{u} + \underline{e}(\hat{\underline{u}}) = \underline{0} . \tag{11-28}$$

The solutions to this vector equation define the $m-k$ dimensional, hyperplane described in the preceding section as the locally-linearized boundary hypersurface. The desired minimum norm correction $\Delta\hat{\underline{u}}$, is then the vector of minimum length from $\hat{\underline{u}}$ to $C(\hat{\underline{u}})$. Analytically it is given by

$$\Delta\hat{\underline{u}} = -\left[S^T(SS^T)^{-1}\right](\hat{\underline{u}}) \, \underline{e}\,(\hat{\underline{u}}). \tag{11-29}$$

This correction is illustrated geometrically in Figure 11-1.
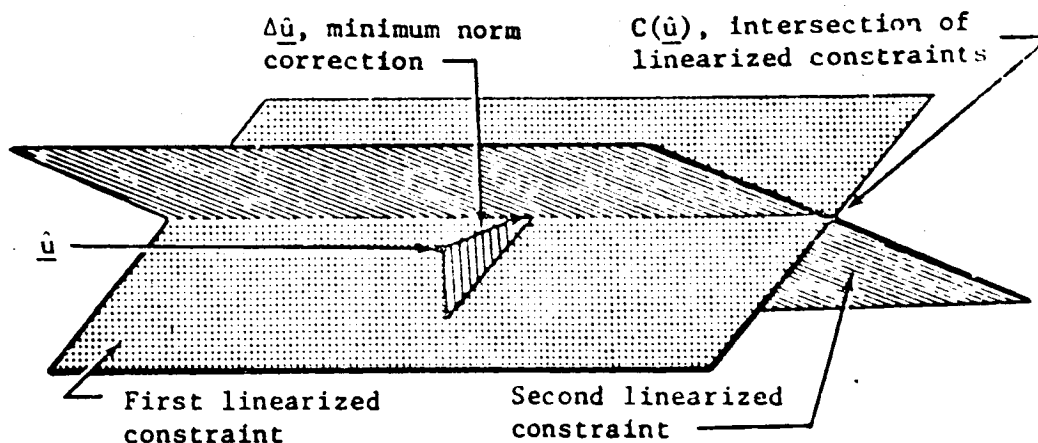
Figure 11-1. Illustration of Minimum-Norm Constraint -Correction Direction
k = 2 < m = 3

(Case 2: k = m) Here the local linearized boundary hypersurface reduces
to a single point. Thus there is a unique solution to the linearized
constraint equation (11-28) without the additional requirement that the
length of the independent variable correction be minimized. The minimum
norm correction formula then reduces to the familiar Newton-Raphson equation

$$\Delta \hat{\underline{u}} = -S^{-1}\underline{e}(\hat{\underline{u}}) \,. \tag{11-30}$$

The Newton-Raphson correction is illustrated geometrically in Figure
11-2.

Figure 11-2. Illustration of Newton-Raphson Constraint -Correction
Direction for k = m = 3

Substantial nonlinearity in the constraint parameters can cause the
constraint-correction logic to fail when either the minimum norm or the
Newton-Raphson search directions are used. The gist of the problem is that
a significant nonlinearity in one or more of the active inequality con-
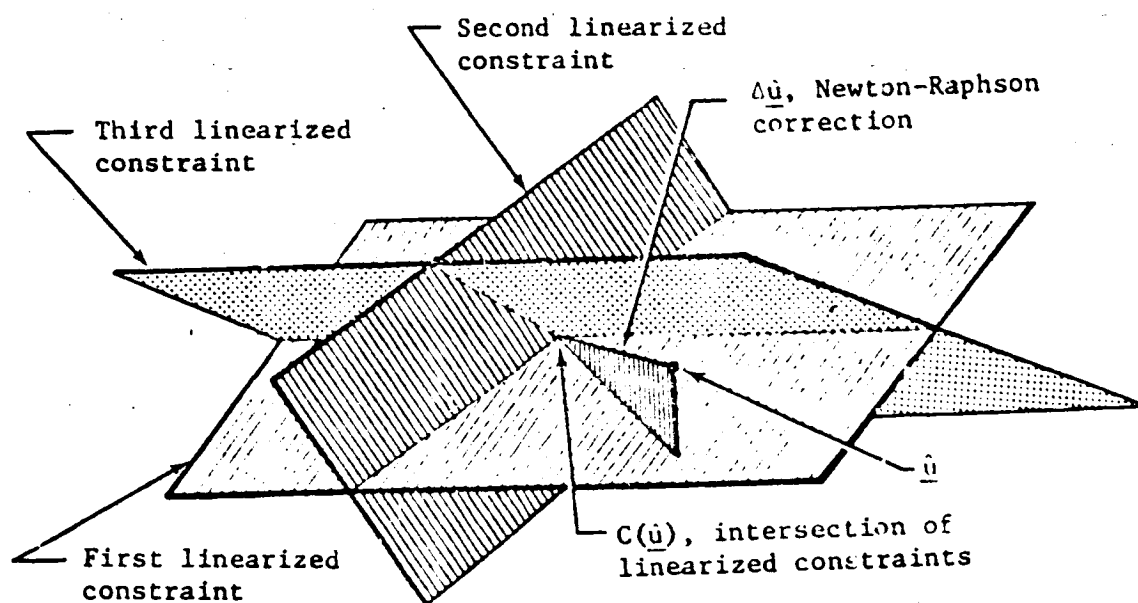straints precludes the active-constraint system of equations from having a
solution and causes the linearized search directions to vary erratically.
No difficulty arises when the nonlinear feasible region is empty. However,
if it is nonempty it may contain solutions which the minimum-norm or Newton-
Raphson directions miss because they hold all solutions on the boundaries
of the satisfied tight inequality constraints. Thus an unsatisfied con-
straint which could be satisfied by moving into the feasible half spaces
of certain satisfied constraints will remain unsatisfied. Figure 11-3 is
a geometrical illustration of this situation.
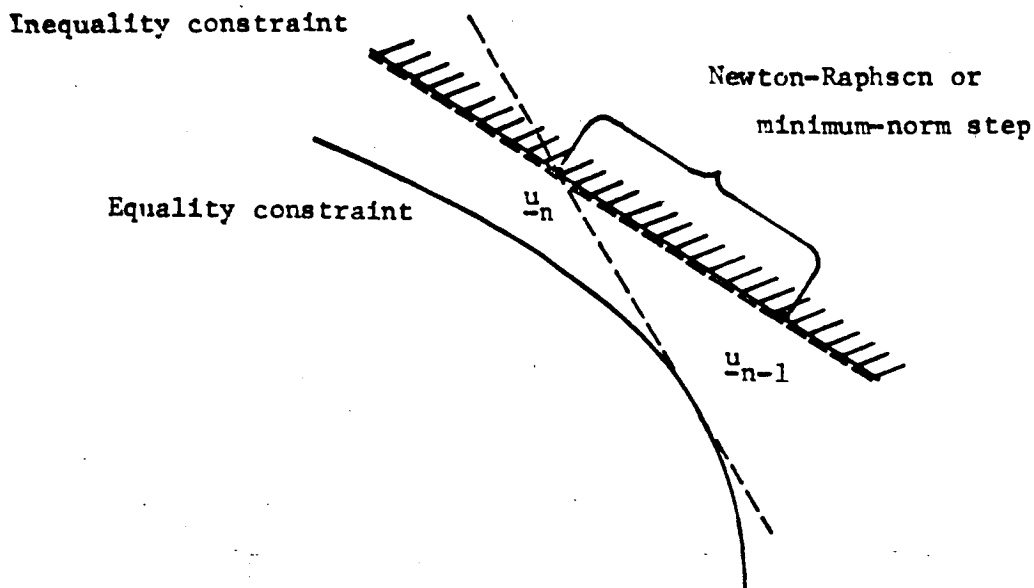
Figure 11-3. Illustration of Failure of Newton-Raphson and
              Minimum-Norm Steps on Nonlinear Constraint System

The algorithm solves this problem by dropping from the active con-
straint set those inequality constraints which are on the verge of vio-
lation but whose feasible half spaces will be entered when the constraint
correction step is taken. A set, R, of relaxable constraints can be ar-
rived at and deleted from the active constraint set, $K(\underline{u})$, by the follow-
ing stepwise procedure.

1. $R = \emptyset$

2. Form the set $T = \{t: (\alpha_t = "\geq") \text{ and } (c_t(\hat{\underline{u}}) = 0)\} - R$

3. If T is empty, delete the elements in R from the active constraint set $K(\hat{\underline{u}})$ and proceed with the normal constraint correction logic

4. For each $t\epsilon T$ form the matrix $S^t(\underline{u})$ from the sensitivity matrix $S(\hat{\underline{u}})$ by deleting the row corresponding to constraint t. Similarly form the vector $e^t(\hat{\underline{u}})$ from the error vector $e(\hat{\underline{u}})$ by deleting the component corresponding to constraint t.

5. Compute the tentative search directions

$$\sigma^t(\hat{\underline{u}}) = -[S^T(SS^T)^{-1}]^t(\hat{\underline{u}})e^t(\underline{u}) \qquad (11\text{-}31)$$

for all $t\epsilon T$.

6. Compute

$$\rho^t = \min \{\nabla c_t(\hat{\underline{u}})\sigma^t(\hat{\underline{u}}), \min_{r\epsilon R} [\nabla c_r(\hat{\underline{u}})\sigma^t(\hat{\underline{u}})]\} \qquad (11\text{-}32)$$

7. Find $t*\epsilon T$ such that

$$\rho^{t*} = \min_{t\epsilon T}\rho^t \qquad (11\text{-}33)$$

8. If $\rho^{t*} \geq 0$, add $t*$ to R and return to step 2.

(Case 3: $k > m$) In this situation a simultaneous solution of all the linearized constraint equations does not exist; that is the linearized boundary hypersurface is empty. Hence an entirely new criteria for choosing a linearized constraint correction, $\Delta\hat{\underline{u}}$, must be devised. The accelerated projected gradient algorithm selects that correction which minimizes the sum of the squares of the residues of the constraint equations, (11-28). Thus the quadratic functional

$$f(\Delta\hat{\underline{u}}) = \left\| S(\hat{\underline{u}})\Delta\hat{\underline{u}} + e(\hat{\underline{u}}) \right\|^2 \qquad (11\text{-}34)$$

is minimized with respect to $\Delta\hat{\underline{u}}$. The formula for this "least squares" correction is readily shown to be

$$\Delta\hat{\underline{u}} = -(S^T S)^{-1}S^T e(\hat{\underline{u}}) . \qquad (11\text{-}35)$$

Figure 11-4 illustrates the least squares correction geometrically.
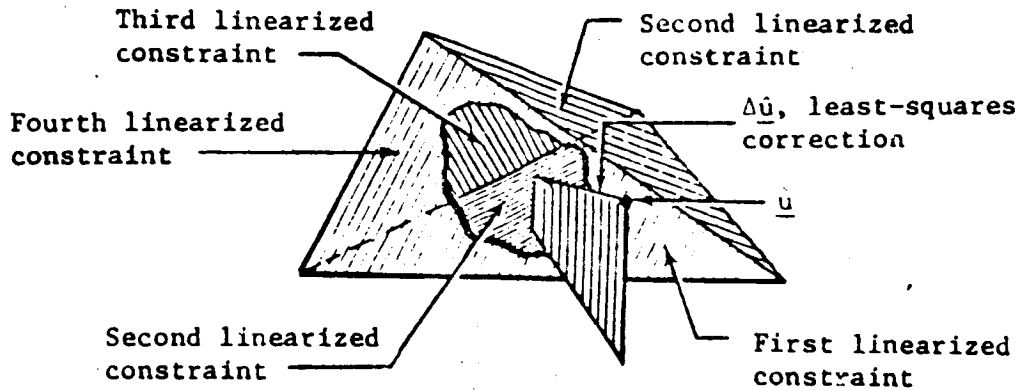
Figure 11-4. Illustration of Least Squares Constraint-Correction Direction for k = 4 m = 3

Consider next the optimization search direction $s^0(\hat{\underline{u}})$. When the number k of active constraints is less than the number of independent variables at $\hat{\underline{u}}$ it is possible to reduce the cost function by searching in the direction of the negative gradient projected into the locally linearized boundary hypersurface $C(\hat{\underline{u}})$. To compute this tentative optimization direction, $s^0(\hat{\underline{u}})$, it is only necessary to apply to the unconstrained negative cost gradient the projection operator $P(\hat{\underline{u}})$ which projects any vector in the control parameter space into its orthogonal component in $Q(\hat{\underline{u}})$, the unique linear space that can be translated into coincidence with the linear manifold $C(\hat{\underline{u}})$; that is

$$s^0(\hat{\underline{u}}) = -[P(\hat{\underline{u}}) \nabla F(\hat{\underline{u}})]^T / ||P(\hat{\underline{u}}) \nabla F(\hat{\underline{u}})||. \qquad (11-36)$$

Figure 11-5 illustrates geometrically the direction of the negative projected gradient for the case of a single active constraint.

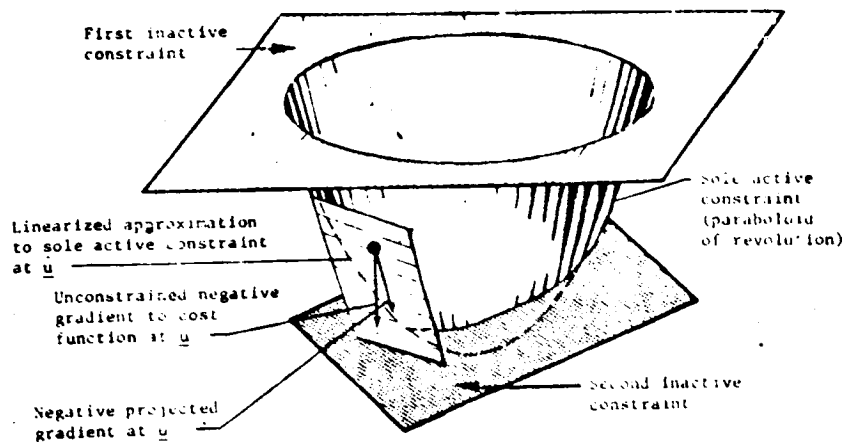**Figure 11-5.** Direction of Negative-Projected Gradient for k = 1 and m = 3 (feasible region is that region inside paraboloid, above lower plane, and below upper plane; ccst-function is vertical height).

Such a projected gradient scheme would, however, be only asymptotically convergent. What is desired is a sequence of one dimensional searches which would be quadratically convergent. Thus once $C(\hat{u})$ remains essentially the same $(m - k)$ dimensional linear manifold from iteration to iteration, the algorithm should converge in at most $(m - k)$ further steps. This acceleration can be achieved by assuming that the cost function is a quadratic form in the $(m - k)$ variables of the manifold $C(\hat{u})$. Defining an iteratively updated deflection matrix, H_R, in the manner of reference [11-6] the accelerated search direction, $s^a(\underline{u})$, is computed through the following inductive procedure where the super- or subscript "ν" refers to the current iteration number:

(1) If $\nu = 0$, set $H_\nu = I_m$ and go to step 5.

(2) If $K(\underline{u}^\nu) \neq K(\underline{u}^\nu$), set $H_\nu = I_m$ and go to step 5.

(3) Compute $\Delta\underline{u}^\nu = \underline{u}^\nu - \underline{u}^{\nu-1}$ and $\underline{g}^\nu = P(\underline{u}^\nu)\nabla^T F(\underline{u}^\nu) - P(\underline{u}^{\nu-1})\nabla^T F(\underline{u}^{\nu-1})$ (11-37)

(4) Form $A_\nu = (\Delta\underline{u}^\nu \Delta\underline{u}^{\nu T})/(\Delta\underline{u}^{\nu T}\underline{g}^\nu)$,   (11-38)

     $B_\nu = (H_{\nu-1}\underline{g}^\nu \underline{g}^{\nu T} H_{\nu-1}^T)/(\underline{g}^{\nu T} H_{\nu-1}\underline{g}^\nu)$, and   (11-39)

     $H_\nu = H_{\nu-1} + A_\nu + B_\nu$.   (11-40)

(5) Compute the accelerated optimization direction and the initial trial step length as

     $s^a(\underline{u}^\nu) = H_\nu P(\underline{u}^\nu)\_\nabla^T F(\underline{u}^\nu) / \| H P(\underline{u}^\nu)\nabla^T F(\underline{u}^\nu)\|$ and   (11-41)

     $s^a_o(\underline{u}^\nu) = \| H_\nu P(\underline{u}^\nu)\nabla^T F(\underline{u}^\nu)\|$.   (11-42)

If there are no equality constraints and if all of the inequality constraints are inactive, then the algorithm reduces to the deflected gradient procedure of Fletcher and Powell for solving unconstrained minimization problems.

11.3.2.3 Step-Size Calculation

At any particular point $\hat{u}$ in the control space, the accelerated projected gradient algorithm proceeds by reducing the multidimensional problem to a one-dimensional search along either the constraint or optimization directions. In either case, once the initial point, $\hat{u}$, and the search direction $\underline{s}(\hat{u})$ are specified, the problem is to numerically minimize a function of a single variable, namely the step size. The algorithm performs this minimization via polynomial interpolation based on function values along the search ray and the function value and slope at the starting point, $\hat{u}$. Consider then in detail the functions to be minimized along the respective search directions as well as the computation of their starting values and slopes.

The function to be minimized along the constraint direction, $\underline{s}^c(\hat{u})$, is the sum of the squares of the constraint violations; namely

$$h_c(\gamma) = ||\underline{e}[\hat{u} + \gamma \underline{s}^c(\hat{u})]||^2 \tag{11-43}$$

Obviously

$$h_c(0) = ||\underline{e}(\hat{u})||^2. \tag{11-44}$$

Differentiation via the chain rule yields

$$h_c{}'(0) = 2\underline{e}^T(\hat{u}) S(\hat{u}) \underline{s}^c(\hat{u}) \tag{11-45}$$

The function to be minimized along the optimization direction, $\underline{s}^o(\hat{u})$, is the estimated net cost. This function consists of the change in the cost function that results from a step of length γ along the search ray plus an estimate of the deterioration in the cost that will arise from correcting back to the feasible region. More precisely

$$h_o(\gamma) = \underbrace{F(\hat{u}+\gamma\underline{s}^o)-F(\hat{u})}_{\substack{\text{change in cost} \\ \text{function pro-} \\ \text{duced by a step} \\ \text{of length } \gamma \\ \text{along } \underline{s}^o(\hat{u})}} - \underbrace{\nabla^T F(\hat{u})[S^T(SS^T)^{-1}](\hat{u})\underline{e}[\hat{u}+\gamma s^c(\hat{u})]}_{\substack{\text{linearized approximation to} \\ \text{change in cost function re-} \\ \text{quired to perform minimum} \\ \text{norm correction back to the} \\ \text{feasible region}}}. \tag{11-46}$$

Clearly

$$h_o(0) = -\nabla^T F(\underline{\hat{u}}) [S^T(SS^T)^{-1}](\underline{\hat{u}})\underline{e}(\underline{\hat{u}}) .$$ (11-47)

Differentiation again by the chain rule gives

$$h_o'(0) = \nabla^T F(\underline{\hat{u}})\underline{s}^o(\underline{\hat{u}}).$$ (11-48)

Thus the second term in equation (39) contributes nothing to the initial slope of h_o. The basic properties of the estimated net cost function are illustrated graphically in Figure 11-6.
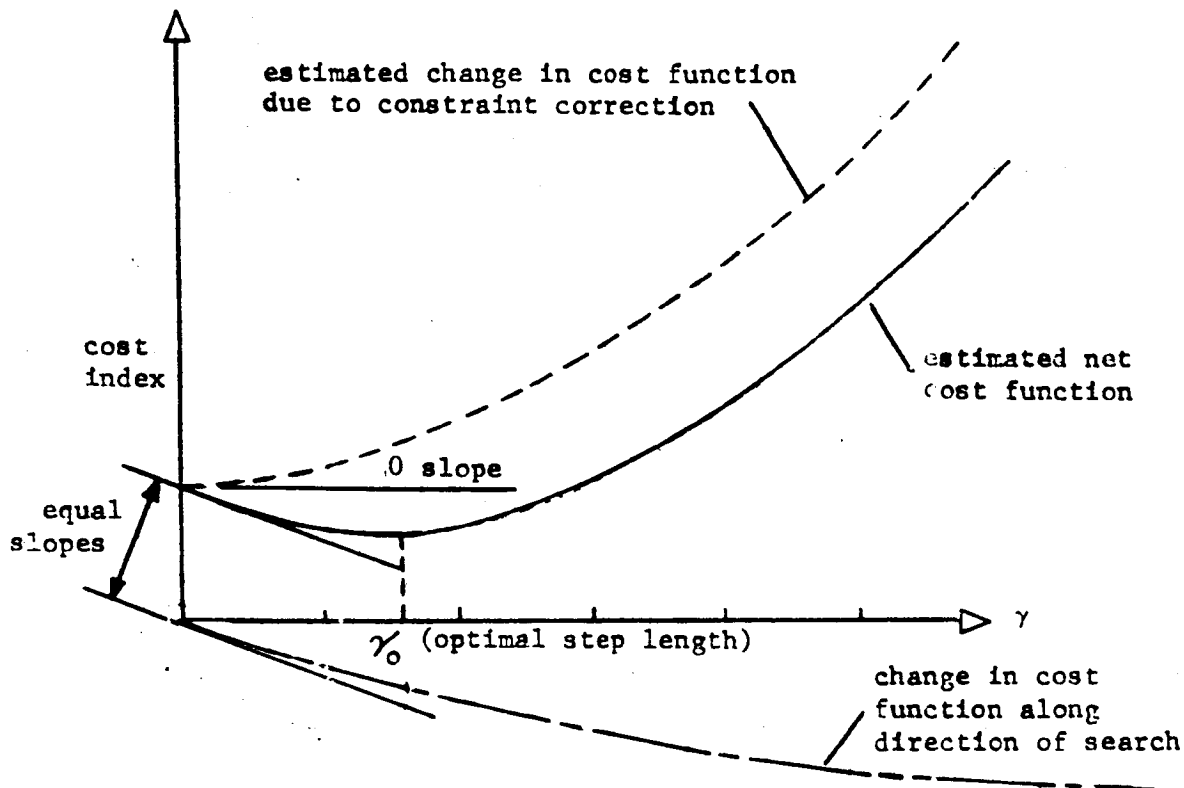
Figure 11-6. Properties of Estimated Net Cost Function

Both the constraint and optimization directions are based upon an assumed set of active constraints. Hence for searches in the optimization direction it is necessary to limit the step size so that the set of active constraints does not grow. Such a limit based on linear approximation can readily be obtained. Let $L(\underline{\hat{u}})$ denote the set of constraints which are loose at $\underline{\hat{u}}$; that is

$$L(\underline{\hat{u}}) = \{i: c_i(\underline{\hat{u}}) > 0\}.$$ (11-49)

11-22

To each element ℓ in L compute the linearized directional derivative, d_ℓ, along the search ray, $s^o(\hat{\underline{u}})$.

$$d_\ell = \underline{\nabla}c_\ell(\hat{\underline{u}})s^o(\hat{\underline{u}}) \qquad \text{for } \ell\epsilon L(\hat{\underline{u}}). \qquad (11\text{-}50)$$

Then the approximate distance along the search ray to the region of infeasibility for constraint ℓ is

$$\lambda_\ell = \begin{cases} -c_\ell(\hat{\underline{u}})/d_\ell & \text{if } d_\ell < 0 \\ R & \text{if } d_\ell \geq 0 \end{cases} \qquad \text{for } \ell\epsilon L(\hat{\underline{u}}) \qquad (11\text{-}51)$$

where R is a large positive constant. Hence a reasonable upper bound on the step length is

$$\lambda(\hat{\underline{u}}) = \min_{\ell\epsilon L(\hat{\underline{u}})} \lambda_\ell. \qquad (11\text{-}52)$$

11.3.2.4 One-Dimensional Minimization

Monovariant minimization in the projected gradient algorithm is performed exclusively by polynomial approximation. In general the minimizing step length, γ, of a function, $f(\gamma)$, along the search ray $\underline{s}(\underline{u}^\nu)$ is to be found to determine a new iterate of control parameters as

$$\underline{u}^{\nu+1} = \underline{u}^\nu + \gamma\underline{s}(\underline{u}^\nu). \qquad (11\text{-}53)$$

The function, f, is fitted with a sequence of successively more refined low-degree polynomials;

$$P_m(\gamma) = \sum_{i=0}^{3} a_i^m \gamma^i \approx f(\gamma) \text{ for } 0 \leq \gamma \leq \lambda(\underline{u}^\nu). \qquad (11\text{-}54)$$

Since the degree of the approximating polynomial never exceeds three, its minimizing abscissa value γ_m^* can be evaluated in closed form. If γ_m^* exceeds $\lambda(\underline{u}^\nu)$, then the algorithm takes

$$\gamma = \lambda(\underline{u}^\nu). \qquad (11\text{-}55)$$

If, on the other hand, γ_m^* is less than $\lambda(\underline{u}^\nu)$, two tests are conducted to determine whether or not it is an adequate approximation to γ^*, the true minimizing abscissa of f. These tests are the conditions

$$\left|\gamma_m^* - \gamma_{m-1}^*\right| < \mathcal{E}_1\gamma_o \qquad (11\text{-}56)$$

where γ_o is the length of the initial trial step generated when the search direction is computed and

$$\left|P_m(\gamma_m^*) - f(\gamma_m^*)\right| < \mathcal{E}_2. \qquad (11\text{-}57)$$

If either condition (11-56) or (11-57) is satisfied, the algorithm takes

$$\gamma = \gamma_m^* . \qquad (11\text{-}58)$$

If not, the algorithm fits f with the next polynomial p_{m+1} in the sequence. If the current polynomial is the last one in the sequence, the set E of abscissa values for which f has been evaluated is examined to determine the step size γ_5 with the smallest value of f; that is

$$\gamma_5 = \min_{\gamma \epsilon E} f(\gamma). \qquad (11\text{-}59)$$

The algorithm then takes

$$\gamma = \gamma_5. \qquad (11\text{-}60)$$

The one dimensional minimization routine makes ingenious use of all the information it accumulates about f in generating its sequence of approximating polynomials, $\{p_m\}_{m=1}^{4}$. The first polynomial, p_1, is a quadratic determined by the requirements that

$$p_1(0) = f(0), \qquad (11\text{-}61)$$

$$p_1'(0) = f'(0), \qquad (11\text{-}62$$

and

$$p_2(\gamma_o^*) = f(\gamma_o^*) \qquad (11\text{-}63)$$

where $\gamma_o^* = \gamma_o$, the initial trial step estimate. The coefficients for the quadratic are

$$a_o^1 = f(0) \qquad (11\text{-}64)$$

$$a_1^1 = f'(0) \qquad (11\text{-}65)$$

$$a_2^1 = \{[f(\gamma_o^*)-a_o]/\gamma_o^*-a_1\}/\gamma_o^*. \qquad (11\text{-}66)$$

The abscissa value that minimizes p_1 is

$$\gamma_1^* = -a_1/2a_2. \qquad (11\text{-}67)$$

The second polynomial in the sequence is a cubic based upon the four requirements that

$$p_2(0) = f(0), \qquad (11\text{-}68)$$

$$p_2'(0) = f'(0), \qquad (11\text{-}69)$$

$$p_2(\gamma_o^*) = f(\gamma_o^*), \qquad (11\text{-}70)$$

and

$$p_2(\gamma_1^*) = f(\gamma_1^*). \qquad (11\text{-}71)$$

The coefficients for the cubic are

$$a_0^2 = f(0) \tag{11-72}$$

$$a_1^2 = f'(0)$$

$$a_2^2 = \frac{\{\gamma_1^{*3}[f(\gamma_0^*)-f(0)-\gamma_0^*f'(0)]-\gamma_0^{*3}[f(\gamma_1^*)-f(0)-\gamma_1^*f'(0)]\}}{(\gamma_0^{*2}\gamma_1^{*3}-\gamma_1^{*2}\gamma_0^{*3})} \tag{11-74}$$

$$a_3^2 = \{[(f(\gamma_0^*)-a_0^2)/\gamma_0^*-a_1^2]/\gamma_0^*-a_2^2\}/\gamma_0^* \tag{11-75}$$

The step length that minimizes p_1 is

$$\gamma_2^* = (-a_2^2 + \sqrt{(a_2^2)^2-3a_1^2a_3^2})/(3a_3^2). \tag{11-76}$$

The third polynomial in the sequence is a quadratic passing through the current best point and its two adjacent points. To be more precise, the accumulated set of sample points, namely $[0,f(0)]$, $[\gamma_0^*,f(\gamma_0^*)]$, $[\gamma_1^*,f(\gamma_1^*)]$, and $[\gamma_2^*,f(\gamma_2^*)]$, is arranged in the order of ascending abscissa values. The first point whose ordinate value is less than that of the following point is selected and designated $[\zeta_2,f(\zeta_2)]$. The preceding point is labeled $[\zeta_1,f(\zeta_1)]$ and the succeeding point as $[\zeta_3,f(\zeta_3)]$. Then p_3 is the quadratic polynomial satisfying the three constraints that

$$p_3(\zeta_1) = f(\zeta_1), \tag{11-77}$$

$$p_3(\zeta_2) = f(\zeta_2), \tag{11-78}$$

and

$$p_3(\zeta_3) = f(\zeta_3). \tag{11-79}$$

The formulas for the coefficients of p_3 are

$$a_1^3 = -(\zeta_2+\zeta_3)f(\zeta_1)/D_1-(\zeta_1+\zeta_3)f(\zeta_2)/D_2-(\zeta_1+\zeta_2)f(\zeta_3)/D_3 \tag{11-80}$$

$$a_2^3 = f(\zeta_1)/D_1+f(\zeta_2)/D_2+f(\zeta_3)/D_3 \tag{11-81}$$

and

$$a_0^3 = f(\zeta_2)-\zeta_2(a_1^3+a_2^3\zeta_2) \tag{11-82}$$

where

$$D_1 = (\zeta_2-\zeta_1)(\zeta_3-\zeta_1) \tag{11-83}$$

$$D_2 = (\zeta_1-\zeta_2)(\zeta_3-\zeta_2) \tag{11-84}$$

$$D_3 = (\zeta_1-\zeta_3)(\zeta_2-\zeta_1). \tag{11-85}$$

The minimizing step size for this quadratic is

$$\zeta_4 = \gamma_3^* = -a_1^3/2a_2^3. \tag{11-86}$$

The fourth and final approximating polynomial is a cubic satisfying the following four requirements:

$$P_4(\zeta_1) = f(\zeta_1), \tag{11-87}$$

$$P_4(\zeta_2) = f(\zeta_2), \tag{11-88}$$

$$P_4(\zeta_3) = f(\zeta_3), \tag{11-89}$$

and

$$P_4(\zeta_4) = f(\zeta_4). \tag{11-90}$$

The formulas for the coefficients of p_4 are

$$a_0^4 = \zeta_2\zeta_3\zeta_4 f(\zeta_1)/D_1 + \zeta_1\zeta_3\zeta_4 f(\zeta_2)/D_2 + \zeta_1\zeta_2\zeta_4 f(\zeta_3)/D_3$$
$$+ \zeta_1\zeta_2\zeta_3 f(\zeta_4)/D_4, \tag{11-91}$$

$$a_2^4 = (\zeta_2+\zeta_3+\zeta_4)f(\zeta_1)/D_1 + (\zeta_1+\zeta_3+\zeta_4)f(\zeta_2)/D_2$$
$$+ (\zeta_1+\zeta_2+\zeta_4)f(\zeta_3)/D_3 + (\zeta_1+\zeta_2+\zeta_3)f(\zeta_4)/D_4, \tag{11-92}$$

$$a_3^4 = f(\zeta_1)/D_1 + f(\zeta_2)/D_2 + f(\zeta_3)/D_3 + f(\zeta_4)/D_4, \tag{11-93}$$

$$a_1^4 = (f(\zeta_2)-a_0^4)/\zeta_2 - \zeta_2(a_2^4 + a_3^4\zeta_2) \tag{11-94}$$

where

$$D_1 = (\zeta_2-\zeta_1)(\zeta_3-\zeta_1)(\zeta_4-\zeta_1) \tag{11-95}$$

$$D_2 = (\zeta_1-\zeta_2)(\zeta_3-\zeta_2)(\zeta_4-\zeta_2) \tag{11-96}$$

$$D_3 = (\zeta_1-\zeta_3)(\zeta_2-\zeta_3)(\zeta_4-\zeta_3) \tag{11-97}$$

$$D_4 = (\zeta_1-\zeta_4)(\zeta_2-\zeta_4)(\zeta_3-\zeta_4). \tag{11-98}$$

The minimizing abscissa value is

$$\zeta_4^* = (-a_2^4 + \sqrt{(a_2^4)^2 - 3a_1^4 a_3^4})/(3a_3^4). \tag{11-99}$$

11.3.2.5 Variable Weighting

If the ranges of the components of the control or constraint vectors differ considerably numerical problems can arise in obtaining and manipulating sensitivity information. If the control parameters differ drastically in their ranges, the selection of perturbation sizes for approximating derivatives as divided differences is complicated. Also extreme sensitivity of the cost function or constraints to certain control parameters can cause the numerical approximation to the desired geometrically-defined search directions to be in significant error.

Proper control parameter scaling can bring such sensitivities more into line. Similarly a constraint parameter whose range differs substantially from those of the others can cause serious problems in search-direction approximation and curve fitting of the error function.

To avoid these numerical problems both the control and constraint parameters are scaled. The user's unweighted control-parameter vector, $\underline{\tilde{u}}$ is replaced by its corresponding scaled-version, $\underline{u}$, given by

$$u_j = w_j \tilde{u}_j \qquad \text{for } j = 1, \ldots, m. \qquad (11\text{-}100)$$

The weighting factors are best taken as the reciprocal of the user's initial control parameter estimate; that is

$$w_j = \begin{cases} 1/|u_j^0| & \text{if } u_j^0 \neq 0 \qquad \text{for } j = 1, \ldots, m \, . \qquad (11\text{-}101) \\ a_j & \text{otherwise} \end{cases}$$

where a_j is a special scaling factor input by the user. Alternatively the user can specify all of the weighting factors. In any case the factors should be chosen to contain the variation of each weighted control parameter in the interval from -1 to 1 with the end points closely approximated.

A similar weighting is defined for the constraint parameters. Let $\tilde{c}_i$ denote the unweighted value of the ith constraint and c_i the weighted value. Then

$$c_i = v_i \tilde{c}_i \qquad \text{for } i = 1, \ldots, n. \qquad (11\text{-}102)$$

The default option for selecting these weights is to take

$$v_i = 1/\mathcal{E}_i \qquad \text{for } i = 1, \ldots, n \qquad (11\text{-}103)$$

where $\mathcal{E}_i$ is the specified tolerance on the ith constraint. This weighting can, however, lead to rather large magnitudes of the constraint parameters. A preferable weighting is to set

$$v_i = 1/\bar{c}_i \qquad \text{for } i = 1, \ldots, n \qquad (11\text{-}104)$$

where $\bar{c}_i$ is reasonably tight upper bound estimate on the magnitude of c_i. This weighting more nearly achieves the desired properties described for the weighted control parameters.

Finally an extreme range of the cost function can cause numerical difficulties in computing its gradient and in the curve fitting of the

estimated net cost function. Thus a weighted cost function F is defined in terms of the user defined cost $\tilde{F}$ as

$$F(\underline{u}) = z\tilde{F}(\underline{u}).$$

(11-105)

The default option for the weighting is

$$z = 1/|\tilde{F}(\underline{u}^0)|.$$

(11-106)

Alternatively the user can specify z directly. The object, as usual, in selecting z is to confine variation of F to the interval from -1 to 1 while closely approximating the end points.

Since the user generally specifies F and $\underline{c}$ in terms of $\underline{u}$ only

$$\tilde{\underline{\nabla}}F = \frac{\partial \tilde{F}}{\partial \tilde{u}}$$

(11-107)

and

$$\tilde{S} = \frac{\partial \tilde{\underline{c}}}{\partial \underline{\tilde{u}}}$$

(11-108)

can be computed by numerical differencing. The equations relating these to the desired corresponding sensitivities of the weighted cost function and constraint parameters with respect to the weighted control parameters are

$$\frac{\partial F}{\partial u_j} = z \frac{\partial \tilde{F}}{\partial \tilde{u}_j}/w_j \qquad \text{for } j = 1,\ldots, m$$

(11-109)

and

$$\frac{\partial c_i}{\partial u_j} = v_i \frac{\partial \tilde{c}_i}{\partial \tilde{u}_j}/w_j \qquad \text{for } j = 1,\ldots, m.$$

(11-110)

11.3.2.6 Algorithm Macrologic

Now that the fundamental components of the algorithm have been described, the controlling logic integrating them into an effective targeting and optimization procedure can be presented. Once a feasible control parameter vector has been found the algorithm generates a sequence of iteration pairs. Each pair consists of an optimization step followed by a constraint step. If the user's initial control-parameter estimate is not feasible, however, a steadily improving sequence of constraint-correction steps is undertaken until a feasible solution is found. Furthermore, the subsequent optimization step is omitted after any constraint-correction step which fails to yield a feasible control-parameter vector.

The unaccelerated optimization search direction that emanates from $\underline{u}^v$ is based on the active-constraint sensitivity matrix, $S(\underline{u}^v)$; that is

11-28

$$\underline{s}^{\,o}(u^{\nu}) = -[P(\underline{u}^{\nu})\nabla F(\underline{u}^{\nu})]^{T}, \tag{11-111}$$

as discussed previously. Hence $\underline{s}^{\,o}(\underline{u}^{\nu})$ lies in the subspace $Q(\underline{u}^{\nu})$. If the set of active constraints has not changed since the last optimization step, an accelerated projected gradient direction, $\underline{s}^{\,a}$, is generated by multiplying the unaccelerated direction by a deflection matrix; that is

$$\underline{s}^{\,a}(\underline{u}^{\nu}) = H_{\nu}\underline{s}^{\,o}(\underline{u}^{\nu}). \tag{11-112}$$

The deflection matrix, H_{ν}, is updated before each application according to the formulas given in the section on search directions. For the case of k active purely linear constraints and a quadratic cost function this acceleration process guarantees convergence in only m-k steps. The value of the control-parameter vector after the one-dimensional minimization along the search ray is then the next iterate; that is

$$\underline{u}^{\nu+1} = (\underline{u} + \gamma_{o}^{*}\,\underline{s}^{\,a})^{\nu} \tag{11-113}$$

where $(\gamma_{o}^{*})^{\nu}$ is the step length that minimizes the estimated net cost function.

The direction for the constraint-correction search then emanates from $\underline{u}^{\nu+1}$. However, since generating a new Jacobian matrix at $\underline{u}^{\nu+1}$ by divided differencing is such an expensive calculation, the old Jacobian at $\underline{u}^{\nu}$ is used in approximating the new constraint direction. Further, the set of active constraints K is frozen from an optimization step to the succeeding constraint step. Hence

$$S(\underline{u}^{\nu}) = S(\underline{u}^{\nu+1}) \tag{11-114}$$

where $\underline{u}^{\nu+1}$ is the solution at the completion of the optimization step. It can be shown by direction computation that

$$\tilde{P}(\underline{u}_{\nu+1})\,s^{c}(\underline{u}^{\nu+1}) = s^{c}(\underline{u}^{\nu+1}) \tag{11-115}$$

Hence $s^{c}(\underline{u}^{\nu+1})$ lies in $\tilde{Q}(\underline{u}^{\nu+1}) = \tilde{Q}(\underline{u}^{\nu})$. Since $Q(\underline{u}^{\nu})$ and $\bar{Q}(\underline{u}^{\nu})$ are orthogonally complementary subspaces, it follows that the constraint correction and the unacceleration optimization directions are exactly orthogonal; that is

$$[\underline{s}^{\,o}(\underline{u}^{\nu})]^{T}\underline{s}^{\,c}(u^{\nu+1}) = 0 \tag{11-116}$$

The value of the control-parameter vector after the one-dimensional minimization along the search ray is the next iterate; that is

$$\underline{u}^{\nu+2} = (\underline{u} + \gamma_{c}^{*}\,\underline{s}^{\,c})^{\nu+1}$$

where $(\gamma_c^*)^{\nu+1}$ is the step that minimizes the sum of the squares of the errors in the active constraints. Figure 11-7 geometrically illustrates a complete projected gradient iteration pair without acceleration.
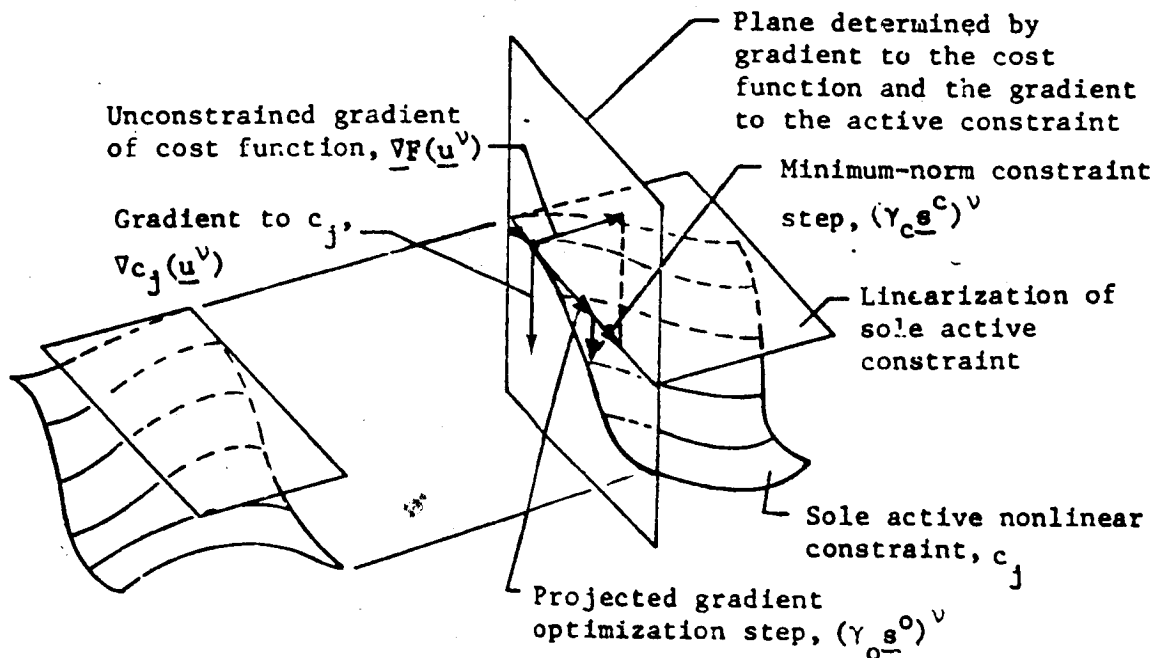
Figure 11-7. Complete PGA Iteration, Consisting of Optimization Step Followed by Constraint Step for k = 1 and m = 3 (feasible region is the unbounded region below the indicated nonlinear constraint manifold).

Finally the algorithm has two stopping conditions. First the search is stopped if both the change in the cost function and the length of the change in the control-parameter vector between two successive optimization steps fall below their respective input tolerances. Symbolically

$$|F(\underline{u}^{\nu+2}) - F(\underline{u}^{\nu})| < \mathcal{E}_F, \tag{11-118}$$

and

$$||\underline{u}^{\nu+2} - \underline{u}^{\nu}|| < \mathcal{E}_u \tag{11-119}$$

where $\underline{u}^{\nu}$ and $\underline{u}^{\nu+2}$ are the control-parameter vectors resulting from the optimization steps in two consecutive iteration pairs. Second, the procedure is terminated if the maximum permissible number of iterations specified by the user is exceeded. Figure 11-8 is a precise summary of the complete macrologic of the accelerated projected gradient algorithm.

11-30
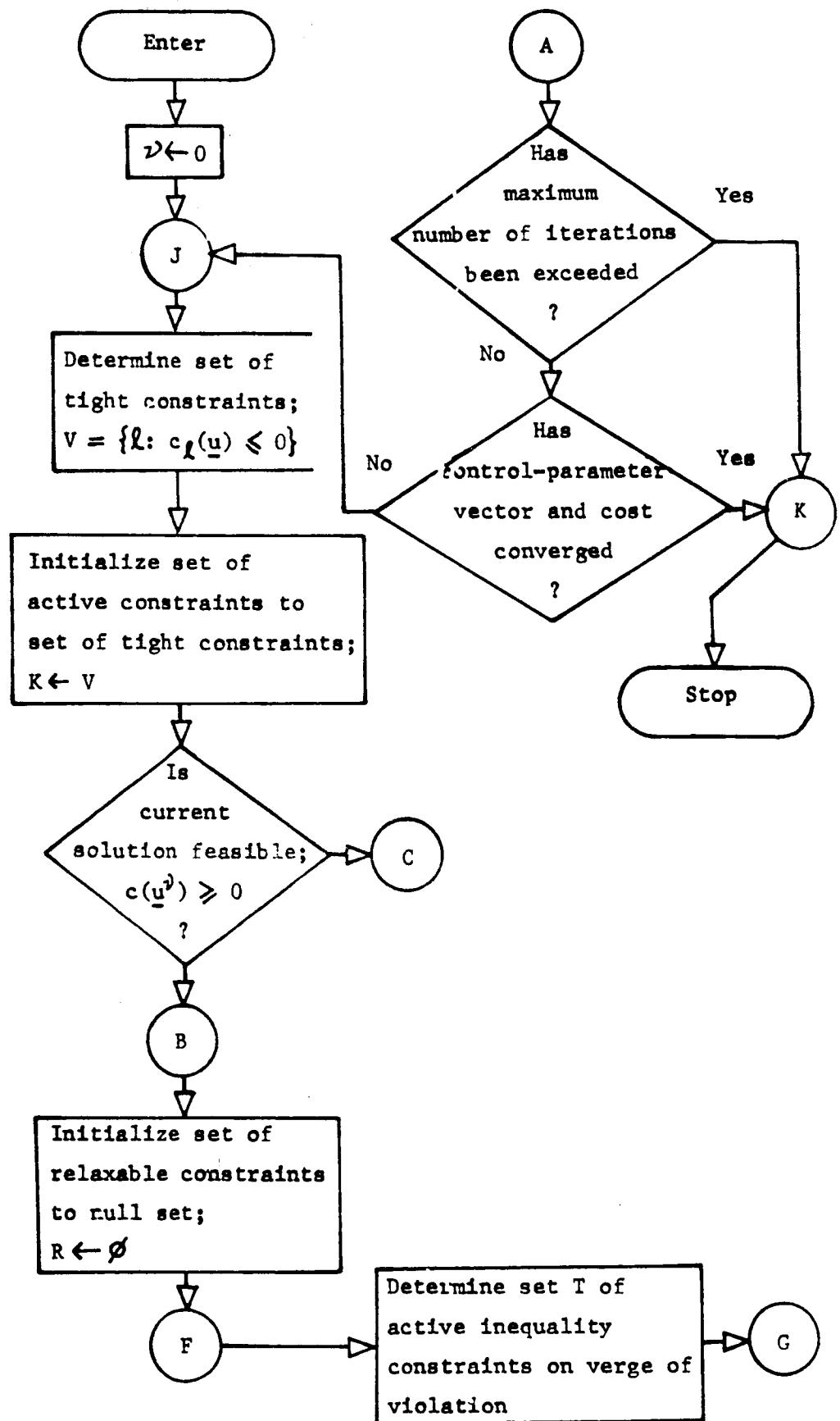
Figure 11-8. Macrologic of Accelerated Projected Gradient Algorithm
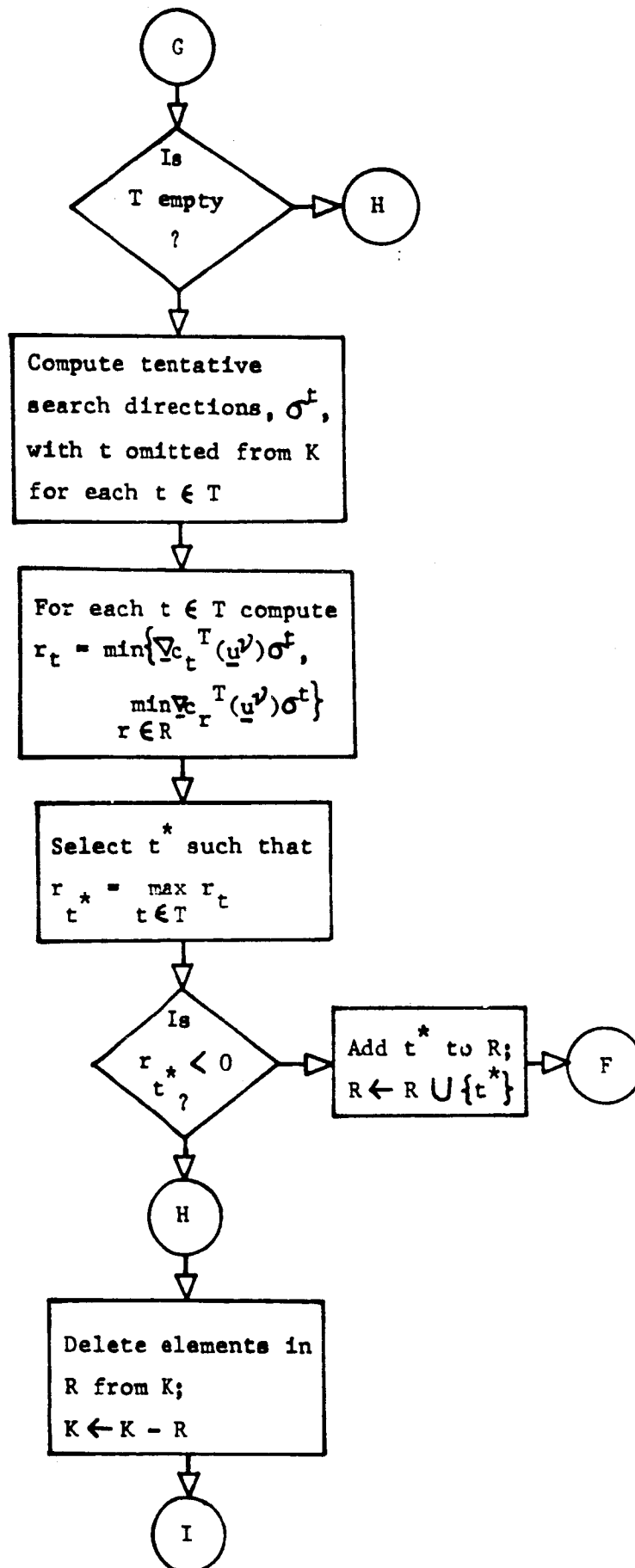
Figure 11-8 (continued). Macrologic of Accelerated Projected Gradient Algorithm

Figure 11-8 (continued). Macrologic of Accelerated Projected Gradient Algorithm

Figure 11-8 (continued). Macrologic of Accelerated Projected Gradient Algorithm

E

Obtain accelerated optimization direction

$$s^a(\underline{u}^\nu) = H_\nu s^0(\underline{u}^\nu)$$

Determine step size, γ_0^*, that minimizes the estimated net cost function

$$h_c(\gamma) = F\left[(\underline{u} + \gamma \underline{s}^a)^\nu\right] - F(\underline{u}^\nu)$$
$$+ \nabla F(\underline{u}^\nu) Ce\left[(\underline{u} + \gamma \underline{s}^a)^\nu\right]$$

without exceeding $\bar{\gamma}_0$

Update current solution and iteration counter

$$\nu \leftarrow \nu + 1$$
$$\underline{u}^\nu \leftarrow (\underline{u} + \gamma_0 \underline{s}^a)^\nu$$

I
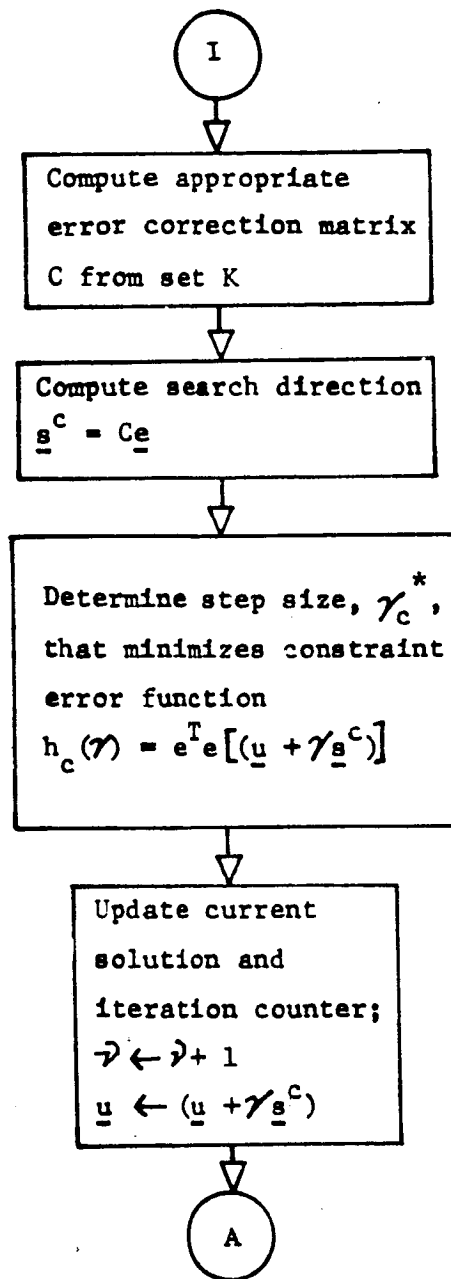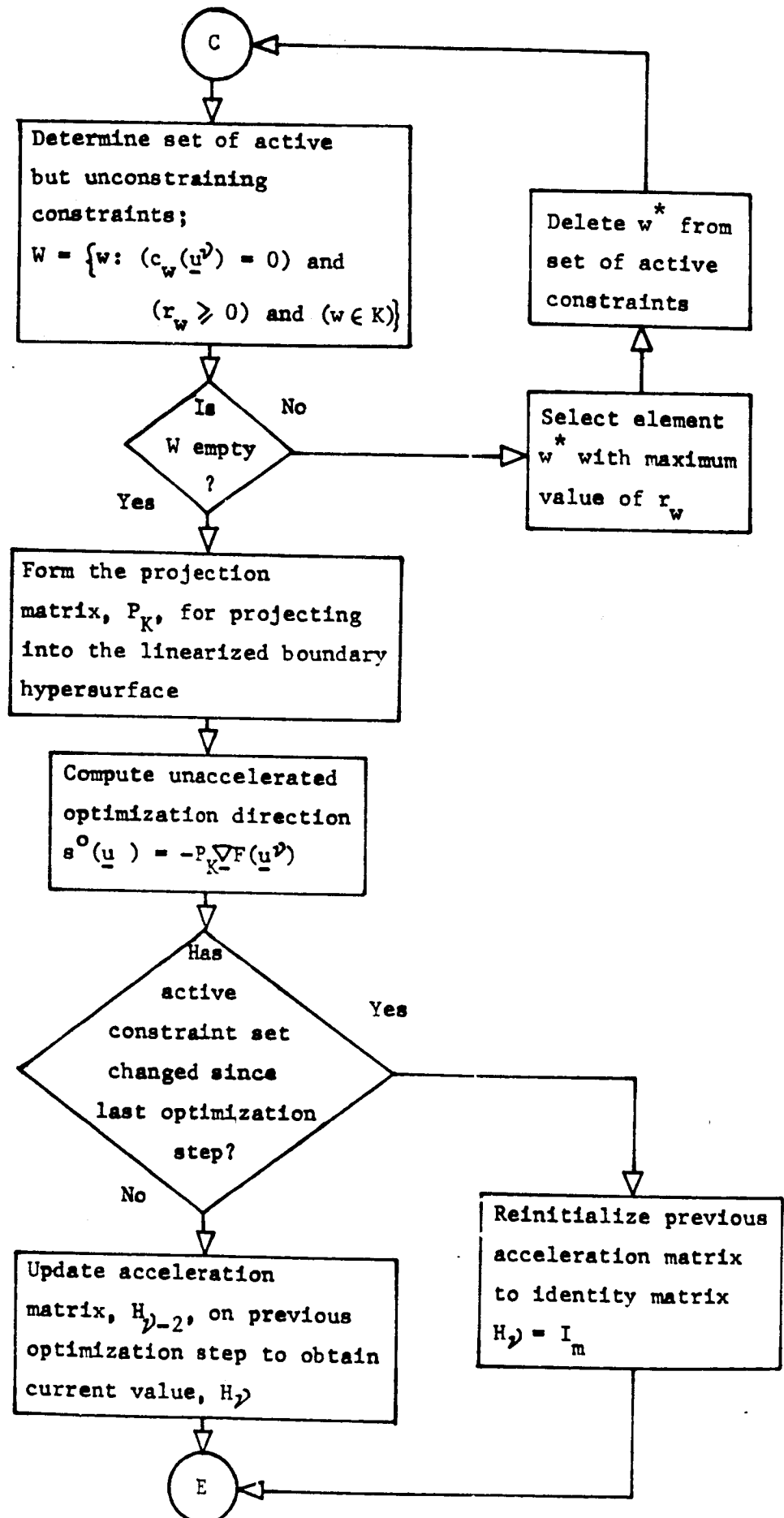
Figure 11-8 (completed). Macrologic of Accelerated Projected Gradient Algorithm

11.3.3 Equality Constraint Algorithms

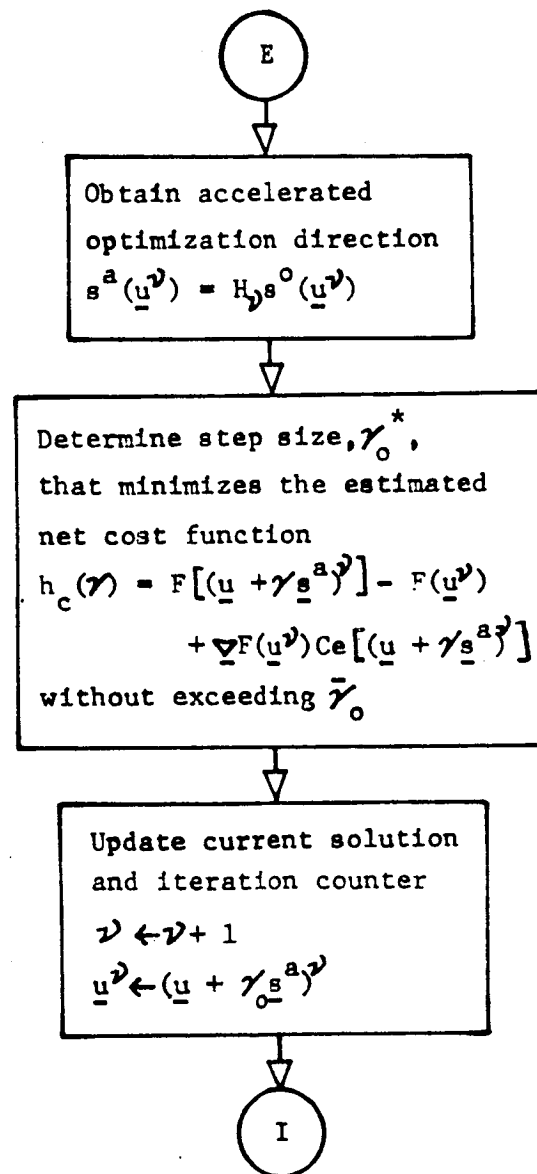Algorithms for solving the general nonlinear programming problem with inequality constraints are particularly unsuited to trajectory problems where the objective and constraint functions are available only implicitly through relatively expensive numerical propagation of the equations of motion. Most inequality-constraint techniques make extensive use of the simplex algorithm and hence require that the objective and constraint functions be explicitly available so that they can be readily approximated as piecewise linear functions over the full range of interest. Examples include separable programming and all other methods based upon inner and outer linearization (see Reference [7]). Other than the projected gradient algorithm the only other two well-known methods not requiring prohibitive initial piecewise linearization are Zoutendijk's method of feasible directions and Fiacco and McCornick's SUMT method (see References [8] and [5], respectively). Neither, however, are very attractive computationally nor do they have the intuitive appeal of the projected gradient method. Further the author knows of no implementation of either for practical trajectory analysis.

Only procedures for solving the specialized problem with equality constraints have found widespread application in trajectory work. Basically two approaches have been used exclusively: (1) minimization of a penalized cost function and (2) zeroing the Lagrangian gradient. The two techniques therefore deserve comment. Reference will be made to the equality constrained program

$$\text{minimize:} \quad F(\underline{u})$$

$$\text{subject to:} \quad c(\underline{u}) = \underline{0}$$

where: $\underline{u}$ is an mx1 matrix of control parameters   (11-120)

F is a scalar cost function of the vector of control parameters

$\underline{c}$ is an nx1 matrix of constraint parameters.

The penalized cost function approach involves forming an augmented cost function, $\hat{F}$, by adding a penalty term to the original cost to penalize constraint violation. The penalty term must be such that the unconstrained minimum of the augmented function and the constrained minimum of the original cost coincide. The augmented cost function can then be minimized by any desired unconstrained optimization technique the best of which is

11-36

is probably Davidon's accelerated version of steepest descent. The penalty term is typically a weighted sum of squares of the constraint errors. Thus

$$\hat{F}(\underline{u}) = F(\underline{u}) + \sum_{i=1}^{n} c_i^2 (\underline{u}) \qquad (11\text{-}121)$$

The problem with the penalty function approach is that the penalty term is only a disguised version of the original constraints, which could better be dealt with directly. As an extreme example if there are precisely m linear constraints, the best quadratically convergent descent scheme would require evaluation of F and $\underline{c}$ at least m(m+1) times (assuming sensitivity approximation by divided differencing) while the projected gradient algorithm would require but 2m+1 such evaluations.

The Lagrangian method involves solving an equivalent but analytically more tractable problem. Lagrange showed that under suitably mild conditions on the differentiability of F and $\underline{c}$ the mathematical program (11-120) is equivalent to finding a point where the gradient of the related Lagrangian function, L, vanishes. Now the Lagrangian is defined to be

$$L(\underline{u}, \underline{\lambda}) = F(\underline{u}) + \underline{\lambda}^T \underline{c}(\underline{u}) \qquad (11\text{-}122)$$

where $\underline{\lambda}$ is an mx1 matrix of Lagrange multipliers. Thus the optimality condition is that at the extreme point (u*, λ*)

$$\left. \frac{\partial L}{\partial \underline{u}} \right|_{\underline{u}*,\underline{\lambda}*} = 0, \qquad (11\text{-}123)$$

and

$$\left. \frac{\partial L}{\partial \lambda} \right|_{\underline{u}*} = 0. \qquad (11\text{-}124)$$

Equivalently

$$\left. \frac{\partial F}{\partial \underline{u}} + \lambda^T \frac{\partial \underline{c}}{\partial \underline{u}} \right|_{u*,\lambda*} = \underline{0} \qquad (11\text{-}125)$$

and

$$\underline{c}(\underline{u}*) = 0. \qquad (11\text{-}126)$$

The Lagrange approach thus reduces to solving the m+n nonlinear equations represented by relations (11-125) and (11-126).

Two fundamental objections can be raised to this method. First the analytical complaint can be made that the number of unknowns has been increased by n with the addition of the Lagrange multipliers. This is significant since problem difficulty typically increases at least exponentially with dimensionality. Second, on numerical grounds exception can be taken to the

requirement of second partial derivatives of F and $\underline{c}$ with respect to the control parameters for solution of the Lagrange equations by the usual Newton-Raphson numerical procedure. Such approximation not only requires an inordinate number of evaluations of F and $\underline{c}$ ([m+1][m+2]/2 per Newton-Raphson iteration) but also is very susceptible to numerical roundoff problems.

11.3.4 Inhibited Least-Squares Algorithm

The MINMAX "nonlinear iterator" currently in use at GSFC solves the following specialized nonlinear program

minimize: $F(\underline{u}) = \sum_{i \varepsilon C_3} [c_i(\underline{u}) - a_i]^2 + \sum_{i \varepsilon C_4} [c_i(\underline{u}) - b_i]^2$

subject to: $c_i(\underline{u}) = d_i$ for $i \varepsilon C_1$

$c_i(\underline{u}) \geq a_i$ for $i \varepsilon C_2 U C_3$

$c_i(\underline{u}) \leq b_i$ for $i \varepsilon C_2 U C_4$

(11-127)

where: $\underline{u}$ is an mx1 matrix of control parameters

$\underline{c}$ is an nx1 matrix of constraint parameters.

$C_1 =$ set of constraint parameters constrained to equality

$C_2 =$ set of constraint parameters constrained to an interval but requiring no optimization

$C_3 =$ set of indices of variables which are to be minimized (b_i should be taken smaller than any value attainable by c_i).

$C_4 =$ set of indices of variables which are to be maximized (a_i should be taken larger than any value attainable by c_i).

$d_i =$ desired value of the c_i which is an element of C_1

$a_i =$ desired lower bound on c_i which is an element of C_2 or artificial lower bound on c_i which is an element of C_3

$b_i =$ desired upper bound on c , which is an element of C_2 or artificial upper bound on c_i which is an element of C_4.

The algorithm is based upon an iterative minimization of the square of the error vector plus a penalty term proportional to the square of the step length in the independent variable. The error vector at control parameter, $\underline{u}$, is defined in terms of the set of active constraints there:

$$K(\underline{u}) = \{i: (i \in C_1) \text{ or } [(i \in C_2 \cup C_3) \text{ and } (c_i(\underline{u}) > b_i)] \text{ or } [(i \in C_2 \cup C_4) \text{ and } (c_i(\underline{u}) < a_i)]\}. \quad (11\text{-}128)$$

Suppose there are k active constraints and that σ_ℓ is the index of the ℓth entry in $K(\underline{u})$. Then the error vector is defined as

$$e_\ell(\underline{u}) = \begin{cases} c_{\sigma_\ell}(\underline{u}) - d_{\sigma_\ell} & \text{if } \sigma_\ell \varepsilon C_1 \\[2mm] c_{\sigma_\ell}(\underline{u}) - b_{\sigma_\ell} & \text{if } (\sigma_\ell \varepsilon C_2 \cup C_3) \text{ and } (c_{\sigma_\ell} > b_{\sigma_\ell}) \\[2mm] a_{\sigma_\ell} - c_{\sigma_\ell}(\underline{u}) & \text{if } (\sigma_\ell \varepsilon C_2 \cup C_4) \text{ and } (c_{\sigma_\ell} < a_{\sigma_\ell}) \end{cases} \quad (11\text{-}129)$$

The MINMAX code attempts to generate a sequence of control parameter values for which the functional

$$R(\underline{u}^\nu) = [e^T \underline{e}](\underline{u}^\nu) \quad (11\text{-}130)$$

decreases monotonically. The generation process is based upon the error sensitivity matrix

$$[S(\underline{u}^\nu)]_{\ell j} = \left. \frac{\partial e_{\sigma_\ell}}{\partial u_j} \right|_{\underline{u}^\nu} \qquad \begin{array}{l} \text{for } \ell = 1,\ldots, k \\ \text{for } j = 1,\ldots, m. \end{array} \quad (11\text{-}131)$$

Assuming the active constraints vary linearly with the controls the exact control-parameter correction to minimize $R(\underline{u})$ is

$$\Delta\underline{u}^\nu = -[(S^T S)^{-1} S^T](\underline{u}^\nu)\underline{e}(\underline{u}^\nu). \quad (11\text{-}132)$$

Nonlinear effects can cause this correction to be quite grossly in error. So instead an augmented functional with a penalty term on the correction step length is minimized; namely

$$\hat{R}(\underline{u}^\nu, \Delta\underline{u}^\nu) = [\underline{e}^T\underline{e}](\underline{u}^\nu) + \lambda_\nu \Delta^T\underline{u}^\nu \Delta\underline{u}^\nu \quad (11\text{-}133)$$

The coefficient λ_ν is called the inhibitor. It is chosen anew at each iteration to satisfy the two conditions

$$\Delta^T\underline{u}^\nu \Delta\underline{u}^\nu < \varepsilon_u^2 \quad (11\text{-}134)$$

and

$$R(\Delta\underline{u}^\nu) < R(\Delta\underline{u}^{\nu-1}). \quad (11\text{-}135)$$

The exact minimum of $\hat{R}$ again assuming linear variation of the active constraints with the control parameters is

$$\Delta \underline{u}^\nu = -[(S^T S + \lambda I) S^T \underline{e}](\underline{u}^\nu) . \qquad (11\text{-}136)$$

At the beginning of iteration ν, λ_ν is estimated as a proper fraction of $\lambda_{\nu-1}$. The control correction $\Delta \underline{u}_\nu$ is then computed from (11-136). Then condition (11-134) is tested. If it is not satisfied λ_ν is increased and the test repeated. This process is continued until satisfaction of relation (11-134) is achieved. Then condition (11-135) is tested. If it is satisfied the iteration is complete and the correction $\Delta \underline{u}^\nu$ is made to the control parameters. If it is not satisfied, λ_ν is increased and the test redone. This procedure is repeated until relation (11-135) is satisfied or λ_ν exceeds some specified upper bound. When the latter occurs, it is concluded that functional R has achieved a local minimum and hence that the program (11-127) is solved.

This algorithm can hardly be considered a state-of-the-art nonlinear programming technique. It is most effective in solving fully determined systems of nonlinear equations—that is, when C_2, C_3, and C_4 are empty. In this targeting mode the code is essentially a Newton-Raphson algorithm if n=m and a Gauss' "least-squares" procedure if n>m. Only a trivial modification to either of these algorithms is made in the MINMAX code to prevent excessive step lengths when the linear extrapolations involved do not apply in minimizing R. The natural question, however, is that if the extrapolations do not apply for R why do they apply for $\hat{R}$. There is no valid answer to this query. Indeed if a reasonably accurate solution estimate is available the performance of the MINMAX code would be no better than that of the appropriate Newton-Raphson or "least-squares" procedures. Further, if the estimate was too inaccurate for convergence of these widely used algorithms the same thing would probably be true of the inhibited iterator. In such cases, a best-step steepest descent algorithm applied to the sum of the squares of the constraint errors would better serve to drive the solution into the range of Newton-Raphson or least-squares convergence.

The objective function of the program (11-127) is too restricted to make MINMAX useful in solving trajectory optimization problems. If $C_3 U C_4$ contains more than one constraint, it is rather difficult to select their relative weighting factors. Further if $C_3 U C_4$ is empty there is no criterion

for selecting a best solution from the multiplicity of feasible solutions. In this situation the projected gradient algorithm chooses that feasible solution closest to the initial control-parameter estimate if the user provides no explicit cost function.

The general accelerated projected gradient algorithm would provide a targeting capability with equal or better convergence properties than MINMAX, plus a completely flexible optimization facility. Indeed, the projected gradient algorithm targets an initially infeasible control parameter estimate by the method of "minimum norm", Newton-Raphson, or least-squares iteration depending upon whether $m<n$, $m=n$, or $m>n$ respectively. It then proceeds to minimize an arbitrary cost function specified by the user while maintaining feasibility. The constrained optimization technique employed is the stable gradient projection technique of Rosen with added acceleration logic to expedite terminal convergence.

REFERENCES

1. G. Hadley, NONLINEAR AND DYNAMIC PROGRAMMING, Addison-Welsey, Reading, Massachusetts, 1964.

2. Leon S. Lasdon, OPTIMIZATION THEORY FOR LARGE SYSTEMS, MacMillan, London, 1970.

3. J. B. Rosen, "The Gradient Projection Method for Nonlinear Programming: Part I-Linear Constraints," SIAM JOURNAL, Number 8, 1960, Pages 181-217.

4. J. B. Rosen, "The Gradient Projection Method for Nonlinear Programming: Part II-Nonlinear Constraints," SIAM JOURNAL, Number 4, 1961, Pages 514-535.

5. A. V. Fiacco and G. P. McCormick, SEQUENTIAL UNCONSTRAINED MINIMIZATION TECHNIQUES FOR NONLINEAR PROGRAMMING, John Wiley and Sons, New York, 1968.

6. R. Fletcher and M. J. D. Powell, "A Rapidly Convergent Descent Method for Minimization," BRITISH COMPUTER JOURNAL, Number 6, 1963, Pages 163-168.

7. A. M. Geoffreon, "Elements of Large-Scale Mathematical Programming Part I: Concepts," MANAGEMENT SCIENCE, Volume 16, Number 11, July, 1970.

8. G. Zoutendijk, METHOD OF FEASIBLE DIRECTIONS, Elsevier Publishing Company, Amsterdam, 1960.

9. R. Ferguson, L. Smith, and F. Orlow, "MINMAX - A Generalized Nonlinear Iterator," Technical Note 7002 (M-67), U. S. Naval Ordinance Laboratory, Silver Springs, Maryland, October, 1965.

12. Tracking Error Analysis

12.1 Introduction

This chapter will be devoted to the description and definition of the linear error analysis tracking model, the mathematical formulation of the required equations relating to the model and the specific algoithms used in the error analysis of the orbit determination process. The real-time orbit determination process is performed by the GTDS, so the GMAS formulations will be addressed primarily towards the pre-flight phase. For consistency and compatibility, the same filter models as used in the GTDS will be included in the GMAS. Other filters such as sequential weighted least squares and Kalman-Schmidt are also included. Features that are very attractive for pre-flight analysis such as the error budget map and generalized covariance analysis will be discussed in Chapter 14.

The measurement models and error sources are given. The GMAS will model range, range-rate, altimeter, right ascension, declination, direction cosine, gimbal angle, azimuth, elevation, and satellite to satellite-range and range-rate. The measurement errors will include biases, timing errors, tracking station location errors, and atmospheric and ionospheric error effects.

12.2   Estimation Processing

12.2.1 Weighted Least Squares Estimation

The weighted least squares estimator assumes that vector observations of the form

$$\bar{y} = \bar{f}(\bar{x}) + \bar{n} \qquad\qquad (12.2\text{-}1)$$

are processed. For a set of m observations the observed m-dimensional vector $\bar{y}$ is equal to the known (i.e. postulated) vector function $\bar{f}$ of a set of p parameters denoted by the p-dimensional vector $\bar{x}$ plus random noise denoted by the vector $\bar{n}$. The trajectory determination problem is to estimate $\bar{x}$ given the functional form of $\bar{f}$, the statistics of $\bar{n}$ and the measurements $\bar{y}$. Since the functional form of $\bar{f}$ is in general non-linear, the solution must be found iteratively using linear theory. From linear theory, the solution of equation (12.2-1) is given by

$$\hat{x} = \bar{x}_o + (F^T W F)^{-1} F^T W \Delta\bar{y} \qquad\qquad (12.2\text{-}2)$$

where $\hat{x}$ is the estimate of $\bar{x}$, $\bar{x}_o$ is the _a priori_ value of $\bar{x}$. F is the observation matrix given by

$$F = \left(\frac{\partial \bar{f}}{\partial \bar{x}}\right)_{(\bar{x}=\bar{x}_o)} \quad \left\{ \begin{array}{l} \text{the m x p matrix of partial} \\ \text{derivatives of } f_{(\bar{x})} \text{ with respect} \\ \text{to } \bar{x} \text{ evaluated at } \bar{x} = \bar{x}_o \end{array} \right\} \qquad (12.2\text{-}3)$$

and W is the weighting time matrix. The quantity $\Delta\bar{y}$ is given by $\Delta\bar{y} = \bar{y} - \bar{f}(\bar{x}_o)$

As a result of the linearization of $\bar{f}$, the correction term on the right hand side of equation (12.2-2) must be small to not violate linearity. If such is not the case, then the process is repeated iteratively in standard Newton-Raphson fashion, each time using the last estimate $\hat{x}$ for the evaluation of F and $\Delta\bar{y}$.

The covariance of the estimate $\hat{x}$ is given by $P_{\Delta x}$, the inverse of the p x p normal matrix $(F^T W F)$ after the estimation process has converged and when the following statistical assumptions of the measurement process are satisfied:

(a) The observation noise is unbiased, i.e., $\mathcal{E}\{\bar{n}\} = 0$.

(b) The errors in the observation vector components are uncorrelated and the covariance of the observation noise vector is known and its inverse is the weighting matrix W. Let σ_1^2 be the variance of the measurement noise component n_1, which corresponds to measurement y_1; σ_2^2 the variance of component n_2, which corresponds to y_2; and so on.

The weighting matrix is

$$
W = \begin{bmatrix} \sigma_1^{-2} & & & \\ & \sigma_2^{-2} & & 0 \\ & & \ddots & \\ 0 & & & \sigma_m^{-2} \end{bmatrix}
\qquad\qquad (12.2\text{-}4)
$$

Equating the inverse of W to the covariance matrix of measurement errors implies that multicomponent observations at a given time (e.g., range, azimuth, elevation) are not spatially correlated and that measurements at different times are not time-correlated.

(c) The mathematical models of the trajectory and observations characterize exactly the physics governing the observation process. All parameters such as biases, tracking station locations and physical constants that are not being estimated are known exactly.

The above criteria can never be met precisely in real spacecraft applications. As a result, the covariance matrix, $(F^TWF)^{-1}$, must be realistically interpreted with regard to the specific application.

For many applications not all of the parameters affecting $\bar{f}$ should be solved-for. In this case the initial assumption that the measurement vector $\bar{y}$, can be related to the state and model parameters is given as

$$
\bar{y} = \bar{f}(\bar{x}, \bar{z}) + \bar{n} \qquad\qquad (12.2\text{-}5)
$$

where two classes of variables are included. The p-dimensional vector $\bar{x}$, designated <u>solve-for vector</u>, contains as components the state and model parameters whose values are known with limited certainty and are to be estimated. The q-dimensional vector, $\bar{z}$, designated <u>consider vector</u>, contains as components all model parameters whose values are known with limited certainty but are not to be estimated. Nevertheless, the uncertainty of $\bar{z}$ is to be considered. A priori values of $\bar{x}$ and $\bar{z}$ are specified to be $\bar{x}_o$ and $\bar{z}_o$ with respective covariance matrices $P_{\Delta x_o}$ and $P_{\Delta z_o}$.

The linearized solution to equation (12.2-5) is exactly the same as for equation (12-1) and is given by equation (12.2-2), that is, the estimate $\hat{x}$ does not depend upon the consider parameters. The more general form of equation (12.2-2) which includes the effect of the <u>a priori</u> estimate $\bar{x}_o$ and its covariance $P_{\Delta x_o}$ is given by

$$\hat{x} = \bar{x}_o + (F^T WF + P_{\Delta x_o}^{-1})^{-1} [F^T W \Delta \bar{y} + P_{\Delta x_o}^{-1} (\bar{x}_o - \hat{x})] \qquad (12.2\text{-}6)$$

The quantity $(\bar{x}_o - \hat{x})$ is non-zero only on the second and subsequent iterations of an iterative solution since $\hat{x}$ is determined by the previous estimate.

The covariance of $\hat{x}$ in the presence of consider parameters is given by

$$P_{\Delta x} = \psi \{ F^T WE P_{\Delta z_o} E^T WF + \psi^{-1}$$
$$+ F^T WEC_{\Delta x_o \Delta z}^T P_{\Delta x_o}^{-1} + P_{\Delta x_o}^{-1} C_{\Delta x_o \Delta z} E^T WF \} \psi^T \qquad (12.2\text{-}7)$$

where the following definitions have been made

$$P_{\Delta z_o} = \mathcal{E} \{ (\bar{z} - \bar{z}_o)(z - \bar{z}_o)^T \} \qquad (12.2\text{-}8)$$

$$C_{\Delta x_o \Delta z} = \mathcal{E} \{ (\bar{x} - \bar{x}_o)(\bar{z} - \bar{z}_o)^T \} \qquad (12.2\text{-}9)$$

$$\psi = (F^T WF + P_{\Delta x_o}^{-1})^{-1} \qquad (12.2\text{-}10)$$

and E is the mxq observation matrix for the consider parameters given by

$$E = \left(\frac{\partial \bar{f}}{\partial \bar{z}} \right)_{(\bar{z} = \bar{z}_o)} \qquad (12.2\text{-}11)$$

It is assumed that no correlation between the measurement noise and the error in the solve-for or consider variables exists. Even if the initial correlation matrix $C_{\Delta x_o \Delta z}$ is zero, a correlation between errors in the solve-for and consider variables will result from the measurement processing. This correlation $C_{\Delta x \Delta z}$ is given by

$$C_{\Delta x \Delta z} = \psi [P_{\Delta x_o}^{-1} C_{\Delta x_o \Delta z} + F^T WE P_{\Delta z_o}] \qquad (12.2\text{-}12)$$

It is seen from equations (12.2-6), (12.2-7) and (12.2-12) that only the estimator requires measurement data. The equations for the covariance and correlation matrices require only the statistics, W, of the observations which are usually known for specific classes of trackers and sensors. Therefore, if one assumes that the a priori reference trajectory, $\bar{x}_o$, is the best estimate, the estimator equation can be omitted and the covariance and correlation matrix can be determined for specific mission sensors and observation profiles. It must also be assumed that the mathematical models in the program accurately characterize the physical situation.

For preflight analysis using GMAS studies can be performed to determine:

o the effect of measurement data errors (random and systematic), measurement time spans, and sampling rates on the accuracy of the estimated state and model parameters

o the effect of the trajectory dynamics and the trajectory/sensor relative geometry on the accuracy of the estimated state and model parameters

o the relative effects of different types of measurements on the accuracy of the estimated state and model parameters.

These kinds of error analysis studies are solely concerned with the influence that errors in problem variables have on the accuracy of the estimate. This type of analysis can strongly influence the design and enhancement of spacecraft missions as well as establish requirements for observation sensor accuracies, sampling rates, tracking times, and sensor locations.

The method of evaluating equations (12.2-7) and (12.2-12) are very similar to the corresponding calculations associated with the reduction of real data in GTDS (Reference 12.1). An a priori estimate of the solve-for and consider variables, $\bar{x}_0$ and $\bar{z}_0$, respectively, along with their covariance matrices, $P_{\Delta x_0}$ and $P_{\Delta z_0}$, is specified. The measurement schedule and measurement uncertainty, W, is also specified a priori. The program then proceeds to integrate the nonlinear differential equations of motion and their corresponding variational equations to the measurement times and compute the measurement partials. The rows of the matrices F and E in equations (12.2-7) and (12.2-12) are accumulated as the measurement statistics are processed. Ultimately the covariance and correlation matrices $P_{\Delta x}$ and $C_{\Delta x \Delta z}$ are calculated at the epoch time. The covariance and correlation matrices may then be propagated to specified times T_1, T_2,. . . T_s as described in Section 14.2.3. Since the estimation equation is not being solved, iterating is unnecessary.

It would appear that since an estimate is not actually being determined, it should make little difference whether model parameters are associated with the solve-for vector, $\bar{x}$, or the consider vector, $\bar{z}$. A subtle difference does exist. Components of the consider vector, $\bar{z}$, are maintained at their a priori specified values throughout the processing, and therefore have no possibility for improvement through estimation. As a result, their covariances are never improved compared to that initially specified, i.e., $P_{\Delta z_0}$. The solve-for variables, $\bar{x}$, have their values continually improved through the estimation process, and this is reflected through the usually reduced variance elements in $P_{\Delta x}$. Because of the coupling, the uncertainty of the state components is affected differently if the same model parameter is associated with $\bar{x}$ than if it is associated with $\bar{z}$.

For compatibility calculations in GMAS and GTDS should be performed as nearly identically as possible. This will allow error analysis studies performed with GMAS to be realistic in their prediction of the types of uncertainties to be expected on a given mission.

12.2.2 Partitioning of the Augmented State Covariances

It has been found (Reference 12.2) that for error analysis applications, considerable savings both in the number of computations and core storage requirements can be achieved by partitioning the matrices and vectors involved in equations(12.2-7)and(12.2-12). This is due to the fact that many studies will involve the error analysis of several arcs of data which may have different state parameters associated with them as well as other solve-for and/or consider parameters which may be associated with one or all arcs.

The solve-for parameters are partitioned as

$$\bar{x} = \begin{bmatrix} \bar{a} \\ \bar{b} \\ \bar{c} \end{bmatrix} = \begin{bmatrix} \bar{a}_1 \\ \vdots \\ \bar{a}_n \\ \bar{b}_1 \\ \vdots \\ \bar{b}_n \\ \bar{c} \end{bmatrix} \tag{12.2-13}$$

where $\bar{a}_i$ contains the ith arc orbital elements or epoch state, $\bar{b}_i$ contains all of the other ith arc solve-for parameters, and $\bar{c}$ contains the solve-for parameters common to all arcs. Similarly the consider parameters are partitioned as

$$\bar{z} = \begin{bmatrix} \bar{d} \\ \bar{e} \end{bmatrix} = \begin{bmatrix} \bar{d}_1 \\ \vdots \\ \bar{d}_n \\ \bar{e} \end{bmatrix} \tag{12.2-14}$$

where $\bar{d}_i$ contains the consider parameters associated with the ith arc and $\bar{e}$ contains the consider parameters common to all arcs.

The observation matrices F and E are partitioned similarly with the resulting normal matrix being partitioned as

$$(F^T W F) = \begin{bmatrix} F_a{}^T W \ F_a & | & F_a{}^T W \ F_b & | & F_a{}^T W \ F_c \\ --- & + & --- & + & --- \\ F_b{}^T W \ F_a & | & F_b{}^T W \ F_b & | & F_b{}^T W \ F_c \\ --- & + & --- & + & --- \\ F_c{}^T W \ F_a & | & F_c{}^T W \ F_b & | & F_c{}^T W \ F_c \end{bmatrix} \qquad (12.2\text{-}15)$$

where

$$F = [F_a \quad F_b \quad F_c] \qquad (12.2\text{-}16)$$

and

$$E = [E_d \quad E_e] \qquad (12.2\text{-}17)$$

The other matrix expressions in equations(12.2-7)and(12.2-12)are partitioned similar to equation (12.2-15).

12.2.3 Sequential Weighted Least Squares

By treating the m components (or sub-groupings of them) of the m-dimensional observation vector $\bar{y}$ described by equation(12.2-1)sequentially, an alternative formulation of the weighted least squares may be obtained. The first measurement or group of measurements is processed in exactly the way described in Section 12.2.1, then that result is used as the a priori for the second measurement or group of measurements and this process is continued through the entire sequence. This process is recursive in nature and the recursion relation for the estimation equation is given by

$$\hat{x}_{N+1} = \hat{x}_N + P_{N+1} \ F_{N+1}^T \ W_{N+1} \ \Delta \bar{y}_{N+1} \qquad (12.2\text{-}18)$$

where the subscripts N and N+1 refer to the measurement being processed. Thus if individual measurements are being processed (the generalization to groups of measurements is straightforward) then F_{N+1} is the (N+1)th row of F and W_{N+1} is the (N+1)th diagonal element of W which is the inverse of the noise variance for the (N+1)th measurement. The covariance of the estimate after (N+1) measurements, P_{N+1}, is determined from

$$P_{N+1}^{-1} = F_{N+1}^T \ W_{N+1} \ F_{N+1} + P_N^{-1} \qquad (12.2\text{-}19)$$

The recursive procedure defined by equations(12.2-18)and(12.2-19)is initialized with the a priori values

$$\hat{x}_o = \bar{x}_o \qquad (12.2\text{-}20)$$

$$P_o = P_{\Delta x_o} \qquad (12.2\text{-}21)$$

To this point there is no real advantage to the sequential formulation either for the estimation problem or for error analysis, in fact each step of the sequential processing would involve the inversion of the matrix P_N which is of the same dimension as the solve-for parameter vector, $\bar{x}$. It is thus necessary to manipulate equation (12.2-19) to produce a recursive procedure that involves no matrix inversions (at least for scalar measurements, an n-dimensional measurement will involve inversion of an nxn matrix). The result is derived in reference 12.1 and is given by

$$P_{N+1} = P_N [I - \beta_{N+1}^T (\beta_{N+1} P_N \beta_{N+1}^T + I)^{-1} \beta_{N+1} P_N] \qquad (12.2-22)$$

where the matrix β is defined by

$$\beta_{N+1}^T = F_{N+1}^T W^{\frac{1}{2}} \qquad (12.2-23)$$

since W is positive definite the matrix $W^{\frac{1}{2}}$ is well defined. The matrix to be inverted in equation (12.2-22) is of the same dimension as the measurement, so that for scalar measurements no matrix inversion is involved. For this latter case equation (12.2-22) reduces to

$$P_{N+1} = P_N [I - F_{N+1}^T (F_{N+1} P_N F_{N+1}^T + q_{N+1})^{-1} F_{N+1} P_N] \qquad (12.2-24)$$

where q_{N+1} is the variance of the noise on the (N+1)th scalar measurement.

It should be noted that for the application of error analysis the sequential processing of a series of measurements using equation (12.2-24) will give exactly the same result (within numerical round-off errors) as processing those measurements using the batch process equation. This is due to the fact that the a priori state $\bar{x}_o$ is used as the best estimate for the calculation of the observation matrices in both processes. For estimation applications it should be noted that in sequential processing, as each measurement is made the updated state estimate $\hat{x}_N$ is used in the calculation of the observation matrix F_{N+1}. In general then, several iterations through all of the measurements may be necessary to obtain a converged solution when using sequential processing as well as for batch processing. If a unique solution exists and if both sequential and batch processing of the measurements converge, then they both will converge to the same solution, although not necessarily in the same way.

For analyses involving the inclusion of consider parameters, the batch processing equations are given in equations (12.2-6) and (12.2-7). To use sequential processing which is equivalent to the batch processing, it must be noted that a characteristic of batch weighted least squares is that the estimation equation (12.2-6) depends only on the solve-for parameters and hence only the

covariance equation(12.2-7)is affected by the consider parameters. The sequential processing equations(12.2-18)and(12.2-24)must be modified to account for this behavior in the following way. The covariance P_{N+1} in equation (12.2-18) must be replaced by P'_{N+1} which is the covariance which would be obtained at that measurement, from processing the same set of measurements in the <u>absence</u> of consider parameters. The equations for the covariance P_{N+1} and the correlation matrix $C_{\Delta x \Delta z_{N+1}}$ must also be modified. The equations are given by

$$\hat{x}_{N+1} = \hat{x}_N + P'_{N+1} F_{N+1} q_{N+1}^{-1} \Delta \bar{y}_{N+1} \qquad (12.2\text{-}25)$$

$$P_{N+1} = P_N - K_{N+1} A_{N+1}^T - A_{N+1} K_{N+1}^T + K_{N+1} J_{N+1} K_{N+1}^T \qquad (12.2\text{-}26)$$

$$C_{\Delta x \Delta z_{N+1}} = C_{\Delta x \Delta z_N} - K_{N+1} B^T$$

where the weighted least squares gain matrix K_{N+1} is given by

$$K_{N+1} = P'_{N+1} F_{N+1} q_{N+1}^{-1} \qquad (12.2\text{-}27)$$

The form of equation(12.2-26)applies for any arbitrarily defined gain matrix. The quantities A_{N+1}, B_{N+1}, J_{N+1} are given by

$$A_{N+1} = P_N F_{N+1}^T + C_{\Delta x \Delta z_N} E_{N+1}^T \qquad (12.2\text{-}28)$$

$$B_{N+1} = C_{\Delta x \Delta z_N}^T F_{N+1}^T + P_{\Delta z_o} E_{N+1}^T \qquad (12.2\text{-}29)$$

$$J_{N+1} = F_{N+1} A_{N+1} + E_{N+1} B_{N+1} + q_{N+1} \qquad (12.2\text{-}30)$$

12.2.4 Kalman-Schmidt Estimation

The estimation theory described in this section (Reference 12.3) is similar in many ways to the sequential weighted least squares theory described in the previous section. There are two basic differences between the methods—one major and one minor. The minor difference is simply that rather than relating an observation to an epoch state by the observation matrix F, the observation is related to the state at the observation time by the observation matrix H. For linear analysis this will make no difference. For a general non-linear problem, again the convergence may be different, but assuming convergence and a unique solution the final result will be the same. The covariance associated with the solve-for parameters will also be the same, given the proviso that it is related to the epoch state or elements through the proper state transition matrix. Thus for linear error analysis, this difference of processing at each time point is unimportant.

The major difference between the two methods involves the treatment of consider parameters. In weighted least squares estimation, the consider parameters have no effect upon the estimator equation, which was implicit in the batch formulation (equation 12.2-6) and was explicit in the sequential formulation (equation 12.2-25) since a gain involving P'_{N+1}, the covariance without consider parameters, had to be introduced. In Kalman-Schmidt estimation theory the consider parameters do affect the estimation as well as the covariance. Simply put, the estimation and covariance equations are derived as though the consider parameters were solve-for parameters also. Thus the gain matrix applied to the solve-for parameters, depends upon the consider parameters exactly as though it were the partition of an augmented solve-for vector which included the consider parameters. Then at the measurement, the consider parameters are simply not modified nor is the covariance associated with them reduced by the measurement.

The general effect of this method is that for estimation, the final result is in general different from that of weighted least squares. The estimate of the solve-for state is more heavily influenced by the later measurements in the time sequence (over and above the inherent noise associated with each measurement), than by the earlier measurements. The rationale behind this is similar to that for using consider parameters in the first place. Namely that no matter how carefully a dynamic system is modeled, in the real world there are influences which are either not modeled at all or are improperly modeled. Thus it makes sense in estimating a state and its uncertainty at a certain time, to give greater weight to the measurements nearer to it in time than to those farther away.

For the application of error analysis the covariances generated by the Kalman-Schmidt consider filter generally lie somewhere between those derived from weighted least squares without consider parameters and weighted least squares with the consider parameters. The estimator and covariance equations for the Kalman-Schmidt consider filter, using notation similar to that of the previous section, are given in Reference 12.3 as

$$\hat{x}_{N+1} = \hat{x}_N + K_{N+1} \, \Delta \bar{y} \tag{12.2-31}$$

$$P_{N+1} = P_N - K_{N+1} \, A^T_{N+1} \tag{12.2-32}$$

$$C_{\Delta x \Delta z_{N+1}} = C_{\Delta x \Delta z_N} - K_{N+1} \, B^T_{N+1} \tag{12.2-33}$$

where the Kalman gain matrix K_{N+1} is defined by

$$K_{N+1} = A_{N+1} \left(H_{N+1} A_{N+1} + G_{N+1} B_{N+1} + q_{N+1} \right)^{-1} \tag{12.2-34}$$

and where the auxiliary matrices A and B are defined by

$$A_{N+1} = P_N H_{N+1}^T + C_{\Delta x \Delta z_N} G^T \qquad (12.2\text{-}35)$$

$$B_{N+1} = C_{\Delta x \Delta z_N}^T H_{N+1}^T + P_{\Delta z_o} G^T \qquad (12.2\text{-}36)$$

The observation matrices relating the observation to the current solve-for state parameters and consider parameters are H and G, respectively. The general form of the update equation for the covariance P_{N+1} given in equation (12.2-26) reduces to equation (12.2-32) when the gain matrix is defined by equation (12.2-34.

Range Rate.

The range rate derivative deserves special attention. Remembering that

$$\dot{\bar{\rho}} = \dot{\bar{r}} ,$$
(12.3-10)

We write

$$\dot{\rho} = \hat{u} \cdot \dot{\bar{\rho}}$$
(12.3-11)

Thus

$$\ddot{\rho} = \dot{\hat{u}} \cdot \dot{\bar{\rho}} + \hat{u} \cdot \ddot{\bar{\rho}}$$
(12.3-12)

Because

$$\dot{\bar{\rho}} = \frac{d}{dt} (\rho \hat{u}) = \rho \dot{\hat{u}} + \dot{\rho} \hat{u}$$
(12.3-13)

we may substitute in equation (12.3-12) above for $\dot{\hat{u}}$, giving

$$\ddot{\rho} = \frac{1}{\rho} (\dot{\bar{\rho}} \cdot \dot{\bar{\rho}} - \dot{\rho} \hat{u} \cdot \dot{\bar{\rho}}) + \hat{u} \cdot \ddot{\bar{\rho}}$$
(12.3-14)

12.3 MEASUREMENT MODELS

The observation matrices referred to in the previous section require that the various types of measurements be mathematically defined and that the partial derivatives of these measurements with respect to both solve-for and consider parameters be computed. The equations for the following basic types of observations will be taken directly from Reference 12.2

- o range and range rate

- o altimeter height

- o right ascension and declination

- o direction cosines

- o X and Y gimbal angles

- o azimuth and elevation

- o satellite satellite-range and range-rate

These measurements are geometric in nature. The computed values for the observations are obtained by applying geometric relationships to the computed values for the relative positions and velocities of the satellite and the observer at the desired time.

12.3.1   Range and Range Rate

Range:

Consider the station-satellite vector:

(12.3-1)

$$\bar{\rho} = \bar{r} - \bar{r}_{ob} \qquad /(12\text{-}37)$$

where

$\bar{r}$ is the satellite position vector (x,y,z) in the geocentric Earth-fixed system, and

$\bar{r}_{ob}$ is the station vector in the same system.

The magnitude of this vector, ρ, is the (slant) range, which is one of the measurements.

Range rate:

The time rate of change of this vector $\bar{\rho}$ is

$$\dot{\bar{\rho}} = \dot{\bar{r}} \qquad (12.3-2)$$

as the velocity of the observer in the Earth-fixed system is zero. Let us consider that

$$\bar{\rho} = \rho\hat{u} \qquad (12.3-3)$$

where

$\hat{u}$ is the unit vector in the direction of $\bar{\rho}$. Thus we have

$$\dot{\bar{\rho}} = \dot{\rho}\hat{u} + \rho\dot{\hat{u}} \qquad (12.3-4)$$

The quantity $\dot{\rho}$ in the above equation is the computed value for the range rate and is determined by

$$\dot{\rho} = \hat{u} \cdot \dot{\bar{r}} \qquad (12.3-5)$$

The partial derivatives of range and range rate with respect to the satellite position and velocity are given below. All are in the geocentric, Earth-fixed system. (The r_i refer to the Earth-fixed components of $\bar{r}$.)

Range:

$$\frac{\partial \rho}{\partial r_i} = \frac{\rho_i}{\rho} \qquad (12.3\text{-}6)$$

Range rate:

$$\frac{\partial \dot{\rho}}{\partial r_i} = \frac{1}{\rho} \left[\dot{r}_i - \frac{\dot{\rho}\rho_i}{\rho} \right] \qquad (12.3\text{-}7)$$

$$\frac{\partial \dot{\rho}}{\partial \dot{r}_i} = \frac{\rho_i}{\rho} \qquad (12.3\text{-}8)$$

The derivatives of range and range rate with respect to time are presented below. All are in the Earth-fixed system.

Range:

$$\dot{\rho} = \hat{u} \cdot \dot{\bar{r}} \qquad (12.3\text{-}9)$$

12.3-3

or, as

$$\dot{\rho} = \hat{u} \cdot \dot{\bar{\rho}} \qquad (12.3-15)$$

we may write

$$\ddot{\rho} = \frac{1}{\rho} (\dot{\bar{\rho}} \cdot \dot{\bar{\rho}} - \dot{\rho}^2 + \bar{\rho} \cdot \ddot{\bar{\rho}}) \qquad (12.3-16)$$

The gradient of the potential U with respect to the Earth-fixed position coordinates of the satellite is the part of $\ddot{\bar{\rho}}$ due to the geopotential:

$$\frac{\partial U}{\partial r_i} = -\frac{GM}{r^3} \left[1 - \frac{3 a_e^2 C_{20}}{2 r^2} \left(5 \sin^2 \phi - 1 - 2 \frac{z}{r_i} \right) \right] r_i \qquad (12.3-17)$$

We must add to this the effect of the rotation of the coordinate system. (The Earth-fixed coordinate system rotates with respect to the true of date coordinates with a rate $\dot{\theta}_g$, the time rate of change of the Greenwich hour angle.) The components of $\ddot{\bar{\rho}}$ are then

$$\ddot{\rho}_1 = \frac{\partial U}{\partial r_1} + [\dot{x} \cos \theta_g + \dot{y} \sin \theta_g] \dot{\theta}_g + \dot{r}_2 \dot{\theta}_g \qquad (12.3-18)$$

$$\ddot{\rho}_2 = \frac{\partial U}{\partial r_2} + [-\dot{x} \sin \theta_g + \dot{y} \cos \theta_g] \dot{\theta}_g - \dot{r}_1 \dot{\theta}_g \qquad (12.3-19)$$

$$\ddot{\rho}_3 = \frac{\partial U}{\partial r_3} = \frac{\partial U}{\partial z} \qquad (12.3-20)$$

where $\dot{x}$ and $\dot{y}$ are the true of date satellite velocity components.

12.3.2 Altimeter Height

The altimeter height is unique in that the satellite is making the observation. While this is actually a measurement from the satellite to the surface of the Earth, it is taken to be a measurement of the spheroid height and the time rate of change of that quantity for obvious reasons. Using the formula for spheroid height

$$H_{alt} = r - a_e - \frac{3}{2} a_e f^2 \left(\frac{z}{r}\right)^4$$

$$+ \left(a_e f + \frac{3}{2} a_e f^2\right) \left(\frac{z}{r}\right)^2$$

(12.3-21)

where

a_e is the Earth's mean equatorial radius,

f is the Earth's flattening, and

z is r_3, the z component of the Earth-fixed satellite vector.

For error analysis purposes, the partial derivatives of the altimeter measurement with respect to the satellite position, velocity, and time are needed. These are derived directly from the analytical expression for H_{ALT}.

$$\frac{\partial H_{alt}}{\partial r_i} = \frac{r_i}{r} + \frac{1}{r}\left[\left(2\,a_e\,f + 3\,a_e\,f^2\right)\left(\frac{z}{r}\right)\right.$$

(12.3-22)

$$\left. - 6\,a_e\,f^2\left(\frac{z}{r}\right)^3\right] \chi \left[\frac{\partial z}{\partial r_i} - \frac{z x_i}{r^2}\right]$$

The time derivative of altimeter range is given by

$$\dot{H}_{ALT} = \frac{\partial H_{ALT}}{\partial r_1}\dot{r}_1 + \frac{\partial H_{ALT}}{\partial r_2}\dot{r}_2 + \frac{\partial H_{ALT}}{\partial r_3}\dot{r}_3 \qquad (12.3-23)$$

The altimeter measurement is actually made to the geoid surface instead of the spheroid surface. A detailed geoid is necessary, however, to model the altimeter measurements to properly exploit their full accuracy.

12.3.3 Right Ascension and Declination

The topocentric right ascension α and declination δ are inertial coordinate system measurements as illustrated in Figure 12.1. These angles are computed from the components of the Earth-fixed station-satellite vector and the Greenwich hour angle θ_g.

$$\alpha = \tan^{-1}\left(\frac{\rho_2}{\rho_1}\right) + \theta_g \qquad (12.3-24)$$

$$\delta = \sin^{-1}\left(\frac{\rho_3}{\rho}\right) \qquad (12.3-25)$$

12.3-7
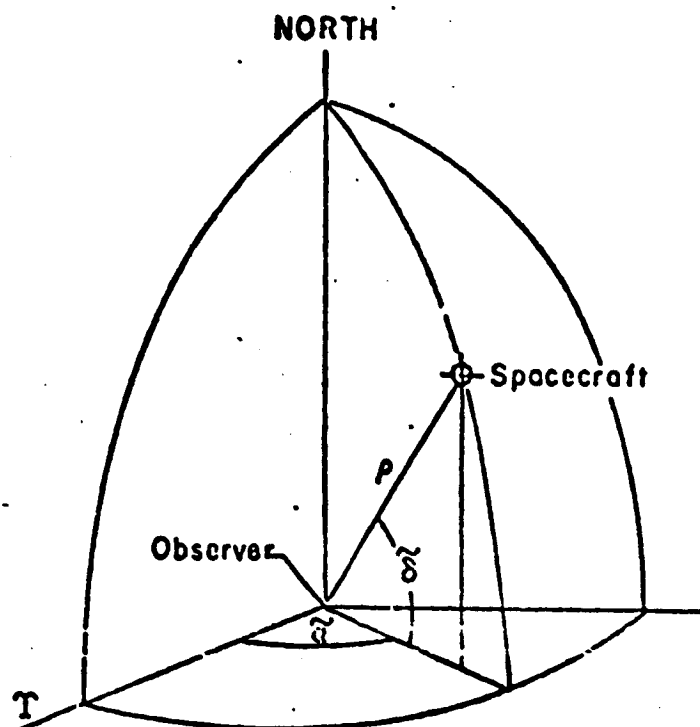
Figure 12.3-1. Topocentric right ascension & declination angles

The partial derivatives of these measurements with respect to the Earth-fixed satellite position vector $\vec{r}$ are given by

Right Ascension:

$$\frac{\partial \alpha}{\partial r_1} = \frac{-\rho_2}{\sqrt{\rho_1^2 + \rho_2^2}} \qquad (12.3\text{-}26)$$

$$\frac{\partial \alpha}{\partial r_2} = \frac{\rho_1}{\sqrt{\rho_1^2 + \rho_2^2}} \qquad (12.3\text{-}27)$$

$$\frac{\partial \alpha}{\partial r_3} = 0 \qquad (12.3\text{-}28)$$

Declination:

$$\frac{\partial \delta}{\partial r_1} = \frac{-\rho_1 \rho_3}{\rho^2 \sqrt{\rho_1^2 + \rho_2^2}}$$

(12.3-29)

$$\frac{\partial \delta}{\partial r_2} = \frac{-\rho_2 \rho_3}{\rho \sqrt{\rho_1^2 + \rho_2^2}}$$

(12.3-30)

$$\frac{\partial \delta}{\partial r_3} = \frac{\sqrt{\rho_1^2 + \rho_2^2}}{\rho^2}$$

(12.3-31)

The time derivatives are given by

Right ascension: $\dot{\alpha} = \dfrac{u_1 \dot{r}_2 - u_2 \dot{r}_1}{\rho (1 - u_3^2)}$ (12.3-32)

Declination: $\dot{\delta} = \dfrac{\dot{r}_3 - \dot{\rho} u_3}{\rho \sqrt{1 - u_3^2}}$ (12.3-33)

where the unit vector $\hat{u}$ is defined as

$$\hat{u} = \frac{\bar{\rho}}{|\bar{\rho}|}$$

(12.3-34)

12.3.4 Direction Cosines

There are three direction cosines associated with the station-satellite vector in the topocentric system. Description of these measurements requires the $\hat{N}$, $\hat{Z}$, and $\hat{E}$ (north, zenith and east baseline unit vectors which describe the tropocentric system along with the $\hat{u}$). The direction cosines are computed as:

$$\ell = \hat{u} \cdot \hat{E} \tag{12.3-35}$$

$$m = \hat{u} \cdot \hat{N} \tag{12.3-36}$$

$$n = \hat{u} \cdot \hat{Z} \tag{12.3-37}$$

The partial derivatives of the direction cosines with respect to the satellite position vector are given by

$$\frac{\partial \ell}{\partial r_i} = \frac{1}{\rho} \left[E_i - \ell u_i \right] \tag{12.3-38}$$

$$\frac{\partial m}{\partial r_i} = \frac{1}{\rho} \left[N_i - m u_i \right] \tag{12.3-39}$$

$$\frac{\partial n}{\partial r_i} = \frac{1}{\rho} \left[Z_i - n u_i \right] \tag{12.3-40}$$

where

$$E_i = \text{component of } \hat{E} \text{ in the } r_i \text{ direction} \qquad (12.3\text{-}41)$$

$$N_i = \text{component of } \hat{N} \text{ in the } r_i \text{ direction} \qquad (12.3\text{-}42)$$

$$Z_i = \text{component of } \hat{Z} \text{ in the } r_i \text{ direction} \qquad (12.3\text{-}43)$$

The time derivatives of the ℓ and m direction cosines are given by

$$\dot{\ell} = \frac{\dot{\bar{\rho}} \cdot \hat{E} - \ell \dot{\rho}}{\rho} \qquad (12.3\text{-}44)$$

$$\dot{m} = \frac{\dot{\bar{\rho}} \cdot \hat{N} - m \dot{\rho}}{\rho} \qquad (12.3\text{-}45)$$

12.3.5 <u>x and y Angles</u>

The x and y angles, as illustrated in Figure 12.2, are computed in a tropocentric coordinate system as

$$X_a = \tan^{-1} \left(\frac{\ell}{n} \right) \qquad (12.3\text{-}46)$$

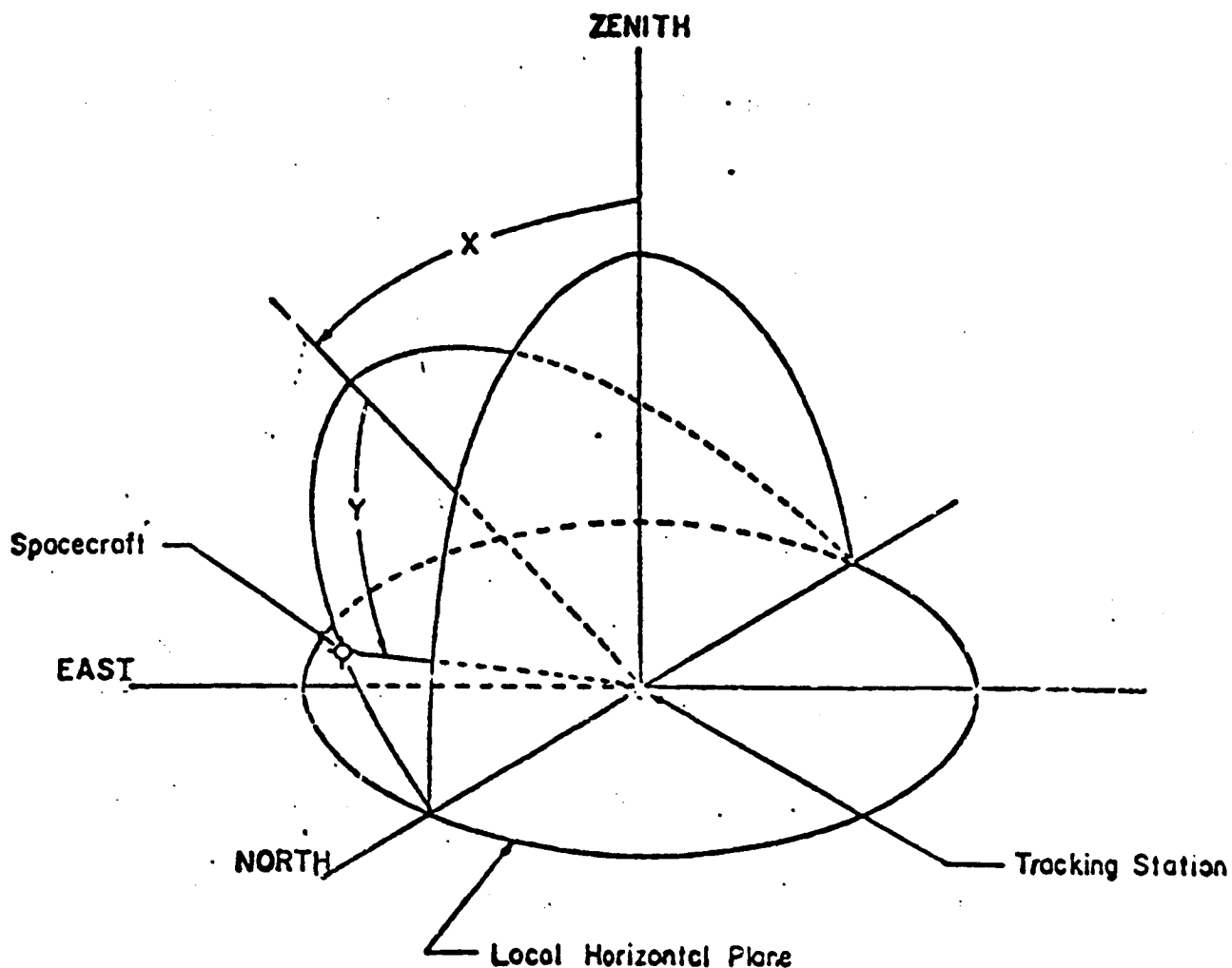$$Y_a = \sin^{-1} (m) \qquad (12.3\text{-}47)$$

Figure 12.3-2. X and Y Angles

The derivatives of the x and y angles with respect to the satellite position vector are

$$\frac{\partial X_a}{\partial r_i} = \frac{n E_i - \ell Z_i}{\rho(1-m^2)}$$

(12.3-48)

$$\frac{\partial Y_a}{\partial r_i} = \frac{N_i - m u_i}{\rho \sqrt{1-m^2}}$$

(12.3-49)

and the time derivatives are given by

$$\dot{X}_a = \frac{\dot{\bar{\rho}} \cdot (n\,\hat{E} - \ell\hat{Z})}{\rho\,(1-m^2)} \qquad (12.3-50)$$

$$\dot{Y}_a = \frac{\dot{\bar{\rho}} \cdot \hat{N} - m\dot{\rho}}{\rho\,\sqrt{1-m^2}} \qquad (12.3-51)$$

12.3.6 Azimuth and Elevation

Figure 12.3-3 illustrates the measurement of azimuth and elevation. These angles are computed in the topo-centric coordinate system as

$$A_z = \tan^{-1}\frac{\ell}{m} \qquad (12.3-52)$$

$$E_\ell = \sin^{-1}(n) \qquad (12.3-53)$$

The partial derivatives with respect to the satellite position vector are given by

$$\frac{\partial A_z}{\partial r_i} = \frac{mE_i - \ell N_i}{\rho\sqrt{1-n^2}} \qquad (12.3-54)$$

$$\frac{\partial E_\ell}{\partial r_i} = \frac{Z_i - nu_i}{\rho(1-n^2)} \qquad (12.3-55)$$
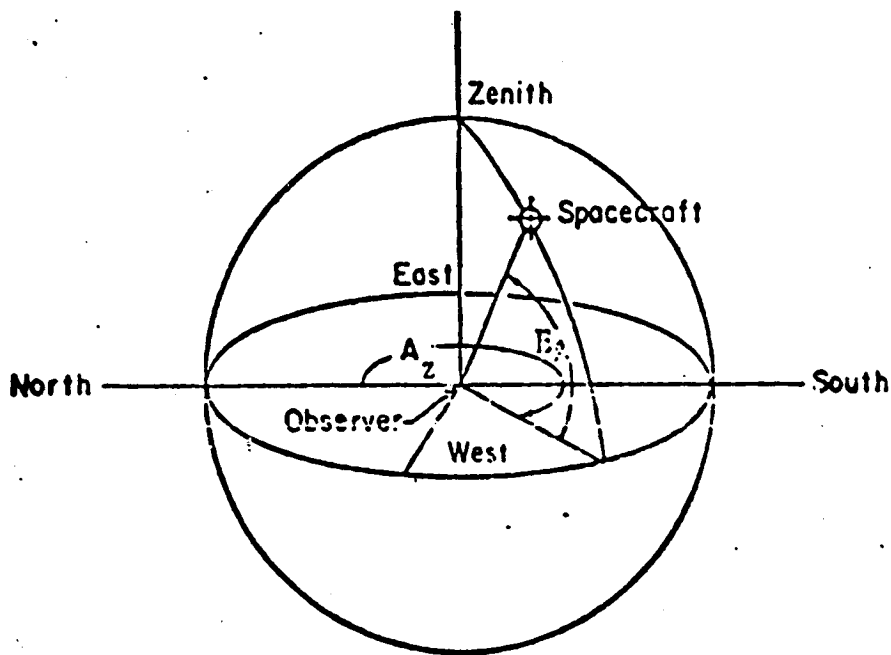
Figure 12.3-3. Azimuth and Elevation Angles

and the partial derivatives with respect to time are

$$\dot{A}_z = \frac{\dot{\bar{\rho}} \cdot (m\hat{E} - \ell\hat{N})}{\rho \, (1 - m^2)} \qquad (12.3\text{-}56)$$

$$\dot{E}_\ell = \frac{\dot{\bar{\rho}} \cdot \hat{Z} - m\dot{\rho}}{\rho \, \sqrt{1 - m^2}} \qquad (12.3\text{-}57)$$

12.3.7 Satellite-Satellite Range and Range Rate

The range measurement from one satellite to another is computed as follows.

Let $\vec{X}_1$ be the inertial coordinates of the transmitting satellite and $\vec{X}_2$ the inertial coordinates of the receiving satellite. Then the range (or distance) between the two satellites is given by

$$R = \sqrt{(\vec{X}_2 - \vec{X}_1) \cdot (\vec{X}_2 - \vec{X}_1)} \; . \qquad (12.3\text{-}58)$$

The time rate of change of range, or just range rate, is calculated by differentiating (12.3-58) with respect to time

$$\dot{R} = \frac{(\vec{X}_2 - \vec{X}_1) \cdot (\dot{\vec{X}}_2 - \dot{\vec{X}}_1)}{R} \qquad (12.3\text{-}59)$$

Relay range and range rate measurements can also be simulated. Relay range is simply the sum of two range measurements: the range from some transmitting station to a satellite plus the range from that same satellite to another satellite. This configuration is given in Figure 12.3-4. Thus, according to the notation in Figure 12.3-4, the relay range is defined as

$$R_{Relay} = \left| \vec{R}_1 \right| + \left| \vec{R}_2 \right| .$$
$$= R_1 + R_2 \qquad (12.3\text{-}60)$$

Likewise, the relay range rate is the time derivation of (12.3-60) or

$$\dot{R}_{Relay} = \dot{R}_1 + \dot{R}_2 . \qquad (12.3\text{-}61)$$

Since the partial derivative of a sum is equal to the
sum of the individual partial derivatives, any partial
derivative of R_{Relay} or $\dot{R}_{Relay}$ can be found by summing
the individual partials of the two quantities in the
sum. Specifically, if one wants the partial with respect
to some parameter σ, then

$$\frac{\partial R_{relay}}{\partial \sigma} = \frac{\partial R_1}{\partial \sigma} + \frac{\partial R_2}{\partial \sigma} , \tag{12.3-62}$$

$$\frac{\partial \dot{R}_{relay}}{\partial \sigma} = \frac{\partial \dot{R}_1}{\partial \sigma} + \frac{\partial \dot{R}_2}{\partial \sigma} \tag{12.3-63}$$
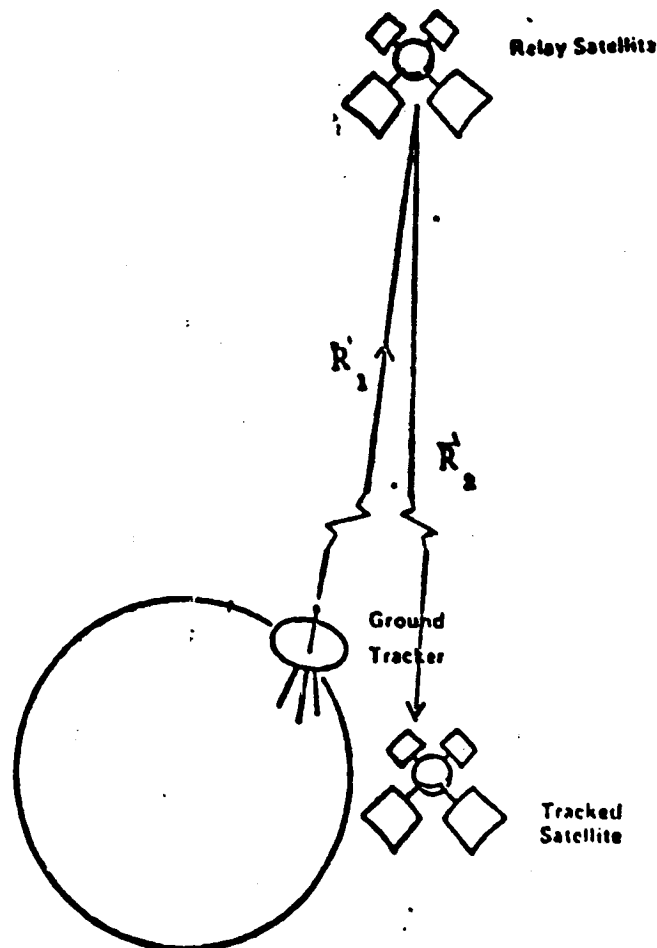
Figure 12.3-4. Geometry for Satellite-Satellite Tracking

12.4 MEASUREMENT ERRORS

This section discusses the individual measurement error sources and the mathematics used to model them. The equations are taken directly from Reference 12.2.

The simplest type of measurement error to model is a bias in the measured quantity itself. Bias errors are considered as constants which must be added on to the computed value in order to better represent the observed value. Thus

$$Z_c = Z_c' + b \qquad\qquad (12.4-1)$$

where

Z_c is the computed measurement corrected for any biases

Z_c' is the computed measurement based only on satellite geometry

b is the bias

Thus

$$\frac{\partial Z_c}{\partial b} = 1 \text{ for all measurement types.} \qquad (12.4-2)$$

12.4.1   Timing Errors

Should the time tag of the measurement be incorrect, then a correction to this time tag is called a correction to timing. Any error in this correction can be found by computing the partial derivative of the computed measurement and multiplying by the time error, or

$$\frac{\partial Z_c}{\partial t} \Delta t = \Delta Z_{c_{Tim}} \qquad\qquad (12.4-3)$$

where Δt is the timing error, but

$$\frac{\partial Z_c}{\partial t} = \frac{\partial Z_c}{\partial \bar{r}} \cdot \frac{\partial \bar{r}}{\partial t}$$

$$= \frac{\partial Z_c}{\partial \bar{r}} \cdot \frac{\dot{\bar{r}}}{r} \qquad\qquad (12.4\text{-}4)$$

where

$\bar{r}$ is the satellite position vector

$\dot{\bar{r}}$ is the satellite velocity vector.

Thus

$$\Delta Z_{c_{\text{Tim}}} = \frac{\partial Z_c}{\partial \bar{r}} \cdot \dot{\bar{r}} \ \Delta t \qquad\qquad (12.4\text{-}5)$$

The time tag assigned to the measurement is usually the time at which the station receives the signal. But the satellite retransmitted the signal to the receiving station at some earlier time. Therefore, two times are involved. To simplify matters somewhat, the observed measurements usually have been corrected so the computation process of the computed values can assume the satellite and station at the same time. An error in this transit time correction is similar to the timing error just discussed, but now the systematic error is some fractional part of the estimated transit time, i.e.,

$$\Delta Z_{c_{\text{transit time}}} = \frac{\partial Z_c}{\partial \bar{r}} \cdot \dot{\bar{r}} \ \Delta T \qquad\qquad (12.4\text{-}6)$$

where ΔT is the error in the transit time. If p is the fractional error in transit time correction, then

$$\Delta T = p\left(\frac{R}{c}\right)$$

(12.4-7)

where

R   is range

C   is speed of light

12.4.2   Tracking Station Location Errors

In the preceding sections measurement equations have been developed for a relative satellite-station geometry. These measurements are used to determine satellite position and motion in an inertial coordinate system at some epoch time. In transforming from the relative coordinate system at the time of measurement to the inertial system at epoch we must account for both the movement of the satellite and the movement of the station in inertial coordinates during the time period between measurement and epoch. The equations of motion for the satellite are given in Chapter 6. 6 The station movement is due to the movement of the Earth (considered as a solid body) and to the movement of the Earth's crust relative to the central mass. Station co-ordinates are referenced to a particular epoch time (usually 1900.0) and the movement of the station since this time is included in the computation of a station-satellite measurement. The solid body component of station motion is due to the Earth's rotation, nutation and precession. These are very well known and make negligible contributions to station location error.

The remaining components are due to uncertainties in the movement of the Earth's crust relative to the central mass. These are:

$\Delta \bar{r}_{SE}$ = error due to solid Earth tidal displacements. This is relatively a local error.

$\Delta \bar{r}_{OL}$ = error due to ocean loading displacement. This is also a relatively local error which depends upon the distance of the station from the shoreline.

$\Delta \bar{r}_{p}$ = error due to polar motion

12.4.3 Errors Due to Atmospheric and Ionized Particle Effects

Uncertainties in range and range-rate due to the following transmission medium effects are treated.

- Tropospheric refraction

- Ionospheric refraction

- Space plasma

Except at very low elevation angles, (<5°), the primary effect of the troposphere is a decrease in the velocity of propagation. At the Earth's surface, this decrease is about 300 parts per million, decreasing to about 1 part per million at a height of 30 km. Considering the Earth's atmosphere to be horizontally stratified, as is almost always done in data reduction, a good approximation to the integrated tropospheric effect on range measurements is

$$\Delta R_{T} = \frac{2.77(N_{s}/328.5)}{.026 + \sin E} \text{ meters} \qquad (12.4\text{-}8)$$

The effect of an error in station location on the computed measurement can be determined by the following expression

$$\Delta Z_{c_{STA}} = -\frac{\partial Z_c}{\partial \bar{r}} \cdot \Delta \bar{r}_{STA} \qquad (12.4-9)$$

where

$\Delta Z_{c_{STA}}$ is the error in the computed measurement due to an error in station position

$\bar{r}$ is the satellite position vector

$\Delta \bar{r}_{STA}$ is the error in station position (in same coordinate system as $\bar{r}$)

This is obvious if one considers, for example, a range measurement from a station to a satellite. If the station height were raised, the same effect on the measurement would occur if the satellite height were lowered.

At any measurement time the total station location error can be expressed as

$$\Delta \bar{r}_{STA} = \Delta \bar{r}_S + \Delta \bar{r}_E + \Delta \bar{r}_{SE} + \Delta \bar{r}_{OL} + \Delta \bar{r}_p \qquad (12.4-10)$$

where the components are defined as

$\Delta \bar{r}_S$ = survey error. This is the error in a station's location relative to the local datum. Each station on the same local datum will have a different value of $\Delta \bar{r}_S$.

$\Delta \bar{r}_E$ = station location error due to uncertainty in location of the local datum with respect to the center of mass of the Earth. All stations on the same local datum will have the same $\Delta \bar{r}_E$.

where

$$R_{OBSERVED} = R_{COMPUTED} + \Delta R_T,$$

N_s is the deviation of surface index of refraction from unity in parts per million, and

E is the elevation angle.

The most serious error in applying this correction to data is due to errors in the surface index of refraction at the tracking site. For this reason, tropospheric refraction errors are modeled as

$$\frac{\partial (\Delta R_T)}{\partial N_s} = \frac{(2.77/328.5)}{.026 + \sin E} \qquad (12.4\text{-}11)$$

The systematic effect of tropospheric refraction on range rate errors is obtained by differentiating the range error with respect to time,

$$\frac{\partial (\Delta \dot{R}_T)}{\partial N_s} = \frac{(-2.77/328.5)}{(.026 + \sin E)^2} \cos E \ \dot{E} \qquad (12.4\text{-}12)$$

Elevation:

For elevation observations, the partial with respect to refraction is

$$\frac{\partial E}{\partial N_s} = \frac{10^3}{16.44+930} \ \tan E \qquad (12.4\text{-}13)$$

Azimuth is not affected by refraction.

Direction Cosines:

$$\frac{\partial \ell}{\partial n_s} = -\sin A_z \sin E \frac{\partial E}{\partial n_s} \qquad (12.4\text{-}14)$$

$$\frac{\partial m}{\partial m_s} = -\cos A_z \sin E \frac{\partial E}{\partial m_s} \qquad (12.4\text{-}15)$$

X and Y angles:

$$\frac{\partial X}{\partial n_s} = \frac{\sin A_z}{(\sin^2 E + \sin^2 A_z \cos^2 E)} \frac{\partial E}{\partial n_s} \qquad (12.4\text{-}16)$$

$$\frac{\partial Y}{\partial n_s} = -\frac{\cos A_z \sin E}{\sqrt{1 - \cos^2 A_z \cos^2 E}} \frac{\partial E}{\partial n_s} \qquad (12.4\text{-}17)$$

The effect of the ionosphere on a range measurement is evaluated by considering

$$R_{OBSERVED} = R_{COMPUTED} + \Delta R_I \qquad (12.4\text{-}18)$$

The correction ΔR_I is modeled by fitting a polynomial to curves taken from JPL SPS 37-41, Volume III, page 8. The polynomial takes the form

$$\Delta R_I = C_0 + C_1 \sin E + C_2 \sin^2 E + C_3 \sin^3 E \qquad (12.4\text{-}19)$$

where E is the elevation angle and the C_i are obtained by a least squares fit to selected points from the curves. Errors in range rate are obtained by differentiating ΔR_I.

An estimate of the error in ΔR_I is given by the above reference to be 10% on a day-to-day basis for a particular location.

Space plasma represents another type of propagation
error. Unlike the ionosphere, which is assumed to terminate
somewhere near 600 KM above the Earth's surface, space plasma
continues ad-infinitum, and is reasonably represented by
a $1/r^2$ law. Therefore, no closed-form solution exists for
its effect on measurements, and an integration process must
be performed. Let

$$R_{OBSERVED} = R_{COMPUTED} + \Delta R_{SP} \tag{12.4-20}$$

where ΔR_{SP} is modeled by the relationship

$$\Delta R_{SP} = \frac{44.3}{f^2} \int N_p \, ds \tag{12.4-21}$$

and

f = frequency of wave (Hz)

N_p = proton density per cubic centimeter

s = ray path

The proton density is taken to be a 4th degree polynomial

$$N_p = K_0 + K_1 R + K_2 R^2 + K_3 R^3 + K_4 R^4 \tag{12.4-22}$$

as a function of the distance from the sun.

12.5 References

12.1 W. E. Wagner and C. E. Velez. "Goddard Trajectory Determination Subsystem Mathematical Specifications." March, 1972.

12.2 W. E. Hatch and C. C. Goad. "Mathematical Description of the ORAN Error Analysis Program." Wolf Research and Development Corporation Planetary Sciences Department Report No. 009-73 under Contract NAS5-11932-29, August, 1973.

12.3 G. L. Adams, et al. "Space Trajectories Error Analysis Programs Version II (Update) Volume I - Analytical Manual." Martin Marietta Corporation under Contracts NAS5-11795 and NAS5-11873. December, 1971.

13. MANEUVER ERROR ANALYSIS

13.1 Introduction

The analysis of the errors associated with spacecraft maneuvers is a very important part of GMAS. General error models are defined for attitude determination and control errors (pointing) and engine characteristics (proportionality, resolution and timing) for both impulsive and finite burn models of spacecraft orbit change maneuvers. The purpose of the analysis is to assess the errors which may result after performing a burn maneuver and the impact that these errors may have upon the mission success.

In the Monte Carlo mode of analysis, the various error sources are sampled to generate actual states which are then propagated through the mission, statistics are then collected upon various mission parameters of interest in the analysis. In the linear mode of analysis, actual trajectories are not analyzed, but rather the ensemble of possible cases as described by the nominal trajectory and covariances of state errors and covariances of the various error sources. All error sources are assumed to have gaussian distributions. In the linear analysis state covariances are propagated by the use of the state transition matrixes.

In many cases where it is necessary to model the maneuver as a finite burn, the burn is short enough that a simplified model for the state and state transition matrix propagation over the burn arc is sufficient. The equations for this model are also given in this section.

13.2 Impulsive Maneuver Error Modeling

The execution errors resulting from performing a velocity change maneuver $\Delta\bar{V}$, are based upon an execution error model defined by four independent error sources. The first two error sources are in the direction of the $\Delta\bar{V}$ but affect its magnitude. The proportionality error is determined by the proportionality factor k. The resolution error s is also in the direction of $\Delta\bar{V}$ but is independent of its magnitude and corresponds to a thrust tailoff error from the engines. The error in the direction of $\Delta\bar{V}$ is thus given by

$$\epsilon_{\Delta V} = k\,\Delta\bar{V} + S\,\frac{\Delta\bar{V}}{\Delta V} \qquad (13.2-1)$$

where ΔV has been written for $|\Delta\bar{V}|$.

The pointing error is formulated as two independent errors along mutually orthogonal axes which are both orthogonal to the maneuver impulse direction. For purposes of unique specification let one pointing error angle $\delta\alpha$ be measured in the xy plane of the coordinate system in which $\Delta\bar{V}$ is expressed, then the error due to $\delta\alpha$ (which is presumed to be a small angle) is given by

$$\epsilon_\alpha = \Delta V\,\delta\alpha\left[\frac{\Delta V_y}{u}\,\hat{\imath} - \frac{\Delta V_x}{u}\,\hat{\jmath}\right] \qquad (13.2-2)$$

where the x and y subscripts refer to those components of $\Delta\bar{V}$, $\hat{\imath}$, $\hat{\jmath}$, $\hat{k}$ are the unit vectors in the xyz system in which $\Delta\bar{V}$ is expressed, and the auxillary variable u is defined by

$$u = (\Delta V_x^2 + \Delta V_y^2)^{\frac{1}{2}} \qquad (13.2-3)$$

The second pointing angle $\delta\beta$ is in the direction orthogonal to both $\delta\alpha$ and ΔV. Presuming $\delta\beta$ to also be a small angle the velocity error corresponding to it is

$$\epsilon_\beta = \delta\beta\left[\frac{\Delta V_x \Delta V_z}{u}\,\hat{\imath} + \frac{\Delta V_y \Delta V_z}{u}\,\hat{\jmath} - u\,\hat{k}\right] \qquad (13.2-4)$$

Combining equations(13.2-1),(13.2-2)and(13.2-4),the complete description of the execution error vector ϵ is written as

$$\epsilon = \left[(k + \frac{S}{\Delta V})\Delta V_x + \frac{\Delta V \Delta V_y \,\delta\alpha + \Delta V_x \Delta V_z \delta\beta}{u} \right] \hat{i}$$

$$+ \left[(k + \frac{S}{\Delta V})\Delta V_y - \frac{\Delta V\, \Delta V_x\, \delta\alpha - \Delta V_y \Delta V_z\, \delta\beta}{u} \right] \hat{j}$$

$$+ \left[(k + \frac{S}{\Delta V})\Delta V_z - u\delta\beta \right] \hat{k} \qquad\qquad (13.2\text{-}5)$$

The four error sources are generally taken to be independent, zero mean, gaussian distributed variables. A more general error model might presume correlated, non-zero mean, or non-gaussian distributed variables, but the above model is generally quite sufficient. Since the four error sources are independent, equation(13.2-5)is suitable for use in Monte Carlo analysis directly, with actual values of k, s, $\delta\alpha$, and $\delta\beta$ being sampled from zero-mean distributions with variances σ_k^2, σ_s^2, σ_α^2 and σ_β^2 respectively.

For the purposes of linear error analysis, the execution error covariance matrix $Q = \mathcal{E}\{\epsilon\,\epsilon^T\}$ is necessary. The components of Q are given below, presuming the assumptions made above.

$$Q_{11} = \Delta V_x^2 (\sigma_k^2 + \frac{\sigma_s^2}{\Delta V^2}) + \frac{\Delta V^2 \Delta V_y^2\, \sigma_\alpha^2}{u^2} + \frac{\Delta V_x^2 \Delta V_z^2\, \sigma_\beta^2}{u^2}. \qquad (13.2\text{-}6)$$

$$Q_{12} = Q_{21} = \Delta V_x\, \Delta V_y \left[\sigma_k^2 + \frac{\sigma_s^2}{\Delta V^2} - \frac{\Delta V^2 \sigma_\alpha^2}{u^2} + \frac{\Delta V_z^2 \sigma_\beta^2}{u^2} \right] \qquad (13.2\text{-}7)$$

$$Q_{13} = Q_{31} = \Delta V_x\, \Delta V_z \left[\sigma_k^2 + \frac{\sigma_s^2}{\Delta V^2} - \sigma_\beta^2 \right] \qquad (13.2\text{-}8)$$

$$Q_{22} = \Delta V_y{}^2 \left(\sigma_k{}^2 + \frac{\sigma_s{}^2}{\Delta V^2}\right) + \frac{\Delta V^2 \Delta V_x{}^2 \sigma_\alpha{}^2}{u^2} + \frac{\Delta V_y{}^2 \Delta V_z{}^2 \sigma_\beta{}^2}{u^2} \qquad (13.2-9)$$

$$Q_{23} = Q_{32} = \Delta V_y \Delta V_z \left[\sigma_k{}^2 + \frac{\sigma_s{}^2}{\Delta V^2} - \sigma_\beta{}^2\right] \qquad (13.2-10)$$

$$\dot{Q}_{33} = \Delta V_z{}^2 \left(\sigma_k{}^2 + \frac{\sigma_s{}^2}{\Delta V^2}\right) + u^2 \sigma_\beta{}^2 \qquad (13.3-11)$$

The state covariance after a ΔV maneuver is performed is then given by

$$P^+ = P^- + \left[\begin{array}{c|c} 0 & 0 \\ \hline 0 & Q \end{array}\right] \qquad (13.2-12)$$

where the + and − superscripts denote after and before the maneuver respectively.

Equations (13.2-1) through (13.2-11) are taken primarily from Reference 13.1. They are essentially equivalent to the corresponding equations of References 13.2 and 13.3 with a few minor exceptions. Reference 13.2 does not develop the covariance Q, using only the Monte Carlo form in which the resolution error is modeled as a uniform distribution rather than gaussian. Both References 13.2 and 13.3 determine the direction of the erroneous ΔV as the nominal ΔV plus pointing errors only. The proportionality and resolution errors are then added to the nominal magnitude which is then used along the direction which includes the pointing errors. For small execution errors the difference between the formulation given above and that of References 13.2 and 13.3 will only be of second order and is hence generally quite negligible.

13.3 Finite Burn Maneuver Error Modeling

The execution errors resulting from performing a velocity change maneuver which takes an appreciable time span are based upon four independent error sources as is the case for impulsive maneuvers. For a burn with a fixed thrust level and direction, the error sources which are in the direction of the thrust are the thrust magnitude error and an error in the duration of the burn. As in the impulsive case, two independent pointing errors are modeled.

As was the case for an impulsive burn, either an erroneous state (Monte Carlo application) or a covariance describing the ensemble of erroneous states (linear analysis application) is necessary at the completion of the burn. For the Monte Carlo application, actual values of the errors in thrust (δT), pointing ($\delta\alpha$, $\delta\beta$) and timing (δt_B) are sampled from zero-mean gaussian distributions with variances σ_T^2, σ_α^2, σ_β^2 and σ_t^2 respectively. A slightly more complicated error model could replace the single timing error δt_B by errors in the time of burn initiation and the time of burn termination. Once the sampled errors are added to the nominal thrust parameter values, then these erroneous thrust parameters are used by the propagation model which has been specified - whether high precision numerical integration or an approximate scheme - to generate the sampled state vector after the burn as a function of the initial state which may also have included sampled errors.

For the linear error analysis application the situation is somewhat more complex. The state errors at burn completion will arise from two sources, namely the state dispersions at the start of the burn, which must be propagated through the burn, and the actual execution errors related to the burn itself. The effects of both of these error sources are found by the use of the state transition matrices Φ and Θ. The first of these is the 6x6 state to state transition matrix, relating deviations in the final state to deviations in the initial state. The second is the 6x4 control to state state transition matrix relating deviations in the final state to deviations in the thrust control parameters. For the finite burn model considered here, the four

control parameters are the thrust magnitude (T), the two angles specifying the inertial direction of the burn and the duration of the burn (t_B). The two state transition matrices may be calculated by high precision numerical integration or some approximate scheme, but in either case the column of Θ corresponding to t_B is simply

$$\frac{\partial X}{\partial t_B} = \begin{bmatrix} 0, & 0, & 0, & A_x, & A_y, & A_z \end{bmatrix}^T \tag{13.3-1}$$

where X is the state vector and A_x, A_y and A_z are the components of the thrust acceleration given by

$$A = \begin{bmatrix} (T/m) \cos \alpha \cos \beta \\ (T/m) \sin \alpha \cos \beta \\ (T/m) \sin \beta \end{bmatrix} \tag{13.3-2}$$

where m is the spacecraft mass. The covariance of state errors after the burn (P^+) is given by

$$P^+ = \Phi P^- \Phi^T + \Theta U \Theta^T \tag{13.3-3}$$

where P^- is the state covariance at the burn initiation and U is the diagonal covariance of control errors with elements σ_T^2, σ_α^2, σ_β^2 and σ_t^2 giving the statistics of the finite burn errors. The above equations are taken primarily from Reference 13.4.

For some approximate analyses, it is useful to assume that the burn is short enough so that the state is sufficiently approximated by linear motion. In this case the state at the conclusion of the burn is given by

$$\bar{R}_F = \bar{R}_o + \dot{\bar{R}}_o t_B - \frac{\bar{R}_o \mu t_B^2}{2 R_o^3} + \bar{T} \frac{t_B}{m} \left[\frac{(m_o + \dot{m} t_B)}{\dot{m} t_B} \ln \left(\frac{m_o + \dot{m} t_B}{m_o} \right) - 1 \right] \tag{13.3-4}$$

$$\dot{\bar{R}}_F = \dot{\bar{R}}_o - \frac{\bar{R}_o \mu t_B}{R_o^3} + \frac{\bar{T}}{\dot{m}} \ln\left(\frac{m_o + \dot{m} t_B}{m_o}\right) \qquad (13.3\text{-}5)$$

where $\bar{R}_o$ and m_o are the position vector and mass before the burn, $\dot{m}$ is the mass flow rate, $\bar{R}_F$ is the position vector after the burn, μ is the gravitational parameter, t_B is the burn time, $\bar{T}$ is the thrust vector, and R_o and R_F are the magnitudes of $\bar{R}_o$ and $\bar{R}_F$. The state transition matrix Φ is given by

$$\phi_1 = I - \frac{\mu t_B^2}{2 R_o^3}\left[I - 3\frac{\bar{R}_o \bar{R}_o^T}{R_o^2}\right] \qquad (13.3\text{-}6)$$

$$\phi_2 = t_B I \qquad (13.3\text{-}7)$$

$$\phi_3 = -\frac{\mu t_B}{R_o^3}\left[I - 3\frac{\bar{R}_o \bar{R}_o^T}{R_o^2}\right] \qquad (13.3\text{-}8)$$

$$\phi_4 = I \qquad (13.3\text{-}9)$$

where Φ has been partitioned as

$$\Phi = \begin{bmatrix} \phi_1 & \phi_2 \\ \phi_3 & \phi_4 \end{bmatrix} \qquad (13.3\text{-}10)$$

The first three columns of the state transition matrix Θ can be expressed as

$$\Theta_3 = \begin{bmatrix} \dfrac{\partial \bar{R}}{\partial \bar{T}} \\[2mm] \dfrac{\partial \dot{\bar{R}}}{\partial \bar{T}} \end{bmatrix} \left[\dfrac{\partial \bar{T}}{\partial(T, \alpha, \beta)}\right] \qquad (13.3\text{-}11)$$

13.3-3

where

$$\frac{\partial \bar{T}}{\partial(T, \alpha, \beta)} = \begin{bmatrix} \cos\alpha \cos\beta & -T\sin\alpha \cos\beta & -T\cos\alpha \sin\beta \\ \sin\alpha \cos\beta & T\cos\alpha \cos\beta & -T\sin\alpha \sin\beta \\ \sin\beta & 0 & T\cos\beta \end{bmatrix}$$

$$(13.3\text{-}12)$$

and where

$$\frac{\partial \bar{R}}{\partial \bar{T}} = \frac{t_B}{\dot{m}} \left[\left(\frac{m_o + \dot{m}t_B}{\dot{m}t_B} \right) \ln \left(\frac{m_o + \dot{m}t_B}{\dot{m}t_B} \right) - 1 \right] \; I$$

$$+ \frac{t_B}{\dot{m}} \left[2 - \left(\frac{2m_o + \dot{m}t_B}{\dot{m}t_B} \right) \ln \left(\frac{m_o + \dot{m}t_B}{\dot{m}t_B} \right) \right] \frac{\bar{T}\bar{T}^T}{T^2}$$

$$(13.3\text{-}13)$$

and

$$\frac{\partial \dot{\bar{R}}}{\partial \bar{T}} = \frac{1}{\dot{m}} \ln \left(\frac{m_o + \dot{m}t_B}{\dot{m}t_B} \right) \; I$$

$$+ \frac{1}{\dot{m}} \left[\left(\frac{\dot{m}t_B}{m_o + \dot{m}t_B} \right) - \ln \left(\frac{m_o + \dot{m}t_B}{\dot{m}t_B} \right) \right] \frac{\bar{T}\bar{T}^T}{T^2} \qquad (13.3\text{-}14)$$

The fourth column of Θ is as given in equation (13.3-1), so that now with Φ and Θ equation (13.3-3) may be used to calculate the covariance at the end of the burn. Equations (13.3-4) through (13.3-14) are based primarily upon References 13.5 and 13.6.

13.4 References

13.1 G. L. Adams, et al. "Space Trajectories Error Analysis Programs Version II (Update) Volume I - Analytical Manual." Martin Marietta Corporation under Contracts NAS5-11795 and NAS5-11873. December, 1971.

13.2 D. A. Lutzky, W. S. Bjoekman and C. Uphoff. Final Report for Radio Astronomy Explorer-B In-Flight Mission Control System Development Effort. Analytic Mechanics Associates, Inc. Report No. 73-8 under Contract No. NAS5-11900. March, 1973.

13.3 Unknown. "Preliminary User's and Programmer's Guide for SMS/MAESTRO." Analytic Mechanics Associates, Inc. Report No. 74-? under Contract No. NAS5-21963. September, 1974.

13.4 D. V. Byrnes, et al. Space Trajectory Error Analysis Program (STEAP) for Halo Orbit Missions Volume I - Analytic and User's Manual." Martin Marietta Corporation Report No. MCR 74-98 under Contract No. NAS5-24067. May, 1974.

13.5 D. P. Muhonen. "TBERR Two-Body Error Analysis Program." Goddard Space Flight Center X-551-71-238. May, 1971.

13.6 Unknown. "User's Manual for the Advanced Mission Analysis Programs (Subroutine THRUST). Philco-Ford Corporation Corporation Space and Re-Entry Systems Division Report No. TR-DA1621 under Contract No. NAS5-10029. December, 1967.

14. LINEAR AND MONTE CARLO ANALYSIS

14.1 Introduction

One of the tasks to be performed by GMAS is the analysis of the effect of errors upon various missions. Errors or uncertainties arise from many sources. Chapter 12 discussed the modeling of measurement errors involved in the spacecraft tracking process. Random noise and fixed biases can occur in various quantities which are measured by ground- or spacecraft-based instruments as well as in dynamical quantities such as the mass of the earth, gravitational harmonics, spacecraft drag, reflectivity and engine characteristics, ephemeris errors, etc. Uncertainty can also arise from modeling all of the effects involved in an analysis in too simple a manner. All of these sources of uncertainty must be assessed in pre-mission planning to be able to predict mission feasibility and to assist in both mission and spacecraft design. During a mission, also, the effect of current and expected uncertainties must be assessed for the impact upon the continued success of the mission.

Error analysis can be addressed from two points of view. The first point of view assumes that all errors and uncertainties are "small". When this is the case all equations of motion, measurement equations, any mathematical representation of the dynamics under consideration, can be linearized about the nominal or best estimate of the values of all of the parameters. This allows a much more tractable mathematical representation. The second point of view makes no assumption about the size or effect of any error source, the only assumptions made are that all important effects are properly modeled and that the uncertainties in all parameters are described by gaussian distributions which may be correlated with one another. Monte Carlo analysis can be performed by statistically sampling from the various parameter distributions to obtain simulated actual values for the parameters. These actual cases may then be used in the full non-linear form of the model to obtain distributions of the resulting parameters of interest. The Monte Carlo analysis

although generally more realistic, is of course far more costly in terms of computation time due to the large number of samples required for reasonable statistics to be obtained.

This chapter will also cover error sensitivities, error budget analysis and the linear propagation of errors, as well as Monte Carlo techniques. The sensitivity of an estimated state to the parameters which are known to be uncertain but are not estimated (consider parameters) is frequently of great interest in mission analysis. These sensitivities, like covariances, can be calculated for error analysis purposes without actual data being necessary. Error budgets allow the identification of the effects of various error sources as they contribute to the total uncertainty. Monte Carlo methods are frequently a necessary technique, but must be used with great care due to the high cost involved and the possibilities for misinterpretation of the statistics involved.

14.2 Linear Error Analysis

14.2.1 Error Sensitivities

In Chapter 12, the expressions in equations 12.2-6, 12.2-7, and 12.2-12 were given for the batch weighted least squares estimator and covariance equations in the presence of consider parameters. Within the restrictions of linearity, the estimator equation 12.2-6 prescribes the computations necessary to obtain the "best" estimate of the solve-for parameters. By calculating the derivative of $\Delta\hat{x}$, the correction to be applied to the initial estimate, with respect to the vector of consider parameters, it is possible to obtain the sensitivity of the estimate to the consider parameters.

This is given by

$$\frac{\partial \Delta\hat{x}}{\partial z} = -\psi F^T W E \qquad (14.2\text{-}1)$$

Where ψ is the inverse of the normal matrix as defined by equation (12.2-10) and F and E are the observation matrices for the solve-for and consider parameters respectively. Substituting this into equation (12.2-7) leads to the expression for the covariance in terms of the sensitivity matrix

$$P_{\Delta x} = \psi + \left(\frac{\partial \Delta\hat{x}}{\partial z}\right) P_{\Delta z}\left(\frac{\partial \Delta\hat{x}}{\partial z}\right)^T$$
$$- \left(\frac{\partial \Delta\hat{x}}{\partial z}\right) C_{\Delta x_o \Delta z}^T P_{\Delta x_o}^{-1} \psi - \psi P_{\Delta x_o}^{-1} C_{\Delta x_o \Delta z}\left(\frac{\partial \Delta\hat{x}}{\partial z}\right)^T \qquad (14.2\text{-}2)$$

The first term in equation (14.2-2) is due to measurement noise and the _a priori_ covariance. The second term is easily identifiable as the contribution due to the consider parameters. The last two terms occur only if there is an initial correlation between the solve-for and consider parameters. The sensitivity equation is useful for assessing the dependence of the estimate upon assumed values of the consider parameters.

14.2.2 Covariance Propagation

The linearized dynamic model which relates errors on deviations in the state at one time to those at another has the form

$$\Delta x_k = \phi_{k,k-1} \Delta x_{k-1} + \theta_{k,k-1} \Delta z_{k-1} + q_{k,k-1} \qquad (14.2\text{-}3)$$

Where the state to state and consider parameter to state state transition matrices are given by ϕ and θ over the time interval (t_{k-1}, t_k). The effect of dynamic process noise over the interval is given by $q_{k,k-1}$ and the vectors of solve-for and consider parameters are given by x and z respectively. The corresponding equations for the propagation of the covariances discussed in Chapter 12 are given by

$$P_{\Delta x_k} = \phi P_{\Delta x_{k-1}} \phi^T + \theta C^T_{\Delta x \Delta z_{k-1}} \phi^T$$

$$+ \phi C_{\Delta x \Delta z_{k-1}} \theta^T + \theta P_{\Delta z_o} \theta^T + Q_{k,k-1} \qquad (14.2\text{-}4)$$

and

$$C_{\Delta x \Delta z_{k-1}} = \phi C_{\Delta x \Delta z_{k-1}} + \theta P_{\Delta z_o} \qquad (14.2\text{-}5)$$

where the subscript k, k-1 is presumed on all of the state transition matrices. The quantity $Q_{k,k-1}$ is the contribution due to dynamic process noise.

14.2.3 Error Budget Analysis

In standard error analyses the normal result of performing the error analysis of a set of measurements is the covariance matrix P which describes the effect of all error sources which were assumed for the analysis. The individual contributions of the various error sources to P are thus not identifiable. To be able to identify the contributions of the error sources to P it would normally be necessary to make repeated analyses each with a specific error source turned on. A formulation which at each step of a sequential analysis gives the contribution due to each error source is therefore highly desirable.

The equations for an error budget analysis, wherein the components of the total error budget can be propagated in a single set of calculations are given below. The covariance P_N, based upon all measurements up to and including the Nth, is given by

$$P_N = S_x(N) \, \mathcal{E}\{\Delta\bar{x}_o\Delta\bar{x}_o^T\} \, S_x^T(N) \; + \; S_z(N) \, \mathcal{E}\{\Delta\bar{z}\Delta\bar{z}^T\} \, S_z^T(N)$$

$$+ \; S_m(N) \, \mathcal{E}\{\Delta\bar{m}\Delta\bar{m}^T\} \, S_m^T(N) \; + \; P_u(N) + P_s(N) \qquad (14.2-6)$$

where as before x refers to the solve-for parameters. The consider parameters which were previously denoted by z have been broken into two classes - dynamical consider parameters z and the measurement consider parameters m. The sensitivity matrices $S_x(N)$, $S_z(N)$ and $S_m(N)$ relate the various error sources to the current state estimate. The $P_u(N)$ and $P_s(N)$ matrices are the contribution to the state uncertainty due to state process noise and measurement noise respectively. The quantities Δx_o, Δz and Δm are the initial solve-for and consider parameter errors given by

$$\Delta\bar{x}_o = x(0) - \bar{x}(0) \qquad\qquad (14.2-7)$$

$$\Delta\bar{z} = z - \bar{z} \qquad\qquad (14.2-8)$$

$$\Delta\bar{m} = m - \bar{m} \qquad\qquad (14.2-9)$$

The initial solve-for and consider parameter second moment matrices are given by

$$\mathcal{E}\{\Delta\bar{x}_o\Delta\bar{x}_o^T\} = P_{\Delta x_o} + \left[\bar{x}(0) - \bar{x}_A(0)\right]\left[\bar{x}(0) - \bar{x}_A(0)\right]^T \quad (14.2-10)$$

$$\mathcal{E}\{\Delta\bar{z}\Delta\bar{z}^T\} = P_{\Delta z} + \left[\bar{z} - \bar{z}_A\right]\left[\bar{z} - \bar{z}_A\right]^T \qquad (14.2-11)$$

$$\mathcal{E}\{\Delta\bar{m}\Delta\bar{m}^T\} = P_{\Delta m} + \left[\bar{m} - \bar{m}_A\right]\left[\bar{m} - \bar{m}_A\right]^T \qquad (14.2-12)$$

where the possibility for an initial mismatch or non-zero mean for the parameters has been allowed for. The subscript A indicates the mean of the actual distribution and the $P_{\Delta x_o}$, $P_{\Delta z}$ and $P_{\Delta m}$ are the initial covariances.

The proceedure of the error budget analysis is to use recursive relations for the matrices S_x, S_z, S_m, P_u and P_s instead of the covariance

matrix P. The relations are given by

$$S_x(N) = \left[I - K_N F_N\right] \phi_{N, N-1} S_x(N-1) \tag{14.2-13}$$

$$S_z(N) = \left[I - K_N F_N\right]\left[\phi_{N, N-1} S_z(N-1) + \Theta_{N,N-1}\right] - K_N E_{z_N} \tag{14.2-14}$$

$$S_m(N) = \left[I - K_N F_N\right] \phi_{N, N-1} S_m(N-1) - K_N E_{m_N} \tag{14.2-15}$$

$$P_u(N) = \left[I - K_N F_N\right]\left[\phi_{N, N-1} P_u(N-1)\phi^T_{N, N-1} + Q_{N, N-1}\right]\left[I - K_N F_N^T\right] \tag{14.2-16}$$

$$P_s(N) = \left[I - K_N F_N\right]\left[\phi_{N, N-1} P_s(N-1) \phi^T_{N, N-1}\right]\left[I - K_N F_N^T\right] + K_N R_N K_N^T \tag{14.2-17}$$

The initial values are given by

$$S_x(0) = I \tag{14.2-18}$$

$$S_z(0) = S_m(0) = P_u(0) = P_s(0) = 0 \tag{14.2-19}$$

The state to state and dynamic parameter to state state transition
matrices ϕ and Θ are over the interval (t_{N-1}, t_N) as indicated, the
dynamic process noise and measurement noise are given by $Q_{N,N-1}$ and R_N
respectively. The observation matrices F_N, E_{z_N} and E_{m_N} are the same as
defined in Chapter 12, except that the consider parameter matrix has been
partitioned into dynamic (z) and measurement (m) parameters.

It has been tacitly assumed in the above equations that no correlation
between the dynamic and measurement consider parameters exists, if there
is it can always be removed by defining a new set of dynamic parameters
by

$$z' = z - C_{\Delta z \Delta m} P_{\Delta m}^{-1} m \tag{14.2-20}$$

and then z' is treated just as z was.

In general, even though there may be no initial correlation between the solve-for and consider parameters, a correlation will result from measurement processing. The equations for these correlations are given by

$$C_{\Delta x \Delta z_N} = S_z(N) \, \mathcal{E}\{\Delta \bar{z} \Delta z^T\} \qquad\qquad (14.2-21)$$

and

$$C_{\Delta x \Delta m_N} = S_m(N) \, \mathcal{E}\{\Delta \bar{m} \Delta \bar{m}^T\} \qquad\qquad (14.2-22)$$

The theoretical development behind the equations given above for the error budget analysis is contained in Reference 14.1.

The generalized covariance technique described in Reference 14.2 is specifically concerned with filter sensitivity to differences between the assumed (by filter) and actual models of the world. Either the standard formulation of error analysis equations as summarized in Chapter 12, or the formulation given above in the error budget analysis may be used, noting that the consider parameters z and m are further subdivided into parameters which are not estimated but affect the computation of the gain matrix (consider), and parameters which are neither estimated nor affect the gain matrix (ignore). Essentially then, the generalized covariance technique generates sequentially both actual and assumed statistics. The differences between assumed and actual error statistics can involve differences in means, standard deviations, and correlation coefficients. Actual error statistics are also defined for the ignore parameters whose uncertainty has not influenced the filter design.

14.3 Monte Carlo Techniques

The GMAS Monte Carlo capability will be used primarily to supplement the linear error analysis. Monte Carlo analysis may be used to test linearity assumptions and to analyze the cumulative effect upon dispersions in mission parameters due to a sequence of maneuvers each affecting the next. Each particular Monte Carlo sample will be run exactly as a deterministic case, with the uncertain parameters being sampled as described below to generate the particular case, and the statistics of the parameters of interest being accumulated.

The standard method of sampling from the distribution described by the nominal vector of parameters $\hat{x}$ and associated covariance $P = \mathcal{E}\left\{(x-\hat{x})(x-\hat{x})^T\right\}$ requires the computation of the eigenvalues and associated eigenvectors of the matrix P. The matrix S of the eigenvectors is the orthogonal matrix which diagonalizes P giving the diagonal matrix D, defined by

$$D = S^T P S \tag{14.3-1}$$

whose diagonal elements are the eigenvalues of P. The Monte Carlo samples from the distribution defined by $\hat{x}$ and P are generated by first defining a vector, $\bar{\xi}$, of k normally distributed random numbers, where k is the dimension of $\hat{x}$. The components of $\bar{\xi}$ are given by

$$\xi_j = d_j n(0,1) \tag{14.3-2}$$

where d_j is the j-th diagonal element of D and $n(0,1)$ is a random number from a gussian distribution of mean 0 and variance 1. The Monte Carlo samples are given by

$$x = \hat{x} + S\bar{\xi} \tag{14.3-3}$$

An alternative scheme for sampling a distribution which may be computationally faster when the eigenvalues and eigenvectors of P have not been calculated for other purposes, is given in Reference 14.3. The matrix P is factored into the product given by

$$P = R^T R \qquad\qquad (14.3\text{-}4)$$

where the square root matrix R is an upper-triangular matrix. The Monte Carlo samples are then simply given by

$$x = \hat{x} + R^T r(0,1) \qquad\qquad (14.3\text{-}5)$$

where $r(0,1)$ is a k-dimensional vector of (independent) random numbers $n(0,1)$. The elements of the matrix R are given by the recursive relations

$$R_{ii} = \sqrt{P_{ii} - \sum_{j=1}^{i-1} R_{ij}^2} \qquad , \; i=1,\ldots,k \quad (14.3\text{-}6)$$

$$R_{ji} = \begin{cases} 0 & , \; j < i \\ \dfrac{1}{R_{ii}} \left(P_{ji} - \displaystyle\sum_{m=1}^{i-1} R_{jm} R_{im} \right) & , \; j=i+1,\ldots,k \end{cases} \qquad (14.3\text{-}7)$$

Whenever random numbers are obtained for the purpose of generating Monte Carlo samples, the covariances which are sampled should always be reconstructed from the actual samples which are generated. This is so that comparison between the covariance and its reconstructed equivalent can be made to assure that at least no gross mistakes have been made. It may be desirable to apply more or less sophisticated techniques of confidence level verification and testing to the reconstructed covariances as well as the distributions of the mission parameters for which the Monte Carlo analysis is being performed.

For certain mission analysis situations, it may be desirable to perform a combined linear-Monte Carlo analysis. That is, linear methods of covariance propagation and modification may be applied to certain parts of the analysis where it is known that the linearity assumption is perfectly valid. Other parts of the analysis, where linearity does not hold, may be treated with Monte Carlo methods.

In situations such as assessing a series of midcourse maneuvers, the error sources may be sampled directly without having to sample from a covariance. This will be possible only when the various error sources are independent of one another.

14.4 References

14.1 Excerpt from personal communication from C. E. Velez (GSFC).

14.2 G. L. Adams, et al. "Space Trajectories Error Analysis Programs Version II (Update) Volume I - Analytical Manual." Martin Marietta Corporation under Contracts NAS5-11795 and NAS5-11873. December, 1971.

14.3 Unknown. "Preliminary User's and Programmer's Guide for SMS/MAESTRO." Analytic Mechanics Associates. Inc. Report No. 74-? under Contract No. NAS5-21963. September, 1974.